UNIVERSITY OF SOUTHAMPTON

DEPARTMENT OF OCEANOGRAPHY

WATER AND SEDIMENT MOVEMENT IN THE VICINITY OF LINEAR SAND BANKS: THE NORFOLK BANKS, SOUTHERN NORTH SEA

Huw Joseph Powell

Submitted in fulfilment of the requirements for the degree of Doctor of Philosophy.

March 1996

For Peter and Valerie

UNIVERSITY OF SOUTHAMPTON

ABSTRACT

FACULTY OF SCIENCE
OCEANOGRAPHY

Doctor of Philosophy

WATER AND SEDIMENT MOVEMENT IN THE VICINITY OF LINEAR SAND BANKS: THE NORFOLK BANKS, SOUTHERN NORTH SEA.

by Huw Joseph Powell

Self-recording current meter data have revealed patterns of water movement in the vicinity of the Broken Bank, southern North Sea. The M_2 harmonic is dominant throughout the area; the M_4 component is, however, more distinctive at locations adjacent to the banks within the present study area. This may be indicative of local (topographic) generation of M_4 tidal currents.

Tidal currents are strongly rectilinear, creating narrow tidal ellipses. The axis of the Broken Bank is, on average, orientated at approximately 20° in an anticlockwise sense to the direction of the dominant flow.

Along the eastern flank of the Broken Bank residual flow is directed towards the southeast and is, therefore, largely parallel to the axis of the Broken Bank. Flow along the western flank is more variable, but directed generally towards the northwest. In the swale between the Broken and Well Banks, the observed near-bed residual current direction is in an offshore (northeasterly) direction.

Within the present study area, it has been found that linear wave theory does not reproduce accurately wave-induced orbital velocities observed near the sea bed.

Concurrently recorded hydrodynamic data reveal that sea bed profiles, interpreted from near-bed photographs, are not controlled explicitly by either waves or currents. Rather, observed ripple dimensions exhibit some agreement with formulae derived for both wave- and current-dominated conditions. The bed roughness 'felt' by the flow is related here to the ripple height and the angle made between the ripple crests and the direction of tidal current flow. This relationship improves considerably on the performance of existing roughness formulae. Rates of ripple migration have been used to investigate the ability of existing predictive sediment transport formulae to reproduce observed transport rates. A predictive formula has been presented which improves significantly on the performance of existing formulae.

Regional sediment transport patterns have been determined using formulae developed as part of the present investigation. These patterns reveal that this area is highly active; critical erosion velocities may be exceeded by up to 77% of the time. Currents along each flank of the Broken Bank are equally capable of transporting sediment. Sediment movement is directed predominantly towards the southeast on the eastern flank and towards the northwest on the western flank. However, on the western side, northwesterly and southeasterly sediment movement is comparable; as such the southeasterly residual on the eastern flank is much greater than the northwesterly residual on the western flank. Hence, this represents a net southward movement over the area. The supply of sand to the crestline occurs continuously from the eastern flank and intermittently from the western flank. Sediment movement in the swale between the Broken and Well Banks is directed towards the northeast. This suggests that sediment is being transported offshore under 'normal' (tidal and low wave) hydrodynamic conditions.

CONTENTS

ACKNOWLEDGEMENTS

For his supervision throughout this investigation, for funding the project and for critically reading the manuscript, I am indebted to my supervisor, Professor MB Collins.

I must thank also Dr George Voulgaris for help with the STABLE data; Dr Shu Gao for his comments regarding the manuscript; and Dr Graham Evans for his insight into North Sea sediment dynamics. Finally, I must thank Dr Leslie Whitcombe for critically reading the manuscript and for numerous discussions concerning this subject.

LIST OF TABLES

LIST OF FIGURES

LIST OF SYMBOLS

a	wave amplitude
a_{1m}	free stream particle amplitude
A_b	wave orbital diameter
A_H	coefficient of horizontal momentum transfer
C_D	drag coefficient (C_{100} = at 1 m above bed)
D	grain diameter
D_{50}	median grain diameter
E	sea surface elevation; turbulent kinetic energy
f	focal length
g	gravity
h	water depth; vertical height between sea bed and camera
H	wave height
I_b	immersed weight transport rate
k	wavenumber
k_s	physical bed roughness
N_z	eddy viscosity
P	error parameter for assessing roughness formulae
Q_E, Q_M	predicted and measured transport, respectively
Re	Reynolds number
Re_*	grain Reynolds number
Re_w	wave Reynolds number
s	ρ_s/ρ
S	$(\tau-\tau_c)/\tau_c$
t	time
T	wave period
u	velocity
u	east-west component of fluid velocity; fore-aft component of fluid velocity relative to STABLE bedframe
u_b	wave-induced orbital velocity
u_*	friction velocity

u_{*n}	friction velocity as a result of grain roughness only
u_{*w}	wave friction velocity
u_{cr}	critical threshold velocity
U_{rms}	root mean square wave-induced orbital velocity
U_0	mean current speed (harmonic analysis)
$<U>$	depth integrated velocity
v	north-south component of fluid velocity; transverse component of fluid velocity relative to STABLE bedframe
W	immersed weight of grain
z	height above bed
z_0	roughness length
δ	boundary layer thickness
δ_{cw}	combined boundary layer thickness
η	bedform height; sea surface elevation
θ	Shields' parameter
θ_c	Shields' criterion
θ_{cr}	angle between ripple crest and current direction
θ_s	direction of surface current
θ_b	direction of near-bed current
κ	von Karman's constant (=0.4)
λ	bedform wavelength; (wave) wavelength
μ	molecular viscosity
Ξ	Yalin parameter
π	pi
ρ	density of sea water
ρ_s	density of sediment
τ	shear stress; τ_0=bed shear stress; τ_b=total bed shear stress
τ_{cr}	critical threshold shear stress
τ_{cu}	current shear stress
τ_w	wave shear stress
τ_{wc}	combined wave-current shear stress

ϕ	phase difference between orbital velocity and wave shear stress
ϕ_{Ib}	direction of sediment transport
ϕ_{wc}	angle between wave and current directions
χ	period parameter
Ω	angular velocity of Earth
∇	$\partial i/\partial x + \partial j/\partial y$

INTRODUCTION

BACKGROUND

The prediction of the behaviour of coastal and shelf seas is fundamental to a wide range of human activities including coastal defence, navigation, waste disposal, fisheries, dredging, oil and gas extraction, recreation, power generation (from waves and tides), defence (military), search and rescue operations, and response to oil spills and other pollution incidents. In addition, there is concern about the long term impacts of climatic change and sea level rise on coastal defence. The recognition of the need to manage coastal and shelf seas, combined with increasing reliance on 'soft' defences, requires a major improvement of our existing predictive capability especially in relation to longer time-scales, and increasingly complex and interacting coastal processes.

Elongate sand deposits which are shaped by tidally- and/or storm- generated currents are defined as linear sand banks or sand ridges. Such deposits occur extensively on continental shelves, where sand is present and there exists an hydrodynamic regime which is able to transport it. The global distribution of such deposits has been described by several investigators (Off, 1963; Chakhotin *et al.*, 1972 and Swift *et al.*, 1978).

Changes may be produced by the interaction of hydrodynamic and sediment transport processes with these morphological features. These mechanisms are coupled closely with feedback between them. Through such coupling and feedback, the system is assumed to be striving continuously to an optimum, or equilibrium, state in which both processes and morphological form achieve maximum stability (Wright and Thom, 1977). The behaviour of such systems has received much attention, through numerical modelling studies (see, for example, Zimmerman, 1981; Huthnance, 1982a, 1982b; Boczar-Karakiewicz and Bona, 1986; De Vriend, 1990; Boczar-Karakiewicz *et al.*, 1990, 1991; Hulscher *et al.*, 1993) and from field (observational) investigations (see, for example, Houbolt,

1968; Swift *et al.*, 1973; Swift and Field, 1981; Heathershaw and Hammond, 1980a and Pattiaratchi and Collins, 1987). In spite of these extensive earlier studies, there is no general agreement as to which processes are responsible for sand bank formation; and their morphodynamic behaviour. Indeed, the processes responsible for the present maintenance of sand banks may not necessarily be the same processes that formed them initially (Collins *et al.*, 1995a). Originally, sand banks may have been relict features which the prevailing (hydrodynamic and sediment transport) regime have modified and activated; strictly, they are possibly palimpsest features.

The study of sand bank dynamics is not only of scientific interest, but is also of practical relevance. Sand banks may be present in shallow water areas which are hazardous for shipping, whilst lateral movements may affect the stability of pipelines and oil rigs. Also, such deposits may constitute potential sources for the offshore abstraction of sand as a marine aggregate. Geologically, ancient sand banks can form reservoirs for oil due to their textural characteristics (porosity and permeability).

AIMS AND OBJECTIVES

Water and sediment movements in the vicinity of the Broken Bank (one of the Norfolk Banks) in the southern North Sea are investigated. The investigation has three broad aims which can be summarised as: (i) to study the horizontal and vertical patterns of water movement; (ii) to obtain an improved understanding of the combined wave-current boundary layer over a rippled sand sea bed through an investigation into the wave-induced velocity profile above the sea bed, combined with a study of the factors controlling the roughness of a rippled bed, including identification of the processes controlling rates of ripple migration; and (iii) to investigate patterns of sediment movement in the vicinity of the Broken Bank in relation to possible mechanisms of formation and maintenance of linear sand banks and longer-term changes of sea bed bathymetry.

This investigation combines data from a number of different sources: (i) high-frequency hydrodynamic data; (ii) photographic data of the sea bed; and (iii) tidal current data obtained from self-recording current meters deployed around the Broken Bank.

THESIS STRUCTURE

A description of the overall setting of the study area (Chapter 1) includes: the geological setting of the region; coastal development, bathymetry and sediment distribution; an outline of the general pattern of water (predominantly tidal) circulation; and the regional/local wave climate.

Possible methods by which linear sand banks are formed and subsequently maintained are reviewed in Chapter 2. Included within the review are: geomorphology of linear shelf bodies; and tidal flow in the presence of sand banks.

Those aspects of sediment and fluid interaction which are relevant to the present investigation are reviewed in Chapter 3. The literature review includes: the main properties of unidirectional and oscillatory flow, both separately and in combination, together with the associated structure of the boundary layer; the concept of sea bed roughness; and sediment threshold considerations, integrated with selected sediment transport equations used for the prediction of sediment transport rates and pathways.

The description of the self-recording current meter data and the results of the analysis of these data are presented in Chapter 4. Regional water movements are investigated on the basis of self-recording current meter data obtained around the Broken Bank. Included are: data collection techniques; analysis techniques; overall record and tidal cycle descriptions; harmonic analysis; energy considerations; and phase differences.

The results of an investigation into the structure of the bottom boundary layer over a rippled sea bed under combined wave and current flow are presented in Chapter 5. The form of the wave-induced velocity profile is examined. An investigation into the relationship between the roughness 'felt' by the wave-current boundary layer as a result of flow over a rippled sand bed is undertaken; this roughness is examined in terms of ripple dimensions on the sea bed and the hydrodynamic flow characteristics. The performance of existing predictive formulae have been assessed in terms of observed ripple migration rates and concurrently recorded high frequency hydrodynamic data.

Sediment transport patterns within the present study area, based on a predictive approach (developed as part of Chapter 5) and current meter data (described in Chapter 4) are investigated; the results are described in Chapter 6. Regional patterns established here are compared within the context of the published literature.

The processes controlling sediment transport in the particular area under investigation are discussed, finally, in Chapter 7. Included are: discussion of the techniques employed; and an evaluation of the formulae developed here. Comparisons are made, at the same time, with other local areas and similar environments elsewhere. Sediment transport patterns described here are discussed within the context of longer-term, regional changes. The Chapter concludes with a consideration of the implications of the results obtained as part of the present investigation, on the wider, morphological, development of the area.

The thesis is concluded with a summary of the present investigation in Chapter 8.

Chapter 1
BACKGROUND TO THE INVESTIGATION

1.1 THE STUDY AREA

The area of the North Sea is 575,000 km^2, constituting one of the world's most extensive shelf seas; it is bordered by 7 countries (UK, France, Belgium, Netherlands, Germany, Denmark and Norway) and, hence, there is considerable interest in the prevailing oceanographic conditions. The water volume contained within the system is 40,300 km^3, connecting the Atlantic Ocean through the English Channel (Dover Straits), the Scottish continental shelves and the Norwegian Sea; with the Baltic, through the Skagerrak (Figure 1.1).

The mean water depth (around 70 m) in the North Sea increases generally northwards, from 20 to 40 m in the Southern Bight (south of 54°N) and German Bight, to 100 m near 58°N, where there is a somewhat steeper slope to about 150 m. Important bathymetric features of the North Sea are: (i) the Norwegian Trench, about 100 km in breadth and typically 300 m in depth, increasing to 700 m in the Skagerrak; and (ii) numerous sand banks rising typically to within 10 m of the sea surface in the Southern Bight, off the English and continental coastlines, and in the vicinity of the Dogger Bank (around 1 to 4°E, 54 to 55°N) where they rise to within 20 m of the water surface.

Sand banks are common features in the Southern Bight of the North Sea, and are found in a variety of hydrodynamic settings. Amongst the sand bank fields that have been identified (e.g. van Veen, 1936; Houbolt, 1968) are: (i) the Zeeland Banks and Hinder Group in the southern part of the Dutch Shelf; (ii) the Flemish Banks along the Belgian coast; (iii) sand banks within and adjacent to the Thames estuary (D'Olier, 1981); and (iv) along the East Anglian coastline (Robinson, 1966) and the Norfolk Banks (Howarth and Huthnance, 1984). Only the Dutch ridges and the Norfolk Banks are found in what may be referred to as an 'open

shelf setting' (Pattiaratchi and Collins, 1987).

1.2 REGIONAL HYDRODYNAMICS

1.2.1 Tides

Over much of the North Sea, the variation in both sea surface elevation and tidal currents is principally semi-diurnal in character. Semi-diurnal tides propagate cyclonically around the North Sea, with the largest amplitudes occurring along the coasts of eastern England and the German Bight. Tidal amplitudes are small at the amphidromes in the central Southern Bight and to the west of Denmark; they have generally less than a 0.5 m mean range off the northeast of England after energy loss from the tidal wave (primarily through friction) as it propagates. Mean spring currents are typically 0.2 m s^{-1} in the northern and eastern parts of the North Sea, but generally exceed 0.5 m s^{-1} south of 54°N and near to the English coasts and Scottish promontories. Locally, currents exceeding 1.2 m s^{-1} occur off East Anglia and in the Dover Strait. Neap tidal elevations and currents are typically 50 to 60% of those on spring tides, but increase to more than 80% for currents in the inner German Bight; this is related to the reduction in the spring tidal currents in response to shallow water frictional effects (Huthnance, 1991).

The higher harmonics of the tide are generated by non-linearities within the system i.e. advection, significant tidal range/water depth and friction; these are measurable, especially in the Southern Bight and German Bight and (in terms of currents) localised with respect to sand banks and headlands (see Pattiaratchi and Collins, 1987). Non-zero tidal residuals averaged over a tidal cycle are also generated, which may be locally important to net sediment transport rates and directions. Sediment may be transported in response to asymmetric peak tidal currents, in addition to any time-average variations.

Broken Bank is located in an area of moderate tidal energy, with mean spring and neap tidal ranges at Lowestoft of 1.9 m and 1.1 m, respectively.

1.2.2 Waves

Instantaneous water levels and currents may include a contribution from wave activity which is, consequently, important in terms of coastal defence; offshore engineering; turbulence and mixing; and the initiation of sediment movement and transport in water.

Draper (1968) has investigated the wave climate of the sea area to the north of the Norfolk Banks. Over the course of a year, marked seasonality in wave characteristics is evident. During the winter months, the significant wave height at the 50% exceedence level is of the order of 1.3 m; this reduces to 0.7 m during the summer. Wave periods (zero crossing) cluster around 5.8 s and range between 3.5 and 9.5 s. Statistical analysis of the data has shown that the wave period tends to be greatest during the winter.

Average and extreme wave heights decrease generally towards the south and inshore. An 8 m extreme wave height in the north corresponds to just over a median significant wave height of 1 m offshore of eastern England (see Bacon, 1989; Clayson and Ewing, 1988).

1.2.3 Surges and extreme currents

Variations in atmospheric pressure, coupled with strong winds, are effective in forcing currents and associated elevations in the extensive shallow waters of the North Sea. In the central-northeastern areas, these may be greater than tidal motion; elsewhere they are comparable on occasions.

Fifty-year return values have been inferred and contoured for surge elevations and depth-averaged currents over the whole of the North Sea (Flather, 1987). Elevations range from a minimum of around 0.7 m in the north, to 4 m in the inner German Bight. Corresponding values for currents are generally 0.4 m s^{-1} to 0.6 m s^{-1}, but increase locally to over 1 m s^{-1} off the Scottish promontories, within

the Dover Strait, to the west of Denmark and over the Dogger Bank. Such extreme currents, in a similar manner to the tides, tend to progress cyclonically around the North Sea coastline, then into the Skagerrak.

1.3 GEOLOGICAL SETTING

1.3.1 General

Holocene (some 10,000 years old) sediments over the area form generally a thin veneer over Pleistocene or older formations. Exceptions are the thick coastal accumulations in areas such as the Humber, Wash and Thames estuaries, and in the vicinity of sand banks. Whilst the present-day bathymetry of the North Sea approximates generally to the morphology of the pre-Holocene land surface, some areas have been modified substantially by sediment accretion and erosion.

1.3.2 The Holocene sea-level rise

In response to the retreat of the Weichselian glaciers, sea level began to rise from a eustatic low of around 120 m below the present-day level for the period of the glacial maximum (Fairbanks, 1989). Regional sea levels were approximately 65 m below present at the beginning of the Holocene. Periglacial sands had been deposited to the south of a line running approximately from The Wash to the Dogger Bank. During this time, fluvial sands may have been deposited by rivers flowing across this land surface from eastern England, or from the European mainland.

In the early stages of the Holocene transgression, the Southern Bight contained a somewhat quiescent shallow sea of low tidal range. Once a connection between the English Channel and the North Sea had been established, there was probably a rapid transition to strong tidal currents and a large tidal range. Mathematical modelling has suggested that this transition occurred when sea levels were approximately 10 to 15 m below those of the present day (Austin, 1991). Such an

increase in the tidal currents may have led to the significant erosion of early Holocene intertidal flat sediments (Stride, 1989).

A simple pattern of sea level rise after the melting of Weichselian ice sheets is complicated by the effects of regional uplift and subsidence. In Scotland and northern England, isostatic uplift was responsible for the preservation of Holocene raised beaches, whereas in the southern North Sea region there has been regional subsidence of up to 2 mm yr^{-1} during the last 4000 years (Shennan, 1989). Sediment input from rivers may have varied throughout the Holocene, reducing as vegetation cover increased. More recently, mans activities have had a significant effect on Holocene sedimentation, through: intertidal flat and saltmarsh reclamation; coastal engineering projects and flood defence; farming practices; and offshore aggregate exploitation.

1.3.3 Bedforms

Three important bedform types can be identified on the floor of the southern North Sea. Sand ribbons and sand banks are longitudinal bedforms which lie parallel or sub-parallel to the dominant tidal flow; in comparison, sand waves are flow-transverse bedforms.

(a) Sand ribbons

Sand ribbons vary greatly in size, but have lengths of up to the order of several kilometres, and widths of tens of metres; their thickness is always small, from a few grains up to about a metre (Belderson *et al.*, 1982). Such deposits may consist of trains of small sand waves resting on a scoured bedrock or gravel. Sand ribbons are characteristic of areas of strong, rectilinear tidal currents with a limited supply of sand; they have been reported to occur in areas off north-eastern East Anglia (McCave and Langhorne, 1982).

(b) Sand waves

Sand waves are present over large areas of the sea floor of the southern North Sea; they occur in water depths of between 18 m and 60 m. The absence of sand waves in waters shallower than 18 m is attributed to the effects of storm-wave activity (Terwindt, 1971; McCave, 1971). However, in sheltered nearshore areas they occur within the intertidal zone. Many such deposits occur on the flanks of large tidal sand ridges but, where the sand supply is sufficient, large areas of the sea floor may also be covered in sand waves. The height and wavelength of the features vary greatly; heights may reach 10 m and wavelengths vary typically between 50 m and 500 m; as such these bedforms may be considered to be two-dimensional large and very large dunes (Ashley, 1990).

Maximum lee slopes of sand waves are of the order of 10° to 12°, with stoss slopes of 1° to 3° (Terwindt, *op. cit.*). It is not known how rapidly these bedforms migrate. Indeed, Terwindt (*op. cit.*) was unable to detect movement within the accuracies of navigation, over a 3-year period.

Sand waves on the flanks of sand banks usually have their crests aligned obliquely to the ridge crest; on the lower parts of the flanks the sand waves are at right angles to the bank, with a tendency to 'turn' towards the crest on higher parts of the deposit. The direction of transport, as indicated by the steeper faces of the sand waves, may be in opposing directions on opposite sides of the banks (Houbolt, 1968; Caston, 1981). Around the ends of banks, sand waves of opposing symmetry may be separated by a zone of symmetrical sand waves (McCave and Langhorne, 1982; Caston, *op. cit.*).

(c) Sand banks

Sand banks are the largest bedforms present on continental shelves. Extensive areas of the southern North Sea are covered by sand banks that are orientated obliquely with respect to the strongest tidal currents. An extensive field of such

sand banks, the Norfolk Banks, extends over the U.K. sector of the North Sea continental shelf from the East Anglian coast (Figure 1.2). The Norfolk Banks occur mostly parallel to one another; their origins are, to a large extent, determined by the history of Holocene sea-level rise and the associated evolution of the coastline. One of these sand banks, the Broken Bank, is the subject of the present investigation (see Appendix 2 for detailed bathymetry).

The Norfolk Banks rest on a relatively flat surface in water depths of 20 m to 30 m depth. The deposits consist of accumulations of sand lying on an erosional surface of Pleistocene deposits which, in the interbank areas, may be exposed or covered by a thin lag gravel. The largest of these banks, the Well Bank, is over 50 km long, 1.7 km wide and rises to 38 m above the adjacent sea floor. Some of the banks are even higher, at over 42 m above the surrounding sea bed (Caston, 1972).

The Norfolk Banks can be subdivided into: (i) a group of more nearshore parabolic banks, connected by low cols to form a zig-zag pattern; and (ii) an outer group of more linear banks. The linear banks are generally asymmetrical in cross-section, with steeper slopes facing towards the northeast; these slopes may be up to 5°. Internal seismic reflectors within some of the banks dip towards the northeast (Houbolt, 1968) indicating a migration in that direction which may be continuing at present. These internal reflectors represent probably the boundaries between cross-bedded sets of sediments (McCave and Langhorne, 1982).

Broken Bank is approximately 35 km long and 1.5 km wide, with its crestline orientated approximately northwest-southeast. The height of the ridge extends up to 22 m above the adjacent sea bed. Sections of the bank's crestline come to within 8 m of the sea surface. The bank is asymmetrical in cross section; its eastern slope is approximately 1°, whilst the slope of the western flank is approximately half this value. Water depths over the region range between 23 m and 40 m. Hence, in relation to their considerable size and 'steep' slopes, the Norfolk Banks should be regarded as significant morphological features of the sea

bed.

The banks consist of fine- to medium-grained sands, which show a high degree of sorting. On the Haisborough Sand, McCave and Langhorne (1982) found the sand to become finer-grained across the bank from southwest to northeast, with the best sorting being towards the bank crestline. The shell content within the Norfolk Banks sediments is low i.e. less than 5% on the Well Bank (Houbolt, 1968). Very little is known about the internal composition of the Norfolk Banks or, indeed, any of the tidal sand banks. Houbolt (*op. cit.*) found no vertical gradation of grain size in samples obtained from a borehole through Ower Bank. A borehole through a moribund sand bank to the northwest of the Dogger Bank has revealed only subtle vertical trends in the grain size distribution (Davis and Balson, 1992).

The sand bank under investigation (Broken Bank) is covered with uniform well-sorted fine-grained sand, with a mean grain size of 0.2 mm (2.3 ϕ) (Shimwell, 1990).

1.3.4 Distribution and sources of sea bed sediments

The sediments on the floor of the southern North Sea may be derived from a variety of sources. The contribution of each source varies geographically, temporally, and in relation to the grain size of the sediment being considered.

Redistribution of 'relict' deposits has constituted a very important process in the formation of the present-day sea bed sediment distribution; much of this may have taken place during the early Holocene transgression over the land surface.

Large volumes of sediment may be supplied to the Norfolk Banks by the reworking of the sea bed by hydrodynamic forces. Sediment may also be added to this region by the reworking of material deposited within glacial channels to the north of the present study area.

Coastal erosion has been an important source of sedimentary material throughout the Holocene; it has yielded a large volume of sediment into the offshore area. The present coastline of eastern England, to the south of the Humber, is dominated by unconsolidated low cliffs and dunes. Coastal recession in these areas has been at a high rate, at approximately 4.5 km during the past 5000 years (Clayton, 1989).

The major rivers of eastern England input presently only silt- and clay-sized sediment into the southern North Sea, although their ability to transport sediment may have varied throughout the Holocene. Large amounts of fine-grained sediment may be transported into the area by water masses flowing from the North Atlantic, the Baltic and, particularly, through the Dover Strait from the English Channel (Eisma and Kalf, 1979; Eisma, 1981).

(a) Gravel

The largest area of gravelly sediments in the southern North Sea occurs between the Norfolk coastline and Flamborough Head. These sediments are mostly less than a few tens of centimetres thick; they rest on an erosional surface of till or, near the Norfolk coast, on a bedrock of chalk. This thin gravel sheet is overlain in places by deposits of sand, including the Norfolk Banks.

(b) Sand

Sand-sized sediments dominate over much of the sea bed of the southern North Sea. Much of the sediment is mobile under present-day hydrodynamic conditions and, therefore, its distribution relates to modern sand transport processes.

At present, the main input of sand into the North Sea is from coastal erosion; an important contribution from cliff erosion originates from the Norfolk coastline between Weybourne and Happisborough, where cliffs of glacial sediments are receding at a rate of approximately 0.9 m yr^{-1} (Clayton, 1989). Whilst sediment

derived from this erosion is transported to the west and southeast along the beaches, by longshore drift, the dominant direction of transport is towards offshore. A coarsening of sand grain size on the beaches in the direction of transport has been identified by McCave (1978); this has been interpreted as being the result of winnowing of finer-grained sand from the beaches, by wave action, followed by transport into the nearshore zone where the sand is removed by tidal currents.

Lowestoft Ness and Caister Ness (to the south of Cromer) are associated with shoreline-attached sand banks, which are connected through the complex of nearshore parabolic banks to the offshore Norfolk Banks. Sand derived from coastal erosion may be transported offshore, therefore, along a complex transport pathway. Such transport rates and directions maintain the offshore bank system, some tens of kilometres away from the present coastline (Stride, 1988); this concept will be considered in more detail as part of the present investigation.

(c) Mud

Muddy sediments in the southern North Sea have only a restricted distribution, which is confined mostly to intertidal areas within the estuaries and tidal inlets.

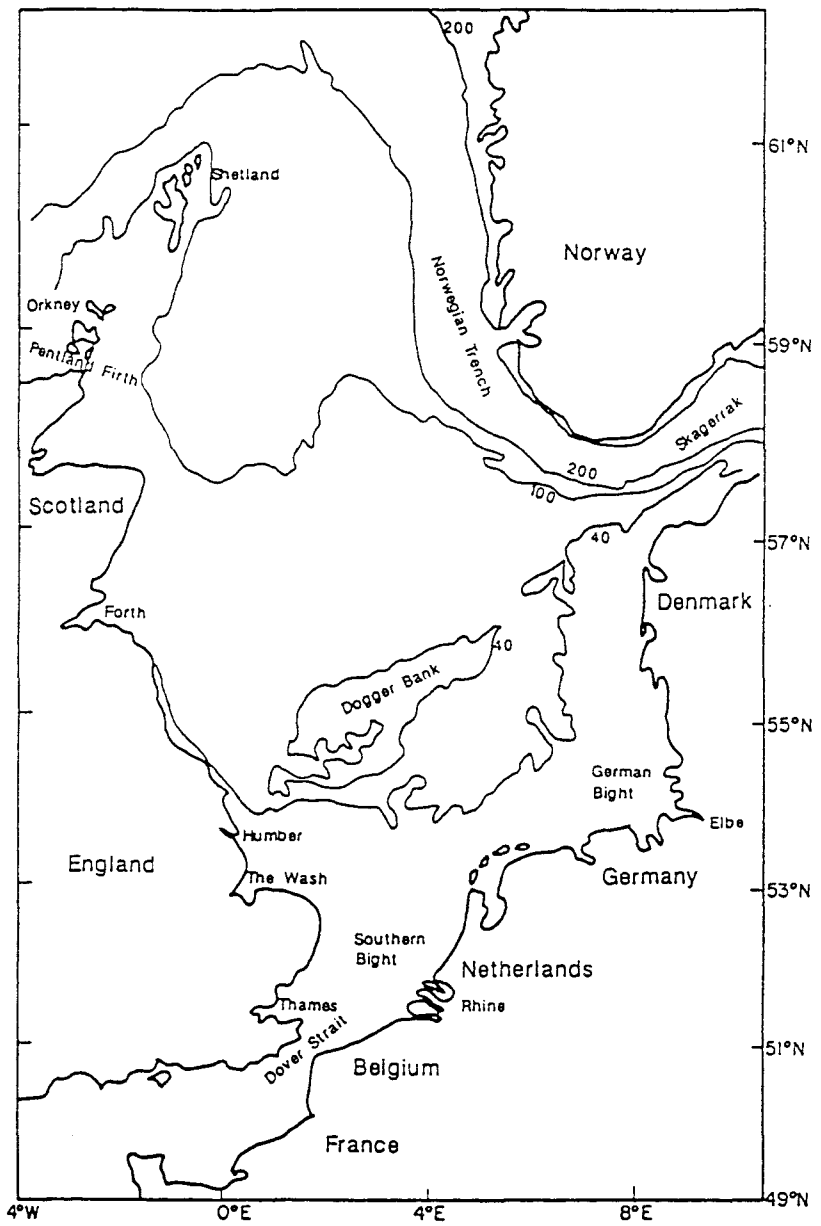

Figure 1.1 North Sea extent and bathymetry (depths are expressed in m) (after Huthnance, 1991).

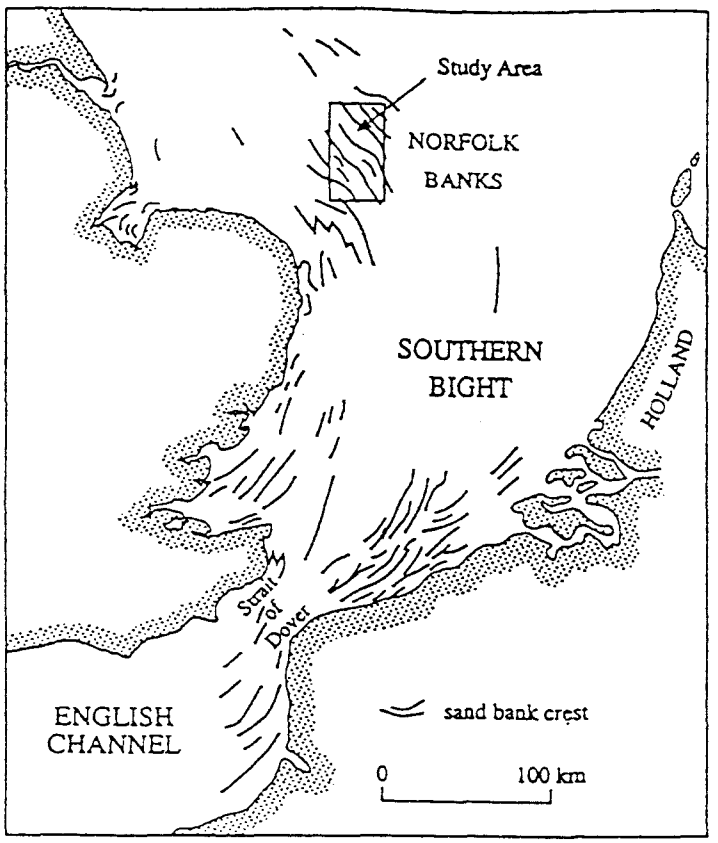

Figure 1.2 Location of the Norfolk Banks and the present study area, in relation to the southern North Sea (after Collins *et al.*, 1995a).

Chapter 2
SAND BANKS: LITERATURE REVIEW

2.1 GEOMORPHOLOGY OF LINEAR SAND BODIES

The term 'linear sand bodies' was used originally by Off (1963) and refers to straight-crested sand banks, orientated parallel or slightly obliquely to the strongest (tidal) currents. Linear sand bodies are found in a variety of geomorphological settings (Off, *op. cit.*; Pattiaratchi and Collins, 1987); they occur on open shelf seas, adjacent to coastlines, in estuaries and off headlands. Several categories of sand banks have been identified (Pattiaratchi, 1985). The present investigation is concerned with a field of banks located off an open coastline, which lie essentially parallel to that coastline. Linear sand bodies which occur in open shelf seas are frequently divided into two groups: those found in tidally-dominated settings (linear sand banks); and those located in areas of wave dominance. In particular, linear sand banks occur in shallow tidal seas in regions of strong tidal current activity (greater than 0.5 m s^{-1} (Off, *op. cit.*)) and an abundant supply of sand. In contrast, sand ridges occur in storm dominated areas (Stride *et al.*, 1982; Amos and King, 1984; Belderson, 1986; Harris *et al.*, 1992). Tidal sand banks should not be confused, however, with the shoreface-connected sand ridges of continental shelves with weak tidal currents. Here, most of the sand transport is caused by wind-induced currents associated with occasional severe storms, or with nearshore bars related to a zone of breaking waves (Stride, 1982).

Typical lengths of linear sand bodies range from a few kilometres up to 70 km; the spacing between banks ranges from 0.5 km to 30 km, whilst slope angles are up to 7° but are usually less than 1° (Amos and King, *op. cit.*; Belderson, *op. cit.*). Off (*op. cit.*) has shown that the ratio between sand bank height and their spacing can be constant (approximately equal to 0.003), albeit with a high degree of variability. The spacing within groups of sand banks tends to increase with increasing depth of tidal flow between the banks (Off, *op. cit.*; Allen, 1968),

although this relationship is poorly developed (Stride, 1982). Sand bank crests are usually straight, but crestlines can be sinuous. The latter characteristic is considered to be associated with mutually-evasive ebb and flood channels (Caston, 1972). Linear sand banks are aligned with the strongest tidal flows, or are orientated obliquely with respect to the dominant flow, at angles of up $\pm 60°$ (Belderson, 1986); they may be depositional or erosional features, or a combination of both processes.

Amos and King (1984) and Belderson (1986) consider that there are significant differences between tidally-dominated sand banks and storm-dominated sand ridges. Three significant modes in ridge height have been distinguished (Amos and King, *op. cit.*), which relate to differences in formation: 7 m for typical storm ridges; 13 m for active tidal sand banks; and 27 m for submerged barriers. An overview of the morphological characteristics of tidal sand banks and storm-generated ridges has been presented by Belderson (*op. cit.*). These investigators identified morphological differences which suggest different origins for the two bank types. For both types, tidal and/or wind-driven currents and wind waves may affect sediment mobility. Further, the processes responsible for the formation and maintenance of the sand banks may also differ in both settings; the extent of this is relatively unknown. On this basis, any strict distinction between these two types of sand bodies (cf. Belderson, *op. cit.* and Harris *et al.*, 1992), is not presently supported by any theoretical basis. The presence of linear sand banks in tidally-dominated areas appears to be associated with peak surface tidal currents in excess of 0.9 m s^{-1} and an abundant supply of sand (Belderson, *op. cit.*). Storm-dominated settings have very low tidal currents (much lower than 0.9 m s^{-1}), but strong storm activity and storm-driven currents (Amos and King, *op. cit.*; Belderson, *op. cit.*).

There is a strong association between the occurrence of linear sand banks and sand waves (Off, 1963; Chakhotin *et al.*, 1972). Sand waves are found usually in areas where the depth-averaged peak tidal currents exceed 0.5 m s^{-1} (Belderson *et al.*, 1982; Belderson, *op. cit.*). The sand waves may be superimposed upon the linear

banks, with their crestlines veering usually towards the crestline of the linear sand bank (Houbolt, 1968; Caston and Stride, 1970; Caston, 1972). When current speeds are high, but there is only a limited supply of sand, sand ribbons are found on the sea bed- rather than sand banks (Belderson *et al.*, 1982). Likewise, moribund ridges are present in regions where the near-surface peak tidal currents are lower than 0.9 m s^{-1}. Such deposits are considered to be fossil ridges, which are not in equilibrium with the present hydrodynamic regime. It has been assumed that they were formed during periods of lower sea levels and stronger tidal currents (Kenyon *et al.*, 1981).

Shelf sand bodies occur frequently in fields, often with a relatively constant spacing between the banks. The factors controlling this lateral coherence are still largely unknown; they are probably related closely, however, to the mechanism by which the sand bodies are formed. Three possible modes of formation of a sand bank field have been identified: (i) the ridge fields may have been formed, diachronously, as a response to a steady change in conditions, such as a rise in sea level with the associated flooding and shoreline retreat (e.g. Duane *et al.*, 1972); (ii) simultaneously, as a response of the sea bed to a particular hydrodynamic regime, comparable with the formation of small-scale bedforms under specified hydrodynamic conditions (Huthnance, 1982a; Boczar-Karakiewicz and Bona, 1986; De Vriend, 1990; Hulscher *et al.*, 1993); and (iii) by sand bank multiplication (Caston, 1972). The latter mechanism is associated with the presence of mutually-evasive ebb and flood channels. The banks are considered to have grown between opposing ebb and flood channels, to evolve into unstable S-shaped ridges and eventually multiply into a set of smaller linear ridges. The banks are assumed to migrate offshore as multiplication continues, in this way forming a field of sand banks (Caston, *op. cit.*; Harris *et al.*, 1992).

In the tidally-dominated setting of the North Sea, shoreline retreat related to a rise in sea level has been hypothesized as controlling the formation of sand ridge fields. Swift (1975) has presented a stratigraphic model for the evolution of these large-scale bedforms, which are considered to mark the retreat of the coastline

during periods of marine transgression. A sand body is considered to have accumulated in areas where the littoral drift of sand converges, attached to the shoreline. In response to sea level rise, a sequence of offshore sand bodies would result, as the tidal ridges became detached from their nearshore origins. Once isolated from the nearshore sand supply, a linear tidal ridge would interact with the regional tidal flow field. The bedform would reach then an equilibrium state, with sand transport continuing within the ridge/swale system.

2.2 HYDRODYNAMICS ASSOCIATED WITH SAND BANKS

2.2.1 Equations of motion

The Norfolk Banks are located within an area of the continental shelf which is subjected to strong spring tidal currents (greater than 1 m s^{-1}). The tidal currents are assumed, therefore, to be an important mechanism in controlling the formation and maintenance of these ridges. There are a number of basic hydrodynamic equations which express the conservation of horizontal momentum and the conservation of mass. The vertically-integrated equation of motion has been discussed by Heaps (1978) and can be expressed as (Pingree, 1978):

$$\frac{\partial u}{\partial t} + u.\nabla u + 2\Omega \times u = -g\nabla E - \frac{C_D u|u|}{h + E} + A_H \nabla^2 u \qquad (2.1)$$

(For a list of definitions, see List of Symbols). Variations in the velocity vector described by Equation 2.1 are the results of changes in acceleration arising from (Pingree, *op. cit.*; Howarth and Pugh, 1983):

a) advection, resulting from spatial gradients in velocity ($u.\nabla u$);

b) the effect of the earth's rotation ($2\Omega xu$);

c) the sea surface slope ($-g\nabla E$);

d) the frictional drag on the sea bed ($-(C_D u|u|)/(h+E)$); and

e) the transfer of horizontal momentum by mixing ($A_H \nabla^2 u$).

The non-linear terms in the equation (advection and bottom friction) contain the product of two components at the same tidal frequency. This association results in the generation of an harmonic at twice this frequency and a residual water movement (Pingree and Maddock, 1978). M_4 tidal currents and a corresponding residual circulation can be generated, therefore, by M_2 tidal currents. M_4 tidal currents are also generated locally by topographic features on the sea bed (Huthnance, 1973) and by headlands and islands (Pingree, 1978; Zimmerman, 1981). In the presence of headlands and/or sand banks, therefore, the generation of M_4 tidal currents is enhanced. The flow dynamics associated with these features have been studied extensively in terms of vorticity dynamics (Tee, 1976; Pingree, 1978; Pingree and Maddock, 1979; Zimmerman, 1981; and Robinson, 1981, 1983).

When suitable topographic features (i.e. depth gradients) are present, a tidally oscillating velocity field at a single frequency will generate tidal vorticity by the mechanisms of column stretching and squeezing, together with bottom friction. Both the advection term and the bottom friction term are non-linear in u, v and vorticity (ω). As a result, ω will have a component of the fundamental tidal frequency and of higher harmonics (Heathershaw and Hammond, 1980b; Robinson, 1981).

2.2.2 Tidal flow in the presence of sand banks

When a tidal current flows across a sand bank, the water column is compressed; hence, the flow accelerates towards the bank's crest. Flow on the downward side decelerates with distance away from the crestline. Hence, for potential vorticity to be conserved over the sand bank, the water column experiences a slightly lower relative vorticity (ζ) on its shallower side than on its deeper side. This process occurs irrespective of the direction in which the tide is flowing (Figure 2.1A). The net effect of this process is to generate clockwise vorticity on the shallow part of the bank, and anti-clockwise vorticity in the surrounding deeper waters. The resultant current pattern flow runs parallel to the axis of the sand bank

(Zimmerman, 1981; Robinson, 1983).

Vorticity is generated also by bottom friction, which will have a greater effect in shallow water than in deep water. Thus, for flow aligned obliquely with the sand bank, the tidal flow will experience a torque which is stronger over the shallower side of the water column. The frictionally-induced vorticity is advected with the tide. The sign of the vorticity (clockwise or anti-clockwise) depends upon the orientation of the sand bank, with respect to the flow. For both situations, however, the sense of rotation in deep and shallow water is independent of the tidal phase. As a result, mean vorticity and residual currents are generated in the sense shown in Figure 2.1B and C.

When a sand bank located in the northern hemisphere is orientated anti-clockwise with respect to the tidal flow, clockwise vorticity is generated as the flow moves on to the sand bank on the flood or ebb phase of the tide and anticlockwise vorticity as it moves off the bank. Overall, clockwise vorticity is generated on the bank and anticlockwise vorticity over the surrounding deeper water. The resulting flow is shown in Figure 2.1C. If the bank is orientated clockwise with respect to the tidal flow (Figure 2.1B) then, from the same arguments, the mean vorticity and residual flow would be directed in the opposite direction (Zimmerman, *op. cit.*; Robinson, *op. cit.*).

For a sand bank orientated anticlockwise in relation to the tidal flow, the effects of bottom friction and column stretching reinforce each other. Clockwise vorticity results from both mechanisms during the flood and ebb phases of the tide, so that a residual influx of clockwise vorticity (in the northern hemisphere) produces a residual (clockwise) circulation around the sand bank (Zimmerman, *op. cit.*). When the sand bank is orientated clockwise to the flow, the effects oppose each other; this results in a weaker net water circulation pattern.

In general, it has been shown that sand banks are orientated most frequently in an anticlockwise sense with respect to the dominant tidal flow (Kenyon *et al.*, 1981).

Robinson (1983) has suggested that this is due to the presence of some form of feedback mechanism, from the residual circulation to the process of sand bank growth i.e. that sand banks have a preferred orientation to the tidal flow, extending in this direction such that stronger residual circulation is produced. The optimisation of the residual circulation is considered to increase subsequently the stability of the sand banks. The current pattern which results from the effects described above is shown in the form of an asymmetric tide, with flood dominance on one side of the bank and ebb dominance on the other. This interpretation has been confirmed by the results of an analytical model investigation developed by Huthnance (1982b), which predicts that a sand bank would rotate to align itself towards the axis of greatest deposition (Section 2.3.1).

Huthnance (1973), using a 2-dimensional model, has demonstrated also that residual eddies are generated by the Coriolis force and bottom friction, due to the interaction between the tidal current and bottom topography. However, no preferred orientation of the sand bank was required for such mechanisms. Thus, the residual circulation is clockwise or anti-clockwise depending upon the orientation of the sand bank with respect to the tidal flow.

Residual eddies in the vicinity of sand banks have been observed on the Atlantic shelf of North America (Smith, 1969; Ludwick, 1972), in the Bristol Channel (Davies, 1980), and in the North Sea (Cloet, 1954; Caston and Stride, 1970; Caston, 1972; Stride, 1974; Harvey and Vincent, 1977; Lees, 1983a; Howarth and Huthnance, 1984). Such patterns of water movement are considered with the context of the present investigation in Chapter 4.

2.3 MECHANISMS OF SAND BANK FORMATION AND MAINTENANCE

Several models have been proposed, based upon field observations and theoretical analyses, for the formation and maintenance of linear sand banks on continental shelves. In the succeeding text, the application of these models to the present study area will be considered.

2.3.1 The Norfolk Banks

Houbolt (1968) made a series of observations relevant to sand banks in the southern North Sea. For a series of successive parallel ridges separated by channels, the tidal currents were found to be slower over the crests of the sand banks than in the channels (swales) between them. In order to compensate for these differences in the velocity field, a secondary flow circulation system was postulated (Houbolt, *op. cit.*). Water was considered to flow in two counter-rotating helixes, in such a way that the near-bed currents are directed from the inter-bank channel to converge on the sand bank crest. Compensatory surface currents are directed away from the banks, towards the centre of the swale (Figure 2.2). The existence of banks with asymmetrical cross-sections was attributed to the dominance of the secondary (helical) current on one side of the bank. Evidence to support this hypothesis was provided by current rips observed on the sea surface, corresponding to the convergence of water masses over the swales and divergence or upwelling over the crests, and by the foreset direction of asymmetric megaripples. Further evidence for such secondary flows was provided by the laboratory experiments of Casey (1935), who generated spiral currents in a flume. Similar flow features are considered to maintain the presence of sand ribbons on the sea bed (Pantin *et al.*, 1981).

A possible tidal current measurement station, located to the north of a sand bank and with the tidal flow in an east-west direction is shown on Figure 2.3. For the Houbolt hypothesis to be correct, the direction of the near-bed current (θ_b) should be to the right of the surface current direction (θ_s), when the tide flows from west to east (flood) i.e. $\theta_s - \theta_b < 0$. Similarly, during the ebb flow and to the north of the bank, $\theta_s - \theta_b > 0$. The opposite pattern of movement should relate to a station located to the south of the bank (see Figure 2.3).

Indirect evidence for the above hypothesis has been provided by Caston and Stride (1970), who described sand waves progressing up the flanks of the banks and converging at the crestline. Swift *et al.* (1973) identified the grain size

distributions across ridge and swale topography to be compatible with the 'spiral flow' concept. However, considerable evidence has been presented which is at variance with these results; on the (storm-dominated) North American Atlantic continental shelf, Swift and Field (1981) found no evidence to support the bottom flow convergence theory. McCave (1979), on the basis of the analysis of current meter data obtained in the vicinity of the North Hinder Bank (southern North Sea), concluded that the observed changes in flow direction did not conform to the pattern of a helical secondary flow. Rather, that the changes in direction throughout the water column were due to Ekman veering (i.e. the Coriolis effect). Likewise, Soulsby (1981) did not identify any evidence of near-bed convergence in the current data obtained near the Skerries Bank (Start Bay, English Channel). Similar data obtained near the Well Bank (southern North Sea) also showed no evidence to support the 'spiral flow' hypothesis (Howarth and Huthnance, 1984). However, Heathershaw and Hammond (1980a) found that, in the vicinity of Scarweather Sands (Swansea Bay, Bristol Channel), θ_s - θ_b changes sign consistently with the ebb and flood tide, giving rise to secondary currents.

It has been demonstrated that helical flows are caused by laterally constricted channels (Prandtl, 1927), flow curvature such as the bend in a river (Bathurst *et al.*, 1977; Thorne and Hey, 1979) and differential bed roughness (Tanner, 1963; Pantin *et al.*, 1981). There is neither theoretical nor experimental evidence to suggest that helical flows exist in unbounded channels. Hence, the model suggested by Houbolt (1968) could apply only to the maintenance of linear sand bank fields which are already formed (by, say, a different mechanism), in which the banks laterally constrain the flows in the intervening swales. The model is not a mechanism by which the sand banks are formed initially from a plane bed.

Growth of the sand banks has been suggested to be related to the cross-bank component of the current flow (Smith, 1969). This investigator has extended, to sand banks, a theory developed originally to explain the formation of sand waves. An erosion equation for the transport of sand has been formulated in which deposition will occur when the shear stress decreases in the direction of the flow

and erosion will occur when the shear stress increases in this direction.

Smith (1969) has argued that the theory remains valid for sand banks which are orientated obliquely to the dominant tidal flow pattern. This assumption is adopted on the basis of the fact that a current directed at some angle to the sand bank will have a transverse component of flow. The ridge will behave, therefore, as a sand wave with respect to the transverse component of the current. Even if the axis of the sand bank coincides with the major axis of the tidal current ellipse, the sand bank will grow during periods when the current velocity is directed at a small angle to the axis of the bank.

The model presented here is for sand bank (and sand wave) maintenance only; it requires an initial perturbation of the sea bed. Smith (*op. cit.*) utilises a relict topographic 'high' for the location of a sand bank. Subsequent growth of the sand bank is limited then only by the water depth and the presence of surface wind waves. In this situation, the maximum height of the sand bank will be determined by the balance between: (a) the erosional forces of the wind wave internal velocity oscillations; and (b) the rate of growth of the bank, due to the mean (tidally-induced) flow. If it is assumed that wave induced velocities are proportional to wave height, then it would be expected that sand banks will be closer to the surface in sheltered (from wave action) areas than in exposed areas; this is consistent with observations in the southern North Sea.

In another investigation, Swift and Field (1981) found that the coarsest sediments occurred on the upstream flanks of sand banks. These investigators interpreted the changes in grain size, across the sand banks, to be the result of the mechanism proposed by the above theory. Such a pattern was interpreted as being the result of the winnowing of fine-grained material, in response to the positive shear stress gradient on the up-current slope, leaving behind a coarse residual deposit. Fine-grained material would be transported and deposited in the zone of negative shear stress gradient, on the crestline and lee slope of the bank.

Various investigators (McCave, 1979; Swift *et al.*, 1978; and Ferentinos and Collins, 1980) have concluded, on the basis of studies undertaken in a number of areas, that the model could operate in association with other models (such as 'helical flows', see above), to contribute to the evolution and maintenance of the sand banks.

Detailed observations on sand waves and tidal currents in the southern North Sea have shown that the sand banks form partitions between flood-dominant tidal currents, on one side of the bank, and tidal currents with an ebb-dominance on the other side (Caston and Stride, 1970; Caston, 1972). Robinson (1966) has identified similar flood-ebb channel characteristics at inshore locations. Hence, sand circulation cells are present which consist of closed (or nearly closed) loops around, for example, individual sand banks within the Norfolk Banks system. Caston (*op. cit.*) identified that, on the bank itself, the strongest near-bed currents (and the net sand flow) were directed towards the crestline of the bank.

Along both sides of the bank, the orientation of the sand waves showed that the sand transport pathways converge towards the crestline. Convergence of the sand streams results, therefore, in an accumulation of sand which provides material for the growth of the bank. Caston (*op. cit.*) has suggested that the bank could grow both vertically (limited by the water depth) and laterally (parallel to the direction of the tidal currents), as the result of two processes: (a) up-slope oblique movement of sand, under the influence of near-bed currents; and (b) periodic downslope dispersion of sand, by wave action (Caston, *op. cit.*). Fluid-dynamical analysis support for the above mechanism has been provided by Huthnance (1982a, 1982b). Asymmetry of a sand bank is considered to be indicative of the dominance of the currents along one side of the bank (Caston, *op, cit.*; Kenyon *et al.*, 1981), or due to a lag-effect in the entrainment and settling of sediment throughout a tidal cycle (Stride, 1974).

The approaches described above have dealt with maintenance only of sand banks. Possible modes of formation have frequently been investigated separately.

Belderson *et al.* (1982) have proposed that headland-associated sand banks in a tidally-dominated environment result from a sand spit becoming detached from the headland. Under a unidirectional current or longshore drift regime, the sand spit would be attached. Detachment would occur in response to locally-concentrated reverse flow, adjacent to the headland.

The interaction between tidal flow and headlands can result in the formation of a residual eddy in the vicinity of the headland. Pingree (1978) suggests that sand banks may form on either side of the headland, depending upon the balance between inertial and Coriolis forces. Hence, it has been shown (Pingree, *op. cit.*; Heathershaw and Hammond, 1980b) that sand banks are formed when the ratio of absolute vorticity ($\omega+f$) to the planetary vorticity (f) is greater than 1 or less than -1. In the northern hemisphere, both residual circulation and planetary vorticity have the same sense of rotation on the right-hand side of a headland (viewed from the sea). On the left-hand side of a headland, ω and f are opposed. Considering the balance of forces in purely circular motion and including the effects of bottom friction and the Coriolis force, Pingree (*op. cit.*) has shown that the circulation described will result in a low pressure region at the centre of the eddy; giving rise to flow convergence at the sea bed and, by continuity, flow divergence at the surface. Flow convergence at the sea bed was presumed to produce an accumulation of sediment at the centre of the eddy. Hence, for headland associated banks, a mechanism has been proposed by which sand banks may be initiated and then maintained.

That one mechanism initiates the formation of (offshore) tidal sand banks and that another is responsible for the maintenance of these banks, does not provide a very elegant conclusion. However, a mode of formation, and subsequent maintenance, of sand banks across the continental shelf has been presented by Huthnance (1982a). In this approach, a stability model has been developed to investigate the growth rate of slight topographic irregularities on the sea bed. The model considered only parallel depth bathymetric contours and is based on the following assumptions:

(a) depth-uniform currents, constant during each half of the tidal cycle, lying at an arbitrary angle to the crestline;

(b) a greater than linear increase in the sand transport rate, with increasing current velocity; and

(c) downhill preference for sand transport, due to gravity effects on the slopes of the bank.

The growth rate of a sand bank was found to be dependent upon the angle between the depth contours and the peak current direction (α), in combination with a normalised wave number k where:

$$k = \frac{2\pi h}{C} L \tag{2.2}$$

and h is the mean water depth, C is a drag coefficient, and L is the sand bank spacing (morphological wavelength). Oblique orientation of the sand banks, with respect to the dominant tidal flow, is required for the banks to grow. Maximum growth was predicted for $\alpha = \pm 28°$ and $k = 10$, corresponding to a ratio of sand bank spacing to mean water depth of 250 (i.e. $L = 250$ h). Sand banks lying effectively parallel to the flow prevent any sand being transported on to the crest of the bank; in this way the banks cannot grow. Sand banks that lie normal to the flow direction must, in order to satisfy the continuity consideration, experience flow acceleration across the crest. Consequently, sand will not be deposited.

As the flow passes along the up-current flank of an obliquely-inclined bank, the cross-bank component of the flow accelerates to maintain continuity; and because it accelerates, the current veers towards the ridge axis and erodes the surrounding sea bed. However, the top of the sand bank is so broad and shallow that the bottom drag makes the cross-ridge component of the flow decelerate. Although the initial current speed across the upper section of the bank is initiated considerably above the regional mean value, ending above it, deceleration occurs. Thus, as the flow loses power across the crest, sand entrained through erosion of the up-current flank is deposited on the crest of the bank. In a reversing tidal current regime,

such dynamical conditions provide the mechanisms for the convergence of sediment transport pathways at the crestline. This process would explain, however, sand deposition and ridge development even in unidirectional flows.

When the flow is oblique to the sand bank, the cross-bank flow component must also accelerate over the crest. However, the along-bank component experiences frictional drag and decelerates, resulting in sand deposition. The frictional drag exerted by the crest on the water slows also the current speed as it enters deeper water, compared with the current directed towards the bank. The inertial effect depends upon the wavelength of the bank, compared with the adjustment length of the flow. If the sand bank is short, the inertial effect will be strong i.e. the effect is transferred to the next bank crest, instead of the trough; if it is long, then the inertial effect is weak and remains close to the crestline. For any particular water depth, the influence of this mechanism is at a maximum when the ridge spacing compares with the distance required for the flow field to re-adjust to the topography.

The veering effect depends upon the orientation of the sand bank with respect to the direction of the tidal current. If the current crosses the bank almost perpendicularly, veering is weak and the frictionally-induced vorticity is at a minimum. If the current is flowing largely parallel to the bank, the friction induced vorticity is maximum, but it is not advected over the bank. The current turns (veers) towards the crestline, due to frictional drag, as it moves on to the bank. The sediment transport pathways are controlled by this veering, as the current leaving the bank during the reverse tidal half-cycle is weaker (see above). Net transport is directed, therefore, towards the bank. Caston (1972) and Kenyon *et al.* (1981) have observed current patterns and sediment transport pathways similar to those predicted by the model for sand banks in the southern North Sea.

Since the stability of sand banks is only weakly dependent upon their orientation, external factors (such as the proximity of the coastline and wave action) may influence this orientation. The model has predicted that, in the absence of wave

activity and with an unlimited supply of sand, a sand bank will grow until it reaches the sea surface. The equilibrium profiles depend strongly on the amount of sand available. A reduction in the sand supply will decrease the bank width to approximately one-fifth of the spacing; it will also reduce the height of the bank. However, wave effects have a more significant influence on the sand bank morphology, causing the top of the bank to become much flatter and broader as the bank grows higher.

If flood- and ebb- tidal currents were unequal in magnitude and/or direction (i.e. an asymmetry in the tidal flow was present), then the model would have predicted the sand bank to have an asymmetric equilibrium profile with the steeper side of the bank facing the direction of net transport. The Coriolis term was found to enhance the growth of banks aligned cyclonically (anti-clockwise in the northern hemisphere), relative to the current.

Huthnance (1982a) compared the relationship $h=0.004L$ with the observations presented by Off (1963), establishing good agreement between the model and observations. Similarly, Figueiredo *et al.* (1981) found 'good qualitative agreement' between the predictions of the model and the morphometric data obtained from the Mid-Atlantic Bight ridge (sand bank) fields. Elsewhere, Parker *et al.* (1982) have concluded that the fluid dynamical, geomorphological and sedimentological data collected from the sand banks of the Inner Argentine Shelf could be explained "most simply and economically" by the model described above.

In a subsequent publication (Huthnance, 1982b), the model described above was extended to include two-dimensional topography. Vorticity generated by flow over a bump was found to cause deposition of sediment at the bump. Scour bands extended from the bump in line with, and perpendicular to, the tidal current. Deposition occurred between the scour bands. In the case of an elliptical bank, the predicted depositional pattern was smooth in comparison with that for a bump. A sand bank tended to align itself with the axis of greatest deposition. A bank tended also to contract laterally (unless very narrow) and to extend itself lengthwise,

providing that the angle between the tidal current and the sand bank (α) was within the range $18° < \alpha < 48°$. Finally, the bank had a tendency to rotate towards an inclination of $\alpha = 27°$, identified earlier.

In the model with parallel depth contours (see above) sand bank growth was restricted by sand supply, wave action and the inclination of the sand bank to the tidal current. With non-parallel contours, it was predicted that the flow would avoid the particularly shallow regions, where the strong influence of bottom friction reduced the flow, encouraging deposition until the bank reached the water surface.

The model predicted also a gradual lengthening of the bank, with deposition taking place at the ends of the bank where the net currents and the rates of sand transport were lower. Reversal of the tidal currents across the ends of the bank was predicted, producing an area of zero mean currents. Such a prediction has been supported by observations of areas of symmetric sand waves at the end of sand banks in the North Sea (Caston, 1981; McCave and Langhorne, 1982).

A sloping sea bed, in the direction of the tidal current, has been found to have a destabilizing effect and to prevent the formation of stationary sand banks. However, with tidal currents flowing along the depth contours, such as near a coast, the destabilizing effect was identified as being only slight. Consequently, an equilibrium sand bank was formed, with the bank being higher and broader in deeper water i.e. the crest of the bank was level. This particular prediction is supported, once again, by the findings of Swift *et al.* (1978). These investigators undertook a comparison between the shore-connected sand banks of the American and European shelves; they identified that the banks were level with respect to the water surface, although a gradient in the water depth was present.

The models presented by Huthnance (1982a, 1982b) describe the growth of *insignificant* irregularities on the sea bed and their associated equilibrium profiles, under differing conditions (wind-wave action, availability of sand etc.). The

models provide a mechanism for sand bank *maintenance*; differing from most others, they provide also a mechanism for sand bank *formation*. Several features are predicted by both of the models described, these include the orientation of sand banks to the tidal currents, asymmetric bank profiles, and veering of the tidal currents and sediment transport pathways across the sand banks. All of these features have been observed, by various investigators, in the field (see Houbolt, 1968; Caston, 1972; Kenyon *et al.*, 1981; and Stride, 1982).

Modelling studies conducted recently, based on Huthnance's earlier work (De Vriend, 1990), have evaluated the effect of a number of controls on the growth rate and stability of sand banks. Processes investigated include: (i) complex tidal flow (tidal water level variations, tidal ellipses other than a single line, additional residual currents); (ii) the mode of sediment transport (bedload or suspended load); and (iii) the impact of wind waves (sediment stirring, additional transport by wave asymmetry). Analysis of a particular reference case (similar to that presented by Huthnance (1982a)) indicates that the growth of sand banks orientated obliquely to the flow can be predicted for any combination of velocity amplitude, mean water depth, bottom roughness and sediment transport mechanism.

That sand bank evolution is a non-linear process has been asserted by Hulscher *et al.* (1993). Hence, the linear theory presented by Huthnance (*op. cit.*) and De Vriend (1990) yields information concerning only which modes tend to grow initially, not on their amplitude evolution. Once the bed has evolved into a sand bank system of finite amplitude, therefore, the linear approach is no longer valid. For example, the initial and fastest growing mode may differ from the dominant mode in the fully-developed sand bank system. Thus, non-linear analysis is necessary to overcome this particular problem. However, as the analysis of a full non-linear system is complicated, Hulscher *et al.* (*op. cit.*) have studied weakly non-linear sand bank dynamics under conditions where the perturbations first start to grow. In order to be able to undertake such an analysis, a critical parameter should exist at which the morphodynamic system changes its stability properties. Hulscher *et al.* (*op. cit.*) have shown that such a situation exits for a rotary tidal

current.

A sequence has been described to explain the movement and development of a system of sand banks (Caston, 1972). This is associated with the growth of the ebb and flood tidal channels (Figure 2.4). A linear sand bank is formed between two mutually-evasive ebb and flood channels (Stage A, Figure 2.4). Inequality in the rate of transport leads to the destruction of the straight crestline of the bank (Stages B and C). The resulting double curve develops into an incipient pair of flood and ebb channels (Stage D). The channels continue to lengthen until the central ridge is parallel with those on either side (Stage E). This cycle may now be repeated, but now in relation to three sand banks.

The model described above is a mechanism by which banks may be maintained and, consequently, evolve into a system of sand banks. However, the initial condition required for development of the sand bank system is the existence of a individual sand bank. The origin for this initial bank has not been described, within the context of the mechanisms outlined.

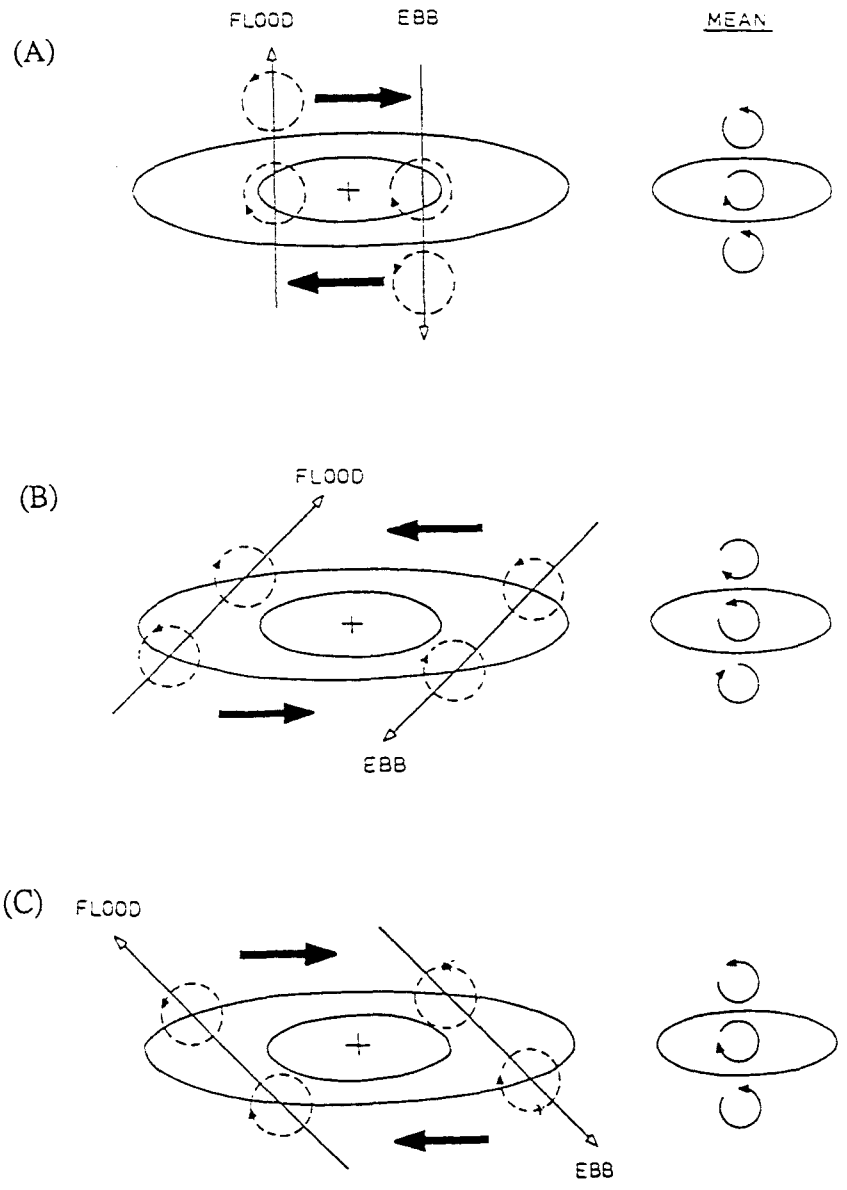

Figure 2.1 The generation of vorticity in the vicinity of a sand bank: (A) due to column stretching and squeezing over the bank; (B) due to bottom friction for a sand bank aligned clockwise to the tidal flow; and (C) with anti-clockwise alignment (after Zimmerman, 1981 and Robinson, 1983).

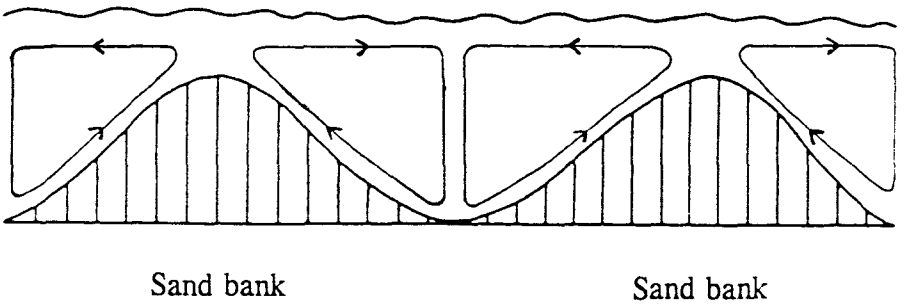

Figure 2.2 Spiral flow structure (after Houbolt, 1968).

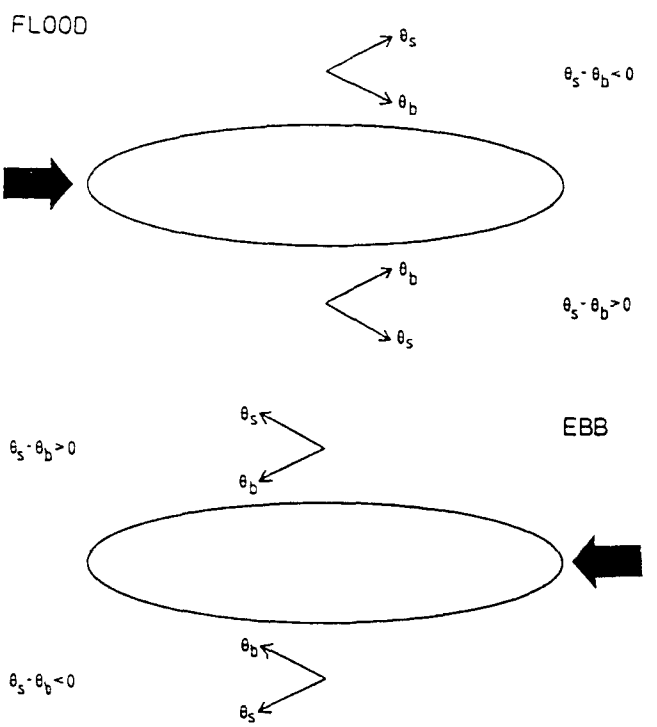

Figure 2.3 Relationship between surface (θ_s) and near-bed (θ_b) current directions for the presence of secondary currents in the vicinity of a sandbank.

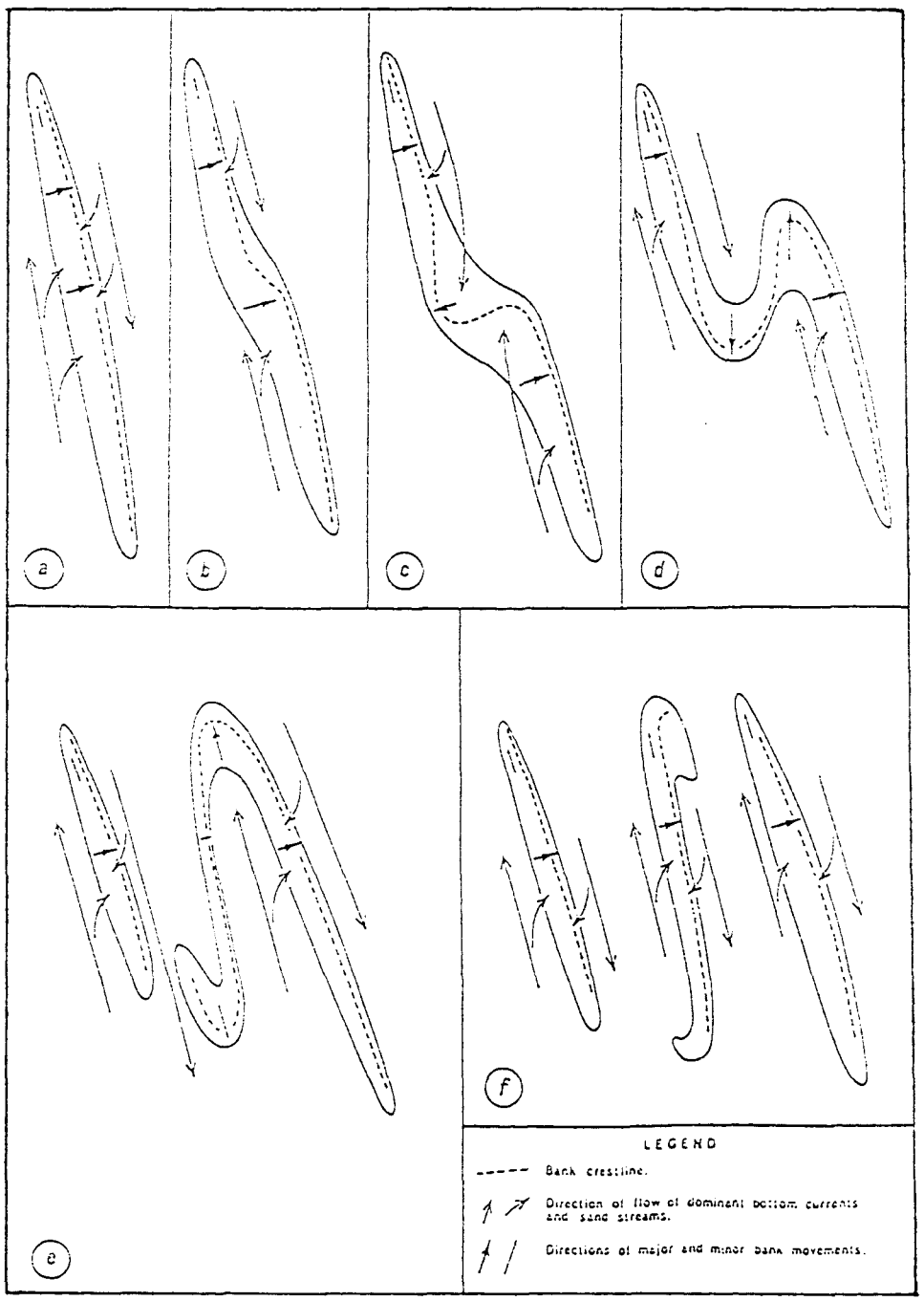

Figure 2.4 Schematic representation of the growth and development of linear sand banks (after Caston, 1972).

Chapter 3
SEDIMENT TRANSPORT THEORY

3.1 SEDIMENT MOVEMENT UNDER UNIDIRECTIONAL FLOW

When a fluid moves over a solid boundary it exerts a drag force on the surface of that boundary. This frictional drag is caused by fluid shearing and is dependent upon the viscosity of the fluid, the roughness of the surface and on the character of the near-surface flow. The boundary layer is the region in which the flow velocity changes from zero at the bed (no-slip condition) to a maximum (the free stream velocity, U_∞) at some height above the bed. A velocity gradient is produced, therefore, above the bed. The turbulent energy and shear stress also vary within this region, from a maximum at the bed to zero at the top of the boundary layer.

The boundary layer may occupy a part of the water depth, or the complete water column. When all of the depth is occupied, the boundary layer is referred to as 'depth limited'; as such, it may not reach it's free stream velocity. The thickness of the boundary layer may be defined in terms of the fluid velocity. The top of the layer is taken usually as that height above the bed where the flow velocity is 99% of the free stream value (Heathershaw, 1988). In the sea, relatively strong current speeds and shallow water depths means that the boundary often occupies the entire water depth over large areas of the inner continental shelf and coastal zone (Figure 3.1). Such conditions are characteristic of the area under investigation.

On the basis of laboratory flume experiments, natural flows may be classified as either laminar or turbulent. In the marine environment, however, laminar flow is rarely observed (Dyer, 1986). On this basis laminar flow conditions will not be discussed here in any detail.

3.1.1 Laminar flow

When fluid moves slowly over a surface, the drag created is related to the viscosity of the fluid. Along planes parallel to the wall (or boundary), a shear stress is produced which is dependent upon the velocity gradient and the fluid viscosity. A layer of molecules with zero velocity form a layer along the boundary, where the shear stress is at a maximum. Above this layer, movement between the various layers takes place and mixing (momentum transfer) occurs in a direction perpendicular to the wall on the molecular scale only. The shear stress (τ) is defined as:

$$\tau = \mu \frac{du}{dz} \tag{3.1}$$

where μ is the molecular viscosity, and du/dz is the velocity gradient above the boundary. In laminar flow, all the particles passing a particular point within the flow will follow the same pathway.

3.1.2 Turbulent flow

Turbulent flow consists of random movements of small eddies within the fluid. Therefore, particles passing a point in the flow do not necessarily follow the same pathway (see above). The turbulent motion about an average streamline is much larger than the corresponding molecular movements. Momentum exchanges and the shear stresses are also greater. The resulting turbulent shear stress has been observed experimentally to be proportional to the square of the time-averaged velocity:

$$\tau \propto u^2 \tag{3.2}$$

Equation 3.2 can be linearised, in a way which is analogous for that adopted for linear flow:

$$\tau = N_z \frac{d\bar{u}}{dz} \tag{3.3}$$

where N_z is the eddy viscosity. The eddy viscosity is a property of the flow and not of the fluid. The value of the eddy viscosity is not constant; it varies, for example, with the mean velocity. The viscosity is likely to change, therefore, throughout the water column.

The transition from laminar to turbulent flow occurs as the flow rate is increased. Experiments undertaken by Osborne Reynolds investigated flow in pipes; these indicated that turbulence is random, with respect to both time and distance along the pipe. Studies undertaken with tubes of different diameters, with various fluids, showed that the onset of turbulence can be represented by a dimensionless Reynolds number (Re); this is dependent upon flow velocity, pipe diameter (in this particular example) and the kinematic viscosity of the fluid ($\upsilon = \mu/\rho$). The transition has been shown to occur at a constant value of Re; at this point, flow resistance in the pipe increased. The properties of flow in the sea and within open channels are similar to those observed in pipes (Dyer, 1986).

The turbulent boundary layer can be classified using the grain Reynolds number ($Re_* = u_*D/\upsilon$) (Table 3.1). Sternberg (1968) has suggested that this classification may be applicable to the marine environment, if the values 3.5 and 68 are replaced by 5.5 and 165, respectively (Table 3.1).

In smooth turbulent flow, a thin sublayer is present close to the wall where the flow is dominated by molecular viscosity; this is referred to as the viscous sublayer. Whilst the fluid motion within this region is not laminar, the mean longitudinal velocity profile is linear (Figure 3.2). Above the viscous sublayer is a buffer layer. This 'intermediate' layer extends upwards to the overlying fully turbulent logarithmic layer, in which the velocity profile is logarithmic in relation to height above the bed.

The transition from smooth to rough turbulent flow occurs when the roughness elements on the boundary just protrude through the viscous sublayer, into the overlying flow. In rough turbulent flow, the viscous sublayer and the buffer zone are absent and the logarithmic layer extends down to the bed (Figure 3.2). Within the fully turbulent logarithmic layer, the flow is determined by distance from the boundary; hence, it is independent of the individual roughness elements. The flow is also independent of the free stream velocity, if the boundary layer is not 'depth limited'. This layer may extend for up to a few metres above the bed. Above this level is the outer layer (Figure 3.2), which extends typically up to a few tens of metres above the bed. If the water depth is great enough, then this layer will extend up to a height above the bed where the fluid velocity approaches the free stream velocity.

The flow speed within the logarithmic layer can be described by the relationship:

$$u_z = \frac{u_*}{\kappa} \ln \frac{z}{z_0} \tag{3.4}$$

where u_z is the current speed at height z above the sea bed, u_* is the friction velocity, z_0 is the sea bed roughness length and κ is von Karman's constant. Various measurements (including those of Charnock (1959), Caldwell and Chriss (1979) and Soulsby and Dyer (1981)), have confirmed that a von Karman constant of 0.4 is appropriate to the sea. This relationship describes steady uniform flow of an unstratified fluid. The velocity profile represents a straight line when ln z is plotted against u_z (Figure 3.3). The slope of the line is proportional to u_* and, therefore, the bed shear stress (τ_0), where

$$\tau_0 = \rho u_*^2 \tag{3.5}$$

can be determined readily from the slope of the line. The bed roughness length (z_0) is obtained, similarly, from the intercept on the ln z axis. However, substantial errors in the values of τ_0 and z_0 (35% and 77%, respectively, with 6 current meters) can be introduced if data from an insufficient number of levels are used to determine the relationship (Wilkinson, 1984). The errors are reduced with

an increase in the number of velocity measurements collected at different heights above the sea bed. Considerable care must be taken in fitting a logarithmic profile to the observed data. Effects that may alter the velocity profile from this form include acceleration and deceleration of the flow, the presence of bedforms and wave orbital motions.

In many situations, it is not possible to obtain sufficient data in order to produce a velocity profile. Instead, the flow velocity may have been recorded at a single elevation above the sea bed (typically, 1 m). In these circumstances, the presence of the logarithmic velocity profile is often assumed. It is necessary to prescribe, therefore, a value of z_0 based upon the sea bed sediment type and the presence of any bedforms (Table 3.2).

The bed shear stress may be determined in a number of ways. A simple alternative to the logarithmic velocity profile approach is to relate the stress to the current measured at a fixed height above the sea bed (usually 1 m), using a quadratic stress relationship. It has been shown experimentally that, in turbulent flow, the shear stress is proportional to the square of the mean velocity. Introducing a drag coefficient, C_D:

$$\tau = \rho C_D u^2 \tag{3.6}$$

When measurements are obtained at 1 m (100 cm) above the bed, Equation 3.6 becomes

$$\tau = \rho C_{100} u_{100}^2 \tag{3.7}$$

Typical values for the drag coefficient are presented in Table 3.2. In general, use of the logarithmic profile with a prescribed value of z_0 is preferred because it is not height specific and can be related directly to bed geometry.

Another method used for determining the variation in velocity with height above the bed is a simple power law relationship. The expression referred to most commonly is:

$$\frac{u}{u_\delta} = \left(\frac{z}{\delta}\right)^{\frac{1}{7}} \tag{3.8}$$

where u_δ is the velocity at the outer edge of the boundary layer. This formula can be regarded only as an approximation, since the exponent has been found to vary between 1/5 and 1/10 (Dyer, 1986).

3.1.3 Threshold of sediment movement

As the velocity of a fluid flowing over a sediment bed is increased gradually, a point is reached where any additional increase in flow velocity will cause the bed to become unstable and the sediment grains to move. Conditions which are slightly less than those necessary to cause initial movement are known as 'threshold'. Any conditions slightly greater than those required to cause threshold will produce a small amount of sediment transport.

The precise conditions required to cause the threshold of movement of particles depend on the nature of the sediment bed, the properties of the fluid and the definition of threshold.

Mechanics of threshold

The forces acting on a (non-cohesive) particle resting on the surface of a bed, caused by a unidirectional current, are shown in Figure 3.4.

A force F is produced by skin friction as the flow travels over the surface of the grain, where:

$$F = C_D \frac{1}{2} \rho u^2 \frac{\pi D^2}{4} \tag{3.9}$$

The lift force (L), is caused by the difference in dynamic pressure between the

upper and lower surfaces of the grain. The pressure is greater at the lower surface of the grain acting upwards; this has the effect of attempting to lift the grain upwards. L can be expressed in terms of:

$$L = C_L \frac{1}{2} \rho u^2 \frac{\pi D^2}{4} \tag{3.10}$$

Hence, the lift force is related to the drag force by

$$L = \frac{C_L}{C_D} F \tag{3.11}$$

The coefficients C_D and C_L are both functions of the grain Reynolds number.

Hence, for the fluid forces:

$$L \propto \tau_0 D^2 f\left(\frac{u_* D}{\nu}\right) \tag{3.12}$$

and:

$$F \propto \tau_0 D^2 \tag{3.13}$$

The immersed weight of the grain is expressed by:

$$W \propto (\rho_s - \rho) g D^3 \tag{3.14}$$

Reference to Figure 3.4 illustrates that the fluid forces are attempting to dislodge the grain, whilst the immersed weight of the grain and the inter-grain friction (not shown) provide the restoring force necessary to retain it in position.

The fluid forces attempt to rotate the grain about a contact position P. Analysis of moments about the point of contact (P) yields the fluid force necessary to cause the grain to become unstable. At the moment of equilibrium,

$$FDf_1\left(\frac{u_* D}{\nu}\right) + LDf_2\left(\frac{u_* D}{\nu}\right) = const\ WD \tag{3.15}$$

Applying the appropriate substitutions from above gives:

$$\frac{\tau_0}{(\rho_s-\rho)gD} = f\left(\frac{u_* D}{\nu}\right) = \theta \qquad (3.16)$$

This form was that proposed originally by Shields (1936). When θ, the Shields' parameter, is equivalent to the threshold condition for sediment movement, it is denoted θ_c and is referred to as the Shields' Criterion.

The actual conditions required to move an individual grain will depend upon the physical properties of the grain(s) and the fluid; similarly its position relative to the other grains and the physical properties of the surrounding grains. Hence, in order to dislodge the grain, fluid will have to overcome the gravitational force and the particle interlock.

Shields (*op. cit.*) has produced the threshold curve shown in Figure 3.5, on the basis of dimensional analysis; it has distinct zones, which correspond to the various boundary layer flow regimes (see below).

(a) Up to $Re_* \sim 3$, smooth boundary flow exists and the particles are embedded in the viscous sublayer. The threshold shear in this zone was assumed to be independent of grain diameter, since small grains effectively lost their individuality. In this particular case, the curve should have a slope of 45° and $\theta_c \propto Re_*^{-1}$.

(b) Between $3 < Re_* < 200$ there is a transitional region where the size of a grain is of the same order of magnitude as the thickness of the viscous sublayer. The minimal θ_c value corresponding with this region is about 0.03.

(c) Within the rough turbulent regime, with $Re_* > 200$, θ_c assumes a constant value lying between 0.03 and 0.06.

There have been various studies undertaken on the threshold of sand. Despite the scatter in the data points obtained, the general dip in the curve to about $\theta_c=0.03$ (Re_* is approximately 10) is fairly well established. There have been few studies on threshold at Re_* values greater than about 1000 and, correspondingly, there are relatively large discrepancies between the results. At these high Re_* values, other

factors such as grain shape, protrusion and sorting, become important.

It should be noted that the well-established Shields' curve is based principally on laboratory and flume studies; it applies, in the strictest sense, to plane beds only. Shields assumed that his theory should be restricted to roughly uniform grain sizes and to water depth/particle diameter ratios greater than 40.

In other early investigations of sediment threshold, Hjuström (1935, 1939) related the mean velocity of flow in a river to the diameter of the sediment particles forming the bed. The curves derived are straightforward in their use, but they are restricted to the motion of quartz. Further, the approach is limited to conditions which are characteristic of a river system. Threshold is defined in terms of a reference flow velocity at 100 cm above the bed, but the vertical distribution of the currents may depend upon the flow depth. In this way, apparently different critical velocities may be obtained for the same sediment size, but different water depths (Reineck and Singh, 1980).

In practice, the Shields curve is somewhat difficult to use, as u_* appears on both axes and an iterative procedure is required in the analysis of the data sets. Consequently, other investigators have proposed slightly different predictive methods; these are outlined below.

a) Inman (1949) presented a curve which relates the threshold friction velocity (u_*) to grain diameter (D). However, this approach does not include all the parameters used by Shields to describe fully the fluid and sediment conditions. Consequently, the curve should not be regarded as a general representation and it can not be applied readily to investigations in the marine environment.

b) Sundborg (1956) has related the flow velocity at 100 cm above the bed (u_{100}), against D. This analysis provides a relationship which can be used under limited conditions.

c) Bagnold (1963) derived a relationship between θ_c and D for quartz grains, in water at 20°C.

d) Yalin (1972) proposed a combination of θ_c and Re_* in the analysis to eliminate

u_* from the two axes of the original Shields curve: fluid and grain parameters are retained on the abscissa of the graph.

The Yalin parameter (Ξ), defined by

$$\Xi = \frac{Re_*^2}{\theta_c} = \frac{(\rho_s - \rho)gD^3}{\rho\nu^2} \tag{3.17}$$

generates a curve similar to that of Shields.

Miller *et al.* (1977) have reviewed the various empirical and semi-empirical relationships which have been derived for threshold under steady unidirectional currents. The data used by these authors were confined to experiments using flat beds, under controlled laboratory conditions. These investigators extended the original Shields diagram by three orders of magnitude, in terms of the grain Reynolds number, concluding that the critical velocity at 100 cm above the bed is given by:

$$\begin{aligned} u_{100c} &= 122.6D^{0.29} \qquad \textit{for } D<0.2 \textit{ cm} \\ u_{100c} &= 160.0D^{0.4} \qquad \textit{for } D>0.2 \textit{ cm} \end{aligned} \tag{3.18}$$

However, in general, use of Shields' curve is preferred to Equation 3.18. The former relationship provides the critical shear stress acting directly on the grains, with no assumption concerning the sea bed roughness length (z_0) being made. (Note: The Shields curve is represented usually by a single line, rather than by a band, implying that the threshold of sediment movement is strictly deterministic).

The relationships discussed so far have been concerned with unimodal sediments only. Variation may be encountered when the sea bed sediment is poorly sorted; for example, larger grains may move at lower threshold values than those predicted by the Shields equation (Tomlinson, 1993).

Further inaccuracies may be introduced by differences between the threshold values determined for sediments in the laboratory, compared with those encountered in the marine environment. Further, Tomlinson (1993) has investigated the influence of 'stress history' on the threshold of motion. Experimental studies showed that when the sediment was subjected to subcritical (threshold) conditions prior to the initiation of movement, the shear stress at which sediment movement was eventually initiated increased. This latter condition is likely to represent flows in the marine environment, where grains have rearranged themselves in response to current speeds which increase slowly due to fluctuating oscillatory tidal current patterns.

3.2 SEDIMENT MOVEMENT UNDER OSCILLATORY FLOW

A wave travelling past an observer, at a fixed point, has a wavelength (λ) equal to the distance between two successive crests. The period (T) is the time interval between the passage of the two crests at that particular point. The height of the wave (H) is the difference in elevation between a wave crest and successive trough (also, amplitude (a)=H/2).

Three idealised wave profiles are referred to extensively in the literature (see Allen, 1982):
(a) Airy waves, which have a sinusoidal profile and are of infinitely small amplitude within an inviscid (frictionless) fluid;
(b) Stokes waves, which are trochoidal in profile and of finite amplitude within an inviscid fluid; and
(c) Solitary waves, which are waves of finite amplitude but which have no definite wavelength and are not periodic.

Although the sea surface has an apparent random nature, it is convenient to consider an ideal wave with a sinusoidal profile. Using Airy theory, the form of the sea surface elevation of the waveform (η) can be expressed as:

$$\eta(x,t) = a \sin(kx-\omega t) \tag{3.19}$$

where $k=2\pi/\lambda$ is the wavenumber, and $\omega=2\pi/T$, the angular frequency.

Airy wave theory shows that the water particles beneath the waves move in circular orbits in deep water. As waves move in to shallower water, from offshore, they are influenced by the sea bed. However, in water of intermediate depth the orbits become elliptical, increasing in eccentricity with increasing depth but decreasing in diameter. The effective limit for deep water is taken often as $h>\lambda/2$, intermediate water conditions as $\lambda/20<h<\lambda/2$, and for shallow water $h<\lambda/20$ (where h is the water depth).

In deep water the particle orbits under the wave are circular, with the diameter decreasing exponentially with depth. Under intermediate conditions the wave feels the sea bed and the vertical motion in the orbit becomes restricted. The orbital motion become increasingly flattened with depth, until at the sea bed there is simply a to-and-fro (oscillatory) motion with no vertical travel. The orbital diameter (d) of the horizontal water motion at the sea bed is given by:

$$d = \frac{H}{\sinh\left(\frac{2\pi h}{\lambda}\right)} \tag{3.20}$$

The maximum orbital velocity at the sea bed (u_m) can be determined from:

$$u_m = \frac{\pi H}{T\sinh\left(\frac{2\pi h}{\lambda}\right)} \tag{3.21}$$

The wavelength can be found either graphically or iteratively from the equation:

$$\lambda = \frac{gT^2}{2\pi}\tanh\frac{2\pi d}{\lambda} \tag{3.22}$$

In shallow water, the diameter remains uniform with depth and only the

eccentricity changes. The orbital diameter is given by the equation:

$$d = \frac{HT}{2\pi}\left(\frac{g}{h}\right)^{0.5} \tag{3.23}$$

and the orbital velocity, which is constant with depth, is equal to:

$$u_m = H\left(\frac{g}{d}\right)^{0.5} \tag{3.24}$$

An extension of Airy wave theory has produced the Stokes waveform; this has a more peaked crest and a flatter trough than the sinusoidal waveform. Such asymmetry is reflected also in the orbital velocities under the wave. A major limitation to the use of the Airy (linear) wave theory is that the to-and-fro motion is (effectively) the same with no net water movement; hence, no net sediment movement. With the Stokes theory, the horizontal velocity under the crest in the direction of wave advance is larger than that in the opposite direction under the trough. Hence, the orbits are not now closed: the particles are subjected to mass transport (Stokes drift) in the direction of the wave propagation.

In terms of limitations, it is not possible to generate an irregular sea using Stokes theory. The Airy theory, because of its ease of use, has found wide application in sediment transport studies and is regarded as a stirring mechanism on the sea bed. The theory has been found to estimate well the bottom orbital velocity in most regions (Le Méhauté *et al.*, 1968).

3.2.1 The wave boundary layer

A boundary layer forms beneath waves in a way that is analogous to the formation of a boundary layer beneath tidal currents. However, the dynamics of the wave boundary layer are governed closely by the periodicity of the flow and the nature of the sea bed. Wave boundary layers are usually considerably thinner than those found beneath tidal oscillations; this is because there is much less time between reversals of the flow, for low momentum fluid to be diffused away from the boundary and for the layer to attain its full thickness.

The structure of the wave boundary layer can be classified in terms of a wave Reynolds number (Re_w), given by:

$$Re_w = \frac{u_m A_b}{\nu} \tag{3.25}$$

The boundary layer flow can be either laminar or turbulent, depending upon the bed roughness and the Reynolds number. Numerous classifications exist which define the limits between laminar/turbulent flow and the boundary layer thickness. For example, Jonsson (1967) defines the boundary layer as laminar provided that

$$Re_w < 1.26 \times 10^4 \quad and \quad \frac{A_b}{k_s} > 1.8 Re_w^{\frac{1}{2}} \tag{3.26}$$

For a laminar boundary layer and smooth bed, the maximum wave orbital velocity (u_m) can be determined readily (Equation 3.21) and the velocity profile calculated (Figure 3.6). As can be seen in the Figure, both the phase and amplitude of the velocity oscillations vary throughout the boundary layer: the phase lead increases towards the bed. For a flat smooth bed and laminar flow, the bed shear stress can be determined directly from:

$$\tau_0 = \rho\left(\frac{\nu 2\pi}{T}\right)^{0.5} u_m \tag{3.27}$$

The thickness of the boundary layer (δ) is given by:

$$\delta = \left(\frac{\pi \nu T}{4}\right)^{0.5} \tag{3.28}$$

or

$$\delta = \frac{\pi A_b}{(2 Re_w)^{0.5}} \tag{3.29}$$

(Jonsson, 1967). Turbulent flow can be classified as either smooth, if the roughness of the bed is small in comparison to the thickness of the sublayer, or

rough turbulent when the roughness elements extend through to the overlying flow.

A lower limit for rough turbulent flow ($Re_w > 7 \times 10^7$) (Dyer, 1986) is given by:

$$Re_w = 2000\frac{A_b}{k_s} \tag{3.30}$$

where k_s is the equivalent bed roughness. For Re_w values below this limit:

$$Re_w = 4130\left(\frac{A_b}{k_s}\right)^{0.45} \tag{3.31}$$

(Sleath, 1974). For smooth turbulent flow, the boundary layer properties depend only upon Re_w; they are independent of the relative roughness of the bed. For rough turbulent flow, the properties depend upon the relative roughness (A_b/k_s) only. For a flat bed, $k_s=2.5\ D_{50}$ or $2\ D_{90}$ has been proposed (Heathershaw, 1988); for a rippled bed, $k_s= 4\ \eta$, or $25\ \eta^2/\lambda$, where η is the ripple height and λ is the ripple wavelength.

Unlike the laminar wave boundary where the bed shear stress can be derived directly from the wave velocity profile, the structure of the velocity profile in the turbulent wave boundary layer is somewhat uncertain. The maximum bed shear stress is derived using a wave friction factor f_w (Jonsson, 1967), where

$$\tau_0 = 0.5 f_w \rho u_m^2 \tag{3.32}$$

For a laminar boundary layer, $f_w = 2(Re_w)^{-0.5}$. For laminar and smooth turbulent flow, f_w is dependent on Re_w only; for fully rough turbulent flow, it is dependent also on the relative roughness (A_b/k_s). In nearshore and coastal waters, where the boundary layer is always rough turbulent (Jonsson and Carlsen, 1976), it is important, therefore, to be able to determine accurately the relative roughness of the bed.

3.2.2 Threshold of sediment motion under waves

Maximum near-bed orbital velocities can be determined from measurements of wave height and period (see above); these can be compared then with the threshold velocity for sediment of a particular grain size. As the orbital velocity of water over a bed is increased, there comes a point at which the shear stress exerted on the bed is sufficient to initiate the movement of sediment grains. Similar to unidirectional currents, it is still only possible to predict the threshold of sediment movement under waves using semi-empirical methods. Many equations have been proposed and Silvestor and Mogridge (1971) have examined thirteen different expressions, identifying that predictions for a flat bed vary considerably.

Komar and Miller (1975) have utilised 5 sets of previously published data to analyze the threshold of sediment movement under waves. The data included results from three types of experiment: (a) from an oscillating bed of sediment in still water (Bagnold, 1946; Manohar, 1955); (b) from an oscillating-flow water tunnel (Rance and Warren, 1969); and (c) from ordinary wave tanks (Horikawa and Watanabe, 1967; Eagleson *et al.*, 1959). For non-cohesive sediment with a grain diameter of less than 0.05 cm, an equation can be derived on the basis of an empirical relationship developed by Bagnold (*op. cit.*). With grain sizes less than approximately 0.05 cm, the boundary layer remains laminar: for grain diameters greater than 0.05 cm, the equation is based upon the studies of Rance and Warren (*op. cit.*). The latter investigation represents the ratio of the acceleration forces to the effective gravity force on the grain. For grain sizes larger than 0.05 cm, the flow will become turbulent before sediment motion commences. Using these equations, however, there is some disagreement between investigators on the threshold of movement for grain sizes of around 0.05 cm at low wave periods (Figure 3.7). This discrepancy occurs at the transition between laminar and turbulent flow. In their review of the threshold of sediment movement under waves, Komar and Miller (1973, 1975) presented (Figure 3.7) give two equations which are possibly those used most widely:

$$u_{m(crit)} = \left(0.21g\frac{(\rho_s - \rho)}{\rho} \right)^{\frac{2}{3}} \left(\frac{DT}{\pi} \right)^{\frac{1}{3}} \qquad D<0.05\,cm \qquad (3.33)$$

$$u_{m(crit)} = \left(0.46g\frac{(\rho_s - \rho)}{\rho} \right)^{\frac{4}{7}} (\pi D)^{\frac{3}{7}} T^{\frac{1}{7}} \qquad D>0.05\,cm \qquad (3.34)$$

For a particular grain size and water depth, the wave height and period required to initiate sediment movement can be determined. As discussed by Silvestor and Mogridge (1971), results obtained from these equations may be conservative. This may be caused by the fact that the bottom orbital velocity may be greater than that predicted by the Airy wave theory; this is due to the interaction of wavetrains of varying periods and angles, generating higher instantaneous velocities. Similarly, grain shape and the presence of small protrusions on the bed could cause sediment motion at lower velocities than those implied by the Komar and Miller (1975) analyses.

The movement of sediment grains beneath waves will be influenced by the instantaneous bed shear stress generated by a wave, in the same way that it is affected by the steady bed shear stress from a tidal current. Consequently, similar stresses can be achieved by different near-bed oscillatory and unidirectional currents.

3.3 SEDIMENT MOVEMENT UNDER COMBINED FLOW

The shallow coastal zone along the inner continental shelf is an extremely dynamic region, where fluid motions associated with both surface waves and currents can extend down to the sea floor and interact with the sediments. Many continental shelf processes are influenced by the turbulent mixing and fluid shearing that occurs when wave and current flows interact. Temporal and spatial variation in the bed shear stress is an important factor in developing accurate models of shelf currents, surface wave propagation, sediment erosion and transport patterns, and bedform generation. Such variability influences also a number of biological and

chemical processes, which depend upon boundary layer mixing and substrate stability.

In shallow seas it is likely that the most significant occurrences of sediment transport will occur when the bed stresses induced by tidal movement are enhanced by wave motion. Therefore, it is necessary to consider how to combine the two processes. Wave motion alone does not produce net sediment transport, except for second order mass transport (Stokes drift). However, waves can be an effective stirring mechanism, creating sediment in suspension at lower velocities than a steady current. Once in suspension, such sediment can be moved *en masse* by relatively small steady currents which, in themselves, may not exceed the threshold for sediment movement. In one respect, therefore, the wave orbital motion near the bed can be thought of as an additional turbulence, with the vortices acting in a similar manner to turbulent bursts in entraining the sediment. One of the major difficulties in the analysis is that wave propagation may be at a large angle to that of the tidal current. As a consequence, the resulting sediment transport direction need not be the same as the current direction.

Although there have been numerous investigations into the structure of the combined wave and current boundary layer, there is a lack of field verification of the various models proposed. The approaches available tend also to vary in their ability to reproduce accurately the results obtained from experimental laboratory data. Indeed, Dyer and Soulsby (1988) found significant quantitative variation between the model predictions. Further complications arise from the lack of consistency in defining the boundary layer thickness, which influences the derived bed shear stress. Therefore, it is only possible presently to use a model which best describes the experimental data.

As a consequence, considerable effort has been directed towards the development of quantitative models that can predict bed shear stress, velocity structure, and bed roughness under conditions which involve typically combined wave and current flows over a moveable bed.

3.3.1 The combined boundary layer

One of the most commonly-used approaches to determine combined wave-current shear stresses in engineering studies, because of its ease of application, is that suggested by Bijker (1967). In this approach, the enhancement of the shear stress due to the presence of a steady current, by wave action, is determined. The presence of a viscous boundary layer under steady flow is assumed, whilst the gradient of the combined velocity vector is calculated at this level. A measure of the relative thickness of the wave boundary layer to that of the laminar sublayer is described in terms of a coefficient (p=0.45). The resultant instantaneous velocity is obtained from the steady current velocity and the wave orbital velocity, using the cosine rule. The mean value for the passage of a wave is obtained by integration over the wave period. The intensity of the resultant shear stress for a turbulent flow is given by:

$$\tau = \rho l^2 \left[\frac{du}{dz} \right]^2 \tag{3.35}$$

where the mixing length $l=\kappa z$. The component of the resulting mean bed shear stress in the direction of the current, τ_1, is given by:

$$\tau_1 = \tau_{cu} \left(1 + N \left(\zeta \frac{u_m}{<U>} \right)^{1.5} \right) \tag{3.36}$$

where $<U>$ is the depth-mean average tidal current. The component of bed shear stress perpendicular to the current can be found from:

$$\tau_2 = \tau_{cu} \left(M \left(\zeta \frac{u_m}{<U>} \right)^{1.25} \right) \tag{3.37}$$

where

$$N = 0.36 - 0.14 \cos 2\varphi \tag{3.38}$$

and

$$M = 0.205 \sin 2\varphi \tag{3.39}$$

and

$$\zeta = p \ln\left(\frac{h}{z_0} - 1\right) \tag{3.40}$$

where φ is the angle between the tidal current direction and the wave crests. The resultant total bed shear stress is given then by (Bijker, 1967):

$$\frac{\tau_{wc}}{\tau_{cu}} = \left(1 + \frac{1}{2}\left(\zeta \frac{u_m}{<U>}\right)^2\right) \tag{3.41}$$

The right hand side of Equation 3.41 can be considered as an enhancement factor, which increases rapidly with a decreasing current. Hence, the resultant total bed shear stress under the combined action of waves and currents can be calculated readily from wave measurements combined with: (i) a tidal current velocity profile; or (ii) a single tidal current velocity measurement at some height above the bed, together with an assumed roughness length (Section 3.1).

The simultaneous presence of a low-frequency current and surface wave velocity components, in natural flows over a hydrodynamically rough sea bed, results in a non-linear interaction that modifies both the flows and the associated shear stress (Grant and Madsen, 1986). Two distinct vertical boundary layer scales exist for this combined flow situation. In the immediate vicinity of the bottom, a wave boundary layer develops that is embedded in the large-scale boundary layer. In the wave boundary layer, both waves and currents contribute to the turbulence. Above this region, the turbulence is associated with the low frequency current only. The presence of the combined boundary layer increases the effective bed roughness experienced by the current (Bakker and van Doorn, 1978; Grant and Madsen, 1979).

A linear superimposition of wave and current velocities, as suggested by Bijker (1967), will not predict accurately the structure of the combined flow (Kemp and

Simons, 1983b). The superimposition of even the smallest wave can cause a dramatic increase in turbulence, over the value for the current flow alone. Likewise, the presence of wave-induced vortices in the layer above a rough bed causes a reduction in the mean velocity, together with a large increase in apparent bed roughness and shear stress determined from the mean velocity profiles.

Hence, bottom boundary layer models have been developed (Smith, 1977; Grant and Madsen, 1979; Christoffersen and Jonsson, 1985; Sleath, 1991); these include non-linear wave and current interaction, which produces an increased shear in the current above the wave boundary layer. The steady current above the wave boundary layer will feel an increased roughness, caused by the turbulent combined flow interaction at the bed; this is in addition to the usual friction associated with the bed sediment and larger roughness elements (i.e. bedforms) (cf. Grant and Madsen, 1979; Christoffersen and Jonsson, 1985).

Grant and Madsen (*op. cit.*) present an analytical theory to describe the combined motion of waves and currents in the vicinity of a rough bottom and the associated boundary shear stress. Characteristic shear velocities for the respective wave and current boundary layers are defined on the basis of a combined wave-current friction factor. Turbulent closure is accomplished by use of a time-invariant eddy viscosity, which varies linearly with height above the sea bed. For the current velocity profile above the wave boundary layer, the concept of an apparent bottom roughness is introduced; this depends on the bottom roughness, as well as the wave characteristics. This apparent roughness results in the current above the wave boundary layer feeling a larger resistance, due to the presence of the wave.

The equations governing the near-bottom current yield the current profiles:

$$u_c = \frac{u_{*c}}{\kappa}\left(\frac{u_{*c}}{u_{*cw}}\right)\ln\frac{z}{z_0} \qquad z \le \delta_{cw}$$
$$u_c = \frac{u_{*c}}{\kappa}\ln\frac{z}{z_{0c}} \qquad z \ge \delta_{cw} \tag{3.42}$$

in which z_{0c} is the apparent roughness experienced by the current in the presence of waves (i.e. the roughness determined from the log-profile of current observations, obtained outside the wave boundary layer). Thus, z_{0c} and not z_0 is the appropriate roughness for the current boundary layer in the presence of waves.

The solution for the 'mean' velocity profile inside the wave boundary layer depends upon the physical bottom roughness; it has a shear velocity modified by the term (u_{*c}/u_{*cw}) expressing the effect of the nonlinear wave-current interaction. Such a modification to the current velocity profile has been observed in several field and laboratory studies (e.g. Cacchione and Drake, 1982; van Doorn, 1981, 1982; Kemp and Simons, 1982, 1983a; Coffey and Nielsen, 1984). The model proposed by Grant and Madsen is also applicable only to a wave-dominated (i.e. wave orbital velocities are greater than steady current velocities) environment.

Most wave-dominated models employ an eddy viscosity (ϵ) to relate the shear stress to the velocity gradient in the combined flow, where

$$\frac{\tau}{\rho} = \epsilon\frac{du}{dz} \tag{3.43}$$

It has been assumed frequently (e.g. Grant and Madsen, 1979) that a single eddy viscosity would apply to both the steady current flow and the oscillatory wave motion inside the wave boundary layer. However, measurements obtained by van Doorn (1981, 1982) and Coffey and Nielsen (*op. cit.*) have shown that different eddy viscosities must be applied to the different flow components. Observations made by Sleath (1990) have provided moderate agreement with the laboratory models of Grant and Madsen (1979) and Christoffersen and Jonsson (1985).

The modelled boundary layer stresses can be used to determine sediment transport

rates. However, whilst estimates of sediment transport rates that ignore such interaction will almost certainly be too low (Wiberg and Smith, 1983), it has been found that predictive equations for combined flows often produce widely-differing results derived on the basis of the same input conditions (see, for example, Heathershaw, 1981; Pattiaratchi and Collins, 1985). Many attempts have been made to derive formulae which can describe adequately sediment movement under the combined action of waves and currents. It has been found, however, that none work satisfactorily over the whole range of conditions from:

currents only → waves and currents → waves only

One of the main reasons for this limitation is that most of the sediment transport formulae are based upon adaptations of existing formulae, for derived transport in response to currents alone. The transport equations are adapted usually by replacing the current-induced bed shear stress with that caused by combined wave and current action; it is assumed that the basic transport mechanism remains unchanged.

Uncertainty exists also in the definition of the threshold of sediment movement under the combined influence of waves and currents. However, under combined flow, the critical shear stress required to initiate sediment transport has been found to increase with increasing wave period, grain size and density (Rigler and Collins, 1983). The Shields' curve has been found to be suitable as a general criterion for the definition of threshold, for a wide range of grain densities under oscillatory flow. Based upon flume experiments of combined co-directional flows over a rippled sand bed, threshold conditions have been found to be the same as that under purely unidirectional and oscillatory flows (Kapdasli, 1990). The same studies showed that the threshold of motion did not depend upon wave period.

3.4 INFLUENCE OF BEDFORMS

Estimates of bed shear stress obtained from boundary layer models can then be

used in predictive sediment transport formulae. The velocity profile near the sea bed, even when the flow is not strictly steady or uniform, can be represented by the von Karman-Prandtl equation (Equation 3.4) (Dyer, 1980), enabling the bed shear stress to be calculated.

However, a planar sea bed is not normally present in areas where the sand is mobile. In many areas, the tidal currents are capable of creating ripples which survive over the slack water periods. A considerable difficulty arises, therefore, when there are bedforms present and the bed shear stress is the sum of the skin friction and the form drag.

Form drag is the integral of the horizontal component of the normal pressure distribution over the length of the bedform; thus, it is the skin friction alone that causes the movement of sediment. The bed features create an internal boundary layer within the flow, causing acceleration in the flow over the crest of the bedform and deceleration near the trough. This effect diminishes with height above the bed until, at about 2 or 3 times the bedform height above the crest, the flow is uniform; flow near the bed, although steady, is non-uniform in character (Dyer, *op. cit.*). Nevertheless, logarithmic velocity profiles can be present and used as a measure of the skin friction, which will vary over the bedform (Dyer, 1970). Above the internal boundary layer, a logarithmic profile can again be measured; however, the drag will then be the total drag on the surface of the bed. Consequently, conventional profile measurements over a rippled bed will measure the total bed shear stress. Large errors will result if these bed shear stresses are used to estimate the transport rate of sediment, because of the high power dependence on the shear stress involved.

Studies undertaken by Bagnold (1963) have indicated that the total drag can be between 2 and 5 times that of the skin friction. Elsewhere, Engelund and Hansen (1972) have shown the form drag to be up to 66% of the total applied stress, whilst Smith (1969) and Taylor *et al.* (1976) have used numerical models to investigate the effect of ripples on the current velocity profiles. These latter results

show that, for sinusoidal waveforms, 25 to 33% of the total drag is typically the form drag contribution. However, these models require accurate specification of the bed shape and the surface roughness on the bed form, since the proportion of form drag is sensitive to bedform asymmetry and flow separation. In a wind tunnel experiment, Khanna (1970) has shown that form drag can exceed a value twice that of the skin friction, for an asymmetrical bedform with flow separation. For the Columbia River, Smith (1977) obtained a total shear stress to skin friction ratio of 5.7 to 1 for non-separating flow and 4 to 1 for separating flow over sand waves.

The presence of two logarithmic profile regions, each yielding a different shear stress estimate, has been confirmed by current speed profile measurements made by Chris and Caldwell (1982). The stress calculated from the upper profile reflected the influence of the form drag; it was more than 4 times the bed shear stress determined from the shear in the viscous sublayer. In general, when form drag is significant, the application of the logarithmic profile or Reynolds stress techniques to measurements obtained more than a few tens of centimetres from the bed may yield bed stress estimates inappropriate for use in near-bed sediment transport calculations.

Flume experiments over a rippled sand bed (Kapdasli and Dyer, 1986) have found the form drag component to be between 5 and 12 times that of the skin friction. Similarly, numerical modelling of non-separating flow over bedforms (Richards, 1982) has provided results which are in general agreement with the measurements of Smith (*op. cit.*) and Fredsoe (1982). Average skin friction values equivalent to 34% of the total shear stress were obtained in the model, with the results being dependent upon ripple shape, steepness and grain size.

The various sets of results outlined above exemplify the overall lack of any consistent relationship between form drag and skin friction that can be used in any analysis; this is emphasised by the fact that form drag will be larger for separating, rather than non-separating, flows. Further problems are encountered on

a temporal scale. For example, detailed flow measurements over a rippled bed in a tidally-dominated regime (Dyer, 1980) have shown that the roughness length can vary by 2 orders of magnitude throughout the tidal cycle.

3.5 SEDIMENT TRANSPORT FORMULAE

The subaqueous movement of sand has long been of interest to hydraulic engineers and coastal oceanographers. Research objectives have been to define the relationships between hydrodynamic parameters (see above) and the mass/volume of solid material being moved. Such relationships are referred to as sediment mass transport formulae.

Essentially, the rate of sediment transport represents the total weight of grains passing through a section, in unit time; it is the product of the weight of moving grains present in the water, over a unit area, multiplied by their speed of movement. Formulae have been derived to transform bed shear stresses or flow, at a certain height above the bed (e.g. 1 m), to transport rates. Although the selection of a particular formula for a specific study remains difficult, extensive lists and reviews are available on the subject (e.g. Yalin, 1972; Ackers and White, 1973; Vanoni, 1977; Pattiaratchi, 1981; Sleath, 1984; Pattiaratchi and Collins, 1985; and Hardisty, 1990).

The numerous sediment transport formulae available fall into a number of basic groupings, as outlined below.

(a) *Empirical.* Extensive flume, combined with occasional field, measurements are used to obtain an empirical relationship between transport rate and a characteristic flow variable.

(b) *Deterministic.* The basic physics of the movement of individual grains are developed to provide bulk movement formulae. However, averaging such movements in space and time inevitably involves constants; these have to be

determined experimentally, often showing some variability.

(c) *Dimensional analysis*. Sediment and flow variables are grouped together, to form dimensionless expressions. The various constants and coefficients are determined then from experimental data.

(d) *Probabilistic analysis*. A probability function is used to describe the relationship between flow and particle movement, to determine the sediment transport rate.

Many of the available formulae have been developed for steady unidirectional flow over non-cohesive beds of unimodal sediments; they do not incorporate the presence of waves and, correspondingly, there has been only limited verification in the marine environment.

Ten of the most widely-used and accepted transport formulae have been applied to the present investigation. Each of these approaches is reviewed now (for a description of symbols, see List of Symbols).

3.5.1 Meyer-Peter and Müller (1948)

Extensive experimental results obtained from a laboratory flume, under steady current conditions, has led to the following expression for the estimation of the (immersed weight) sediment transport rate:

$$I_b = 8\rho_s(1-\frac{\rho}{\rho_s})^2 g((s-1)gD^3)^{1/2}\ (\theta-\theta_c)^{3/2} \qquad (3.44)$$

3.5.2 Einstein (1950)

This approach considers that grains move by saltation, as a result of the fluctuating

lift force; they then perform a jump which, on average, has a length of about 100D. Conceptual and practical difficulties were recognised in defining incipient (sediment) motion. Consequently, this formulation does not include an explicit threshold term.

Unlike many expressions, the Einstein formula accounts for spatial and temporal variations in instantaneous bed shear stresses through the inclusion of a term expressing the probability (P) of particle motion. The resulting bedload transport formula is:

$$I_b = \frac{P}{1-P}\frac{\rho_s}{A_*}(\Delta g D^3)^{\frac{1}{2}} \tag{3.45}$$

where the probability of particle motion occurring (P) is defined by the error function integral:

$$P = 1 - \frac{1}{\pi^{1/2}} \int_{-B_*\Psi^{-1/\eta}}^{B_*\Psi^{-1/\eta}} e^{-t^2}\, dt \tag{3.46}$$

A_* and B_* are constants (43.5 and 0.143, respectively) and η=0.5. Ψ is the 'flow intensity', expressed in terms of the shear velocity:

$$\psi = \frac{g\Delta D}{u_*} \tag{3.47}$$

where

$$\Delta = \frac{(\rho_s - \rho)}{\rho} \tag{3.48}$$

3.5.3 Kalinske-Frijlink (1951)

Elzerman and Frijlink's (1951) approximation of Kalinske's (1947) riverine

bedload equation, as modified by van den Berg (1987) for tidal environments, has been used here as follows:

$$I_b = 5\rho_s D_{50}(D_{50}g(s-1)\theta')^{\frac{1}{2}} e^{-0.27/\theta'} \tag{3.49}$$

This modification negates the need for the 'bedform factor', as specified originally. The grain mobility number (θ') relates now the shear stress to the grain roughness.

3.5.4 Yalin (1963)

This particular theory of bedload transport is a combination of dimensional analysis and an extension of Einstein's analysis of saltation. Grains are assumed to move, by saltation, once the threshold condition is exceeded. The relationship between the transport rate and the boundary layer flow regime is given by:

$$I_b = 0.635\rho_s D u_* S\left(1 - \frac{1}{aS}\ln(1+aS)\right) \tag{3.50}$$

where

$$\begin{aligned} a &= 2.45\left(\frac{\rho}{\rho_s}\right)^{0.4}\theta_c^{0.5} \\ \theta_c &= \frac{\tau_c}{(\rho_s-\rho)gD} \\ S &= \frac{(\tau-\tau_c)}{\tau_c} \end{aligned} \tag{3.51}$$

3.5.5 Engelund and Hansen (1967)

This expression relates the total sediment (suspended and bedload) transport rate in terms of a friction factor (C_f), a dimensionless sediment discharge rate (ϕ), and a dimensionless bed shear stress (θ):

$$C_f\phi = 0.1\ \theta^{2.5}$$
$$C_f = \frac{2u_*^2}{\langle U \rangle}$$
$$\phi = \frac{q_t}{\rho_s\left(gD^3\left(\frac{\rho_s}{\rho}-1\right)\right)^{0.5}} \tag{3.52}$$

and

$$\theta = \frac{\tau}{(\rho_s-\rho)gD} \tag{3.53}$$

The transport rate can be found from:

$$I_b = 0.05\rho_s\langle U\rangle^2\left(\frac{D}{g\left(\frac{\rho_s}{\rho}-1\right)}\right)^{\frac{1}{2}}\left(\frac{\tau}{(\rho_s-\rho)D}\right)^{\frac{3}{2}} \tag{3.54}$$

Although it has been developed for dune covered beds with specific boundary layer conditions, Graff (1971) and Collins *et al.* (1981) have recommended its more general use in the marine environment.

3.5.6 Paintal (1971)

This stochastic model assumes that no distinct condition exists for the beginning of sediment movement. Instead, two transport regimes are recognised: (i) relative high transport rates, above the Shields criterion; and (ii) low transport rates, below the Shields criterion.

The bedload expression is derived using a stochastic analysis, which considers that particle exposures are distributed uniformly, turbulence is normally distributed and the step lengths of particles follow a negative exponential distribution. This particular model was calibrated using gravel, with median grain sizes ranging from 2.5 to 22.2 mm. The derived equation relates a dimensionless transport rate (q_{s*})

to a dimensionless shear stress (θ), through the function:

$$q_{s*}=Af(P_o(B\theta))\sqrt{\theta} \tag{3.55}$$

where A and B are parameters derived experimentally (equal to 9.9 and 13.0, respectively). The function f represents the relationship between the probability (P_o) of particle movement and the dimensionless shear stress θ. The final equation for the estimation of the immersed weight sediment transport rate has been re-arranged and is given as:

$$I_b = Ag\rho_s D\sqrt{gD(s-1)}\frac{P_o^3}{1-P_o}\sqrt{\theta} \tag{3.56}$$

where the probability of movement (P_o) was given, graphically, by Paintal (1971) as a function of the Shields parameter. For computational purposes here, the graph has been digitised and a polynomial fit has been applied to the data, producing the following algorithm for the estimation of P_o as function of θ:

$$P_o = 10^y \tag{3.57}$$

where

$$y = -0.2094x^6 - 0.5241x^5 + 0.3690x^4 + 1.0864x^3 - 1.4860x^2 + 1.2970x - 0.8427 \tag{3.58}$$

and

$$x = B\theta \tag{3.59}$$

3.5.7 Ackers and White (1973)

This expression represents a total load equation which is described in terms of three dimensionless numbers as outlined below.

The *Mobility Number* (F_{gr}) is the ratio of shear forces on a unit area of the bed to

immersed weight of the grains and this is given by:

$$F_{gr} = \frac{u_*^{\,n}}{\left(gD\frac{(\rho_s-\rho)}{\rho}\right)^{\frac{1}{2}}}\left(\frac{<U>}{2.46\ln\left(\frac{10h}{D}\right)}\right)^{1-n} \tag{3.60}$$

Sediment Transport (G_{gr}) was presumed to be a function of F_{gr} and D_{gr}. Using the results determined from approximately a thousand flume experiments, the following relationship was presented:

$$G_{gr} = \frac{qg\rho h}{sD}\left(\frac{u_*}{<U>}\right)^n \tag{3.61}$$

The sediment transport rate (G_{gr}) (dry mass, per mass flow rate) is given then using the above equation, in conjunction with the generalised sediment transport formula:

$$G_{gr} = C\left(\frac{F_{gr}}{A}-1\right)^m \tag{3.62}$$

The constants C and A, together with exponents m and n, in Equations 3.60, 3.61 and 3.62 are presented in terms of a function of a dimensionless particle size parameter, D_{gr} (see below):

$$\log(C) = 2.86\log(D_{gr}) - (\log(D_{gr}))^2 - 3.53 \tag{3.63}$$

$$A = \frac{0.23}{\sqrt{D_{gr}}} + 1.34 \tag{3.64}$$

$$n = 1.0 - 0.56\log(D_{gr}) \tag{3.65}$$

$$m = \frac{9.66}{D_{gr}} + 1.34 \tag{3.66}$$

Dimensionless Grain Diameter (D_{gr})

$$D_{gr} = D\left(g\frac{(\rho_s-\rho)}{\rho}\nu^{-2} \right)^{\frac{1}{2}} \tag{3.67}$$

The value of A is very important in the expression, since it is a parameter equivalent to threshold criterion incorporated in other formulae; it represents, in this case, the F_{gr} value at which sediment starts to move. The mass transport obtained from Equation 3.62 is converted to immersed weight, using:

$$I_b = (1-\frac{\rho}{\rho_s})gG_{gr}<U>\rho h \tag{3.68}$$

3.5.8 Hardisty (1983, 1990)

Bagnold (1963, 1966) derived an equation in which the bedload transport was expressed in terms of stream power, combined with an efficiency factor. It was suggested that, as a minimum critical bed stress is required to move sediment grains, stream power can be formulated in terms of the available stress. Hardisty (1983) modified this formula, in order to include a threshold term. Hence, the $(u^2-u_{cr}^2)$ term in the 'excess stress' formulation of Hardisty (1983) (see below) represents the stress available to move the sediment. The velocity multiplier (u_{100}) represents the distance per unit time, through which the applied force moves:

$$I_b = k_b(u_{100}^2 - u_{100cr}^2)u_{100} \tag{3.69}$$

where

$$k_b = \frac{1}{6.6 \times D_{mm}^{1.23}} \times 10^{-5} \tag{3.70}$$

where D is the mean sediment diameter, in mm. The flume data of Guy *et al.* (1966) was used to calibrate the equation. Subsequently, Hardisty (1990) has used

the datasets of Guy *et al.* (1966) and Williams (1967) to re-evaluate calibration coefficient, k_b. The line of best fit through the data confirmed the correlation between k_b and D, but with different coefficients:

$$k_b = \frac{1.7109}{D_{mm}^{0.7703}} \times 10^{-6} \tag{3.71}$$

3.5.9 van Rijn (1986)

This formula has been derived on the basis of kinematic considerations on sand particles, where it can be shown that

$$I_b = (1-\frac{\rho}{\rho_s}) g E \lambda \tag{3.72}$$

where λ represents the jump or saltation length of a particle, expressed as:

$$\lambda = k\, D_*^{0.6} S^{0.9} D \tag{3.73}$$

and E is an empirical sediment pick-up function, per unit area and time:

$$E = 0.00033\, \rho_s \sqrt{\Delta g D}\; D_*^{0.3} T^{1.5} \tag{3.74}$$

where

$$D_* = D\left(\frac{(\rho_s-\rho)g}{\rho \nu^2}\right)^{\frac{1}{3}} \tag{3.75}$$

and

$$\Delta = \frac{(\rho_s-\rho)}{\rho} \tag{3.76}$$

and

$$T = \frac{(\tau - \tau_{cr})}{\tau_{cr}} \tag{3.77}$$

The constant k in Equation 3.73 was given by van Rijn to be equal to 3, for sand grains.

3.5.10 Soulsby (1993)

A new formula has been presented recently by Soulsby for sand-sized materials. The structure of the expression is similar to that presented by Hardisty (1983, 1990) but with two main differences: (i) the steady velocity term has been replaced by the shear velocity ($u_* = (\tau_b/\rho)^{1/2}$); and (ii) the proportionality coefficient is constant. The expression is as follows:

$$I_b = 12\sqrt{\frac{\tau_b}{\rho}}(\tau_b - \tau_{cr}) \tag{3.78}$$

	Boundary layer classification	
	(a) Laboratory flows	(b) Marine flows
Smooth turbulent	$Re_* < 3.5$	$Re_* < 5.5$
Transitional	$3.5 < Re_* < 68$	$5.5 < Re_* < 165$
Rough turbulent	$Re_* > 68$	$Re_* > 165$

Note: (a) from Heathershaw (1988); (b) from Sternberg (1968).

Table 3.1 Definition of boundary layer flow characteristics using the grain Reynolds number (Re_*, which is equivalent to u_*D/ν).

Sediment type	z_0 (cm)	C_{100}
Mud	0.02	0.0022
Mud/sand	0.07	0.0030
Silt/sand	0.005	0.0016
Sand (unrippled)	0.04	0.0026
Sand (rippled)	0.6	0.0061
Sand/shell	0.03	0.0024
Sand/gravel	0.03	0.0024
Mud/sand/gravel	0.03	0.0024
Gravel	0.3	0.0047

Table 3.2 Typical values of roughness length z_0 and drag coefficient C_{100}, for different sediment types (after Heathershaw, 1988).

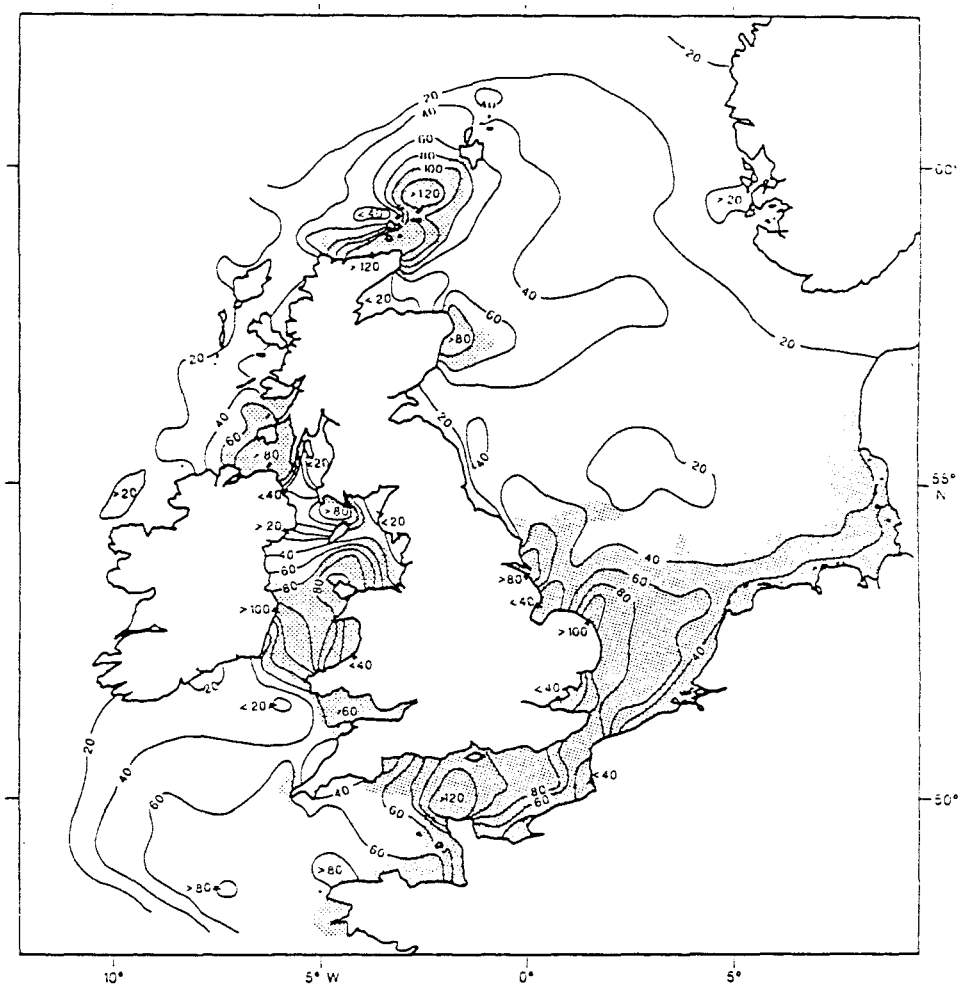

Figure 3.1 Steady current boundary layer thickness (m) for the UK continental shelf. Within the shaded regions, the boundary layer thickness should be assumed to be equal to the water depth (after Soulsby, 1983).

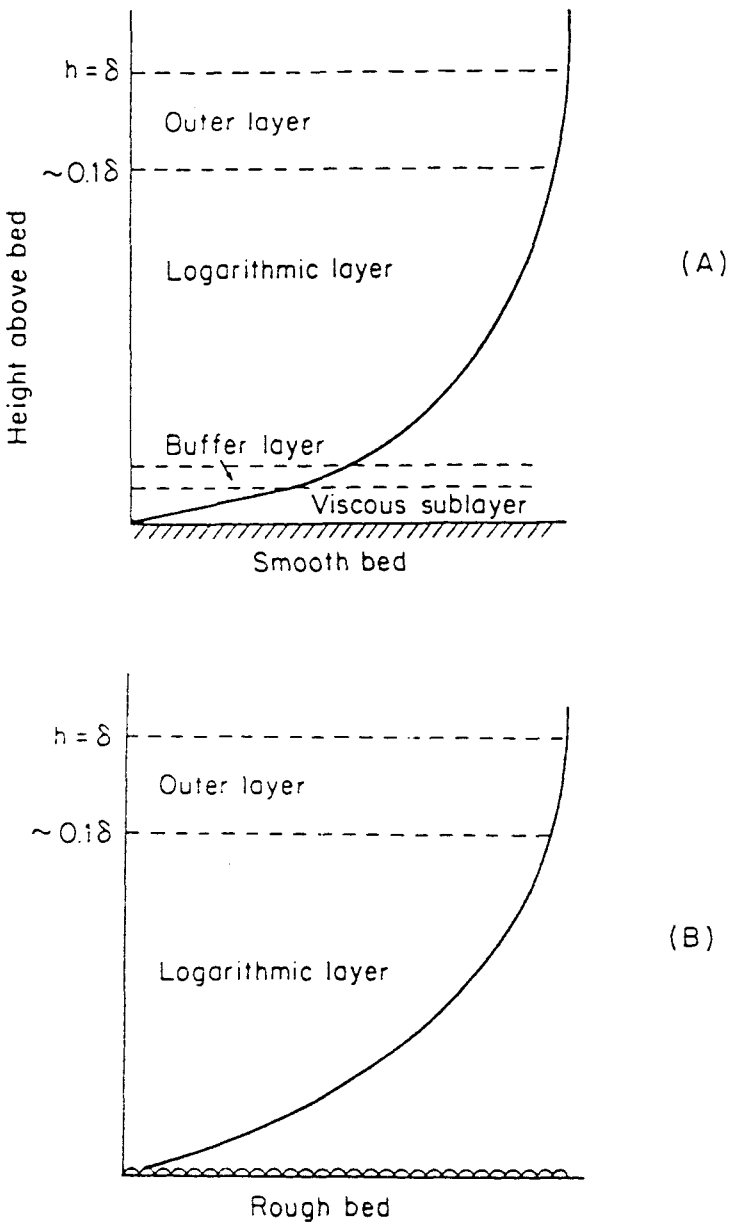

Figure 3.2 Diagrammatic representation of the velocity profiles for (A) smooth turbulent, and (B) rough turbulent flow (after Dyer 1986). The layers are not drawn to scale. Note: δ is the thickness of the boundary layer.

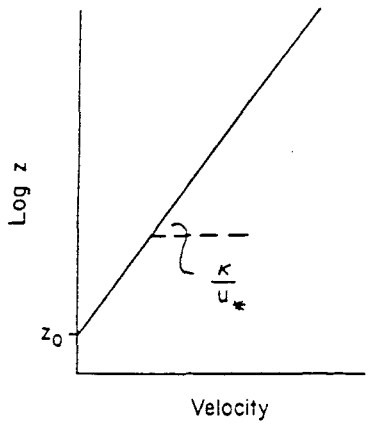

Figure 3.3 Von Karman-Prandtl velocity profile (after Dyer, 1986).

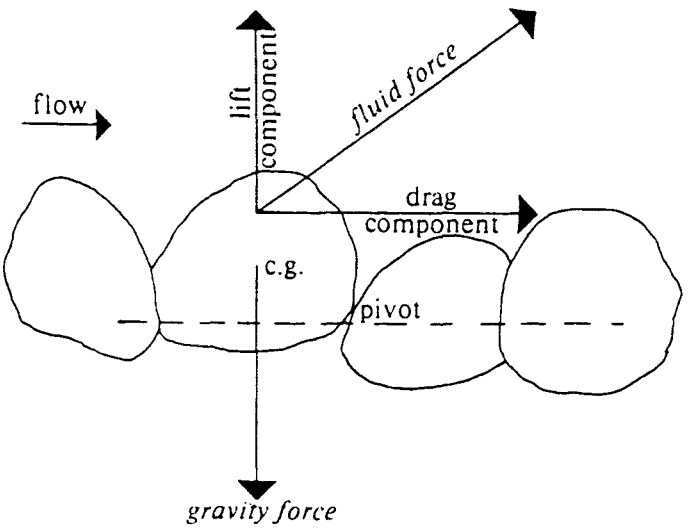

Figure 3.4 Schematic diagram to show the forces acting on a grain, resting on a bed of similar grains, subjected to the fluid flow above it.

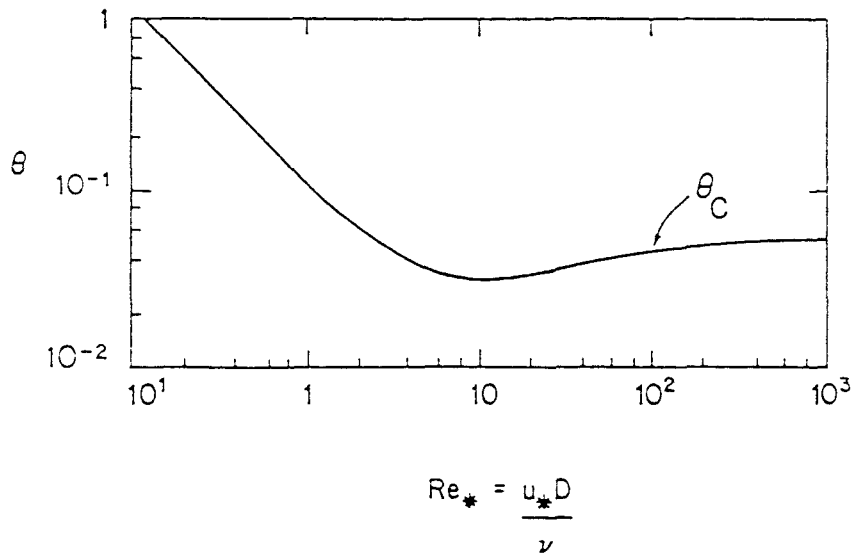

Figure 3.5 Shields threshold curve plotted as a function of Shields parameter (θ) and boundary layer Reynolds number (Re_*).

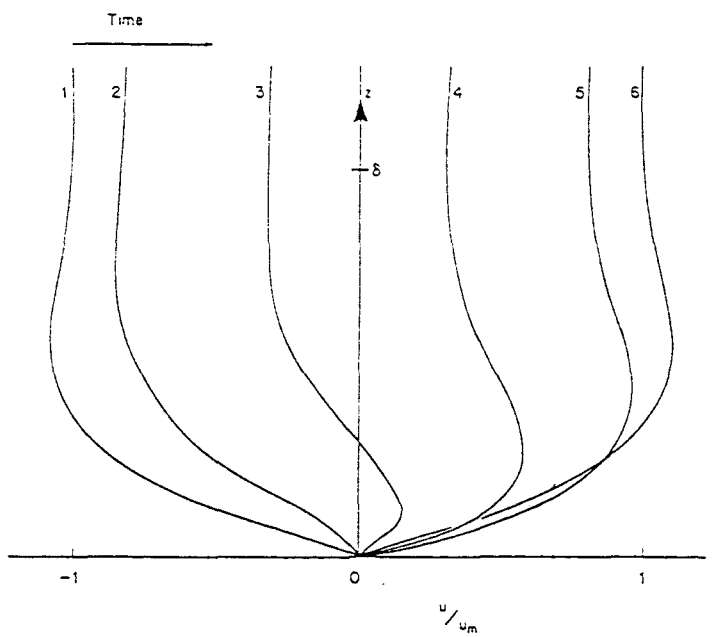

Figure 3.6 Velocity profiles in a laminar wave boundary layer at equal time intervals during half a wave cycle (After Lamb, 1932). Key: δ is the boundary layer thickness.

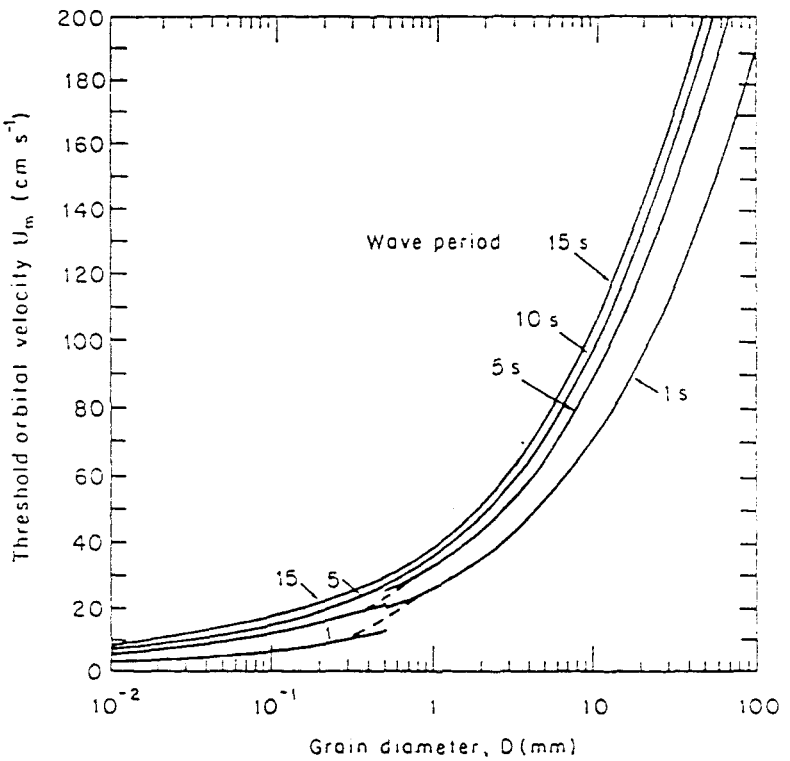

Figure 3.7 Wave period (T) and near-bed orbital velocity (u_m) required to initiate movement of sediment with grain diameter D.

Chapter 4
REGIONAL HYDRODYNAMICS

4.1 INTRODUCTION

Individual grains of sand are set in motion by forces exerted on the sea bed by the overlying water column. Before any insight into the accumulation of sands such as the Broken Bank can be gained, patterns of tidal current flow in the vicinity of such sand banks should be understood.

In order to define such flow patterns, some form of directional convention is required. Hence, the vector time-series of current speed and direction have been resolved into east-west (u) and north-south (v) components: flow is positive in both easterly and northerly directions. In the analyses, corrections have been made to the magnetic directions recorded by the current meters, to those relative to true north, using the magnetic variation at the time of deployment.

Within the text, current meter stations within the study area are identified by a 3- or 4- character code, signifying their location and the height above the bed. Hence, data relating to Station B-12 would have been recovered from Station B, at 12 m above the sea bed.

4.2 DATA COLLECTION

Hydrodynamic data were retrieved as part of the North Sea Community Research Programme, during an RRS Challenger cruise (CH40-88) in November 1988.

Self-recording (rotor and ultrasonic) current meters were deployed at 8 locations (Stations A to H) in the vicinity of the Broken Bank (Figure 4.1) over a period of some 10 days. Near-bottom (at 2 m above the bed) current measurements, at 2 minute intervals, have been obtained from Stations B,C and E. The corresponding

sampling interval was 10 minutes at Stations G and H.

Mid-depth current meters were placed at 10 m above the bed at Stations B, C and E. At Stations G and H, meters were placed at 12 m above the bed. Exceptionally, at Station B, a further current meter was placed at 12 m above the bed.

Current meters from Stations A, D and F were not recovered following the cruise or have, so far, not produced data which can be utilised. Details regarding the position, deployment, height of meter above the bed, meter type and duration of data obtained are presented in Table 4.1. Fortunately, data were recovered from all 3 meters at Station B, providing tidal current information from 3 levels above the sea bed. Data from self-recording instrument 7765 (at Station E-10) was partially corrupted: only measurements collected during the first 6 days of the deployment have been used in the analyses.

Anderaa RCM 4 current meters, fitted with standard Savonius rotors, were used at some of the locations (see Table 4.1). This type of rotor is prone to over-read the current speed, in the presence of superimposed wave action (Hammond and Collins, 1979). In contrast, the Anderaa RCM 4S is a more recent version of the standard meter, incorporating a modified rotor. It has been demonstrated that this type of meter shows a reduced susceptibility to over-reading in the presence of waves, particularly under conditions of low current speeds (Hammond *et al.*, 1986). For example, under wave and current conditions, where errors of between 20 and 50% would occur with the standard rotor, the modified meter is accurate to within $\pm 5\%$ of the current-alone value.

In relation to the present investigation, therefore, specific care was required in the interpretation of the results obtained from the meters deployed at Stations G and H. Spurious observations were identified by visual inspection of a graphical representation of the data recorded. These recordings were replaced by the vector average of the current velocity measured one sampling interval before and after the recording to be replaced.

4.3 TECHNIQUES FOR CURRENT METER DATA ANALYSIS

The time-series analysis of current meter measurements may be presented in a variety of ways; the methods that have been used here are described below.

4.3.1 Statistical analyses

The statistical techniques for analysing the current meter data were the calculation of:

(a) the maximum, minimum and mean current speed values, together with their standard deviation, for each data set;

(b) the presentation of scatter plots for the vectorial current meter data recorded over the entire period of deployment- these are useful in presenting bi-variate data and represent the tidal current regime in the vicinity of each of the stations;

and (c) the derivation of frequency distributions for recorded current speeds and directions.

4.3.2 Residual currents

Residual currents were determined, to establish a mean current vector over a tidal day (equivalent to a period of two M_2 tidal cycles i.e. 24 hrs 50 mins). In this way, residual currents reflect a net water movement independent of tidal forcing. Residual flow over the length of deployment may be determined then using the flow vectors, given by:

$$\vec{u}_R = \frac{1}{N} \sum_{i=1}^{N} \vec{u}_i \qquad (4.1)$$

where N is the number of observations equivalent to a tidal day. Obtaining a mean value over 12.4 hours provides a regular difference between consecutive tidal cycles, related to the diurnal inequality between successive tides.

Tidal residual currents have been obtained elsewhere, by other investigators (e.g.

Pattiaratchi, 1985), by applying a filter to the data sets. The tidal current data are filtered (using, for example, Doodson's (1928) X_0 filter) in order to remove all the energy at diurnal and higher frequencies. Residual currents can be obtained by summing these 'residuals' over the period of a tidal day.

Effectively, there is little difference between the results of the filtered data and those obtained by taking a mean value (Dyer, 1986). Similarly, Hill and Ramster (1972) and Heathershaw and Hammond (1979) have found that use of the X_0 filter yields similar residual flow estimates to those obtained from a 24 hr 50 min arithmetic mean.

Variability in the daily residual current speeds and directions, over the whole of the deployment period, were examined using the standard errors of the north-south and east-west components (Heathershaw and Hammond, 1979) and a 'steadiness' factor (the Neumann Factor (see Ramster *et al.*, 1978)). If the standard errors are greater than 50% of the mean residual flow estimates, less confidence should be placed on those particular estimates (Heathershaw and Hammond, *op. cit.*).

The Neumann Factor (B) is an expression of the ratio between the vector mean (u_{vect}) and the scalar mean (u_{scal}); it is expressed as a percentage, where:

$$B = \frac{u_{vect}}{u_{scal}} \times 100\% \tag{4.2}$$

The scalar mean current (u_{scal}) can be determined by:

$$u_{scal} = \frac{1}{N} \sum_{i=1}^{N} u_i \tag{4.3}$$

and u_i are the recorded current speed vectors.

If $B < 70\%$, then the vector mean values become unrepresentative of a significant portion of the sequence of daily residuals from which B has been calculated (Ramster *et al., op. cit.*).

4.3.3 Progressive vector diagrams

A progressive vector diagram (PVD) of a tidal current time-series represents the movement of a parcel of water over the time of the recording of a data set. Orthogonal components of each of the tidal current recordings have been summed here, so that successive tidal current vectors can be added. This procedure creates an overall vector for the complete recording representing the residual water movement. If the PVD is constructed for a time-series encompassing a complete tidal cycle, then the total distance travelled over 12.4 hrs and its direction represents the residual current i.e. the mean current vector over the tide. For the present investigation, successive residual vectors have been determined over the period of the self-recording current meter deployment. PVDs for the complete measurement period have been constructed then using the daily vectors. In this way, net water movements over the 10 day deployment can be investigated.

4.3.4 Harmonic analysis

The basis of harmonic analysis is the assumption that the tidal variations can be represented by a finite number (N) of harmonic terms, of the form:

$$a_n \cos(\sigma_n t - g_n) \tag{4.4}$$

where a_n is amplitude, g_n is a phase lag (in relation to the Equilibrium Tide at Greenwich) and σ_n is the angular speed. In this way, the random appearance of the tidal currents may be represented by means of a current spectrum. This type of analysis is based upon the regularity of astronomical motion (leading to attractive forces), which gives rise to periodicities in the tidal records. The harmonic analysis of tides (including tidal currents) has been described in detail by several investigators (e.g. Doodson, 1928; Pugh, 1987). A tidal current record is decomposed by means of harmonic analysis into a large number of sinusoidal waves of different frequencies, amplitudes and phases:

$$T(t) = U_0 + \sum_{n=1}^{N} a_n f_n \cos[\sigma_n t - g_n + (V_n + u_n)] \qquad (4.5)$$

where the unknown parameters are U_0 and the series (a_n, g_n).

Any curve can be represented by the sum of a series of sinusoidal curves. Therefore, an attempt is made initially to fit a sinusoidal current (curve) with a period spanning the entire length of the record. The current is shifted then to the right and to the left and its amplitude is varied, until a position is found (phase angle g_1) where the amplitude is at its maximum. On a normal tidal current record, no such wave could be fitted: such a component would have an amplitude of zero. Further, a sinusoidal current of half this period (i.e. double the frequency) is investigated in the same manner. The amplitude of this wave may also prove to be zero, but some positive value might be found. During successive trials, original sinusoidal currents with frequencies of three, four, five (etc.) times that of the original current are examined. Current components which coincide with the predominant current frequency within the record can be identified, because they have comparatively large amplitudes. The analytical procedure is continued until components of small periods (large frequencies) are revealed which do not contribute significantly to the overall curve.

Returning to harmonic analysis, only the amplitude and phase are unknown: periodicities of the oscillations are controlled by planetary movements. Current meter measurements made at a single location may be approximated, therefore, by the sum of a number of simple harmonic oscillations. Such oscillations (tidal constituents) are characterised by their period, amplitude and phase.

The fitting of the curves (as outlined above) is based upon the least square procedure of analysis and adjusted so that $\Sigma S^2(t)$, the square of the difference between the observed (O(t)) and computed tidal currents (T(t)),

$$S(t) = O(t) - T(t) \tag{4.6}$$

is at a minimum when summed over all the observed values. In Equation 4.5, f_n and u_n are the nodal adjustments, whilst the terms $\sigma_n t$ and V_n together determine the phase angle of the Equilibrium constituent.

The method was used in the present investigation to analyse the 10-day self-recording current meter data sets. Tidal harmonic analysis of the east-west (u) and north-south (v) components of the observations was performed using the FORTRAN program TIRA (Tidal Institute Recursive Analysis); developed and made available to the author by the Proudman Oceanographic Laboratory (Bidston). Sixteen major constituents may be resolved using this method, whilst a further 15 related constituents were incorporated into the analyses by assuming relationships in amplitude and phase with one of the 16 major constituents (Table 4.2). These relationships were derived on the basis of the Equilibrium tide (Doodson, 1928).

From the analyses, the amplitudes (a_u and a_v) and phases (g_u and g_v) for each tidal constituent were derived for the east-west (u) and north-south (v) components, respectively, at each current meter location. The mean and standard deviation of the observed series are also provided as output to the analysis package, as an indication to the efficiency of the analysis. In general, a ratio between residual and observed standard deviations of 0.1 indicates an efficient analysis. However, this ratio may be as high as 0.5 for the analysis of current meter data (IOS, 1983).

An 'effective' tidal current can be derived using the constituents obtained from harmonic analysis of the current meter data. For each current meter recording, the difference between the predicted and observed values is referred to as the 'residual' (see above). It should be noted that the 'residuals' constitute a time series; they are not Eulerian residual currents (Section 4.3.2).

4.3.5 Energy distribution within the tidal currents

The east-west (u) and north-south (v) components of the current meter records were analysed in order to determine:
(i) the energy contained at all frequencies within each component; and
(ii) for each component, the energy associated with discrete frequencies.

In order to calculate the energy contained within discrete frequency bands, the tidal oscillations were divided into the following frequency categories: long period (greater than 4 days); diurnal (24 hrs 50 mins); semi-diurnal (12 hrs 25 mins); quarter-diurnal (6 hrs 12 mins) and sixth-diurnal (4 hrs 6 mins).

4.3.6 Correlation between observed tidal currents

Propagation of the tidal wave through the study area has been investigated. Initially, observations of flow speed and the orthogonal (u and v) components, recorded at different heights above the bed, have been compared. Hence, the vertical structure of the tidal flow can be investigated.

Secondly, an investigation into the spatial variation of the tidal wave propagation has been undertaken. Flow velocity (u, v and flow speed) variations recorded at 2 m above the bed at stations around the Broken Bank have been compared.

In order to undertake these analyses, a correlation function has been used to identify phases differences of the self-recording current meter records. The time difference between different elevations/stations can, therefore, be obtained.

4.4 RESULTS AND DISCUSSION

4.4.1 General description of overall data

A limited number of spurious recordings were identified (and in need, therefore,

of smoothing (Section 4.2)) within the data files obtained from Stations G and H. Due to corruption of the data during the latter part of the deployment, it was necessary to truncate the record obtained from the self-recording current meter at Station E-10.

The observed velocities obtained from all the current meter data collected during the present investigation, are presented in Table 4.3. The highest maximum near-bed currents (97.2 cm s^{-1}) were recorded at Station H, whilst the lowest maximum (73.7 cm s^{-1}) was at Station G. Observations from the near-bed and mid-depth current meters suggest that the central swale location (Station G) is an area of lower velocity tidal currents. Mean current speeds, at all stations, show an increase with distance above the bed. At Station B, mean current speeds at 12 m above the bed are greater than those experienced 10 m above the bed; this suggests that the flow has not reached its free stream velocity (Section 3.1).

Variations in the north-south (v) and east-west components (u) of the recorded tidal current velocities are presented in Table 4.3. Here, the maximum recorded currents are shown as positive when directed towards the north and east. The minima represent the highest currents recorded in a negative direction (i.e. to the south and west). Unlike the overall current speeds, there is some consistency in the near-bed u and v variations. The north-westerly maxima are greatest at stations lying to the west of the Broken Bank. Southeasterly water movement is apparent to the east of Broken and Well Banks, although it is less dominant than the northwesterly flow. The pattern observed for the mid-depth data is less obvious. The values of the u and v maxima (both in the positive and negative directions) provide little indication of any consistent pattern of water movement around Broken Bank, at intermediate water depths.

Scatter plots of current speed and direction are presented in Figure 4.2; from these, the highly rectilinear nature of the tidal currents in the vicinity of the banks can be distinguished. The predominant directions of the flood (southeasterly) and ebb (northwesterly) flows can be identified in the plots. At Stations B-2, H-2 and

H-12, the ebb flow is an exact reversal of the flood flow. At Stations B-10, B-12 and G-2 there is an approximate 170° difference between the flood and ebb directions. At Station C-2, this difference is approximately 175°. At Stations E-2 and E-10, the difference is similar, although this is reversed at each elevation above the bed. The greatest deviation away from truly rectilinear flow is observed at Station G-12, where the directional difference between flood and ebb currents is approximately 160°.

The pattern of horizontal water movements in the vicinity of the Broken Bank is one of strongly rectilinear tidal currents producing narrow tidal ellipses. The axis of the Broken Bank is, on average, inclined at approximately 20° in an anticlockwise sense to the direction of dominant flow; considerable agreement is obtained, therefore, with the modelling approach of Huthnance (1982b) in which the inclination was found to be between 18° and 48°, with maximum growth occurring for an angle of 27°.

The frequency distributions representative of current speed and direction have been generated for all the data collected during the deployment (Figure 4.3). Current speeds ranged from zero to, typically, 1 m s^{-1}. These results show that the most frequently occurring speed interval represents, at most, around 20% of the total record. Likewise, that Station G-2 experiences the narrowest range of tidal current speeds. The frequency distributions of current direction show bi-modality at each of the stations; this is indicative of the highly rectilinear character of the currents throughout the study area. However, variations occur between the magnitudes of the two main modal classes. To the east of the bank, the southeasterly modal classes (in the flood direction) are generally greater than the northwesterly modal classes (in the ebb direction). To the west of the bank the pattern is reversed. The dominance of the flood flow to the east of the bank, with the ebb to the west, is illustrated once again.

Variations in the tidal current speed recorded around the Broken Bank, averaged over a tidal day (24 hrs 50 mins), show strong overall correlation with the tidal

range experienced locally (at Lowestoft) over the period of the deployment (Figure 4.4).

Pressure data have been obtained from a sensor deployed adjacent to Station C for the period of the investigation (Collins, 1991). Sea surface elevations have been compared against tidal current speeds and, for this area, maximum speeds coincide with high waters; a relationship which is characteristic of a progressive tidal wave.

4.4.2 Tidal asymmetry and hourly vectors

Typical spring and neap tidal cycles have been identified from the current meter records for the period of deployment. Flood and ebb phases of the tides are defined, therefore, in terms of current direction i.e. not in terms of sea surface elevation. The maximum period of flood and ebb flows has been investigated, for each current meter station and over both spring and neap cycles. The percentage time of the flood and ebb components during spring and neap tidal cycles has also been studied. The results of these analyses are presented in Table 4.4.

Along the eastern flank of Broken Bank (Stations B and C), the present investigation has identified the dominance of flood-directed water movements over the entire period of the current meter deployments. Such a pattern is characteristic of spring tidal cycles, but the situation is more variable during neap tides. At Stations B-2 and B-10, ebb flows represent the greater proportion of the tidal cycle. Station E is located within an area dominated by the spring ebb flow, in both flow speed and duration; during the neap tidal cycle, the duration of the ebb flow is greatest, but does not reach the flow speed maxima attained by the flood. The pattern at Station G is variable, with the flow speed maxima and the flow duration variable; it is dependent upon the flood/ebb and the spring/neap. Flood dominance, in terms of both flow maxima and duration, is apparent at Station H.

The mean hourly tidal current vectors over the spring and neap tidal cycles are presented in Figure 4.5. These vectors represent the average flow velocity during

successive hours throughout the tidal cycles. Neap vectors represent, on average, some 60% of the spring tidal values. Vectors over both cycles are highly rectilinear and are aligned closely with the sand ridges. At the mid-channel (Station G), some decrease in the rectilinear nature of the tidal currents is observed; this may be a result of the development of an embryonic sand bank at this location (Collins *et al.*, 1995a).

4.4.3 Residual water movements

The magnitudes and directions of residual current vectors (calculated using a 24 hr 50 min arithmetic mean), the associated Neumann Factor, the standard errors associated with the analyses (Section 4.3.2), together with the length of the current meter record used, are presented in Table 4.5.

The value of the Neumann Factor shows some spatial variation between the different current meter stations. The residual currents at stations to the east of the Broken and Well Banks (Stations B, C and H) show a high degree of stability i.e. the directions of the daily residuals are similar throughout the period of deployment (Section 4.3.2). Hence, high values of the Neumann Factor (with the exception of Station B-12) are observed. The residual current vectors on the western flank of Broken Bank show greater directional variability, associated with lower values of the Neumann Factor.

Residual current speed and direction show also some variation with location within the study area. Such variability is indicated by the standard errors of the observed residual vectors and the Neumann Factors for the various current meter data sets (Table 4.5). In general, the standard errors are small in comparison with the residual flow speeds (less than 50% (Heathershaw and Hammond, 1979)), and the Neumann Factors are high at Stations B, C and H. The more variable residual flow patterns are observed, in general, in the centre of the swale and along the western flank of the Broken Bank.

The magnitude and direction of the residual water movements, described above, are shown in Figure 4.6. Such movements are independent of tidal forcing (Section 4.3.2); they are due, rather, to effects such as bedform topography and meterological forcing. As such, there is no obvious correlation between the observed patterns of residual speed/direction over the period of deployment, with tidal range (Lowestoft) for the period of the deployments (cf. the correlation between the tidal range and the mean flow speeds observed over the deployment (Figure 4.4)).

Differences between the flow on the western flanks of the Broken and Well Banks and other areas are highlighted in Figure 4.6; Stations B, C and H show a significant decrease in the residual flow speed on the 19 November. No corresponding decrease is evident at Stations E and G. This isolated event may be part of a long-term oscillation only part of which has been recorded here. No similar pattern is evident in the residual directional data.

Most of the fluctuation in the residual speed (Stations B, C and H) occurs during the early (neap) section of the record; at this time (external) forcing may be able to influence significantly the results.

4.4.4 Progressive vector diagrams

Progressive vector diagrams (PVDs), for the entire period of deployment, are presented in Figure 4.7. Vectors have been plotted for each tidal day (as points); as such, they represent the net water movements over successive tidal days. The overall movement is represented by the distance between the final vector and the origin.

Progressive vector diagrams representing water movement along the eastern flank of the Broken and Well Banks reveal a pattern dominated by movement towards the southeast. The daily movements observed for these locations are the highest observed within the present study area. Along the western flank of the Broken

Bank, daily movements reflect the variable regime found here; this gives a significantly lower movement over the period of deployment than that observed on the eastern flank of the Broken Bank. Considerable variation exists also in the direction of the flows with height above the bed at Station E; near-bed water movement is directed largely northward (and, hence, towards the bank) whilst the mid-depth water movement, whilst low, is directed predominantly westward (and, hence, away from the bank).

Water movement at both elevations above the sea bed in the cental swale (Station G) can be split into two parts; (a) the early (neap) part of the record when water movements are highly variable in direction; and (b) the latter (spring) part of the record when movements are more stable in (an easterly) direction (towards Broken Bank).

Pattiaratchi (1985) suggested that stable residual currents observed around Scarweather Sands (Bristol Channel) (and in the present study) are being generated by local effects and not by external forces.

4.4.5 Harmonic analysis

Harmonic analyses of the east-west (u) and north-south (v) components of the tidal current data were undertaken on the 10 days of data recorded at each of the current meter stations. The method used was that described in Section 4.3.4. The ratio between the standard deviations of the residual and observed series (R) was predominantly less than 0.35 (Table 4.6); this is indicative of efficient analyses, the values were less than a critical R value of 0.5 (Section 4.3.4).

The results of the harmonic analyses are summarised for the four, typically, largest constituents i.e. M_2, S_2, M_4 and μ_2 in Table 4.7. The other constituents which were derived are listed in Table 4.2. The magnitude of the M_2 constituents is between 22 and 53 cm s^{-1} (except at Station G-12) and, as such, represents the major constituent of the recorded tidal currents; the S_2 harmonic is frequently an

order of magnitude lower (except at Stations B-12 and E-10). An exception to this generalization is the dominance of the S_2 constituent at Station G-12. Throughout the present study area (except at Station B-10), the v component represents generally a significantly larger fraction of the tidal currents than the u component; it is typically 1.5 times greater than the u component.

The amplitudes of the major semidiurnal constituents are much higher than those of the major diurnal tides. The M_2 and S_2 amplitudes reach 53.34 cm and 60.29 cm, respectively. In comparison, the K_1 and O_1 tidal amplitudes are only 5.70 cm and 6.59 cm, respectively. Hence, a Form Factor ($(HK_1+HO_1)/(HM_2+HS_2)$, where HK_1, HO_1, HM_2 and HS_2 represent the K_1, O_1, M_2 and S_2 amplitudes, respectively) less than 0.20 has been determined for the area; this is indicative of predominantly semi-diurnal tides (Pugh, 1987). In contrast, the tidal regime for Station E-10 has been shown to be mixed, although mainly semi-diurnal in character. However, the harmonic analysis undertaken for records from this station is based upon a truncated data set and, as such, less emphasis should be placed upon this particular result.

For each individual recording (observation) of tidal current velocity made by the current meters, the TIRA analysis has predicted the proportion of the signal due to the harmonic constituents. The remainder of the record is due to non-tidal forcing, representing a residual value. An example of the (observed) time-series recorded by the current meters around the Broken Bank, together with the approximation determined by harmonic analysis, is shown in Figure 4.8 (for the v component at Station G-2). The curves can be seen to be reasonably similar.

The residual time-series, representing the difference between the two curves is also plotted on Figure 4.8. The residual curve may be seen to be distributed evenly about zero, for the majority of the record. During the early part of the residual time series, there is evidence of a longer period oscillation; this is due possibly to external forcing, such as a meterological event. Such an oscillatory pattern is evident in the residual time series derived from other current meter data in the

study area. Although not presented here, the oscillation is present, although not strongly, in the v component output for Stations E-2 and H-2. In contrast, it is not found (in the same component) at Stations E-10 or G-12, but is present at Station H-12. In the corresponding u time series, the signature is shown in the records for those stations which display the oscillation in the output from the v component. This phenomenon is particularly characteristic of near-bed flow centred at Station G. Such an oscillation in the residual time series is not found to the east of the Broken Bank.

The self-recording current meter observations and the residuals (determined from the harmonic analysis) have been summed over successive tidal days throughout the period of deployment (Table 4.8). The ratio of the residual to the observed value gives an indication of how successful TIRA has been at replicating the observed currents. Residuals represent approximately 20% (on average) of the observed flow speeds. However, there is considerable variation from 8 to 64%. The smallest residual current speeds, where the harmonic analysis has been most successful in reproducing the observed currents, are found over the latter (spring) section of the record. Here, residuals constitute, on average, approximately 12% of the observed flow speed; over the neap period, when flow rates are lower and more variable (Figure 4.7), this value is approximately 34%.

Variation of the average residual current speed (Table 4.8) shows no dependence on location around the Broken Bank.

Comparison between the residual values obtained using a 24 hr 50 min mean, with the output from TIRA, shows reasonable agreement at Stations B, C and H. At Stations E and G, however, the difference between the residual water movements may vary by up to a factor of 5.

Ellipses for the major tidal current harmonic constituents have been constructed from the TIRA output and are shown on Figure 4.9. The dominance of the M_2 constituent along the eastern flanks of the banks is apparent; here, the S_2

constituent is very small. The M_2 ellipses on the eastern flank of the Broken Bank are inclined at approximately 23.5° to the axis; on the western side, the inclination is, on average, 16.5°. Interestingly, the S_2 ellipse is of a similar magnitude to that of the M_2 ellipses at Station G-12, but is orientated *across* the sand banks. The axes of the M_4 ellipses are very much smaller (typically 6% to 9% of the M_2 harmonic); similarly, they are more variable in their alignment than those constructed for the previous harmonic constituents. However, these ellipses are more distinctive in the vicinity of the banks (rather than the swales); this may provide further evidence of the topographic origin of the M_4 generation process.

4.4.6 Energy distribution within the tidal currents

The total energy contained within each tidal current component (u and v) for each station is presented in Table 4.9. The total amount of energy present within the data is dependent upon the length of the original current meter record. Hence, the results from Station E-10 are lower than might be expected, as this record was corrupted mid-way through the deployment (Table 4.1).

The total energy of the near-bed currents can be seen to vary with location; current flow along the eastern flank of the Broken Bank (Stations B-2 and C-2) contains energy less than 680 x 10^4 cm^2 s^{-2}, whilst that to the west and south of the bank (Stations E-2 and G-2) has energy values greater than 750 x 10^4 cm^2 s^{-2}. The maximum tidal current energy is found at Station H, whilst the minimum is associated with Station B (cf. the maximum and minimum currents, Table 4.3). A less complete picture is obtained from the mid-depth locations, but some evidence supports a similar pattern of energy distribution as determined for the near-bed tidal current flow.

The proportion of the total energy contained within the v component, for both mid-depth and near-bed currents around the Broken Bank, is generally high; this is true especially of stations located to the west of the Broken Bank (Stations E and G), where such energy accounts for up to 84% of the total energy.

Overall, the mid-depth currents contain approximately 30 to 50% more energy than those observed near the bed (Table 4.9).

The energy associated with different tidal frequencies is presented in Table 4.10. The analysis is not efficient for the truncated data files from Station E-10 which produces spurious results.

The u component of the observed tidal currents is dominated by semi-diurnal oscillations. Energy contained within this band accounts for up to (almost) 90% of the total energy, at individual stations. The quarter-diurnal frequency contains the second largest amount of energy, although this is only slightly greater than that contained within the diurnal frequency band. These frequencies contain, however, considerably less energy than at the semi-diurnal frequency. On average, approximately 85% of the total energy is represented by the energy contained within the 5 bands presented.

The dominant tidal frequency is semi-diurnal (containing up to (almost) 90% of the total energy) for the v component. The diurnal components are, however, the second most important frequency band. The quarter diurnal and long period frequencies contain approximately 25% of the diurnal energy. Likewise, the M_4 constituent of the v component represents only approximately 2% of the total energy; this compares with approximately 6% in the u component. However, overall, the v component represents up to (approximately) 80% of the total tidal current energy around the bank (Table 4.9). Lower values have been obtained here for the quarter-diurnal energy within the (more energetic) v component; due to the dominance of the v component, these values actually represent more of the total energy contained within this particular frequency band.

4.4.7 Correlation between observed tidal currents

Propagation of the tidal wave around Broken Bank has been investigated, in terms of phase differences between tidal currents observed at different elevations above

the sea bed and at different locations within the present study area. Phase differences have been identified in records of: (i) the tidal current speed; (ii) the u component; and (iii) the v component.

Generally, the data sets show high degrees of correlation for phase shifts of approximately 12 hours. Least correlation occurs at phase shifts of approximately 6 and 18 hours. Hence, the strongly semi-diurnal character of the flow recorded here is evident; it produces strong correlations at multiples of approximately 12 hours.

(a) Vertical phase differences

Turbulent effects within the water column diminish generally with height above the bed; at such levels, inertia and the Coriolis effect become more important in balancing the pressure force due to the sea surface slope. In an oscillating tidal flow, the waters farthest from the bottom are moving faster than those near the bottom. An effect of bottom friction, identified elsewhere, is to cause the tidal flows near the bottom to reach their maximum values before the surface streams (Proudman, 1953) as flows farther from the bed take longer to respond (Mofjeld, 1976) (Figure 4.10). Typically, changes in the bottom currents lead those in the upper layer by 20 to 40 minutes (Pugh, 1987).

Variation in the tidal wave propagation, with depth, around the Broken Bank has been investigated. The results are presented in Table 4.11.

u component

The records collected at stations along the eastern flanks of the Broken and Well Banks show that the mid-depth flow leads the near-bed flow. Investigation into the flow patterns at Station B reveals a 2 min (equivalent to the sampling interval) phase difference between the lower current meters (8 m vertical distance). In comparison, the 2 m interval between the upper meters yields 10 minutes; this is

equivalent to the sampling interval of the upper current meter. The magnitude of the lag varies between Stations B and H with that at the more energetic Station H (Table 4.9) being greater. The near-bed flow leads that at mid-depth at the central swale location and Station E, to the west of the Broken Bank. The lag at Station G is considerably greater than elsewhere around the bank (70 min). Thus, vertical phase lag varies with position across the interbank channel.

v component

The general trends identified in the u component of the tidal flow are repeated for the v component. However, the two mid-depth current meter records at Station B are, on this occasion, in phase (to within the sampling interval). The magnitude of the phase differences are replicated exactly at Stations E and G.

Speed

Phase differences at Stations B and H are the same as those encountered for the v component. At these stations, the v component is considerably more energetic than the u component (Table 4.9), and as such the speed variations might be expected to mirror those observed within the (dominant) v component. At Stations E and G, variation in phase remains constant for all three conditions investigated.

In making the comparison of the vertical phase differences across the swale between Broken and Well Banks, it has been necessary to compare values from differing elevations above the bed; flow records from Station E-10 have been compared with those obtained from Stations G-12 and H-12. The v component is dominant at both Stations B and E (Figure 4.3); at Station B it was found that there was no difference in phase of the (dominant) v component (and speed) for the flow at 10 m and 12 m above the bed.

In another study in the southern North Sea, Harvey and Vincent (1977) observed that the phases of currents nearest the bed occurred in advance of the

corresponding phases of the currents well above the bed. Agreement with this observation seems to have a spatial dependency; in the present study, near-bed flow at Stations E and G leads (at a constant value for speed, u and v components) the mid-depth flow.

(b) Spatial phase differences

The results of this part of the investigation are presented in Table 4.12. Variations in tidal current speed phase show a delay between Stations B and C, on the eastern side of the bank; this is consistent with this part of the channel being flood dominated (towards the southeast). To the south and west of the bank, tidal flow at the boundaries of the interbank channel leads the flow over its central portion, by 10 mins. The dominant pattern of tides around the bank (Figures 4.2 and 4.3) results in a delay along the eastern side of the bank, of 20 mins. However, variations in the u component along the western flank of Broken Bank (Station E) lead those on the eastern side (at Station C). The u component variation in the central portion of the swale is the same as that on the western side of the interbank channel.

The v component shows, once again, delay between Stations B and C. The v component variations at the central swale location, however, oppose the pattern found for the u component variations; thus, it has the same phase as that on the eastern side of the interbank channel.

The phase lag between Stations B and C is fairly consistent, for both components and the overall speed, at around 24 minutes. The phase differences between the flow to the south and west of the bank exhibit more variation. The u and v components at Station G align themselves with the western and eastern sides of the channel, respectively.

4.5 CONCLUDING REMARKS

Self-recording current meter data have been collected in the vicinity of a linear sand bank system; these permit a considerable insight to be developed into the hydrodynamic setting of such a region.

The tide propagates as a progressive wave through the area, with the associated tidal currents being strongly rectilinear in character. Southeasterly currents are strongest along the eastern side of Broken Bank. The flow pattern is more balanced on the western side; however, northwesterly (ebb) currents are the highest recorded.

Interaction between tidal currents and sand banks produces localised flow effects, which are predicted by theory and have been identified elsewhere in both numerical models and field observations (Zimmermann, 1981; Pingree and Maddock, 1978; Mardell and Pingree, 1981; and Robinson, 1983). The theories associated with such interactions have been discussed in Chapter 2. Interestingly, data collected during the present investigation demonstrate that some local generation of the M_4 tidal currents is occurring. Such localised generation is indicated by the increased size of the M_4 ellipses adjacent to the Broken and Well Banks when compared with those in the swale (which is not planar). Current speed variations are dominated by the M_2 tidal constituent. The M_4 harmonics within the flow introduce distortions to the tidal curve, which may have important implications in determining sand transport pathways (Pingree and Griffiths, 1979). Hence, local generation of the M_4 tidal currents would influence the predicted sand transport paths. Nonetheless, the M_4 harmonics account for only a small proportion of the total tidal energy; therefore, they will have only limited influence on net regional water (and sediment) movements. Locally, the amplitude of the M_4 harmonic is approximately 6% of the amplitude of the M_2 harmonic. Considerable agreement is found, therefore, with theoretical (numerical modelling) investigation of Pingree and Griffiths (1979) who found that, for this area, the M_4 amplitude represented between 5% and 10% of the M_2 amplitude. Pattiaratchi (1985) found

that, around Scarweather Sands (Bristol Channel), the M_4 tidal currents were an order of magnitude lower than the M_2 tidal currents.

A pattern of horizontal residual water circulation, representative of the period of deployment, has been identified over the study area. The 'steadiness' of the residual currents (with high 'Neumann factor' values) indicates that, except for slight variations during the early part of the deployment, the observed residual flow field is related to sea bed topography, rather than due to external forcing. This would (appear to) indicate that the observed pattern is indicative of water movements in the vicinity of the Broken Bank over longer time scales than those that were measured directly as part of the present investigation. Tidal current observations have been made over the majority of the spring-neap cycle. Hence, it seems reasonable that patterns observed here will be representative of those over a full spring-neap cycle and will, therefore, be indicative of macroscale (kilometres and years (Horikawa, 1981)) patterns of water movement.

Near-bed and mid-depth residual currents to the east of Broken Bank are directed towards the southeast. To the west of Broken Bank, the near-bed residual is directed towards the northwest, whilst the mid-depth residual is largely westerly. The pattern of residual water movement identified here shows considerable agreement with the clockwise circulation of water around such sand banks, including the Norfolk Banks system, as proposed by previous investigators (see, for example, Caston and Stride, 1970; Caston, 1972).

Such investigations (see, for example, Pattiaratchi and Collins, 1987) have suggested that the asymmetrical cross section of a sand bank is a reflection of the dominance of the tidal currents along one particular side of the bank. The asymmetry of the Broken Bank, with its steeper slope orientated towards the northeast would suggest, therefore, a dominance of the (northwesterly) tidal current along the western flank of the bank. The findings presented here do not agree with this suggestion. During the present investigation, southeasterly water movements on the eastern flank of the Broken Bank were greater than those

directed towards the northwest (on the western flank). This imbalance produced a large (southeasterly) residual movement. On the western flank of the bank, water movements directed toward the southeast and northwest were of similar duration and magnitude; a significantly smaller (northwesterly) residual movement was produced than that observed to the east of the Broken Bank.

Vertical differences in the observed tidal current velocities indicate that the mid-depth flow leads consistently the near-bed flow at locations to the east of the banks (Stations B, C and H). Such a flow pattern is not to be expected from simple dynamical consideration of oscillatory flow over a boundary (Mofjeld, 1976). In particular, Station G exhibits large differences between the near-bed and the mid-depth flows. Similarly, spatial (horizontal) variation in phase shows maximum variability at Station G where, for different flow components, the phase can be aligned with flow on either side of the interbank channel. For the same area, Huntley *et al.* (1993) report possible changes of phase, with depth, throughout the water column. Unusual phase differences, not explained by inertial effects or tidal wave propagation, may be the result of secondary flow circulation patterns.

Tidal currents are highly variable within the central swale location; the near-bed residual is directed towards the northeast (offshore). This variability may be the result of the possible formation of a new (sand) bank in this particular area (Collins *et al.*, 1995a); as such, flow characteristics in the swale need to be observed away from such topographic irregularities.

Veering of residual currents adjacent to the banks (Stations B, E and H) does not provide any indication of secondary flow patterns consistent with the 'helical flow' concept of Houbolt (1968). In earlier studies, Harvey and Vincent (1977) found that current veering with height above the bed was consistent with that expected for currents resulting from a constant horizontal pressure gradient force in the northern hemisphere. Further investigation into the nature of secondary flows in the vicinity of these sand banks requires detailed information on the vertical current structure. Likewise, current measurements obtained by McCave (1979) in

the vicinity of the North Hinder Bank (southern North Sea) do not conform to the pattern expected for helical secondary flow.

In summary, a series of observation/interpretations can be derived, as outlined below.

(a) The hydraulic environments on either side of Broken Bank have similar tidal energy levels, and mean current speeds.

(b) To the east of the bank, tidal flow, directed towards the southeast, is dominant. Along the western flank of the bank, the northwesterly flow is greatest; residual water movements here may be directed in a sector ranging from west to northwest. Residual water movements, therefore, imply a clockwise water circulation pattern centred upon Broken Bank. The southeasterly flow around the Broken Bank is greater than that directed towards the northwest; as such this suggests a net movement of water around the bank which is directed towards the south. Near-bed residual water movement in the swale between the Broken and Well Banks is directed towards the northeast (offshore).

(c) Localised generation of higher tidal harmonics in the flow (e.g. the M_4) have been identified, but with amplitudes which are insufficient to influence significantly the net patterns of water movement.

(d) Phase differences and veering identified between near-bed and mid-depth flows may be indicative of secondary circulation. Further, more detailed investigation is required into this particular phenomenon.

Mooring (see Figure 4.1)	Latitude (°N)	Longitude (°E)	Water depth (m)	Instrument type	Instrument Reference Number	Height above seabed (m)	Length of useable data obtained (hrs)
40-B	53 19.9	02 06.5	26	RCM4S	7517	2	231.3
				RCM4S	7946	10	231.3
				UCM2	23	12	240.0
40-C	53 15.4	02 16.2	24	RCM4S	6867	2	239.6
40-E	53 14.9	02 15.3	23	RCM4S	7947	2	241.8
				RCM4S	7765	10	146.5
40-G	53 12.7	02 13.4	29	RCM4	3277	2	263.0
				UCM2	20	12	261.3
40-H	53 10.7	02 11.2	31	RCM4	3559	2	259.0
				UCM2	22	12	258.5

Table 4.1 Self-recording current meter deployments during Challenger Cruise CH40-88. Note: water depth is that above the lowest astronomical tide. Key: RCM4 - Anderaa RCM4, with a savonius rotor; RCM4S - Anderaa RCM4S, with a Modified Rotor; UCM2 - Simrad Ultrasonic Current Meter, Model UCM2.

Major	Related
Z0	σ_1
MSF	Q_1
$2Q_1$	ρ_1
O_1	π_1
K_1	P_1
OO_1	S_1
M_2	ψ_1
S_2	ϕ_1
μ_2	J_1
M_3	$2N_2$
M_4	N_2
MS_4	ν_2
S_4	L_2
M_6	T_2
$2MS_6$	K_2
$2SM_6$	

Table 4.2 Tidal constituents obtainable using TIRA (related constituents were evaluated using Equilibrium tide values).

Station	Current Speed (cm s^{-1})				E-W Component (u) (cm s^{-1})				N-S Component (v) (cm s^{-1})			
	Mean	Min	Max	SD	Mean	Min	Max	SD	Mean	Min	Max	SD
B-2	32.5	1.1	89.4	20.9	3.6	-41.3	58.6	23.4	-7.8	-72.6	45.6	29.5
B-10	38.2	1.3	98.9	23.0	8.8	-48.6	82.9	31.1	-4.6	-76.1	54.3	30.5
B-12	43.0	0.3	97.5	22.4	0.5	-61.3	70.8	26.6	-8.8	-86.9	61.2	39.6
C-2	34.2	1.1	88.1	21.7	6.2	-39.0	61.9	23.3	-6.9	-70.3	58.6	31.8
E-2	36.4	1.1	83.6	20.3	0.1	-47.5	49.2	22.1	0.6	-71.3	75.8	35.3
E-10	42.6	0.0	105.1	22.7	-1.0	-69.7	59.6	23.0	-1.9	-88.2	103.0	42.4
G-2	34.5	1.5	73.7	17.7	2.1	-39.2	45.8	19.3	1.1	-65.3	70.0	33.5
G-12	43.4	4.1	90.8	21.0	4.6	-44.3	48.1	18.6	-1.4	-77.1	89.7	44.2
H-2	39.5	1.1	97.2	21.9	7.1	-41.0	71.0	26.6	-8.3	-81.4	51.2	34.8
H-12	45.2	1.7	113.9	25.4	6.9	-46.8	72.0	27.5	-12.5	-95.8	61.3	41.6

Table 4.3 Current speeds and their statistical parameters for the data collected during the present investigation.
Note: Station B-2 refers to data obtained 2 m above the bed at Station B.

Station	Neaps				Springs			
	Flood		Ebb		Flood		Ebb	
	Time (%)	Max (cm s^{-1})	Time (%)	Max (cm s^{-1})	Time (%)	Max (cm s^{-1})	Time (%)	Max (cm s^{-1})
B-2	49.3	50.7	50.7	41.4	51.5	80.2	48.5	53.8
B-10	46.6	48.2	53.4	44.7	51.7	93.5	48.3	61.7
B-12	56.0	58.8	44.0	54.8	52.0	92.6	48.0	66.2
C-2	49.3	54.2	50.7	36.4	51.5	83.1	48.5	63.1
E-2	40.8	40.8	59.2	36.9	46.9	70.1	53.1	83.6
E-10	42.6	43.5	57.4	49.9	No data		No data	
G-2	44.0	38.7	56.0	40.4	50.7	67.6	49.3	73.2
G-12	54.7	48.0	45.3	53.1	48.0	86.4	52.0	80.2
H-2	50.7	57.8	49.3	43.6	54.7	97.2	45.3	61.6
H-12	52.0	62.9	48.0	49.5	54.7	111.9	45.3	64.2

Table 4.4 Flow maxima and asymmetry, in terms of duration, during typical spring and neap tidal cycles.

Station	Residual current		Standard error		Neumann Factor (%)	Days
	Speed (cm s^{-1})	Direction (°N)	u (cm s^{-1})	v (cm s^{-1})		
B-2	9.6	154.0	1.7	2.2	100	9
B-10	11.1	118.7	2.3	2.5	99	9
B-12	9.8	173.5	2.5	8.1	77	9
C-2	8.9	137.7	1.6	1.7	100	9
E-2	1.2	346.0	1.3	1.5	62	9
E-10	2.1	253.3	2.2	1.3	67	5
G-2	2.4	80.5	1.7	2.3	72	10
G-12	4.9	83.0	2.3	2.5	90	10
H-2	11.6	139.6	1.9	2.8	100	10
H-12	15.1	151.1	2.0	2.6	100	10

Table 4.5 The speed and direction of the residual currents, determined using a 24 hr 50 min arithmetic mean on the current meter data recorded throughout the present study area.

Station		Observed series		R
		Mean	sd	
B-2	u	0.360	0.234	0.19
	v	-0.078	0.295	0.18
B-10	u	0.088	0.311	0.21
	v	-0.046	0.304	0.21
B-12	u	-0.005	0.266	0.27
	v	-0.087	0.396	0.30
C-2	u	0.062	0.233	0.19
	v	-0.069	0.318	0.17
E-2	u	0.001	0.221	0.24
	v	0.006	0.353	0.17
E-10	u	-0.010	0.230	0.31
	v	-0.019	0.424	0.18
G-2	u	0.021	0.194	0.23
	v	0.011	0.335	0.15
G-12	u	0.046	0.186	0.34
	v	0.014	0.442	0.23
H-2	u	0.071	0.266	0.21
	v	-0.083	0.348	0.17
H-12	u	0.069	0.274	0.22
	v	-0.124	0.415	0.18

Table 4.6 The mean and standard deviation (sd) of the observed current meter data series (units m s^{-1}). The efficiency of the analysis (R): ratio of the standard deviations of the observed and residual series is presented also.

Station	M_2				S_2				M_4				μ_2			
	u		v		u		v		u		v		u		v	
	H	g	H	g	H	g	H	g	H	g	H	g	H	g	H	g
B-2	.285	198	.368	28	.078	257	.083	78	.020	4	.032	266	.016	151	.047	222
B-10	.378	198	.374	31	.109	258	.094	80	.053	50	.025	324	.027	89	.057	238
B-12	.303	193	.393	39	.086	237	.180	48	.013	12	.014	313	.038	214	.225	322
C-2	.278	208	.391	40	.075	263	.091	93	.033	70	.027	321	.031	226	.029	216
E-2	.255	204	.427	47	.061	262	.106	92	.031	11	.004	45	.059	212	.021	193
E-10	.257	199	.533	45	.106	241	.192	89	.042	328	.044	179	.072	237	.080	162
G-2	.228	207	.413	47	.065	263	.110	94	.021	46	.010	159	.050	257	.024	156
G-12	.087	105	.191	304	.234	114	.603	318	.009	56	.007	94	.127	281	.275	122
H-2	.313	214	.424	41	.092	254	.107	87	.011	21	.039	3	.047	249	.063	133
H-12	.327	199	.505	35	.096	245	.136	78	.014	198	.020	309	.026	221	.033	135

Table 4.7 Amplitude (H, m s^{-1}) and phase (g, ° relative to Greenwich) of the u and v components for the M_2, S_2, M_4 and μ_2 tidal constituents obtained from harmonic analysis of the tidal current data.

Station	Tidal Day																			
	1		2		3		4		5		6		7		8		9		10	
	T	P%	T	P%	T	P%	T	P%	T	P%	T	P%	T	P%	T	P%	T	P%	T	P%
B-2 u	3.9	24	5.1	31	3.2	18	3.8	19	3.9	20	3.2	14	3.0	13	3.3	14	3.3	15	No data	
v	4.1	18	6.5	32	3.0	13	3.8	14	4.6	18	3.7	13	3.3	11	3.6	13	3.9	14		
B-10 u	5.5	26	7.4	35	4.4	18	5.3	20	4.9	16	4.4	15	4.0	13	3.9	12	4.4	14	No data	
v	4.6	21	7.6	36	5.0	21	5.2	19	4.8	17	4.6	16	3.9	13	4.2	14	4.1	14		
B-12 u	8.1	52	8.9	40	5.2	24	5.4	22	4.4	17	4.7	18	4.2	16	3.3	13	4.4	17	No data	
v	17.4	64	13.9	48	8.4	26	5.7	16	5.2	14	6.8	18	5.6	14	4.6	11	7.3	19		
C-2 u	3.9	23	4.5	29	3.2	17	3.5	18	3.6	16	3.4	15	3.4	15	3.2	14	3.4	16	No data	
v	4.2	17	6.1	28	3.4	13	3.8	14	4.1	14	4.0	14	3.6	12	3.7	12	3.9	13		
E-2 u	3.5	23	6.1	36	4.1	24	3.6	17	3.5	16	3.8	17	4.0	20	3.9	20	3.8	19	No data	
v	4.2	18	7.0	26	4.2	15	4.4	14	3.8	11	4.2	12	4.9	16	4.4	14	3.8	12		
E-10 u	3.4	25	7.2	40	4.9	26	5.8	26	5.1	22	No data		No data		No data		No data		No data	
v	4.8	17	8.4	25	6.4	18	5.5	14	4.9	11										
G-2 u	2.8	20	3.9	27	6.1	35	2.7	16	2.6	14	3.1	16	2.7	15	2.7	15	2.7	15	3.0	17
v	3.8	16	5.6	23	7.1	25	3.4	12	3.6	12	2.7	8	3.4	11	2.8	8	3.1	9	2.9	9
G-12 u	5.5	42	5.9	42	7.2	51	6.0	41	4.7	28	4.1	23	3.8	21	3.7	20	2.8	15	4.4	24
v	11.5	37	8.6	29	9.3	27	10.5	28	6.3	15	5.9	14	6.0	14	5.9	13	4.4	10	7.4	17
H-2 u	3.3	18	5.2	28	6.5	29	3.2	14	3.1	12	3.5	13	3.2	12	2.7	10	3.4	12	3.4	13
v	3.2	12	5.6	21	6.9	25	3.0	10	3.4	10	3.4	10	4.2	12	2.9	8	3.6	10	3.4	10
H-12 u	3.3	16	6.0	31	5.9	27	3.6	15	3.7	14	3.9	14	3.9	14	3.6	13	4.1	14	4.3	16
v	4.4	14	6.6	21	6.0	19	4.1	11	4.3	11	4.0	10	5.2	12	4.3	10	4.5	10	5.8	14

Table 4.8 Residual current speeds determined (over successive tidal days) from the time series output from TIRA over a tidal day (T, cm s^{-1}), and the percentage (P%) of the original observation that this value represents.

Station	Total energy ($cm^2 s^{-2}$) x 10^4	Energy ($cm^2 s^{-2}$) x 10^4		Percentage (%) energy	
		u	v	u	v
B-2	615	239	376	39	61
B-10	821	423	398	51	49
B-12	1060	326	733	31	69
C-2	676	240	436	36	64
E-2	759	213	545	28	72
E-10	637	145	492	23	77
G-2	781	193	588	25	75
G-12	1199	194	1005	16	84
H-2	988	373	615	38	62
H-12	1290	399	891	31	69

Table 4.9 Energy distribution within the east-west (u) and the north-south (v) current components. (Note: differences between the totals and the sum of the components are due to rounding of the data presented within the Table).

a) Station	Percentage (%) energy in tidal frequencies					
	Long period	Diurnal	Semi-diurnal	Quarter-diurnal	Sixth-diurnal	Sum
B-2	0.17	0.75	81.21	0.21	0.02	82.36
B-10	0.33	0.49	80.69	1.20	0.03	82.74
B-12	0.42	0.53	83.00	0.04	0.19	84.18
C-2	0.11	0.56	81.50	1.04	0.01	83.22
E-2	0.11	0.70	78.97	0.87	0.03	80.68
E-10	0.23	1.30	56.44	0.22	0.02	58.21
G-2	0.06	0.45	86.98	0.63	0.04	88.16
G-12	0.47	0.14	78.11	1.57	0.09	80.38
H-2	0.01	0.45	88.71	0.25	0.02	89.44
H-12	0.12	0.34	87.90	0.09	0.25	88.70
Mean	0.20	0.57	80.35	0.61	0.07	81.81

b) Station	Percentage (%) energy in tidal frequencies					
	Long period	Diurnal	Semi-diurnal	Quarter-diurnal	Sixth-diurnal	Sum
B-2	0.22	0.86	82.01	0.54	0.06	83.69
B-10	0.29	1.09	82.25	0.29	0.04	83.96
B-12	1.22	0.82	81.26	0.18	0.04	83.52
C-2	0.18	0.87	83.28	0.32	0.12	84.77
E-2	0.17	1.10	83.49	0.04	0.01	84.81
E-10	0.13	1.45	58.79	0.10	0.06	60.53
G-2	0.06	0.81	89.26	0.08	0.02	90.23
G-12	0.06	0.87	85.80	0.02	0.05	86.80
H-2	0.23	0.52	88.86	0.39	0.00	90.00
H-12	0.14	0.47	88.32	0.27	0.01	89.21
Mean	0.27	0.89	82.33	0.22	0.04	83.75

Table 4.10 Percentage energy distribution within the 5 dominant frequencies for a) the east-west (u) tidal current component; and b) the north-south (v) component.

Height above bed (m)	Station			
	B	E	G	H
	Phase difference for u component (mins)			
12	-12	No data	+70	-20
10	-2	+6	No data	No data
2	0	0	0	0
	Phase difference for v component (mins)			
12	-2	No data	+70	-10
10	-2	+6	No data	No data
2	0	0	0	0
	Phase difference for current speed (mins)			
12	-2	No data	+70	-10
10	-2	+6	No data	No data
2	0	0	0	0

Table 4.11 Vertical variation in the phase of the current speed and its orthogonal components.

Flow component	Phase difference (mins)				
	Station				
	B	C	E	G	H
u	0	+20	+14	+24	+24
v	0	+26	+40	+40	+20
speed	0	+24	+32	+42	+32

Table 4.12 Spatial variation in the phase of the current speed and its orthogonal components at 2 m above the bed.

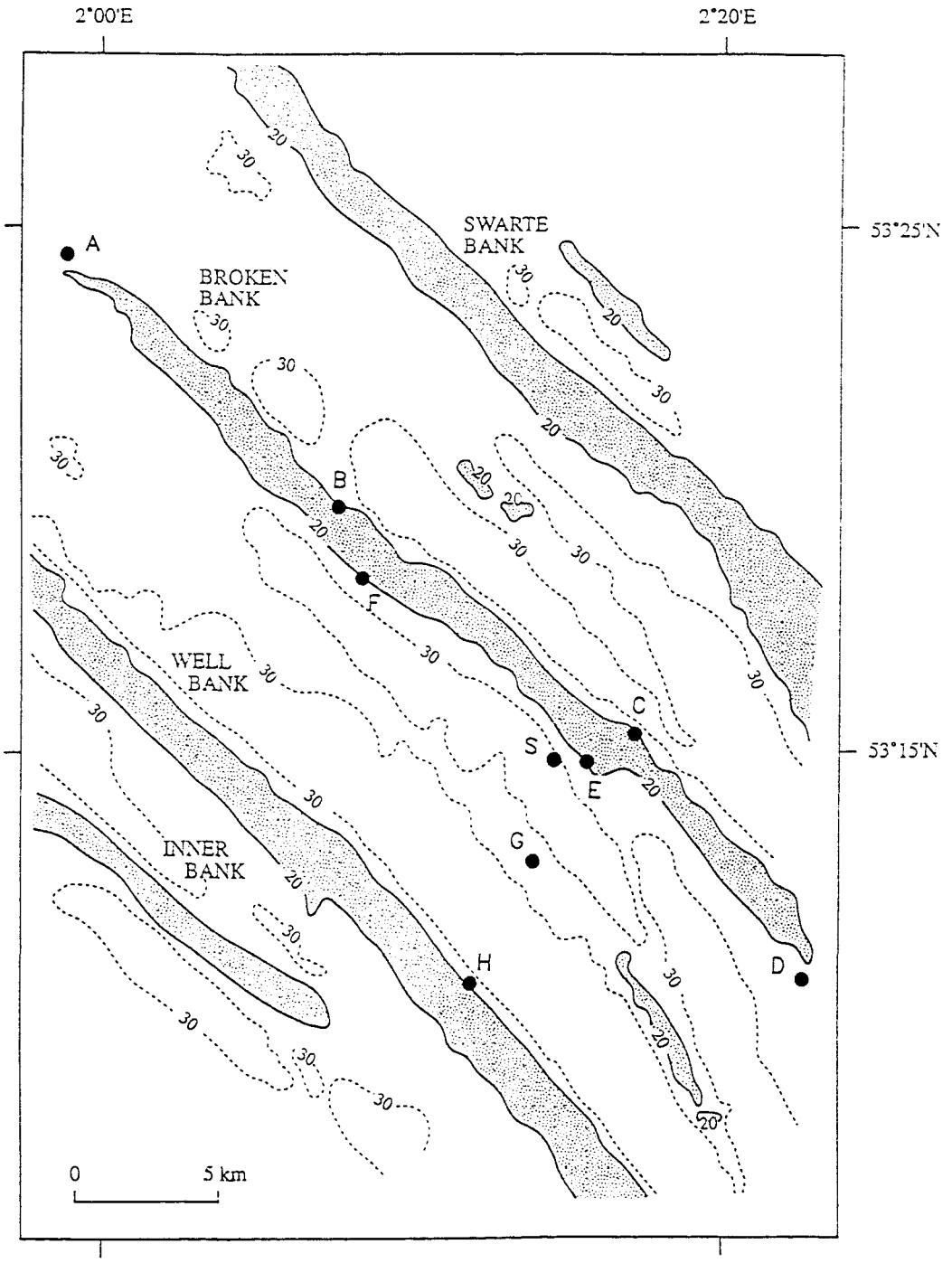

Figure 4.1 Location of the present study area showing positions of the current meter (A to H) and STABLE (S) deployments.

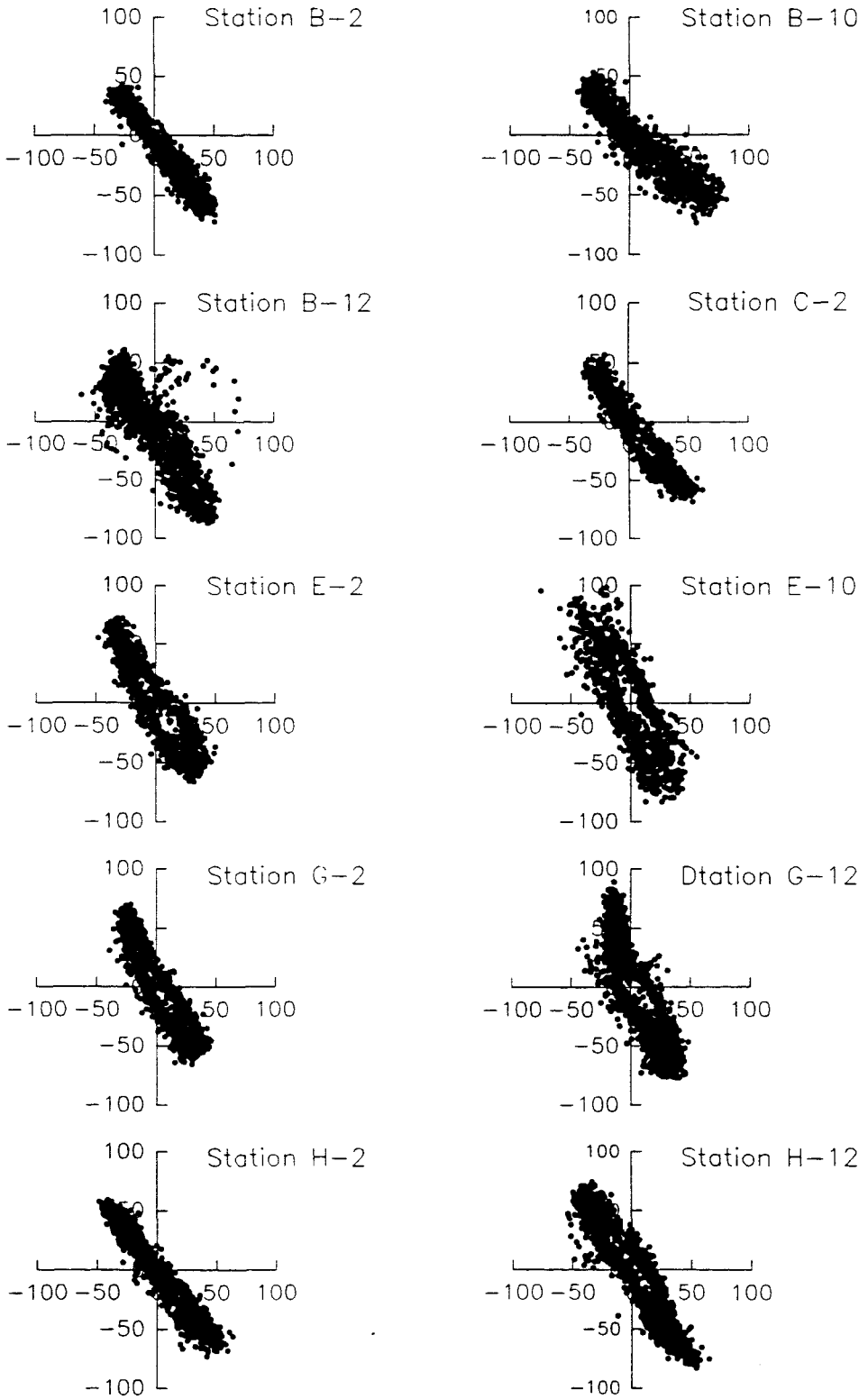

Figure 4.2 Scatter plots of all the data recorded (units cm s^{-1}) at the various stations (for locations, see Figure 4.1).

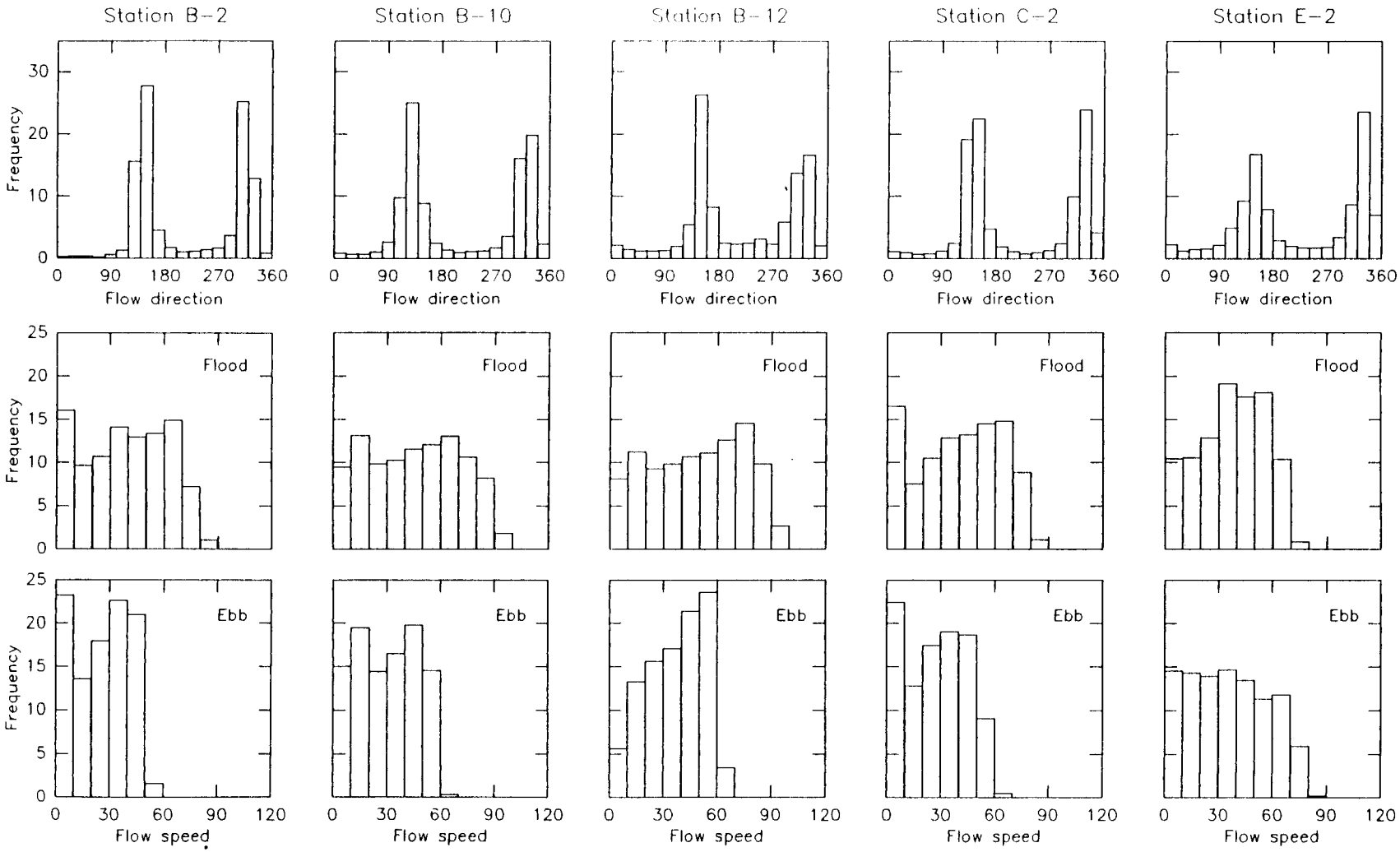

Figure 4.3 Frequency histograms of recorded flow speed and direction at the various stations (for locations, see Figure 4.1).

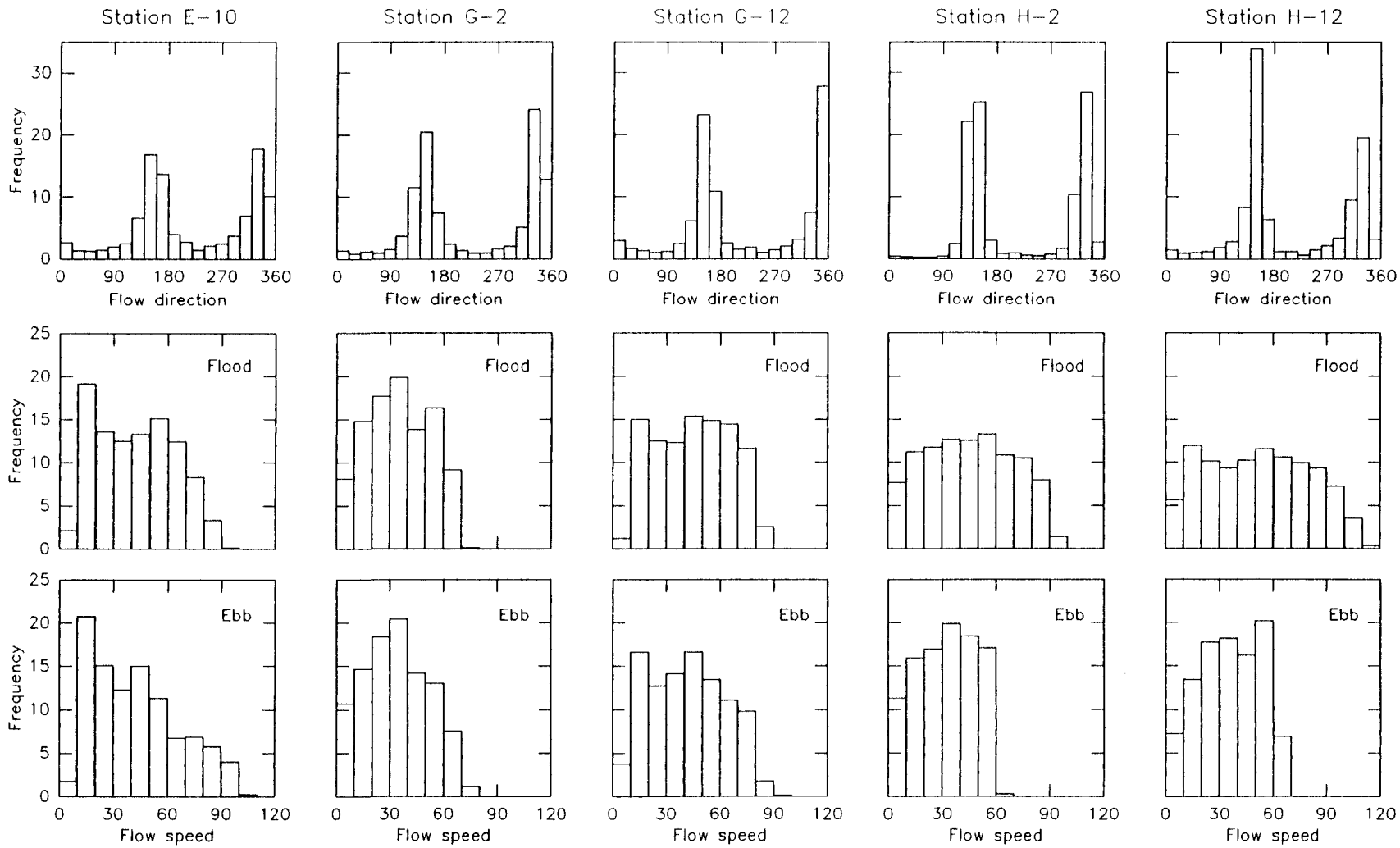

Figure 4.3 continued.

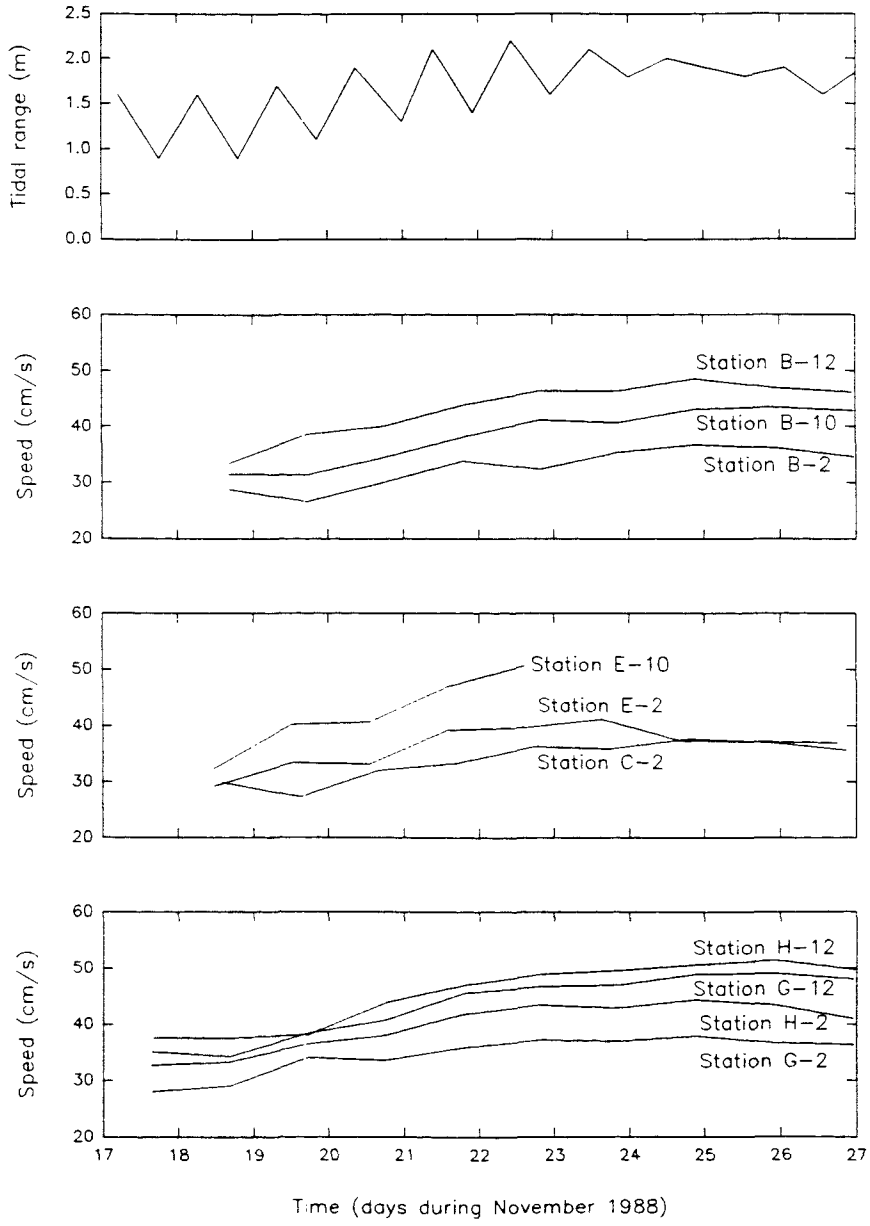

Figure 4.4 Mean flow speed over a 'tidal day', in relation to the tidal range at Lowestoft.

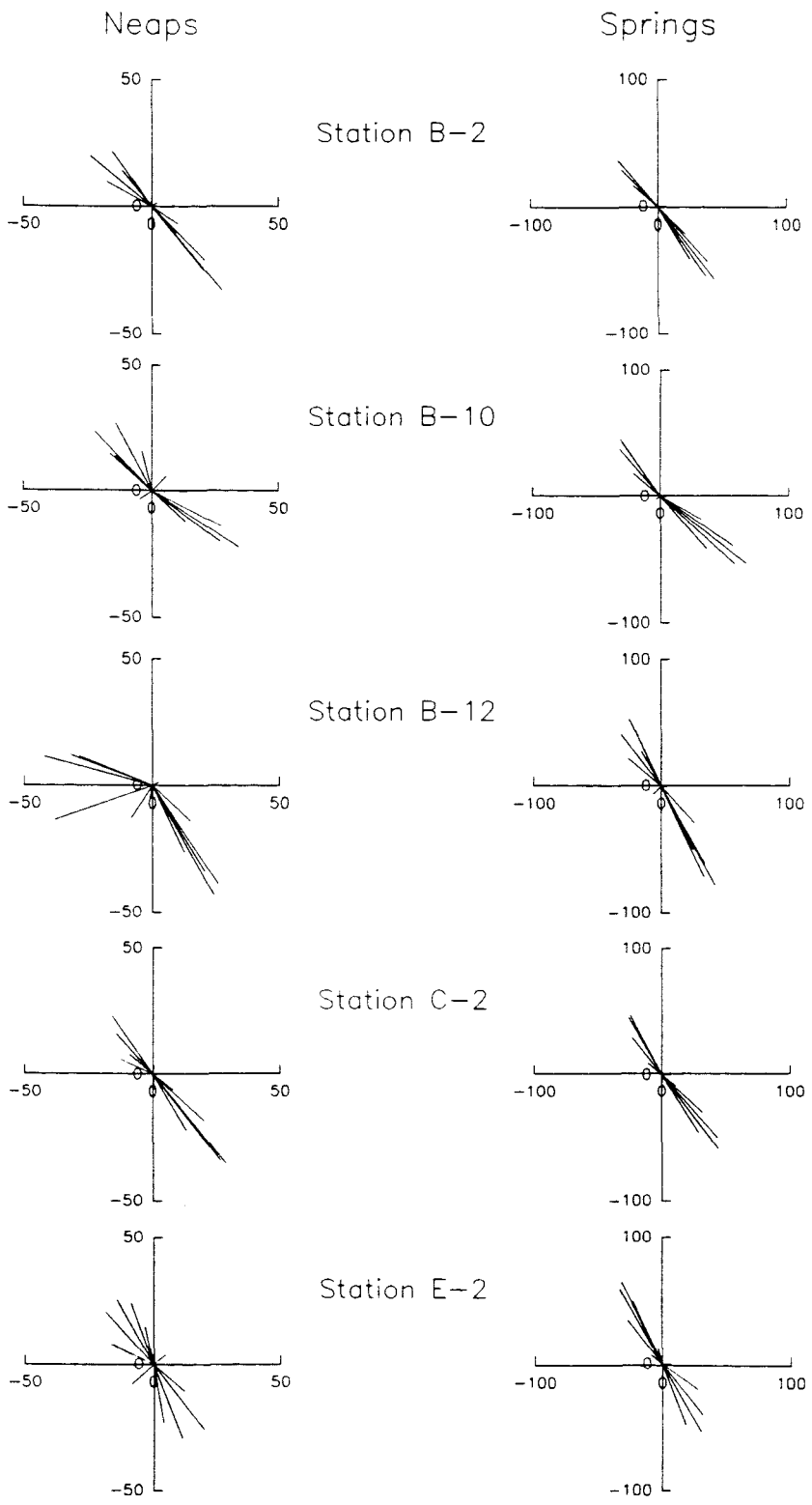

Figure 4.5 Hourly vectors representative of typical spring and neap tidal cycles.

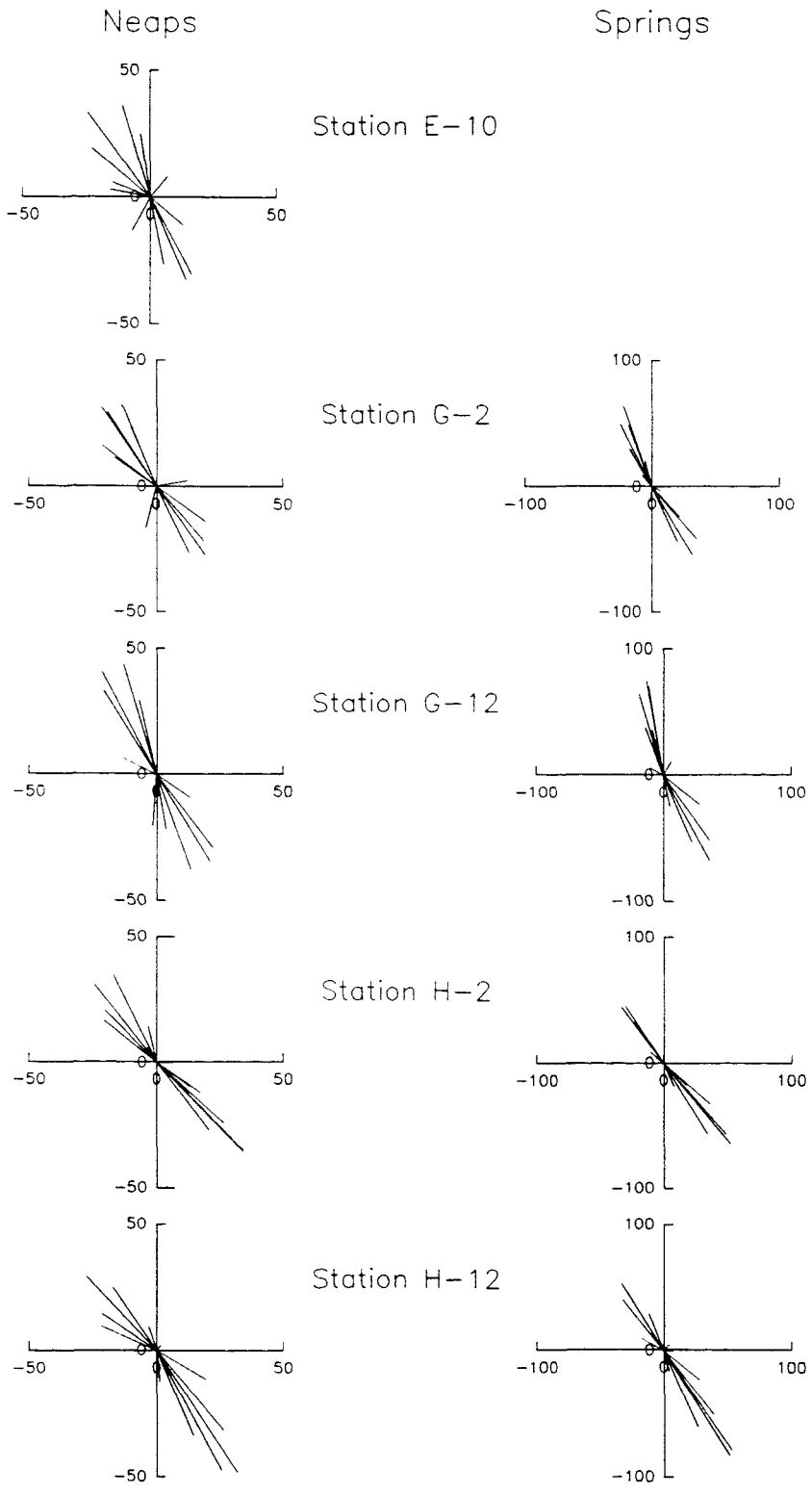

Figure 4.5 continued

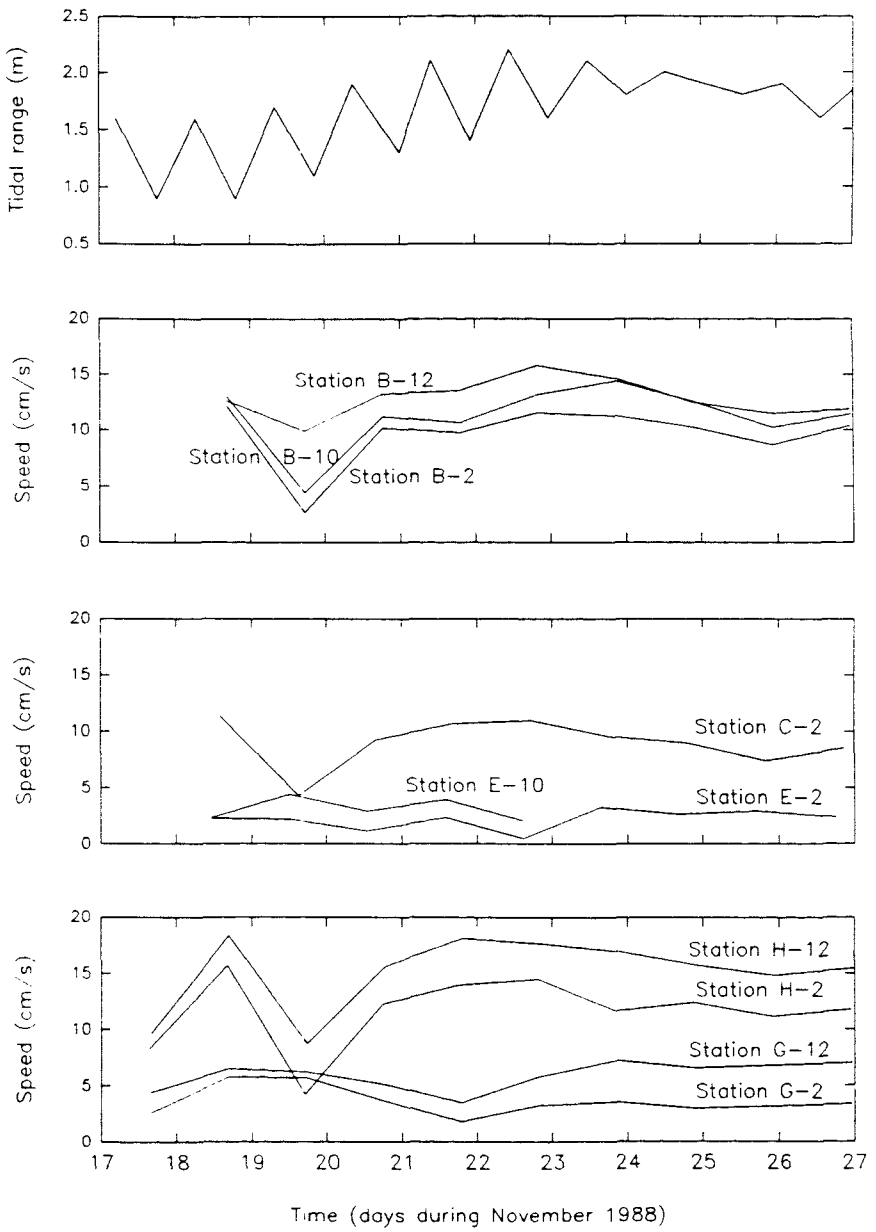

Figure 4.6a Residual current speed shown in relation to the tidal range at Lowestoft.

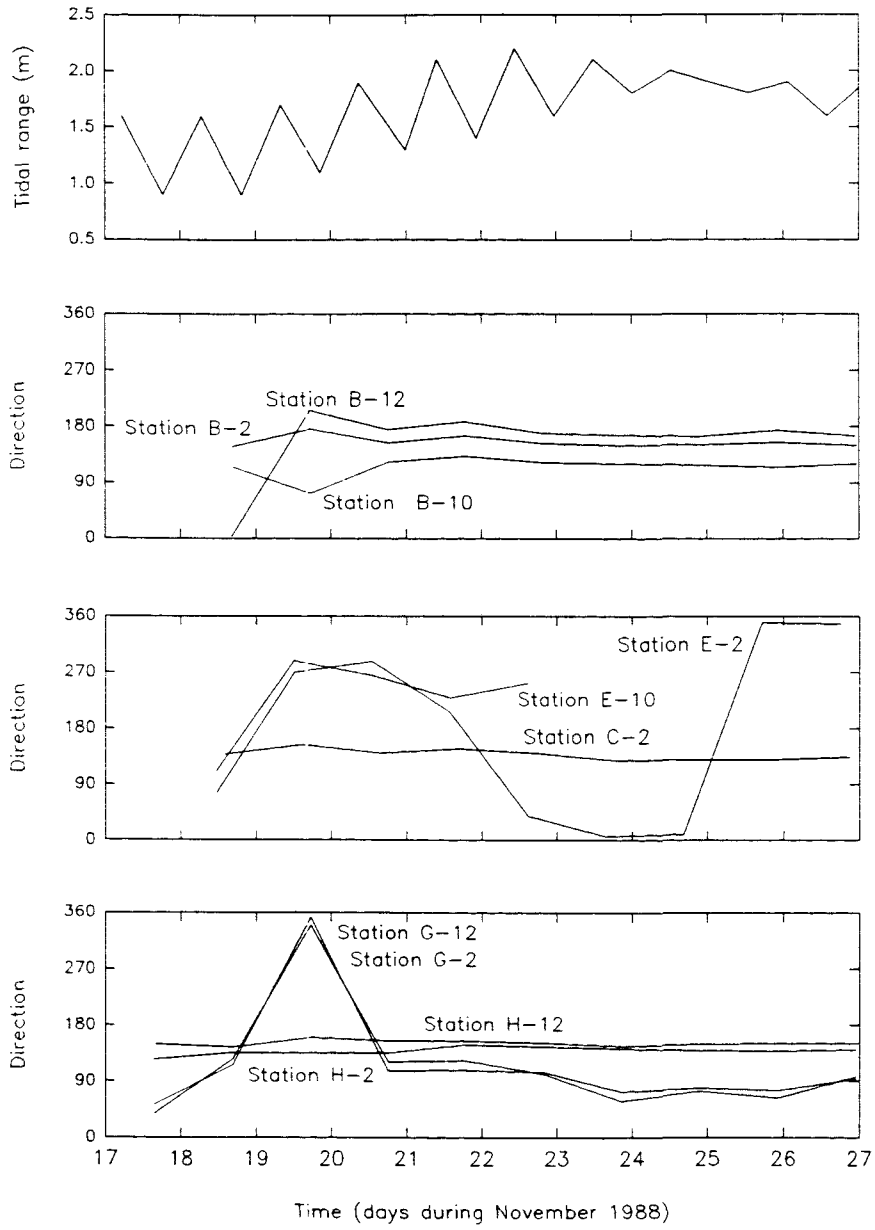

Figure 4.6b Residual current direction (°T) shown in relation to the tidal range at Lowestoft.

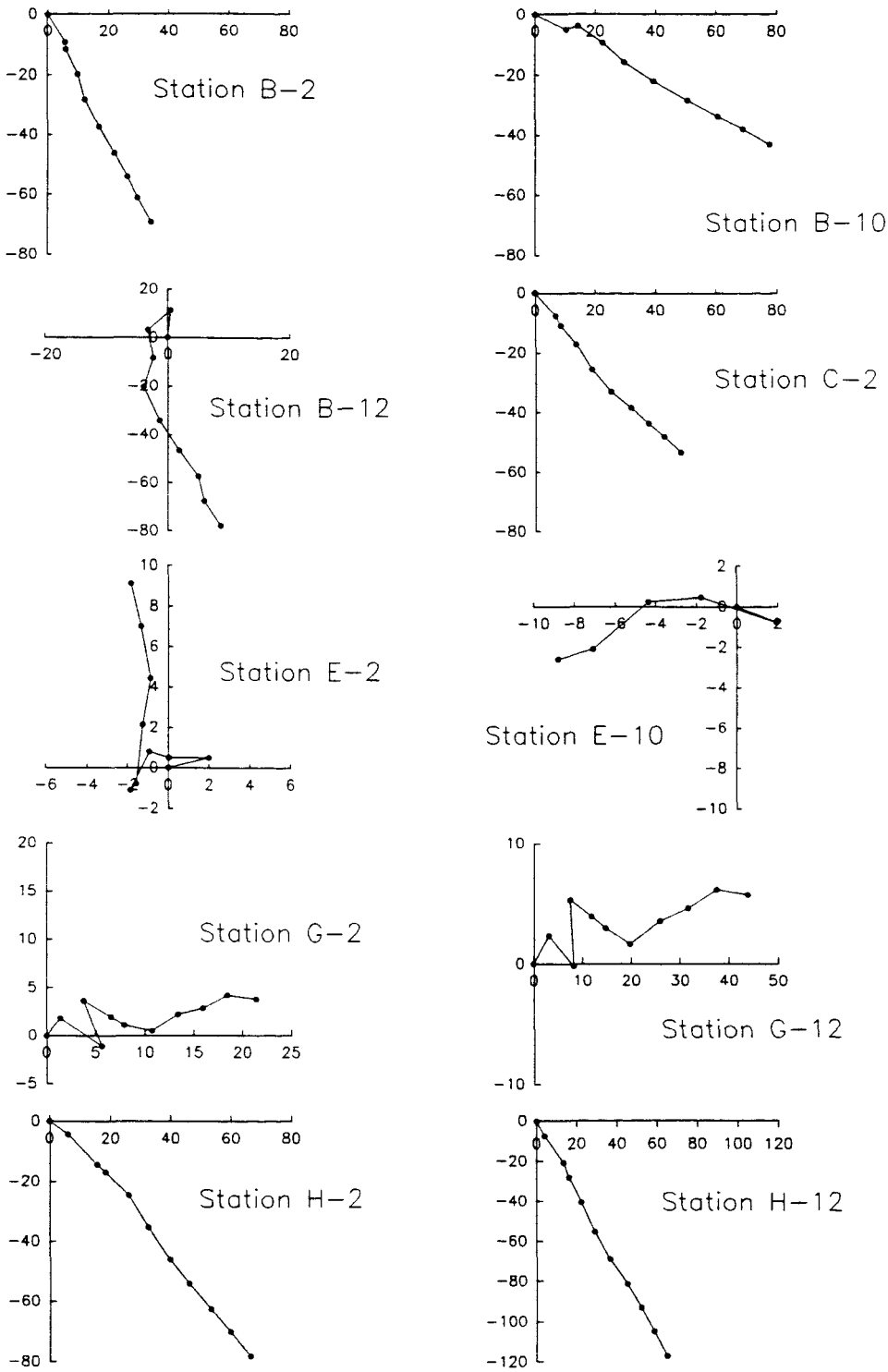

Figure 4.7 Patterns of water movement within the present study area, displayed as progressive vector diagrams. Movement is positive in northerly and easterly directions away from the start of the record (0,0). Black marks have been plotted at the end of each day; the scale is cm s^{-1}.

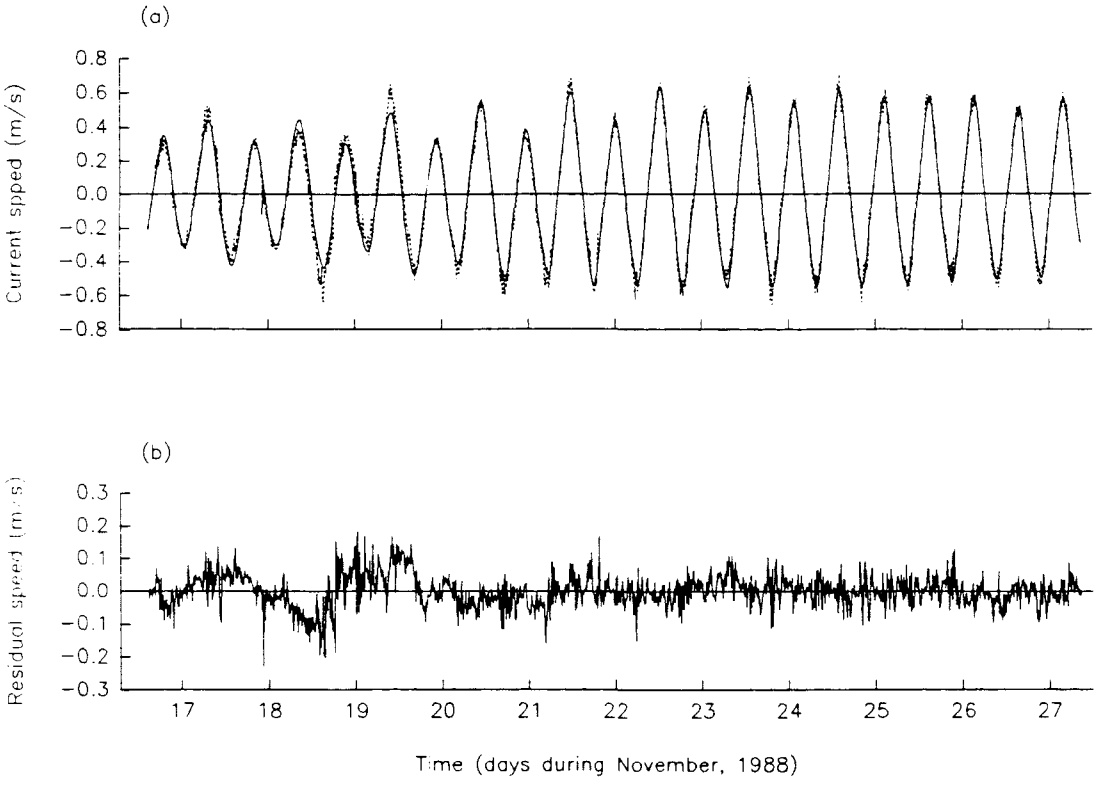

Figure 4.8 TIRA output for the analyses undertaken on the data collected for the north-south (v) component of the water flow at Station G-2: (a) observed tidal current data (dashed curve) and the approximation to the observed data based on harmonic constituents (solid curve); and (b) residual water movements not accounted for by harmonic analysis of the observed data from the self-recording current meter.

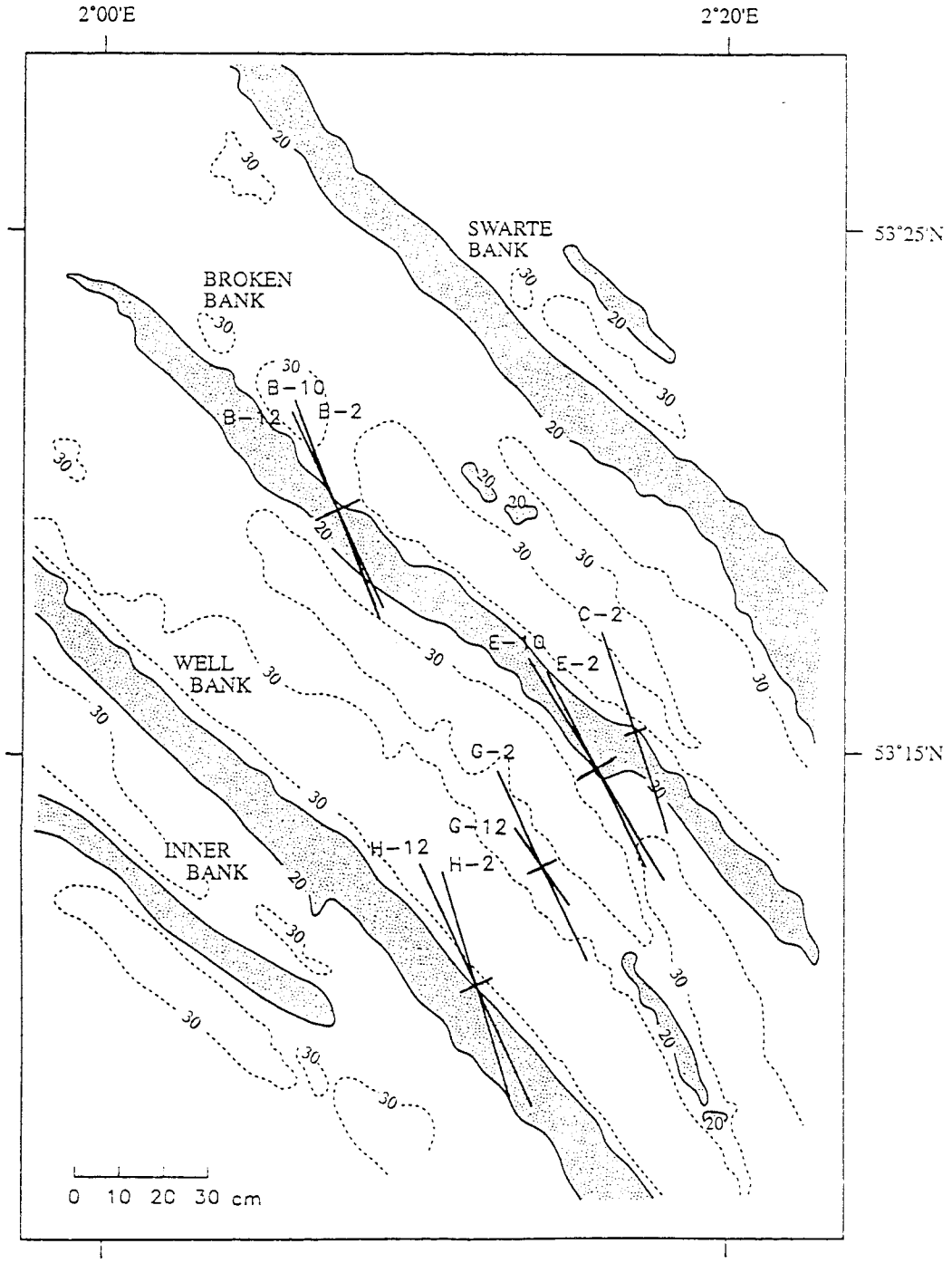

Figure 4.9a Main axes of the tidal ellipses, constructed from the TIRA output, for the M_2 constituent.

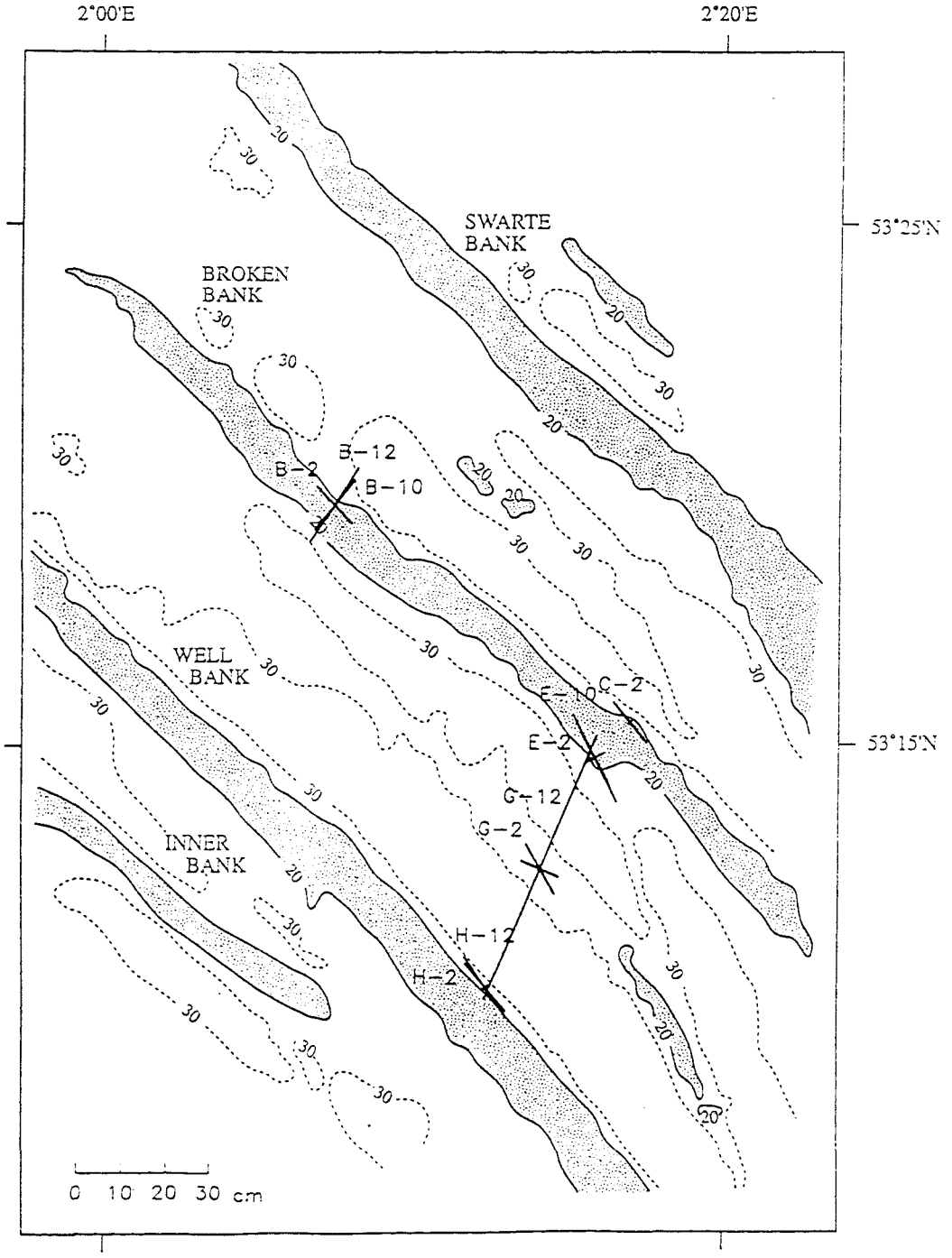

Figure 4.9b Main axes of the tidal ellipses, constructed from the TIRA output, for the S_2 constituent.

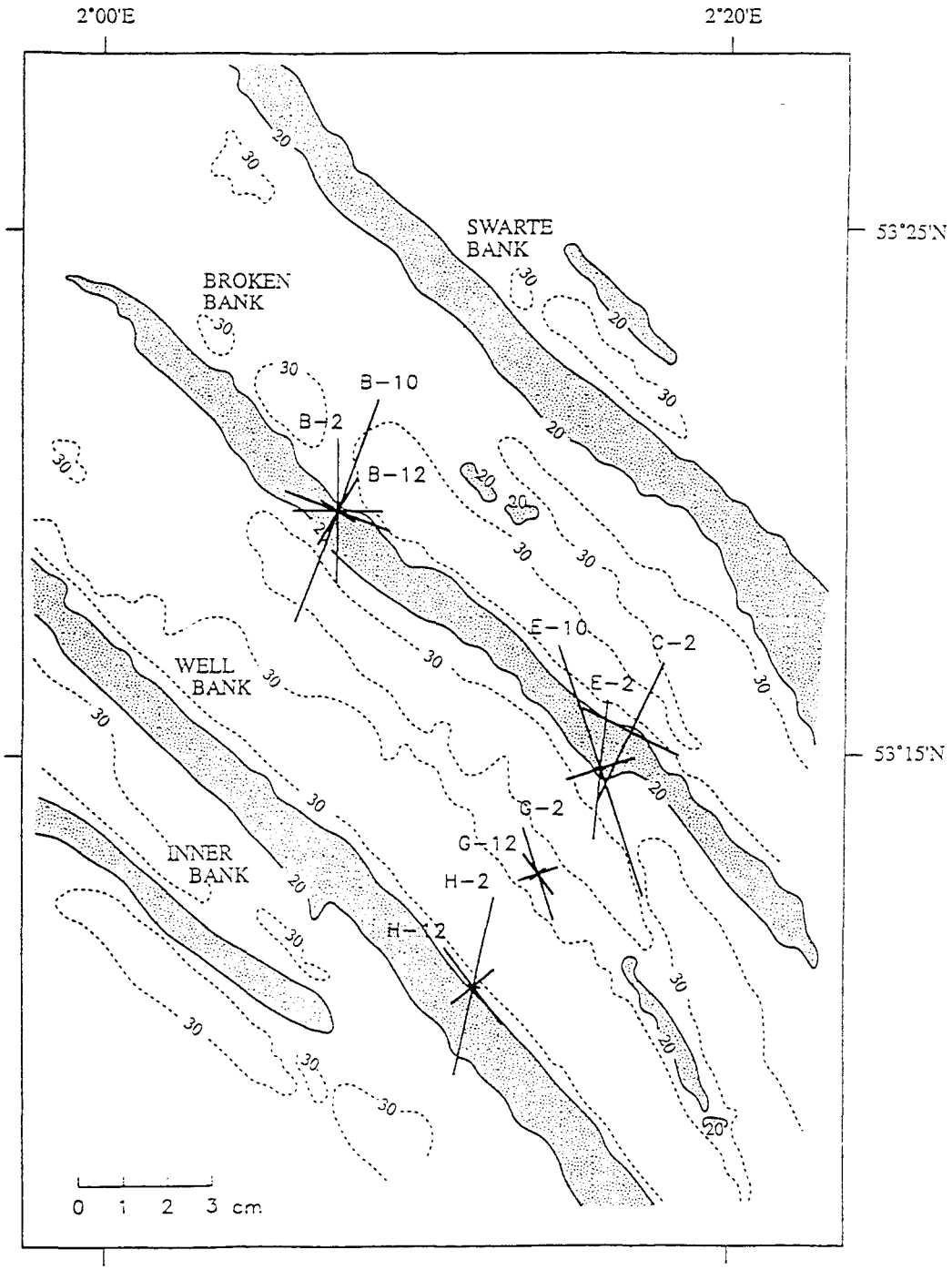

Figure 4.9c Main axes of the tidal ellipses, constructed from the TIRA output, for the M_4 constituent.

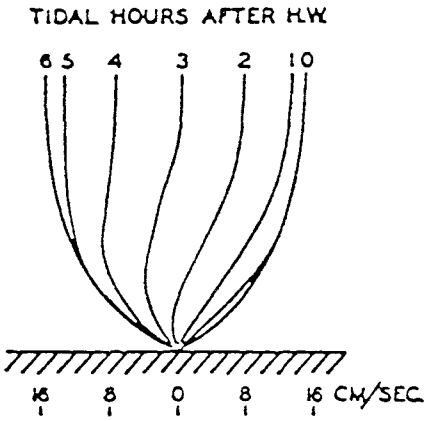

Figure 4.10 Velocity distribution for an idealized progressive wave propagating through water of a finite depth, with turbulent stresses reducing the velocity to zero at the boundary (from Mofjeld, 1976).

Chapter 5
WAVE-CURRENT INTERACTION AND SEDIMENT TRANSPORT

5.1 INTRODUCTION

Geologists, sedimentologists and oceanographers are required frequently to predict sediment transport rates on the continental shelf. The choice of suitable sediment transport equations is, however, far from obvious. In particular, no formulae have been developed for use in the sea under reversing tidal currents; most are based upon steady-flow concepts (Section 3.5); further, none can intrinsically account for the effects of waves.

Whilst there have been extensive comparisons of the predictive ability of these equations in relation to river and flume data (e.g. Ackers and White, 1973), there have been few attempts to compare them with marine transport rate observations (Gadd *et al.*, 1978). This limitation is due largely to the difficulty of obtaining sediment transport measurements in the sea, together with contemporaneous hydrodynamic data.

Sediment transport in the marine environment is the result usually of both tidal currents and wave action. However, before accurate prediction of bedload transport rates can be attempted, detailed knowledge of wave-current interaction and the shear stress distribution within the bottom boundary layer must be known. Complex flow processes in the near-bed region make the estimation of bed shear stress within combined wave-current flows difficult. Wave and steady (in comparison to wave activity) tidal current situations have been modelled separately successfully, whilst a number of theoretical combined wave-current flow models exist (e.g. Grant and Madsen, 1979; Christoffersen and Jonsson, 1985; Davies *et al.*, 1988; and Sleath, 1991).

However, wave-current bottom boundary layer models have not been tested adequately due to an absence of good quality field data. Dyer and Soulsby (1988) have shown, qualitatively, that the models generally predict the enhancement of the bed shear stress and the apparent bed roughness. Quantitatively, the output from model predictions varied significantly. Once the bed shear stress has been derived, further variation is encountered as different bedload transport equations often produce widely differing values from the same input conditions (see, for example, Heathershaw, 1981; Pattiaratchi and Collins, 1985).

In the present Chapter, tidally- and oscillatory wave-induced current data collected within 1 m of a rippled sand substrate (sediment-water interface) on the continental shelf, are used to improve the present level of understanding of physical processes within the near-bed region. Measured instantaneous current velocities have been used for the derivation of mean bed shear stresses (HR, 1991), which have been applied then to examine the relationship between bed roughness and bedform geometry; the magnitude of the form drag component of the total bed shear stress is investigated also. Bedload sediment transport rates, using 10 widely-reported formulae, have been determined using these shear stresses, integrated over a wave cycle. The predicted rates have been compared to sediment transport rates inferred from (observed) ripple migration rates.

5.2 FIELD SITE AND DATA COLLECTION

Hydrodynamic data and sea bed observations were obtained in the vicinity of well-developed sand banks in approximately 30 m of water off the Norfolk coast, UK, during November 1988. An autonomous multi-sensor tripod, STABLE (**S**ediment **T**ransport **A**nd **B**oundary **L**ayer **E**quipment (Humphery, 1987)), was used for this purpose. STABLE is capable of measuring simultaneous hydrodynamic conditions, due to waves and currents, together with the resulting response of the sea bed substrate.

The location of the STABLE bed frame is shown in Figure 4.1; it was deployed on

the southwestern flank of the Broken Bank for a period of approximately 3 days. Some 27 data sets were collected, with a photograph of the sea bed obtained at the beginning and end of each recording period. The mean water depth was approximately 29 m and the bed sediment consisted of well sorted sand, with a mean grain size of approximately 0.22 mm. More details concerning the hydrodynamics of the present study area are presented in Chapter 1. Further information on the deployment and data collection details have been presented by Collins (1991) and HR (1991).

The STABLE instrument suite consists of 2 orthogonally-arranged pairs of annular electromagnetic current meters, at approximate heights of 41 and 80 cm above the bed; these were used to record the 3 components of current velocity. A pressure sensor was utilised to provide estimates of the mean water depth. The instruments were sampled in 'burst' mode, at 4 Hz for a period of 512 s at 2 hourly intervals. Sea bed observations were obtained using a 35 mm camera, located at 1.25 m above the bed and looking vertically downwards. The sea bed was illuminated obliquely by a flashlight, angled at approximately 44° from the horizontal. Shadows were cast on the sea bed by two graduated bars positioned in the path of the flash light, at 0.25 and 0.325 m above the sea bed (Figure 5.1).

The use of STABLE has advantages when investigating near-bed hydrodynamics in that data acquisition can be undertaken at elevations close to the bed. Whilst deployments of this nature are relatively short in duration, the data acquisition can be at high frequencies, and provide an insight into short-term, microscale (Horikawa, 1981) processes.

5.2.1 Additional background information

The subsequent text is concerned with the interaction of steady and oscillatory flows, the influence of a rough boundary on this process and the subsequent movement of the sea bed sediments. As such, the *process* of wave-current interaction is under investigation here. It is felt by the writer, therefore, that the

inclusion here of further detailed background information, in addition to that presented in Chapter 3, is merited.

The formation and disappearance of sediment bedforms occurring under the action of waves and currents is the result of a complex interaction between the fluid and the underlying sediment which is poorly understood yet extremely important in both physical and numerical models of coastal processes. Bedforms affect bottom roughness and shear stresses, wave attenuation, and sediment transport. Improved predictors for bedform geometry will lead naturally to better models of coastal processes involving the movement of sediments.

The boundary shear stress depends upon sea bed roughness; this consists of two components represented by individual sand grains (skin friction) and the presence of bedforms (form drag). The influence of bedforms on bed roughness (k_s) has been related by many investigators to bedform height (η) and steepness (η/λ). Various formulae have been used to determine the roughness parameter. Shinohara and Tsubaki (1959) have suggested the following formula for the roughness parameter:

$$k_s = 7.5\eta\left(\frac{\eta}{\lambda}\right)^{0.57} \tag{5.1}$$

Nielsen (1983) used laboratory measurements of wave energy dissipation and suggests that the physical roughness is dependent upon the steepness alone:

$$k_s = 8\frac{\eta}{\lambda} \tag{5.2}$$

In a recent investigation under wave-dominated conditions, Xu and Wright (1995) have proposed a roughness formula that incorporates Nielsen's (1983) model. van Rijn (1982) analyzed flume and field data and has presented the following formula:

$$k_s = 1.1\eta(1 - \exp^{-25\frac{\eta}{\lambda}}) \tag{5.3}$$

within the limits,

$$\begin{aligned} 0.08 \leq h \leq 0.75\ m \\ 0.25 \leq U \leq 1.1\ ms^{-1} \\ 0.1 \leq D_{50} \leq 2.4\ mm \end{aligned} \tag{5.4}$$

where h and U are the flow depth and velocity respectively. Grant and Madsen (1982) and Raudkivi (1990) suggest, in an approach similar to that of Lettau (1969) and Swart (1976), that k_s is proportional directly to the ripple height and concentration:

$$k_s = \alpha \eta \left(\frac{\eta}{\lambda} \right) \tag{5.5}$$

Grant and Madsen (*op. cit.*) suggest a value of 27.7 for α. Their formula has been derived for wave-generated ripples; it has performed well in situations in which the sediment transport layer was minimal or absent. Raudkivi (*op. cit.*) suggests that the value of α is dependent upon the height, aspect ratio and concentration of the roughness elements on the sea bed, varying between 12.9 and 15.8.

Drake *et al.* (1992), in an approach based upon field observations, have suggested a new formula which is a modification of the Grant and Madsen (*op. cit.*) formula; this permits the angle between ripple crest and current direction (θ_{cr}) to be taken into account:

$$k_s = 27.7 \eta \left(\frac{\eta}{\lambda} \right) - 0.14(90 - \theta_{cr}) \tag{5.6}$$

The geometry of sea bed ripples depends significantly upon the prevailing (superimposed) sediment transport conditions. Ripples have been shown to develop during times when the sediment is moving primarily as bedload (Wiberg and Harris, 1994). Under purely oscillatory flows, bed ripples tend to be symmetrical in their cross section, with broad troughs and narrow crests. The super-position of a mean current on an oscillatory flow can add a degree of asymmetry to the ripples, in the direction of the mean flow; asymmetry in the wave-induced orbital velocities can also cause ripple asymmetry (Clifton and Dingler, 1984). Accurate

specification of the bed roughness for a ripple-covered sea bed is necessary in order that reliable estimates of bed shear stress may be obtained (Section 3.1.2).

5.3 METHODS OF DATA ANALYSIS

5.3.1 Photographic data (ripple characteristics, bedload transport rates)

Wave-current interaction models are heavily dependent upon the (bed) roughness caused by the sediment and the presence of any bedforms. Sequential bottom photographs were used to record the local sea bed topography throughout the deployment; these provided estimates of the ripple characteristics, from which physical bottom roughness estimates could be obtained. Likewise, a recognised way of improving the accuracy of sediment transport predictions is to compare the different formulations against accurate field measurements. However, such measurements of bedload transport are difficult to obtain. The determination of ripple size characteristics and migration rates across the sea bed provides potentially a non-intrusive method of determining bedload transport rates. Thus, by photographing the sea bed, both these requirements can be satisfied. The method adopted here has been described previously by Sternberg (1967) and Kachel and Sternberg (1971). Recently, observations of time-lapse bed geometry at a southern North Sea location have been converted into bedload transport rates by Huntley *et al.* (1991).

Sea bed topography has been investigated by casting the shadow of a known object onto the sea bed. In this way the light source produces, at the bed, the shadow of a solid and straight bar. Distortion of the shadow from a straight, true representation of the bar is due then to local sea bed topography. The distorted shadow can be observed and recorded by photographic means. On the basis of a knowledge of the relative positions of the camera, flashlight and shadow bars, the local variation in the height of the sea bed can be determined directly from the trace of the shadow (see below).

(a) Determination of the sea bed topography

The geometry of the STABLE rig is presented in Figure 5.1. In the Figure it has been assumed that the light source is sufficiently far enough away from the shadow bars so that consecutive light rays passing the shadow bar can be considered to be parallel to one another. Thus, the problem reduces to one of 2-dimensional geometry only. The method of interpretation of the photographs adopted here is similar to that described by Wilkinson *et al.* (1985).

From Figure 5.1 the perpendicular height between the shadow bar (R), and the sea bed at point S must be determined so that the area of the sea bed which has been photographed can be obtained.

a) Determination of focal length

Firstly, the focal length (f) of the camera needs to be derived. From similar triangles:

$$\frac{AB}{AD} = \frac{CB}{RD} \tag{5.7}$$

$$f = AD\frac{CB}{RD} \tag{5.8}$$

RD is the perpendicular distance from the centre of the shadow bar to the centre of the photograph. Substituting the known (measured) values of AD and RD (in cm), gives:

$$f = \frac{99.7}{17}CB \tag{5.9}$$

CB is the distance RD, but measured on the photograph (image plane). From the photographs, it may be determined that:

$$CB = 7.4 + \frac{0.7}{2} = 7.75 \tag{5.10}$$

The 0.7 value is the diameter of the image of the shadow bar. The focal length (f) can now be determined as:

$$f = 45.45 \tag{5.11}$$

b) Definition of h (RG)

From similar triangles,

$$\frac{RS}{GS} = \frac{\sqrt{Z_L^2 + Y_L^2}}{Y_L} \tag{5.12}$$

Substituting for GS gives:

$$RS = \frac{\sqrt{Z_L^2 + Y_L^2}}{Y_L}(RD + ES) \tag{5.13}$$

Using similar triangles

$$\frac{ES}{BS'} = \frac{AE}{f} \tag{5.14}$$

from which ES can be given as:

$$ES = \frac{(AD + DE)BS'}{f} \tag{5.15}$$

which gives:

$$ES = \frac{(AD + h)BS'}{f} \tag{5.16}$$

Substituting Equation 5.16 into Equation 5.13 gives:

$$RS = \frac{\sqrt{Z_L^2 + Y_L^2}}{Y_L}\left(RD + \frac{(AD+h)BS'}{f}\right) \tag{5.17}$$

$$RS = \frac{RD\sqrt{Z_L^2 + Y_L^2}}{Y_L} + \frac{BS'\sqrt{Z_L^2 + Y_{L_2}}}{fY_L}(AD+h) \tag{5.18}$$

From similar triangles,

$$\frac{RS}{h} = \frac{\sqrt{Z_L^2 + Y_L^2}}{Z_L} \tag{5.19}$$

$$RS = \frac{h}{Z_L}\sqrt{Z_L^2 + Y_L^2} \tag{5.20}$$

Substituting Equation 5.20 into Equation 5.18 and then dividing by the terms within the square-root gives:

$$\frac{h}{Z_L} = \frac{RD}{Y_L} + \frac{BS'}{fY_L}(AD+h) \tag{5.21}$$

$$h\left(1 - \frac{Z_L}{Y_L}\frac{BS'}{f}\right) = \frac{Z_L}{Y_L}RD + \frac{Z_L}{Y_L}\frac{BS'}{f}AD \tag{5.22}$$

Therefore,

$$h = \frac{RD + \frac{BS'}{f}AD}{\left(\frac{Y_L}{Z_L} - \frac{BS'}{f}\right)} \tag{5.23}$$

The STABLE rig system was constructed such that it included two shadow bars so that, in principle, both edges of each shadow cast on the sea bed could be used to provide four profiles of the sea bed. The shadow of one bar only was consistently

within the area of sea bed photographed; the shadow of the upper bar was frequently too close to the edge of the field of view to be used. Both edges of the shadow cast by the lower shadow bar were used to obtain local sea bed topography; these were digitised then with each profile requiring 80 to 140 points, depending upon the complexity of the shadow. The area of sea bed photographed and the profile of the sea bed are related to the distance between the shadow cast on the sea bed and the position of the shadow bar (BS'), together with the magnification factor.

The magnification factor (related to the focal length of the camera) was determined using known distances marked along the shadow bar; the distance of the shadow bar below the camera; and the average elevation (for each photograph) between the bar and the sea bed. From similar triangles, combined with the average height (of each edge of the shadow) above the sea bed, the effective size of the 5 cm markings (on the shadow bar) were determined. Thus, the magnification factor between the bed and the photograph was determined.

(b) Observed sediment transport rates

Two methods of determining the volume of sediment in motion, as a ripple migrates across the sea bed, are investigated within the present study.

Adopting a simple approach, the rate of migration was measured using the ripple crests. A simple relationship was assumed then between the migration rate and the volume of bed material being transported. For a ripple of height η, migrating at a rate U, the mean sediment volume per unit width per unit time is approximately equal to $0.5\eta U$ (e.g. Dyer, 1986). The transport rate over the ripple crest is twice this average rate, whilst that at the ripple trough is zero. Allen (1970), Rubin and McCulloch (1980), Langhorne (1981, 1982) and van den Berg (1987) have proposed the relationship:

$$I_b = \frac{1}{2}\,\eta\left[\frac{\lambda}{t}\right](\rho_s-\rho) \tag{5.24}$$

where I_b is the immersed weight transport rate and λ is the wavelength of the ripples observed on the sea bed. Thus, the transported volume is equivalent to the ripple volume (per unit width). Bagnold (1941) and later Kachel and Sternberg (1971) and Yang (1986) proposed the relationship:

$$I_b = \eta\left[\frac{\lambda}{t}\right](\rho_s-\rho) \tag{5.25}$$

These investigators argue that sand transport is equivalent to the trapezoid defined by the prograding face through time i.e. $\eta\lambda$. Mean transport, over the bedform as a whole, is proportional to the mean bedform elevation, $\eta/2$. Allen (1970) has shown that grains are transported twice (on average) during the migration of the ripple form. If no by-passing is assumed, the average distance travelled during the two transportation events can be no greater than λ and gives a mean path length of $\lambda/2$. Thus, mass transport is given by:

$$I_b = 2\frac{\eta}{2}\frac{\lambda}{2}(\rho_s-\rho) \tag{5.26}$$

or

$$I_b = \frac{\eta}{2}\lambda(\rho_s-\rho) \tag{5.27}$$

Viewed simply, the approach suggested by Allen (*op. cit.*), Rubin and McCulloch (1980), Langhorne (1981, 1982) and van den Berg (1987) (Equation 5.26) yields the *mean* transport rate. The approach of Bagnold (*op. cit.*) and later Kachel and Sternberg (*op. cit.*) and Yang (*op. cit.*) (Equation 5.27) yields the *maximum* value. Immersed weight transport rates have been obtained here by adopting the mean value approach.

The second method of determining the volume of sediment in motion is to record the profile of the local sea bed at two instances in time, then overlaying the two

profiles. The cross-sectional area changes due to the migrating ripples can then be measured and used to give estimates of the volumetric bedload transport rate (Huntley *et al.*, 1991). When several ripples are present within the sea bed area being photographed, this method enables multiple estimates of the transport rate to be obtained from each photo-pair. For ripples migrating without any change in shape, these estimates would agree with those based upon ripple dimensions.

5.3.2 Hydrodynamics

Instantaneous horizontal currents (u,v) were measured at heights of 41 cm and 80 cm above the sea bed. Here, u is the fore-aft velocity (positive into STABLE) and v is the transverse velocity (positive from port to starboard of STABLE). The mean tidal speed at each height was calculated by:

$$S = (U^2 + V^2)^{0.5} \tag{5.28}$$

where U and V are the mean current speeds. The mean tidal direction relative to the axes of STABLE, was given by:

$$\psi = \tan^{-1}\left(\frac{V}{U}\right) \tag{5.29}$$

Equivalent parameters for the wave orbital motions have been derived similarly.

'Observed' bed shear stresses have been determined for each burst on the basis of several independent approaches (HR, 1991). Estimates were made based upon the magnitude of the Reynolds stresses at both elevations, and upon the turbulent kinetic energy at both elevations. A further estimate was determined based upon the average of these 4 values. Estimates based upon the turbulent kinetic energy (E) are in closest agreement with the recorded flow data; hence, they have been chosen to represent the stresses active on the sea bed for the remainder of the present investigation. E is determined by:

$$E = \frac{1}{2}\left(\overline{u_t^2} + \overline{v_t^2} + \overline{w_t^2}\right) \tag{5.30}$$

where u_t, v_t and w_t are the turbulence variances in the x, y and z directions, respectively, at 80 cm above the sea bed. The bed shear stress is determined by

$$\tau_0 = a\rho E \tag{5.31}$$

where a is a constant of proportionality, taken to be equal to 0.19 (observed in a wide variety of flows (Soulsby, 1983)).

The wave shear stress (τ_w) has been obtained using the boundary layer model of Sleath (1991) for each burst.

5.3.3 Bed roughness analysis

In the present investigation, an iterative technique using Sleath's (1991) model (and the recorded hydrodynamic data) has been used to determine the roughness parameter for each burst. The roughness parameter is adjusted within the model, so that the mean shear stress produced matches the observed shear stress.

The relationship between the roughness values obtained in this way has been compared with the recorded hydrodynamic data and sea bed observations. The performance of existing formulae (Section 5.2.1) to reproduce the roughness values derived in the present investigation has been investigated.

5.3.4 Predicted bedload transport rates

Estimates of bedload transport rates have been based upon shear stress values described previously. Bed shear stresses and friction velocities determined from flow data recorded 0.8 m above the bed are associated, however, with bed roughness due to both skin friction and form drag. Hence, an attempt has been made to identify the contribution of each roughness component (skin friction and form drag), to the total drag.

For transport applications, the force applied to individual particles should be used

i.e. the total shear stress acting on the rippled bed should not be used, only that proportion which represents the skin friction. Using the boundary layer model of Christoffersen and Jonsson (1985), friction velocities based upon recorded flow data (at 0.8 m above the bed) and k_s equal to the grain diameter and 'measured' bed roughness, have been determined. Assuming a logarithmic velocity profile, the corresponding flow velocity at the height of the wave boundary layer has been evaluated. These velocities (and heights) were used then to obtain friction velocities, with k_s=grain diameter; hence, they are dependent only upon grain roughness (G. Voulgaris, pers. comm.).

The thickness of the boundary layer (δ_w) has been calculated, using

$$\delta_w = A\kappa\frac{u_{*w}}{\sigma} \tag{5.32}$$

where $\sigma=2\pi/T$. Grant and Madsen (1982) and Grant and Glenn (1983) suggest, in the above equation, that $A=2$. In contrast, Christoffersen and Jonsson (*op. cit.*) derived the boundary layer thickness on the basis of a theoretical approach and have suggested that $A=0.367$.

The approach adopted here has been to accept that the velocity profile obtained from Sleath (1991) provides a friction velocity (u_*) and a roughness length (z_0), which are subject to both skin friction and form drag. If these values were to be used to determine sediment transport rates, then the derived rates would be expected to overestimate the naturally-occurring rates.

From the velocity profile, a friction velocity has been evaluated at a height above the bed equivalent to the height of the roughness elements. Below this level, a velocity profile has been shown to exist (Kemp and Simons, 1983b). This logarithmic profile is dependent only upon the grain roughness. The friction velocity obtained this way is independent, therefore, of the influence of form drag of the bedforms (Figure 5.2).

The proportion of the shear stress used in overcoming form drag can be determined. The skin friction component of the total shear stress is given by:

$$\frac{u_{*(n)}}{u_*} \tag{5.33}$$

where $u_{*(n)}$ is the friction velocity resulting from the roughness of the sediment grains alone; whilst u_* is the friction velocity resulting from the roughness of the sea bed sediment and bedforms.

(a) Transport under the combined action of waves and currents

In the marine environment, where waves and currents are superimposed, the forces (stresses) acting on the sea bed sediment can be separated into those resulting from: (i) a steady flow (tidal current) component (τ_c); and (ii) an oscillatory (wave) component (τ_w), which is a time-varying quantity with a period of oscillation equivalent to the period of the waves. Due to the non-linear interaction between these forces, the calculation of each of the above vectors is a complicated procedure. Several authors have developed, however, models to deal with this particular problem (e.g. Grant and Madsen, 1979; Christoffersen and Jonsson, 1985; and Sleath, 1991). The total bed shear stress (τ_b) is provided by the vector sum of the two components, so that the instantaneous bed shear stress is given by:

$$\vec{\tau}_b(t) = (\vec{\tau}_x(t), \vec{\tau}_y(t)) \tag{5.34}$$

where

$$\vec{\tau}_x(t) = \vec{\tau}_w \cos(\frac{2\pi t}{T} + \phi) + \vec{\tau}_c \cos(\phi_{wc}) \tag{5.35}$$

$$\vec{\tau}_y(t) = \vec{\tau}_c \sin(\phi_{wc}) \tag{5.36}$$

where τ_x and τ_y are instantaneous bottom stress components in directions parallel and perpendicular to the wave propagation, respectively; T is the wave period, ϕ is the phase difference between the orbital velocity and wave shear stress, and ϕ_{wc}

is the angle between the waves and the currents (Figure 5.3).

The amount of sediment being transported is dependent upon the magnitude of the bottom shear stress. However, depending upon the relative magnitude of waves and currents, the resultant shear stress can be quite variable (in terms of magnitude and direction) throughout the wave cycle. In order to account for such variability, instantaneous sediment transport rates can be calculated for each (orthogonal) direction:

$$\vec{I}_{bx}(t) = F(|\tau_b(t)|,\tau_{cr})\frac{\vec{\tau}_x(t)}{|\tau_b(t)|} \tag{5.37}$$

$$\vec{I}_{by}(t) = F(|\tau_b(t)|,\tau_{cr})\cdot\frac{\vec{\tau}_y(t)}{|\tau_b(t)|} \tag{5.38}$$

where F is the function associating bottom shear stress to bedload transport rates.

For formulae which require the use of a depth-integrated mean current, the instantaneous mean current is calculated following a similar approach. Hence, the depth-integrated mean current can be estimated by assuming a logarithmic vertical profile (Equation 3.4, here $u(z) \equiv u_z$) and given, by definition, to be:

$$\langle U \rangle = \frac{1}{h-z_o}\int_{z_o}^{h} u(z)\, dz \tag{5.39}$$

An assumption made in the calculation, valid at least for shallow coastal waters, is that the wave-induced velocity remains constant from the top of the wave boundary layer (δ_w) to the mean water surface. No estimation of the vertical distribution of velocity inside the wave boundary layer is considered, since this is very thin (i.e. of the order of 1 to 2 cm); this does not affect, therefore, the results of the transport formulae predictions.

The instantaneous wave-induced orbital velocity is given by:

$$u(t) = U_{rms}\cos(\frac{2\pi}{T}t) \tag{5.40}$$

The instantaneous depth-integrated wave-current velocities, at (400) discrete time intervals (sufficient to obtain reliable results (G. Voulgaris, pers. comm.)) along the direction of wave propagation (x), and perpendicular to the wave propagation (y), $\hat{U}_x(t)$ and $\hat{U}_y(t)$ respectively, are given by:

$$<U>_x(t) = <U>\cos(\phi_{wc}) + U_{rms}\cos(\frac{2\pi}{T}t) \tag{5.41}$$

$$<U>_y(t) = <U>\sin(\phi_{wc}) = constant \tag{5.42}$$

As the x-direction is parallel to that of wave propagation, the combined velocity in the y direction is constant, dependent only upon the tidal current velocity. The x and y components of instantaneous sediment transport rates are presented as described above, for equations where I_b is a function of bottom shear stress (cf. Equations 5.37 and 5.38).

The mean (immersed weight) sediment transport rate, over a wave period is given then for each direction, by:

$$I_{bx} = \frac{1}{T}\int_{t=0}^{t=T} I_{bx}(t)\,dt \tag{5.43}$$

and

$$I_{by} = I_{by}(t) = constant \tag{5.44}$$

Hence, the total sediment transport rate ($\mathbf{I_b}$) and direction (ϕ_{Ib}), with reference the wave direction (x-axis), are given by:

$$I_b = \sqrt{I_{bx}^2 + I_{by}^2} \tag{5.45}$$

and

$$\phi_{I_b}=\tan^{-1}\left(\frac{I_{by}}{I_{bx}}\right) \qquad (5.46)$$

(b) Bedload transport rate formulae

Within the present investigation, the performance of 10 sediment transport equations (see Section 3.5) are examined. Sediment transport is presented either as volumetric or mass transport rates. Here, for consistency, all the formulae have been re-arranged so that their output is presented in terms of an immersed weight sediment transport rate (I_b, W m^{-2}). Also, all the input/output variables are expressed in SI units. In order to use the formulae for rippled bed conditions, the skin friction component of the shear stress (rather than the total stress) is used in the computations.

(c) Threshold criteria for the initiation of sediment movement

For sediment transport rates to be determined it is necessary to adopt a threshold condition, below which the sediment motion is not initiated. The Shields' parameter for the initiation of sediment movement (Section 3.1.3) has been adopted for use within the present investigation.

5.4 RESULTS AND DISCUSSION

Twenty-seven burst data sets were collected with a photograph of the sea bed obtained at the beginning and end of each burst. During the deployment, measured tidal current speeds ranged from approximately 20 cm s^{-1} to 90 cm s^{-1}, whilst the root-mean squared (rms) orbital velocities ranged from approximately 10 cm s^{-1} to 24 cm s^{-1}, obtained using the spectrum splitting technique on the (orthogonal) recorded data, as described by Soulsby and Humphery (1989). The average recorded wave period was 10.3 s.

The transverse velocity component was consistently the dominant flow component, at both elevations above the bed (Figure 5.4). Hence, the flow velocities throughout the experiment were largely unobstructed by the framework of the STABLE tripod system.

The burst-averaged information recorded is shown in Figure 5.4. The tidal ellipse is relatively narrow (Figure 5.5) as tidal current velocities recorded are essentially co-directional. The main tidal axis recorded lies at approximately 320° relative to north and, as such, is approximately parallel to the axis of the Broken Bank. The burst-averaged hydrodynamic data which have been used in the present investigation are presented in Table 5.1.

The mean vertical distance between the shadow bar and the bed, varied throughout the deployment (Figure 5.6); the maximum variation was around 6 cm. The variation in the bed elevation appears to vary independently of the steady current velocity and the oscillatory current. Lower flow speeds might be expected to enhance the rate of settling of the sediment in suspension, raising the bed elevation. The overall bed elevation may be due, in fact, to the progressive settling of the rig into the sea bed sediments.

5.4.1 Wave activity

Wave orbital velocities (u_b) recorded at z=41 and 80 cm are presented in Figure 5.4. These values range from 10.8 cm s^{-1} to 20.0 cm s^{-1} at z=41 cm, and from 13.1 cm s^{-1} to 24.0 cm s^{-1} at z=80 cm. Figure 5.7 shows u_b at z=80 cm plotted against u_b at z=41 cm. The regression line has a slope of 1.22, whilst the orbital velocities exhibit a correlation coefficient between them of 0.99 (27 data points). Linear wave theory suggests that the difference between the orbital velocities at these elevations above the bed should be very small; hence, the slope of the line should be almost unity. Figure 5.7 shows that the orbital velocities at z=80 cm are consistently higher than the orbital velocities at z=41 cm, with the deviation from unity increasing with increasing wave activity.

For comparison, Soulsby and Humphery (1989) have presented data from a previous deployment of the STABLE rig, at a location to the southwest of the Isle of Wight. Here, the mean water depth was 25 m and the waves were of a similar period to those of the present investigation, over a flat featureless mixture of gravel, sand and shell with a median grain diameter of 12.5 mm. These investigators presented wave orbital velocity data recorded at 10 cm and 40 cm above the bed. The observations presented here correlate well with the data presented by these investigators, who found that the slope of the regression line was also 1.22, and with a correlation coefficient of 0.96 (28 data points). In common with the present data, deviation from the line of equality increased with increasing wave activity. Both orthogonal components recorded during the deployment (Figure 5.7) show also a consistent increase in the records obtained at 80 cm above the bed.

In order to explain the difference in orbital velocity with height above the sea bed, additional field data are required to resolve the oscillatory flow adjacent to the bed. Possible explanations of the increase in orbital velocity with height must be derived from theoretical considerations of wave-current interactions, although it would not appear that any mathematical model has simulated the results shown in Figure 5.7. Elsewhere, Davies *et al.* (1988) have shown numerically that the addition of a current ($U_{100} \approx 100$ cm s^{-1}), upon a wave-induced current ($U_0 = 100$ cm s^{-1}), will result in the formation of a wave boundary layer. The thickness of this layer will extend to approximately 10 cm above the bed. Figure 2(b), from Davies *et al.* (*op. cit.*), shows that the near-bed orbital velocity increases with height above the bed up to approximately 10 cm.

The prevailing oceanographic conditions presented by Davies *et al.* (*op. cit.*) are far in excess of the conditions encountered here. However, using Equation 5.32, the thickness of the wave boundary layer can be determined. For the computation, the average conditions encountered during the STABLE deployment have been used ($T = 10.3$ s and $\tau_w = 0.077$ kg m^{-1} s^{-2}). The extent of the wave boundary layer calculated using Grant and Madsen (1982) together with the Grant and Glenn

(1983) value of $A=2$, gives the thickness of the wave boundary layer to be 1.1 cm. Alternatively, the use of Christoffersen and Jonsson's (1985) value of $A=0.367$ derives the thickness of the wave boundary layer as 0.2 cm (ten times the mean diameter of the sediment grains). Jonsson and Carlsen (1976) have suggested the following formula for the determination of the wave boundary layer thickness (δ_w):

$$\frac{30\delta_w}{k} \log_{10}\frac{30\delta_w}{k} = m_\delta \frac{a_{1m}}{k} \tag{5.47}$$

where a_{1m} is the free stream particle amplitude, given by:

$$a_{1m} = \frac{u_{1m}}{\sigma} \tag{5.48}$$

where u_{1m} is the mean free stream velocity amplitude. m_δ is a factor determined by Jonsson and Carlsen from the test data; this was found to have a value of 1.1 cm.

Using the above equation for the average conditions recorded during the present deployment, the boundary layer thickness was found to be 1.1 cm; this is in agreement with the values derived using the formulae suggested by Grant and Madsen (1982) and Grant and Glenn (1983). This value (1.1 cm) agrees also with the studies of Soulsby and Humphery (1989), who used the equations of Jonsson and Carlsen (*op. cit.*) and Lambrakos (1982) to determine the thickness of the wave boundary layer. These investigators calculated that the wave boundary layer occupied a maximum of 1.5 cm of the water flow above the sea bed, to the southwest of the Isle of Wight.

Hannay *et al.* (1994) have suggested that the 10 cm value, presented by Davies *et al.* (1988), could be an underprediction; this would allow the lower sensor of the present investigation to be contained within the wave boundary layer and, hence, explain the differences observed in the orbital velocities at both heights. In light of the information presented earlier, it would appear that this interpretation would require further investigation. Further, it is possible that first order wave theory,

incorporated within most wave-current interaction models, may not be an accurate representation of the orbital velocities at this particular location. It would appear that further investigation into near-bed wave dynamics is required.

5.4.2 Bedform dimensions

A series of sea bed photographs, corresponding to 15 sampling 'bursts', were of high quality and showed clear images of the rippled sea bed; these were subject to detailed analysis. The profiles of 140 ripples were observed from the photographs obtained during the deployment. The maximum number of ripples observed in any single photograph was four; however, typically this value was two. Such data provided multiple estimates of the ripple dimensions relating to a particular burst sampling period.

Figure 5.8 presents two examples of the photographs obtained during the STABLE deployment, showing clearly the position of the shadow cast on the sea bed. At the same time, Figure 5.9 shows the sea bed profiles obtained from these photographs, using the method described above. Ripple heights and wavelengths were measured by observing the angle between the shadow bar and the crests of the bedforms.

The observed ripple profiles were predominantly asymmetric, with heights of between 0.4 and 2 cm (average 1.1 cm), and wavelengths of between 11 and 22 cm (average 15.3 cm). The 'burst-averaged' dimensions of the observed ripples are presented in Table 5.2. During the remainder of the bursts (i.e. those not summarised here), only sediment in suspension could be identified on the photographs (even after optimizing). At such times, the shadow bar on the image could not be distinguished clearly.

The height and spacing characteristics of the ripples observed on the sea bed have been investigated. Considerable variation in the ripple steepness was observed (Figure 5.10). For comparison, Allen (1968) has suggested elsewhere that, based upon field observations, that the relationship between the height of a ripple and its

wavelength is almost linear and is given by:

$$\eta = 0.074\lambda^{1.19} \tag{5.49}$$

where $0.4 \leq L \leq 60$ cm. This relationship is plotted on Figure 5.10 and can be seen to resemble closely the line of best fit for the results of the present investigation, whose equation is:

$$\eta = 0.15\lambda - 0.03 \tag{5.50}$$

This relationship has a correlation coefficient of 0.64 (37 data points). Although these lines exhibit similar gradients, the difference between the representations can be seen to widen with increasing ripple size. However, the results presented by Allen (1968) exhibited considerable scatter; as such they must be treated only as an order of magnitude estimate. Also shown on Figure 5.10 is the line of maximum vortex ripple steepness generated within a wave-dominated environment (Bagnold, 1946); this represents poorly the data observed in the present investigation.

Ripple steepness showed no sequential development, with time, throughout the period of the deployment. Likewise, there was no consistent variation in ripple steepness, with wave orbital velocity or steady current flow (Figure 5.11).

Mogridge *et al.* (1994) have re-evaluated wave-generated bedform geometry data published by various authors. These data have been investigated in terms of a 'period parameter', χ:

$$\chi = \frac{\rho D}{\gamma_s T^2} \tag{5.51}$$

where γ_s is the specific weight of the sediment. The data reviewed by these authors, together with the STABLE data, are shown in Figure 5.12. Two 'groups' of data can be seen, with the field data plotting distinctly away from that determined from experimental data. Mogridge *et al.* (*op. cit.*) have fitted a curve to the maximum bedform (wave) length data (Figure 5.13). On the basis of the

data presented in this Figure, representing the low values of χ (typically field data), there is evidence that the bedform (wave) length is dependent only upon sediment grain size i.e. where the curve is flat. The results from the present investigation plot within that group of data obtained from field investigations i.e. that of Inman (1957), Dingler and Inman (1976), Miller and Komar (1980a) and Nielsen (1981).

The ripple heights observed during the course of the present investigation exhibit less agreement with the results of Mogridge *et al.* (1994). Figure 5.14 shows the ripple height data reviewed in terms of the period parameter. Ripple height is more difficult to measure and, consequently, no observed ripple height data from the field studies reviewed by Mogridge *et al.* (*op. cit.*) were presented. Figure 5.14 is, therefore, only a review of laboratory-generated bedform geometry; this has been shown already to be at variance with field (wavelength) data. This observation is reinforced in relation to the STABLE data which is plotted a significant distance from the other data reviewed (Figure 5.14) and from the results of the curve-fitting exercise performed by Mogridge *et al.* (*op. cit.*) (Figure 5.15).

Results obtained as part of the present investigation are compared with those obtained by Amos *et al.* (1988) in Figure 5.16 together with those obtained by Miller and Komar (*op. cit.*). Miller and Komar (*op. cit.*) investigated laboratory data obtained on the geometry of oscillation ripples collected by a number of investigators using a variety of experimental devices. These investigators established a linear relationship between the wave orbital diameter (d_0) and the ripple spacing (λ, equivalent to the ripple wavelength):

$$\lambda = 0.65 d_0 \tag{5.52}$$

From the results presented in Figure 5.16, it may be seen that the average conditions experienced during the STABLE deployment period plot in the region of the relationship suggested by Miller and Komar (*op. cit.*) when the wave orbital diameter was determined using the root-mean-square wave height. Likewise, the

data presented in this Figure, representing the low values of χ (typically field data), there is evidence that the bedform (wave) length is dependent only upon sediment grain size i.e. where the curve is flat. The results from the present investigation plot within that group of data obtained from field investigations i.e. that of Inman (1957), Dingler and Inman (1976), Miller and Komar (1980a) and Nielsen (1981).

The ripple heights observed during the course of the present investigation exhibit less agreement with the results of Mogridge *et al.* (1994). Figure 5.14 shows the ripple height data reviewed in terms of the period parameter. Ripple height is more difficult to measure and, consequently, no observed ripple height data from the field studies reviewed by Mogridge *et al.* (*op. cit.*) were presented. Figure 5.14 is, therefore, only a review of laboratory-generated bedform geometry; this has been shown already to be at variance with field (wavelength) data. This observation is reinforced in relation to the STABLE data which is plotted a significant distance from the other data reviewed (Figure 5.14) and from the results of the curve-fitting exercise performed by Mogridge *et al.* (*op. cit.*) (Figure 5.15).

Results obtained as part of the present investigation are compared with those obtained by Amos *et al.* (1988) in Figure 5.16 together with those obtained by Miller and Komar (*op. cit.*). Miller and Komar (*op. cit.*) investigated laboratory data obtained on the geometry of oscillation ripples collected by a number of investigators using a variety of experimental devices. These investigators established a linear relationship between the wave orbital diameter (d_0) and the ripple spacing (λ, equivalent to the ripple wavelength):

$$\lambda = 0.65 d_0 \tag{5.52}$$

From the results presented in Figure 5.16, it may be seen that the average conditions experienced during the STABLE deployment period plot in the region of the relationship suggested by Miller and Komar (*op. cit.*) when the wave orbital diameter was determined using the root-mean-square wave height. Likewise, the

STABLE data plot very close to the data observed by Amos *et al.* (1988). These latter investigators used an autonomous, free-standing tripod (*Ralph*), deployed in 22 m of water on the Canadian continental shelf. The mean grain diameter of the sediments was 0.23 mm and the material was well sorted. As such, this particular site is somewhat similar to that used for deployment of STABLE. Interestingly, similar wave characteristics were observed during the two deployments; however significantly weaker tidal currents were observed during the *Ralph* deployment i.e. 35 cm s^{-1} maximum, whereas during the STABLE deployment the maximum tidal flow was 90 cm s^{-1}.

Figure 5.17 shows the relationship between maximum ripple spacing and the grain size of the sea bed sediments. On this Figure, the results of the field, water tunnel and wave flume investigations show reasonable agreement. On this basis, Miller and Komar (1980a) suggested the following empirical relationship between grain diameter and ripple spacing:

$$\lambda = 0.0028 D^{1.68} \tag{5.53}$$

where the grain diameter (D) is given in microns, and the ripple spacing (λ) is in centimetres. However, the ripple spacing/grain diameter relationship of those ripples generated on an oscillating bed mechanism showed a significant departure from this relationship (Figure 5.17). During the investigation undertaken by Amos *et al.* (*op. cit.*) and the present study, wave-induced velocities were lower than the steady (tidal) currents. The ripple geometry data obtained by both investigations are in close agreement with Equation 5.53.

Yalin (1977) has shown that the spacing of equilibrium ripples in quartz-density sand, under unidirectional flows, is dependent only upon the grain diameter and according to the relationship:

$$\lambda = 0.1 D \tag{5.54}$$

where D is again in microns and λ is in centimetres. With an average wavelength over the deployment of the present investigation of approximately 15 cm, for a sea

bed consisting of fine sand (0.2 mm), the ripples observed during the present investigation can be seen to obey closely the relationship suggested by Yalin (1977) (λ=0.08D). In a subsequent paper, Miller and Komar (1980b) found that the accuracy of the relationship given in Equation 5.52 was dependent upon the method of determining d_0 (see above); when there is a range of wave frequencies present, this is made more difficult.

The bedform geometry derived here has been compared with the results from previous investigations. From this analysis and discussion, the bedform geometry obtained from the STABLE deployment exhibits characteristics associated with both wave- and current-dominated ripples (a feature observed also by You (1996)). However, the ripples were observed under current-dominated conditions and were observed to be asymmetrical - a feature not associated with ripples generated under purely oscillatory flows. Nonetheless, on the basis of agreement with previous investigations into wave generated ripples, it would appear that the wave conditions present during the STABLE deployment may have had some influence on bedform geometry.

For many of the bursts of the present investigation, the edges of the shadow were difficult to distinguish clearly; this prevented accurate determination of the shadow profile. Ripple dimensions were found to be highly variable along an axis normal to their crests. Therefore, it is very possible that the shape of the ripples varied along their crests. Consequently, it is possible that the ripple dimensions observed using the photographs, together with the inferred bedload transport rates, are valid only for a small area of the sea bed.

The accuracy of the derivation of the bedform size must also be considered. The photographs were digitised by eye and were, therefore, somewhat subjective. Some of the bursts were associated with significant amounts of suspended sediment; such photographs could not be used to determine bedform dimensions. Hence, the dimensions presented here are related to the relatively lower flow conditions.

5.4.3 Bed roughness

The presence of ripples on a sea bed increases the hydrodynamic roughness of a bed, relative to the influence of grain roughness. Values of z_0 or k_s for ripples are not well established, although it appears that a reasonable estimate of the ripple-generated roughness parameter for symmetrical ripples is given by the product of the ripple height and the ripple steepness i.e. η^2/λ (see Grant and Madsen, 1982; Wiberg and Nelson, 1992).

The roughness derived from comparison of the Reynolds stresses with those obtained from the boundary layer model, is examined now in relation to other recorded data. Values of the roughness parameter (k_s) were found to be dependent upon the height of the roughness elements and, similar to the relationship suggested by Drake *et al.* (1992), the angle between the ripple crests and the steady current direction (Figure 5.18). This relationship can be represented by:

$$\log(k_s) = K_1 \eta \cos\theta_{cr} - K_2 \tag{5.55}$$

The values of K_1 and K_2, based upon a line of 'best fit' through the data, were found to be 4.09 and 3.42, respectively.

These values are, in effect, measurements of bed roughness. As such, these 'measured' roughness values are compared now with the values obtained from the 6 formulae described earlier (Section 5.2.1). The ratio of predicted to measured values has been evaluated in terms of an error parameter P, which is given by:

$$P = \frac{k_s(predicted)}{k_s(measured)} \tag{5.56}$$

The results of this investigation into predicted bed roughness values are presented in Table 5.3, where the wide range of values of P associated with the present investigation can be identified. Equations with P values lying closest to unity have most accurately reproduced the observed roughness values. Overall, three bands of accuracy were investigated: $1/2 \leq P \leq 2$, $1/3 \leq P \leq 3$ and $1/5 \leq P \leq 5$.

Of the formulae investigated here, three provide roughness estimates that are similar to those obtained by comparing the Reynolds stresses with those obtained using the model of Christoffersen and Jonsson (1985). Overall, the roughness values predicted by the formulae of van Rijn (1982), Nielsen (1983) and Raudkivi (1990) were 1.25, 0.87 and 1.36 times the 'measured' values, respectively. However, there is considerable scatter about these mean values; You (1996) found that many existing formulae failed to predict bed roughness accurately. The better performance of the Nielsen model, though slight here, is found also in a recent investigation within a wave-dominated continental shelf environment where bed roughness under moderate wave energy conditions has been found to be predicted adequately by Nielsen's (*op. cit.*) model (Xu and Wright, 1995). For moderate and high energy conditions, however, these investigators proposed a modification to Nielsen's (*op. cit.*) model that was proportional to a maximum skin friction Shields' parameter. Within the present investigation, the formulae of Shinohara and Tsubaki (1959) and Grant and Madsen (1982), however, provided a greater number of roughness estimates within the widest tolerance band. Drake *et al.*'s (1992) modification of Grant and Madsen's (*op. cit.*) formula, when applied to the observations obtained here, produced values which were inconsistent with those 'measured'. In the present investigation, θ_{cr} varied between 18° and 57°, a range similar to that experienced by Drake *et al.* (5° to 46°). However, the hydrodynamic setting in which this investigation was undertaken was subject to relatively low currents and waves and, therefore, considerably different from the present study area.

5.4.4 Bedload transport rates

Transport rates were obtained from the sea bed photographs using two different approaches (see above). The method described by Huntley *et al.* (1991) derived a wide spread of transport rates; this may be due to the problem of correctly identifying the same ripples in consecutive photographs (ripple aliasing), a problem noted by these investigators during a deployment in the southern North Sea. The approach suggested by Allen (1970), Rubin and McCulloch (1980),

Of the formulae investigated here, three provide roughness estimates that are similar to those obtained by comparing the Reynolds stresses with those obtained using the model of Christoffersen and Jonsson (1985). Overall, the roughness values predicted by the formulae of van Rijn (1982), Nielsen (1983) and Raudkivi (1990) were 1.25, 0.87 and 1.36 times the 'measured' values, respectively. However, there is considerable scatter about these mean values; You (1996) found that many existing formulae failed to predict bed roughness accurately. The better performance of the Nielsen model, though slight here, is found also in a recent investigation within a wave-dominated continental shelf environment where bed roughness under moderate wave energy conditions has been found to be predicted adequately by Nielsen's (*op. cit.*) model (Xu and Wright, 1995). For moderate and high energy conditions, however, these investigators proposed a modification to Nielsen's (*op. cit.*) model that was proportional to a maximum skin friction Shields' parameter. Within the present investigation, the formulae of Shinohara and Tsubaki (1959) and Grant and Madsen (1982), however, provided a greater number of roughness estimates within the widest tolerance band. Drake *et al.*'s (1992) modification of Grant and Madsen's (*op. cit.*) formula, when applied to the observations obtained here, produced values which were inconsistent with those 'measured'. In the present investigation, θ_{cr} varied between 18° and 57°, a range similar to that experienced by Drake *et al.* (5° to 46°). However, the hydrodynamic setting in which this investigation was undertaken was subject to relatively low currents and waves and, therefore, considerably different from the present study area.

5.4.4 Bedload transport rates

Transport rates were obtained from the sea bed photographs using two different approaches (see above). The method described by Huntley *et al.* (1991) derived a wide spread of transport rates; this may be due to the problem of correctly identifying the same ripples in consecutive photographs (ripple aliasing), a problem noted by these investigators during a deployment in the southern North Sea. The approach suggested by Allen (1970), Rubin and McCulloch (1980),

Of the formulae investigated here, three provide roughness estimates that are similar to those obtained by comparing the Reynolds stresses with those obtained using the model of Christoffersen and Jonsson (1985). Overall, the roughness values predicted by the formulae of van Rijn (1982), Nielsen (1983) and Raudkivi (1990) were 1.25, 0.87 and 1.36 times the 'measured' values, respectively. However, there is considerable scatter about these mean values; You (1996) found that many existing formulae failed to predict bed roughness accurately. The better performance of the Nielsen model, though slight here, is found also in a recent investigation within a wave-dominated continental shelf environment where bed roughness under moderate wave energy conditions has been found to be predicted adequately by Nielsen's (*op. cit.*) model (Xu and Wright, 1995). For moderate and high energy conditions, however, these investigators proposed a modification to Nielsen's (*op. cit.*) model that was proportional to a maximum skin friction Shields' parameter. Within the present investigation, the formulae of Shinohara and Tsubaki (1959) and Grant and Madsen (1982), however, provided a greater number of roughness estimates within the widest tolerance band. Drake *et al.*'s (1992) modification of Grant and Madsen's (*op. cit.*) formula, when applied to the observations obtained here, produced values which were inconsistent with those 'measured'. In the present investigation, θ_{cr} varied between 18° and 57°, a range similar to that experienced by Drake *et al.* (5° to 46°). However, the hydrodynamic setting in which this investigation was undertaken was subject to relatively low currents and waves and, therefore, considerably different from the present study area.

5.4.4 Bedload transport rates

Transport rates were obtained from the sea bed photographs using two different approaches (see above). The method described by Huntley *et al.* (1991) derived a wide spread of transport rates; this may be due to the problem of correctly identifying the same ripples in consecutive photographs (ripple aliasing), a problem noted by these investigators during a deployment in the southern North Sea. The approach suggested by Allen (1970), Rubin and McCulloch (1980),

Of the formulae investigated here, three provide roughness estimates that are similar to those obtained by comparing the Reynolds stresses with those obtained using the model of Christoffersen and Jonsson (1985). Overall, the roughness values predicted by the formulae of van Rijn (1982), Nielsen (1983) and Raudkivi (1990) were 1.25, 0.87 and 1.36 times the 'measured' values, respectively. However, there is considerable scatter about these mean values; You (1996) found that many existing formulae failed to predict bed roughness accurately. The better performance of the Nielsen model, though slight here, is found also in a recent investigation within a wave-dominated continental shelf environment where bed roughness under moderate wave energy conditions has been found to be predicted adequately by Nielsen's (*op. cit.*) model (Xu and Wright, 1995). For moderate and high energy conditions, however, these investigators proposed a modification to Nielsen's (*op. cit.*) model that was proportional to a maximum skin friction Shields' parameter. Within the present investigation, the formulae of Shinohara and Tsubaki (1959) and Grant and Madsen (1982), however, provided a greater number of roughness estimates within the widest tolerance band. Drake *et al.*'s (1992) modification of Grant and Madsen's (*op. cit.*) formula, when applied to the observations obtained here, produced values which were inconsistent with those 'measured'. In the present investigation, θ_{cr} varied between 18° and 57°, a range similar to that experienced by Drake *et al.* (5° to 46°). However, the hydrodynamic setting in which this investigation was undertaken was subject to relatively low currents and waves and, therefore, considerably different from the present study area.

5.4.4 Bedload transport rates

Transport rates were obtained from the sea bed photographs using two different approaches (see above). The method described by Huntley *et al.* (1991) derived a wide spread of transport rates; this may be due to the problem of correctly identifying the same ripples in consecutive photographs (ripple aliasing), a problem noted by these investigators during a deployment in the southern North Sea. The approach suggested by Allen (1970), Rubin and McCulloch (1980),

Of the formulae investigated here, three provide roughness estimates that are similar to those obtained by comparing the Reynolds stresses with those obtained using the model of Christoffersen and Jonsson (1985). Overall, the roughness values predicted by the formulae of van Rijn (1982), Nielsen (1983) and Raudkivi (1990) were 1.25, 0.87 and 1.36 times the 'measured' values, respectively. However, there is considerable scatter about these mean values; You (1996) found that many existing formulae failed to predict bed roughness accurately. The better performance of the Nielsen model, though slight here, is found also in a recent investigation within a wave-dominated continental shelf environment where bed roughness under moderate wave energy conditions has been found to be predicted adequately by Nielsen's (*op. cit.*) model (Xu and Wright, 1995). For moderate and high energy conditions, however, these investigators proposed a modification to Nielsen's (*op. cit.*) model that was proportional to a maximum skin friction Shields' parameter. Within the present investigation, the formulae of Shinohara and Tsubaki (1959) and Grant and Madsen (1982), however, provided a greater number of roughness estimates within the widest tolerance band. Drake *et al.*'s (1992) modification of Grant and Madsen's (*op. cit.*) formula, when applied to the observations obtained here, produced values which were inconsistent with those 'measured'. In the present investigation, θ_{cr} varied between 18° and 57°, a range similar to that experienced by Drake *et al.* (5° to 46°). However, the hydrodynamic setting in which this investigation was undertaken was subject to relatively low currents and waves and, therefore, considerably different from the present study area.

5.4.4 Bedload transport rates

Transport rates were obtained from the sea bed photographs using two different approaches (see above). The method described by Huntley *et al.* (1991) derived a wide spread of transport rates; this may be due to the problem of correctly identifying the same ripples in consecutive photographs (ripple aliasing), a problem noted by these investigators during a deployment in the southern North Sea. The approach suggested by Allen (1970), Rubin and McCulloch (1980),

Of the formulae investigated here, three provide roughness estimates that are similar to those obtained by comparing the Reynolds stresses with those obtained using the model of Christoffersen and Jonsson (1985). Overall, the roughness values predicted by the formulae of van Rijn (1982), Nielsen (1983) and Raudkivi (1990) were 1.25, 0.87 and 1.36 times the 'measured' values, respectively. However, there is considerable scatter about these mean values; You (1996) found that many existing formulae failed to predict bed roughness accurately. The better performance of the Nielsen model, though slight here, is found also in a recent investigation within a wave-dominated continental shelf environment where bed roughness under moderate wave energy conditions has been found to be predicted adequately by Nielsen's (*op. cit.*) model (Xu and Wright, 1995). For moderate and high energy conditions, however, these investigators proposed a modification to Nielsen's (*op. cit.*) model that was proportional to a maximum skin friction Shields' parameter. Within the present investigation, the formulae of Shinohara and Tsubaki (1959) and Grant and Madsen (1982), however, provided a greater number of roughness estimates within the widest tolerance band. Drake *et al.*'s (1992) modification of Grant and Madsen's (*op. cit.*) formula, when applied to the observations obtained here, produced values which were inconsistent with those 'measured'. In the present investigation, θ_{cr} varied between 18° and 57°, a range similar to that experienced by Drake *et al.* (5° to 46°). However, the hydrodynamic setting in which this investigation was undertaken was subject to relatively low currents and waves and, therefore, considerably different from the present study area.

5.4.4 Bedload transport rates

Transport rates were obtained from the sea bed photographs using two different approaches (see above). The method described by Huntley *et al.* (1991) derived a wide spread of transport rates; this may be due to the problem of correctly identifying the same ripples in consecutive photographs (ripple aliasing), a problem noted by these investigators during a deployment in the southern North Sea. The approach suggested by Allen (1970), Rubin and McCulloch (1980),

Of the formulae investigated here, three provide roughness estimates that are similar to those obtained by comparing the Reynolds stresses with those obtained using the model of Christoffersen and Jonsson (1985). Overall, the roughness values predicted by the formulae of van Rijn (1982), Nielsen (1983) and Raudkivi (1990) were 1.25, 0.87 and 1.36 times the 'measured' values, respectively. However, there is considerable scatter about these mean values; You (1996) found that many existing formulae failed to predict bed roughness accurately. The better performance of the Nielsen model, though slight here, is found also in a recent investigation within a wave-dominated continental shelf environment where bed roughness under moderate wave energy conditions has been found to be predicted adequately by Nielsen's (*op. cit.*) model (Xu and Wright, 1995). For moderate and high energy conditions, however, these investigators proposed a modification to Nielsen's (*op. cit.*) model that was proportional to a maximum skin friction Shields' parameter. Within the present investigation, the formulae of Shinohara and Tsubaki (1959) and Grant and Madsen (1982), however, provided a greater number of roughness estimates within the widest tolerance band. Drake *et al.*'s (1992) modification of Grant and Madsen's (*op. cit.*) formula, when applied to the observations obtained here, produced values which were inconsistent with those 'measured'. In the present investigation, θ_{cr} varied between 18° and 57°, a range similar to that experienced by Drake *et al.* (5° to 46°). However, the hydrodynamic setting in which this investigation was undertaken was subject to relatively low currents and waves and, therefore, considerably different from the present study area.

5.4.4 Bedload transport rates

Transport rates were obtained from the sea bed photographs using two different approaches (see above). The method described by Huntley *et al.* (1991) derived a wide spread of transport rates; this may be due to the problem of correctly identifying the same ripples in consecutive photographs (ripple aliasing), a problem noted by these investigators during a deployment in the southern North Sea. The approach suggested by Allen (1970), Rubin and McCulloch (1980),

Of the formulae investigated here, three provide roughness estimates that are similar to those obtained by comparing the Reynolds stresses with those obtained using the model of Christoffersen and Jonsson (1985). Overall, the roughness values predicted by the formulae of van Rijn (1982), Nielsen (1983) and Raudkivi (1990) were 1.25, 0.87 and 1.36 times the 'measured' values, respectively. However, there is considerable scatter about these mean values; You (1996) found that many existing formulae failed to predict bed roughness accurately. The better performance of the Nielsen model, though slight here, is found also in a recent investigation within a wave-dominated continental shelf environment where bed roughness under moderate wave energy conditions has been found to be predicted adequately by Nielsen's (*op. cit.*) model (Xu and Wright, 1995). For moderate and high energy conditions, however, these investigators proposed a modification to Nielsen's (*op. cit.*) model that was proportional to a maximum skin friction Shields' parameter. Within the present investigation, the formulae of Shinohara and Tsubaki (1959) and Grant and Madsen (1982), however, provided a greater number of roughness estimates within the widest tolerance band. Drake *et al.*'s (1992) modification of Grant and Madsen's (*op. cit.*) formula, when applied to the observations obtained here, produced values which were inconsistent with those 'measured'. In the present investigation, θ_{cr} varied between 18° and 57°, a range similar to that experienced by Drake *et al.* (5° to 46°). However, the hydrodynamic setting in which this investigation was undertaken was subject to relatively low currents and waves and, therefore, considerably different from the present study area.

5.4.4 Bedload transport rates

Transport rates were obtained from the sea bed photographs using two different approaches (see above). The method described by Huntley *et al.* (1991) derived a wide spread of transport rates; this may be due to the problem of correctly identifying the same ripples in consecutive photographs (ripple aliasing), a problem noted by these investigators during a deployment in the southern North Sea. The approach suggested by Allen (1970), Rubin and McCulloch (1980),

Of the formulae investigated here, three provide roughness estimates that are similar to those obtained by comparing the Reynolds stresses with those obtained using the model of Christoffersen and Jonsson (1985). Overall, the roughness values predicted by the formulae of van Rijn (1982), Nielsen (1983) and Raudkivi (1990) were 1.25, 0.87 and 1.36 times the 'measured' values, respectively. However, there is considerable scatter about these mean values; You (1996) found that many existing formulae failed to predict bed roughness accurately. The better performance of the Nielsen model, though slight here, is found also in a recent investigation within a wave-dominated continental shelf environment where bed roughness under moderate wave energy conditions has been found to be predicted adequately by Nielsen's (*op. cit.*) model (Xu and Wright, 1995). For moderate and high energy conditions, however, these investigators proposed a modification to Nielsen's (*op. cit.*) model that was proportional to a maximum skin friction Shields' parameter. Within the present investigation, the formulae of Shinohara and Tsubaki (1959) and Grant and Madsen (1982), however, provided a greater number of roughness estimates within the widest tolerance band. Drake *et al.*'s (1992) modification of Grant and Madsen's (*op. cit.*) formula, when applied to the observations obtained here, produced values which were inconsistent with those 'measured'. In the present investigation, θ_{cr} varied between 18° and 57°, a range similar to that experienced by Drake *et al.* (5° to 46°). However, the hydrodynamic setting in which this investigation was undertaken was subject to relatively low currents and waves and, therefore, considerably different from the present study area.

5.4.4 Bedload transport rates

Transport rates were obtained from the sea bed photographs using two different approaches (see above). The method described by Huntley *et al.* (1991) derived a wide spread of transport rates; this may be due to the problem of correctly identifying the same ripples in consecutive photographs (ripple aliasing), a problem noted by these investigators during a deployment in the southern North Sea. The approach suggested by Allen (1970), Rubin and McCulloch (1980),

Of the formulae investigated here, three provide roughness estimates that are similar to those obtained by comparing the Reynolds stresses with those obtained using the model of Christoffersen and Jonsson (1985). Overall, the roughness values predicted by the formulae of van Rijn (1982), Nielsen (1983) and Raudkivi (1990) were 1.25, 0.87 and 1.36 times the 'measured' values, respectively. However, there is considerable scatter about these mean values; You (1996) found that many existing formulae failed to predict bed roughness accurately. The better performance of the Nielsen model, though slight here, is found also in a recent investigation within a wave-dominated continental shelf environment where bed roughness under moderate wave energy conditions has been found to be predicted adequately by Nielsen's (*op. cit.*) model (Xu and Wright, 1995). For moderate and high energy conditions, however, these investigators proposed a modification to Nielsen's (*op. cit.*) model that was proportional to a maximum skin friction Shields' parameter. Within the present investigation, the formulae of Shinohara and Tsubaki (1959) and Grant and Madsen (1982), however, provided a greater number of roughness estimates within the widest tolerance band. Drake *et al.*'s (1992) modification of Grant and Madsen's (*op. cit.*) formula, when applied to the observations obtained here, produced values which were inconsistent with those 'measured'. In the present investigation, θ_{cr} varied between 18° and 57°, a range similar to that experienced by Drake *et al.* (5° to 46°). However, the hydrodynamic setting in which this investigation was undertaken was subject to relatively low currents and waves and, therefore, considerably different from the present study area.

5.4.4 Bedload transport rates

Transport rates were obtained from the sea bed photographs using two different approaches (see above). The method described by Huntley *et al.* (1991) derived a wide spread of transport rates; this may be due to the problem of correctly identifying the same ripples in consecutive photographs (ripple aliasing), a problem noted by these investigators during a deployment in the southern North Sea. The approach suggested by Allen (1970), Rubin and McCulloch (1980),

Of the formulae investigated here, three provide roughness estimates that are similar to those obtained by comparing the Reynolds stresses with those obtained using the model of Christoffersen and Jonsson (1985). Overall, the roughness values predicted by the formulae of van Rijn (1982), Nielsen (1983) and Raudkivi (1990) were 1.25, 0.87 and 1.36 times the 'measured' values, respectively. However, there is considerable scatter about these mean values; You (1996) found that many existing formulae failed to predict bed roughness accurately. The better performance of the Nielsen model, though slight here, is found also in a recent investigation within a wave-dominated continental shelf environment where bed roughness under moderate wave energy conditions has been found to be predicted adequately by Nielsen's (*op. cit.*) model (Xu and Wright, 1995). For moderate and high energy conditions, however, these investigators proposed a modification to Nielsen's (*op. cit.*) model that was proportional to a maximum skin friction Shields' parameter. Within the present investigation, the formulae of Shinohara and Tsubaki (1959) and Grant and Madsen (1982), however, provided a greater number of roughness estimates within the widest tolerance band. Drake *et al.*'s (1992) modification of Grant and Madsen's (*op. cit.*) formula, when applied to the observations obtained here, produced values which were inconsistent with those 'measured'. In the present investigation, θ_{cr} varied between 18° and 57°, a range similar to that experienced by Drake *et al.* (5° to 46°). However, the hydrodynamic setting in which this investigation was undertaken was subject to relatively low currents and waves and, therefore, considerably different from the present study area.

5.4.4 Bedload transport rates

Transport rates were obtained from the sea bed photographs using two different approaches (see above). The method described by Huntley *et al.* (1991) derived a wide spread of transport rates; this may be due to the problem of correctly identifying the same ripples in consecutive photographs (ripple aliasing), a problem noted by these investigators during a deployment in the southern North Sea. The approach suggested by Allen (1970), Rubin and McCulloch (1980),

Langhorne (1981, 1982) and van den Berg (1987) predicted low transport rates for low energy (wave and tidal currents) situations, and higher rates for the higher energy bursts. In view of the more consistent performance of the approach suggested by these investigators these latter values have been adopted in the subsequent discussion of the results.

The drag effect of the ripples has been evaluated by dividing the friction velocity based upon the grain roughness, by the total friction velocity. The total friction velocity has been evaluated at a height above the sea bed equivalent to the thickness of the wave boundary layer (Equation 5.32). The results are given in Table 5.4. Average drag values with A=2 and A=0.367 are 0.678 and 0.483, respectively. These values lie between those suggested by Smith and McLean (1977), who quote drag values of 0.212 and 0.840, for separated and unseparated flow, respectively.

In this investigation, the proportion of the shear velocity acting on the sediment grains alone has been taken as the mean (58%) of the two values obtained earlier, for each of the bursts (Table 5.4).

Bedload transport rates have been predicted using the (10) formulae described previously (Section 3.5), with skin friction considered to represent 58% of the total drag on the sea bed. This particular proportion of skin friction, compared to the total drag, compares well with the conclusions of previous investigations (Section 3.4). The transport rates determined using the procedures described above are presented in Figure 5.19. A similar pattern of prediction is obtained for all the equations; they all produce a substantial reduction in the volume of material being transported around Burst 19.

Few transport rates predicted using the approach suggested by Ackers and White (1973) have been plotted as the flows during the intervening periods have not exceeded the threshold condition suggested by these investigators. Hence, such occasions are not associated with any bedload transport. Similar results using this

approach have been obtained by Huntley *et al.* (1991), during an investigation into bedload sediment transport rates in the southern North Sea. Hence, transport rates predicted by the Ackers and White (1973) approach are not considered here any further.

Predicted transport rates vary through approximately 3 orders of magnitude. Substantial variation between the output of these equations, using the same input, leads to the conclusion that the selection of which transport equation to use has the greatest influence upon the rates predicted. Thus it would appear that, despite the complexity of modelling stresses in combined wave and current flows, the inaccuracy of these boundary layer models is insignificant compared to that contained within the presently-available sediment transport formulae. During the present investigation, however, 'independent' bedload transport rates are available; against these, each of the predictive methods outlined above can be tested.

The ability of each of the predictive formulae to reproduce the *measured* transport rates is investigated now using the method of Zanke (1987). In this approach, the spread of the results about a line of 'best-fit' is evaluated:

$$r_{i=1,n} = \frac{Q_E}{Q_M} \tag{5.57}$$

where Q_E is the rate predicted by the formula under investigation, and Q_M is the measured transport rate determined from the observed ripple migration rates. For a predicted transport rate which produces an r value of 1/2, the level of accuracy is equivalent to a prediction with an r value of 2. Although the magnitude of the error is different, the factor by which the prediction is in error (in this case by 2) is the same. Zanke (1987) formulated this as:

$$r_i' = r_i \quad if\ r_i < 1 \tag{5.58}$$

$$r_i' = \frac{1}{r_i} \quad if\ r_i > 1 \tag{5.59}$$

All of the r_i' values are multiplied together to give a final value, S:

$$S = \left[Product(r_i')\ \begin{matrix} i=1 \\ i=n \end{matrix}\right]^{\frac{1}{n}} \tag{5.60}$$

The bedload transport formula with S closest to unity is considered to have performed best in the analysis. The results obtained are listed in Table 5.5. Considerable variation in the predicted values is evident. Of the formulae investigated, that of Soulsby (1993) is found to be the most successful in predicting transport rates which lie close to those observed in this particular field investigation. However, the Zanke parameter still lies at around 17. It was found, as part of the present study, that the measured values can be best represented by the following formula:

$$I_b = Bg\left(1 - \frac{\rho}{\rho_s}\right)(\tau_b - \tau_{cr})U_{100} \tag{5.61}$$

where $B = 1.31 \times 10^{-4}\ m^{-2}\ s^4$.

The bedload transport rates predicted by this formula, and the corresponding measured values, are presented in Table 5.6. This formula has a form similar to that suggested by Hardisty (1983, 1990) and by Williams *et al.* (1989) in relation to the movement of gravel, and by Soulsby (*op. cit.*). When the transport values predicted by this formula were compared with those observed, the Zanke parameter was approximately 2.7; this is a considerable improvement upon the (10) formulae investigated here.

Several assumptions are inherent in the method adopted for deriving transport rates from the ripple migration patterns. Ripples formed during periods of bedload transport at the STABLE site have been observed to persist during sub-critical

flows. Sediment transport rates will be inferred from the observed ripple geometry by adopting the approach described earlier i.e. when, in fact, little or no transport may be occurring. Examination of the data recorded by the STABLE bed frame (Figure 5.4), however, reveals only small periods when flow speeds are below those required to initiate and maintain sediment transport. This source of error should, therefore, have limited influence only on the results presented here.

The discussion presented here assumes that all the movement of sand as bedload occurs within the migration of the ripples. Individual sand grains are assumed, therefore, to be contained within the same ripple, with time. Hence, no allowance has been made for sand 'by-passing' particular ripples i.e. grains jumping from one ripple crest to the next. Ripple by-passing by individual grains will occur most often during periods of higher flow i.e. at times when the shadow of the bar on the sea bed has not been clearly identified on the images of the sea bed. Ripple by-passing should not affect greatly, therefore, the results obtained during the present investigation.

Another assumption inherent in the transport rates derived from the photographs is that the layer of mobile sediment is assumed to be equal to the height of the ripples. Hence, the mobile layer (or depth of mixing) has been assumed to extend down to 2 cm into the bed. Shimwell (1990), for the same area of sea bed, measured the depth of burial to be 3.2 cm. Elsewhere, in shallower water depths and, hence, greater wave height to water depth ratios, the estimated depth of mixing was found to be 8 cm (Lees, 1981). Shallow locations, located nearer the shoreline, would be expected to have a greater mobile layer thickness (Bray, 1990). If the mobile layer extends below the level assumed here, then there is sediment transport occurring which cannot be recorded by the photographs. However, in order to make the sediment transport rates predicted by the Hardisty (1983, 1990) equation correlate with the transport rates inferred from the observed rates of ripple migration, the depth of burial would have to be increased by over 2 orders of magnitude. Such an estimate would seem to be unlikely, in this particular case. Alternatively, if these rates were to be accepted, the rate of ripple

migration would be expected to be around 80 m hr^{-1}. For sediment transport to be occurring at these rates, it is likely that the dominant mode of sediment transport will be suspension, thus rendering photographs of the sea bed dark. Further problems may be encountered at these high rates by the substantial volumes of sediment in suspension, creating stratification, calling into question the validity of the boundary layer model.

Empirical formulae for the prediction of bedload transport were derived originally for use with time-varying unidirectional flows, such as those experienced in rivers and canals. Application of these formulae to the marine environment is complicated by the simultaneous presence of 'steady' tidal currents and oscillatory wave action. Considerable variability has been found in the application of these formulae to specific investigations (see, for example, Heathershaw, 1981; Pattiaratchi and Collins, 1985; and Dyer and Soulsby, 1988). Considerable uncertainty also surrounds the threshold of movement in the sea (Pugh, 1987) with the critical velocities and shear stresses applied to the marine environment being based on field and flume results.

5.5 CONCLUDING REMARKS

The transport of sediment in coastal environments is frequently in response to both wave- and current-induced shear stresses. Wave measurements are made often as orbital motions at some distance above the bed, or in relation to surface wave characteristics. In either case, an assumption is required so that these measured parameters can be transferred into parameters required in predictive formulae. First order wave theory is usually assumed in such transformations. However, the results presented here suggest that this assumption may not always be valid and that further investigation is required into wave dynamics in intermediate water depths.

Sea bed geometry can be interpreted successfully from time-lapse photography. During periods of higher flow, however, it may be difficult to distinguish clearly

migration would be expected to be around 80 m hr^{-1}. For sediment transport to be occurring at these rates, it is likely that the dominant mode of sediment transport will be suspension, thus rendering photographs of the sea bed dark. Further problems may be encountered at these high rates by the substantial volumes of sediment in suspension, creating stratification, calling into question the validity of the boundary layer model.

Empirical formulae for the prediction of bedload transport were derived originally for use with time-varying unidirectional flows, such as those experienced in rivers and canals. Application of these formulae to the marine environment is complicated by the simultaneous presence of 'steady' tidal currents and oscillatory wave action. Considerable variability has been found in the application of these formulae to specific investigations (see, for example, Heathershaw, 1981; Pattiaratchi and Collins, 1985; and Dyer and Soulsby, 1988). Considerable uncertainty also surrounds the threshold of movement in the sea (Pugh, 1987) with the critical velocities and shear stresses applied to the marine environment being based on field and flume results.

5.5 CONCLUDING REMARKS

The transport of sediment in coastal environments is frequently in response to both wave- and current-induced shear stresses. Wave measurements are made often as orbital motions at some distance above the bed, or in relation to surface wave characteristics. In either case, an assumption is required so that these measured parameters can be transferred into parameters required in predictive formulae. First order wave theory is usually assumed in such transformations. However, the results presented here suggest that this assumption may not always be valid and that further investigation is required into wave dynamics in intermediate water depths.

Sea bed geometry can be interpreted successfully from time-lapse photography. During periods of higher flow, however, it may be difficult to distinguish clearly

migration would be expected to be around 80 m hr^{-1}. For sediment transport to be occurring at these rates, it is likely that the dominant mode of sediment transport will be suspension, thus rendering photographs of the sea bed dark. Further problems may be encountered at these high rates by the substantial volumes of sediment in suspension, creating stratification, calling into question the validity of the boundary layer model.

Empirical formulae for the prediction of bedload transport were derived originally for use with time-varying unidirectional flows, such as those experienced in rivers and canals. Application of these formulae to the marine environment is complicated by the simultaneous presence of 'steady' tidal currents and oscillatory wave action. Considerable variability has been found in the application of these formulae to specific investigations (see, for example, Heathershaw, 1981; Pattiaratchi and Collins, 1985; and Dyer and Soulsby, 1988). Considerable uncertainty also surrounds the threshold of movement in the sea (Pugh, 1987) with the critical velocities and shear stresses applied to the marine environment being based on field and flume results.

5.5 CONCLUDING REMARKS

The transport of sediment in coastal environments is frequently in response to both wave- and current-induced shear stresses. Wave measurements are made often as orbital motions at some distance above the bed, or in relation to surface wave characteristics. In either case, an assumption is required so that these measured parameters can be transferred into parameters required in predictive formulae. First order wave theory is usually assumed in such transformations. However, the results presented here suggest that this assumption may not always be valid and that further investigation is required into wave dynamics in intermediate water depths.

Sea bed geometry can be interpreted successfully from time-lapse photography. During periods of higher flow, however, it may be difficult to distinguish clearly

migration would be expected to be around 80 m hr^{-1}. For sediment transport to be occurring at these rates, it is likely that the dominant mode of sediment transport will be suspension, thus rendering photographs of the sea bed dark. Further problems may be encountered at these high rates by the substantial volumes of sediment in suspension, creating stratification, calling into question the validity of the boundary layer model.

Empirical formulae for the prediction of bedload transport were derived originally for use with time-varying unidirectional flows, such as those experienced in rivers and canals. Application of these formulae to the marine environment is complicated by the simultaneous presence of 'steady' tidal currents and oscillatory wave action. Considerable variability has been found in the application of these formulae to specific investigations (see, for example, Heathershaw, 1981; Pattiaratchi and Collins, 1985; and Dyer and Soulsby, 1988). Considerable uncertainty also surrounds the threshold of movement in the sea (Pugh, 1987) with the critical velocities and shear stresses applied to the marine environment being based on field and flume results.

5.5 CONCLUDING REMARKS

The transport of sediment in coastal environments is frequently in response to both wave- and current-induced shear stresses. Wave measurements are made often as orbital motions at some distance above the bed, or in relation to surface wave characteristics. In either case, an assumption is required so that these measured parameters can be transferred into parameters required in predictive formulae. First order wave theory is usually assumed in such transformations. However, the results presented here suggest that this assumption may not always be valid and that further investigation is required into wave dynamics in intermediate water depths.

Sea bed geometry can be interpreted successfully from time-lapse photography. During periods of higher flow, however, it may be difficult to distinguish clearly

the shadow of the bar on the sea bed. Clearer identification of the shadow of the bar on the sea bed for a greater period of the deployment may be obtained by use of a video camera rather than discrete photographs. Bedform geometry observed during the present investigation has shown considerable agreement with previous studies of field- and flume-generated ripples.

Existing formulae for describing the sea bed roughness, related to the presence of bedforms, can produce significantly differing results. For the present investigation, k_s was found to be dependent upon the bedform height and the angle between current direction and the ripple crests:

$$\log(k_s) = 4.09\eta\cos\theta_{cr} - 3.42 \qquad (5.62)$$

The ability of several roughness models to reproduce the physical roughness encountered during the present study has been investigated. The roughness encountered here was found to be represented most accurately by Nielsen's (1983) formula.

Ripple migration was observed throughout the (3 day) deployment. The rates of movement provide a means of evaluating the performance of predictive sediment bedload transport rate formulae.

A combined bed shear stress approach has been adopted here to determine sediment transport rates. Combined bed shear stresses have been evaluated by superimposing the instantaneous wave shear stresses upon the measured steady (unidirectional) current shear stress, over a complete wave cycle. The proportion of the total energy responsible for sediment transport (skin friction), in combination with an appropriate bedload transport formula, can provide remarkably good agreement between observed and predicted rates i.e. to within less than a factor of 3 of the observed rates. Within the predictive approach, the proportion of the total friction velocity that is considered to overcome the form drag of the ripples (42%) is within the range suggested by the results of previous investigations (Section 3.4).

the shadow of the bar on the sea bed. Clearer identification of the shadow of the bar on the sea bed for a greater period of the deployment may be obtained by use of a video camera rather than discrete photographs. Bedform geometry observed during the present investigation has shown considerable agreement with previous studies of field- and flume-generated ripples.

Existing formulae for describing the sea bed roughness, related to the presence of bedforms, can produce significantly differing results. For the present investigation, k_s was found to be dependent upon the bedform height and the angle between current direction and the ripple crests:

$$\log(k_s) = 4.09\eta\cos\theta_{cr} - 3.42 \qquad (5.62)$$

The ability of several roughness models to reproduce the physical roughness encountered during the present study has been investigated. The roughness encountered here was found to be represented most accurately by Nielsen's (1983) formula.

Ripple migration was observed throughout the (3 day) deployment. The rates of movement provide a means of evaluating the performance of predictive sediment bedload transport rate formulae.

A combined bed shear stress approach has been adopted here to determine sediment transport rates. Combined bed shear stresses have been evaluated by superimposing the instantaneous wave shear stresses upon the measured steady (unidirectional) current shear stress, over a complete wave cycle. The proportion of the total energy responsible for sediment transport (skin friction), in combination with an appropriate bedload transport formula, can provide remarkably good agreement between observed and predicted rates i.e. to within less than a factor of 3 of the observed rates. Within the predictive approach, the proportion of the total friction velocity that is considered to overcome the form drag of the ripples (42%) is within the range suggested by the results of previous investigations (Section 3.4).

In the present investigation, Equation 5.61 has been found to most accurately reproduce the transport rates inferred from the ripple migration rates. However, shortcomings of the approach adopted to infer transport rates from the photographs have been identified. These may be described briefly as: (i) low flow rates may be sub-critical but ripples may be present on the sea bed, so a transport rate is inferred; (ii) no ripple by-passing by individual sand grains has been assumed; and (iii) the depth of the mobile layer has been assumed.

Within the previous analysis and subsequent discussion, it has been shown that the first two of these shortcomings have limited influence only on the results presented here. Further investigation into the depth of the mobile sediment layer under a rippled sand bed, in combined wave and current flows, needs to be undertaken. Further, the 'velocity profile' within this mobile layer needs to be established in order that improved accuracy of sediment transport rates determined from time-lapse photography of the sea bed may be obtained.

Burst	Water depth (m)	Wave period (s)	Wave orbital velocity (cm s^{-1}) 41 cm 80 cm	Wave-current interaction angle (°)	Current velocity (cm s^{-1}) 41 cm 80 cm
1	28.50	9.11	17.27, 20.96	48.7	48.60, 55.83
2	29.20	9.50	15.93, 19.15	25.7	60.98, 80.80
3	29.06	9.09	15.78, 18.89	5.4	28.39, 37.45
4	29.64	10.60	15.20, 18.40	57.6	17.10, 20.10
5	29.41	11.01	11.85, 13.83	33.4	45.04, 57.58
6	28.67	10.63	13.24, 15.33	22.1	24.36, 31.89
7	28.04	10.25	10.90, 13.09	39.7	21.09, 29.44
8	28.23	10.53	13.87, 16.60	26.0	48.02, 65.67
9	28.85	10.65	12.72, 15.57	9.3	22.04, 30.53
10	29.69	10.72	12.47, 14.70	39.1	32.11, 43.27
11	29.81	10.79	10.82, 13.15	35.1	61.35, 80.51
12	29.41	10.97	13.28, 16.00	24.0	51.68, 68.32
13	28.43	10.86	14.86, 17.96	78.7	12.97, 11.92
14	28.25	8.64	15.94, 19.90	27.4	59.69, 81.84
15	28.59	10.74	16.40, 19.57	16.2	55.70, 78.61
16	29.28	10.90	18.34, 22.40	77.3	7.70, 11.94
17	29.59	10.06	15.10, 17.56	42.4	41.11, 55.80
18	29.06	8.63	15.81, 18.97	29.0	43.75, 59.04
19	28.08	9.96	14.62, 17.80	79.9	15.10, 18.19
20	27.91	8.46	17.00, 20.75	15.8	59.88, 82.07
21	28.36	9.87	19.78, 23.89	19.0	45.75, 64.11
22	29.28	11.10	19.96, 23.99	63.8	11.08, 15.70
23	29.99	12.09	16.70, 19.30	38.2	47.16, 63.44
24	29.85	10.99	15.98, 18.47	30.7	66.01, 88.82
25	29.04	11.07	15.27, 17.56	5.8	25.98, 40.32
26	28.18	10.60	16.56, 19.89	45.0	40.45, 52.39
27	28.47	11.32	17.17, 20.31	19.2	66.44, 90.90

Table 5.1 'Burst-averaged' hydrodynamic data recorded during the deployment. Note: Bursts were approximately 17 mins long, recorded once every 2 hours. Burst 1 was recorded from 1403 hrs on 19/11/88.

Burst	Ripple height (cm)	Ripple wavelength (cm)
2	1.5	22.1
4	0.9	13.5
5	0.9	15.7
7	1.4	17.3
8	1.0	15.2
9	1.0	10.9
10	1.0	14.4
14	0.7	14.7
15	1.6	15.6
16	0.8	16.4
17	1.2	17.0
18	1.4	15.4
19	0.4	12.5
20	0.6	16.0
25	1.7	13.4

Table 5.2 Observed bedform dimensions derived from the photographic data obtained from STABLE. The values presented here are average values for all bedforms observed across the field of view for the two photographs, recorded at the beginning and end of each of the bursts.

Burst	Ripple height (cm)	Ripple wavelength (cm)
2	1.5	22.1
4	0.9	13.5
5	0.9	15.7
7	1.4	17.3
8	1.0	15.2
9	1.0	10.9
10	1.0	14.4
14	0.7	14.7
15	1.6	15.6
16	0.8	16.4
17	1.2	17.0
18	1.4	15.4
19	0.4	12.5
20	0.6	16.0
25	1.7	13.4

Table 5.2 Observed bedform dimensions derived from the photographic data obtained from STABLE. The values presented here are average values for all bedforms observed across the field of view for the two photographs, recorded at the beginning and end of each of the bursts.

Burst	Observed roughness (m)	Ratio of predicted roughness to observed roughness (P)					
		GM82	Nielsen (1983)	Drake *et al.* (1992)	Raudkivi (1990)	ST59	van Rijn (1982)
2	0.029	0.93	0.28	-89.11	0.43	0.81	0.45
4	0.400	0.04	0.00	-17.62	0.02	0.03	0.02
5	0.046	0.29	0.09	-100.03	0.14	0.28	0.16
7	0.118	0.25	0.08	-28.53	0.11	0.20	0.11
8	0.011	1.62	0.46	-318.44	0.76	1.41	0.79
9	0.050	0.48	0.14	-55.33	0.22	0.36	0.19
10	0.010	1.83	0.55	-307.02	0.85	1.57	0.87
14	0.004	1.93	0.64	-865.14	0.90	0.98	1.15
15	0.004	12.58	3.64	-431.41	5.86	9.06	4.49
16	0.400	0.03	0.01	-25.92	0.01	0.03	0.02
17	0.003	7.55	2.19	-782.75	3.51	6.39	3.52
18	0.003	9.39	3.00	-373.03	4.37	7.24	3.78
19	0.009	0.39	0.11	-957.34	0.18	0.47	0.27
20	0.002	2.95	0.82	-817.33	1.37	3.23	1.87
25	0.017	3.58	1.01	-96.69	1.67	2.34	1.06
P mean		2.92	0.87	-351.05	1.36	2.36	1.25
$0.5 \leq P \leq 2$		4	4	-	5	4	5
$0.3 \leq P \leq 3$		7	7	-	6	7	6
$0.2 \leq P \leq 5$		10	8	-	9	10	9

Table 5.3 The application of (six) predictive equations to reproduce the observed roughness values, expressed in terms of a P parameter (see text).
Key: GM82- Grant and Madsen (1982); ST59- Shinohara and Tsubaki (1959).

		GM82, GG83		CJ85		
Burst	**U_{*c} (cm s^{-1})**	**U'_{*c} (cm s^{-1})**	**C_D**	**U'_{*c} (cm s^{-1})**	**C_D**	**C_D (ave)**
2	5.0	3.2	0.64	2.3	0.46	0.55
3	2.3	1.5	0.64	1.0	0.43	0.54
4	1.4	0.8	0.59	0.0	0.32	0.45
5	3.8	2.3	0.59	1.5	0.39	0.49
7	2.3	1.2	0.52	0.6	0.24	0.38
8	3.7	2.6	0.71	2.0	0.55	0.63
9	2.1	1.3	0.59	0.1	0.35	0.47
10	2.4	1.7	0.70	1.3	0.52	0.61
14	4.2	3.3	0.78	2.8	0.66	0.72
15	4.0	3.2	0.80	2.7	0.68	0.74
16	0.1	0.1	0.56	0.0	0.25	0.40
17	2.9	2.3	0.80	1.9	0.66	0.73
18	3.0	2.4	0.79	2.0	0.65	0.72
19	1.1	0.1	0.65	0.0	0.40	0.53
20	4.0	3.4	0.83	2.9	0.72	0.77
25	2.5	1.7	0.66	1.2	0.47	0.56

Table 5.4 Friction velocities based upon total roughness (U_{*c}) and grain roughness only (U'_{*c}), together with the corresponding drag coefficient (C_D). The drag values (C_d) for each burst represent the proportion of the total friction velocity that acts directly upon the sea bed sediment. Values have been determined for two heights (thickness) of the boundary layer.
Key: GM82- Grant and Madsen (1982); GG83- Grant and Glenn (1983); CJ85- Christoffersen and Jonsson (1985).

Sediment transport formula	**Zanke parameter (S)**
Yalin (1963)	.1714E+05
van Rijn (1986)	.1176E+03
Meyer-Peter and Muller (1948)	.3647E+03
Hardisty (1983)	.6514E+03
Paintal (1971)	.1721E+04
Engelund and Hansen (1967)	.1184E+03
Einstein (1950)	.1185E+04
Kalinske-Frijlink (1951)	.5535E+03
Soulsby (1993)	.1773E+02

Table 5.5 Performance of (nine) predictive equations (Ackers and White values omitted as they lie frequently at zero), assessed using the criteria of Zanke (1987) (see text). Those equations with S values nearest unity have performed best.

Burst	Bedload transport rate (kg m^{-1} s^{-1})	
	Observed	Predicted
2	0.016	0.021
4	0.003	0.003
5	0.003	0.009
7	0.005	0.001
8	0.004	0.007
9	0.004	0.001
10	0.007	0.002
14	0.003	0.011
15	0.008	0.010
16	0.004	0.001
17	0.007	0.003
18	0.007	0.003
20	0.003	0.011
25	0.006	0.002

Table 5.6 Bedload sediment transport rates predicted using the formula suggested within the present investigation (Equation 5.61) in relation to those inferred from observations of the sea bed.

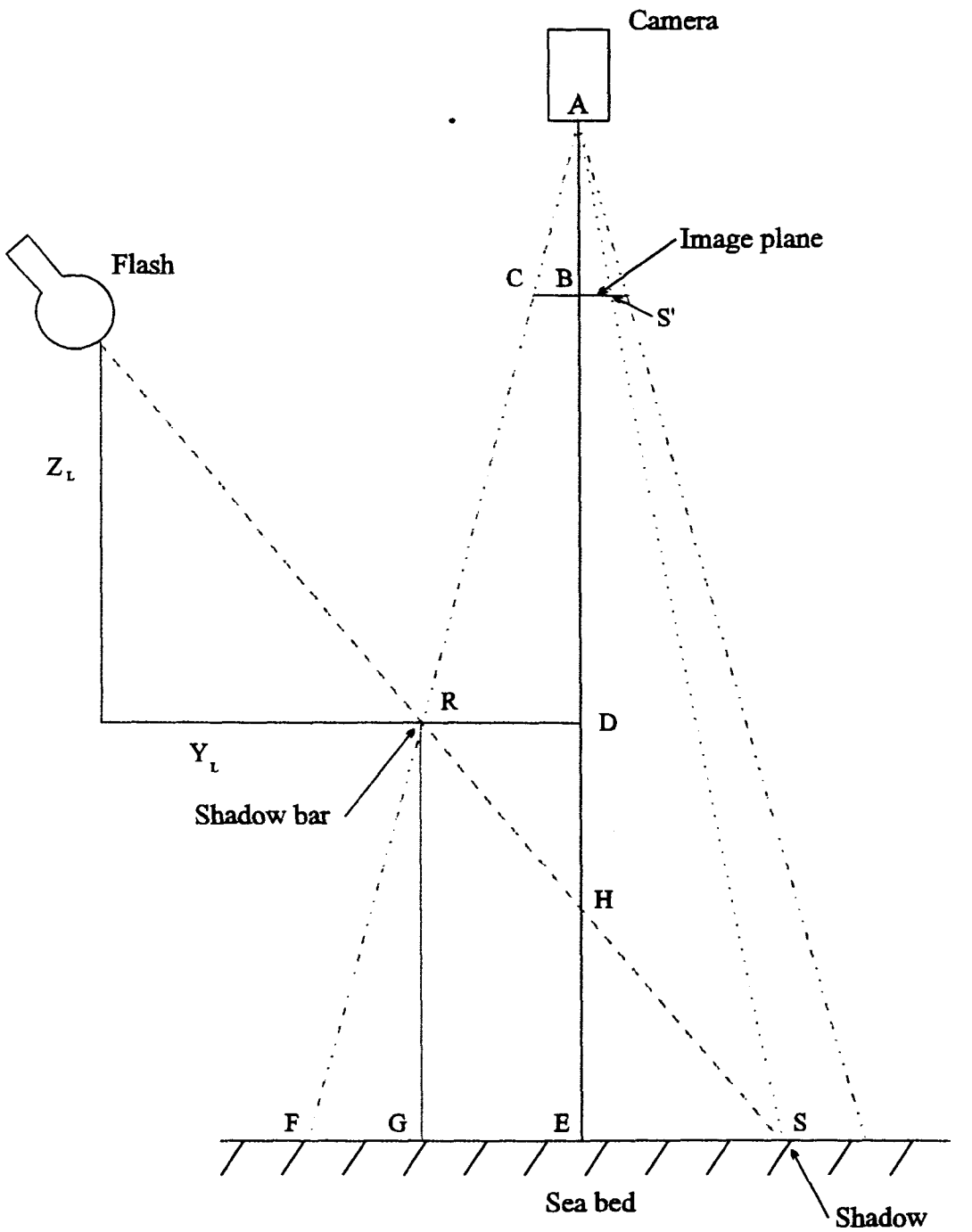

Figure 5.1 Two-dimensional geometry of the STABLE tripod showing camera, flash illumination and sea bed.

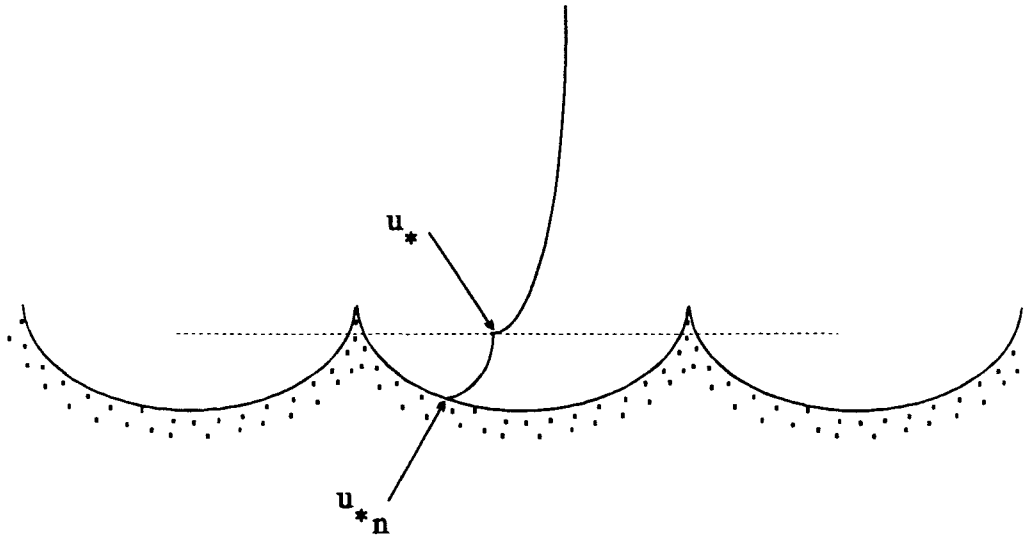

Figure 5.2 Diagram showing the two-stage velocity profile used to obtain friction velocities acting on the bed sediment only.

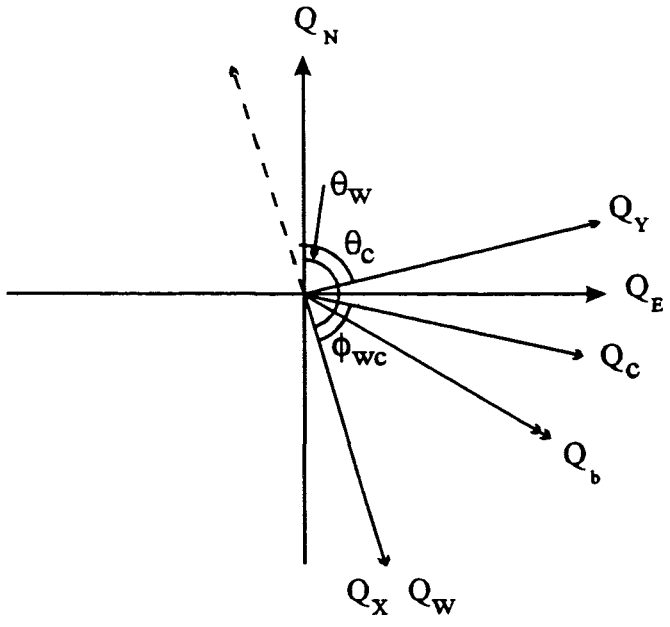

Figure 5.3 Definition diagram of wave-current interaction, as considered within the context of the present study. Key: θ_c, θ_w - direction of tidal currents and waves, respectively; ϕ_{wc} - wave-current interaction angle; Q_c, Q_w - current- and wave-induced, respectively, sediment transport; Q_b - combined wave-current sediment transport vector; Q_X, Q_Y - components of combined transport parallel and perpendicular, respectively, to the wave direction; Q_E, Q_N - easterly and northerly, respectively, components of combined transport.

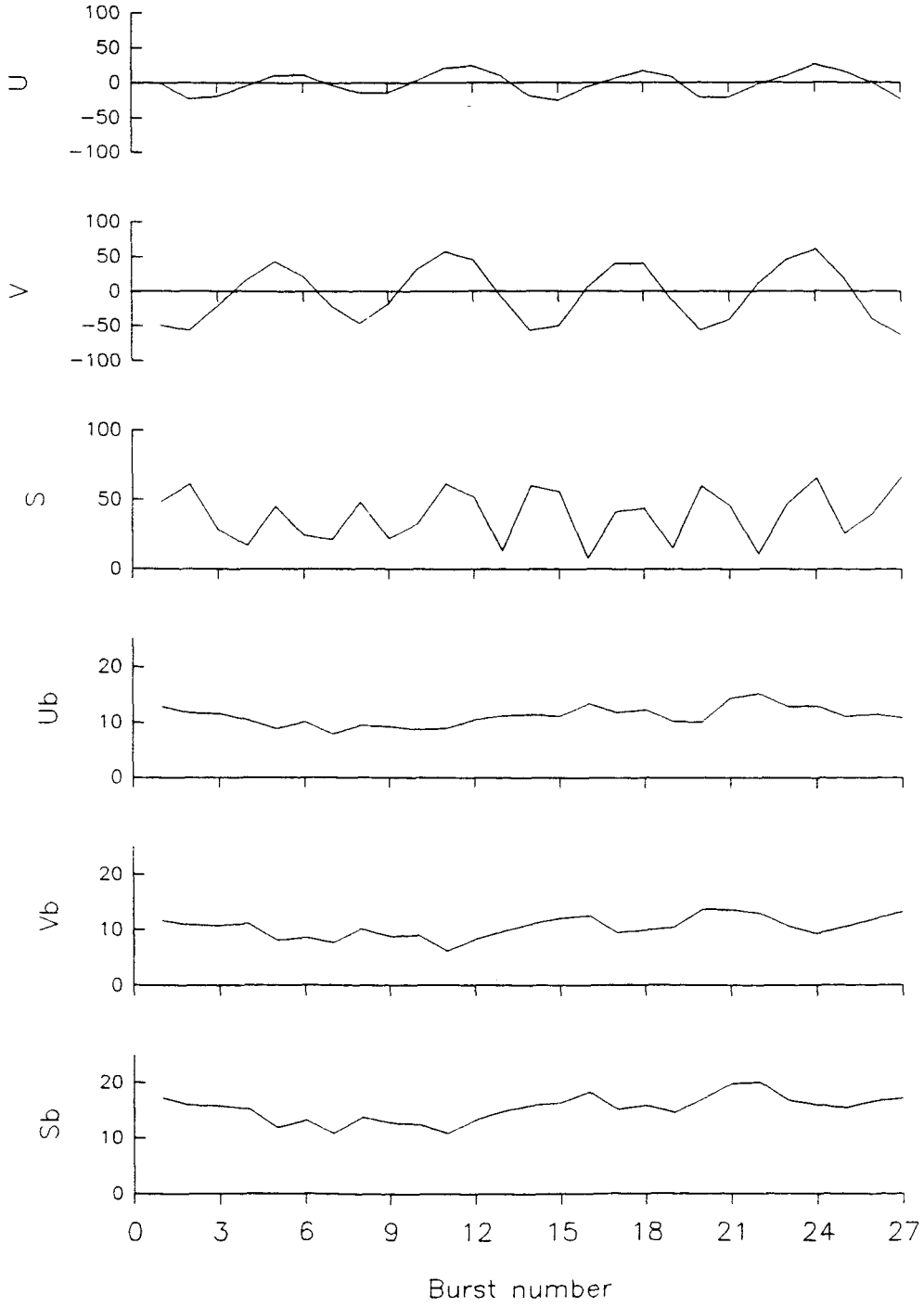

Figure 5.4a Hydrodynamic data recorded by STABLE over the deployment, at 41 cm above the bed.
Key: U, V - orthogonal components of tidal current velocity; S - resultant of U and V; Ub, Vb - orthogonal components of wave orbital velocity; and Sb - resultant of Ub and Vb.

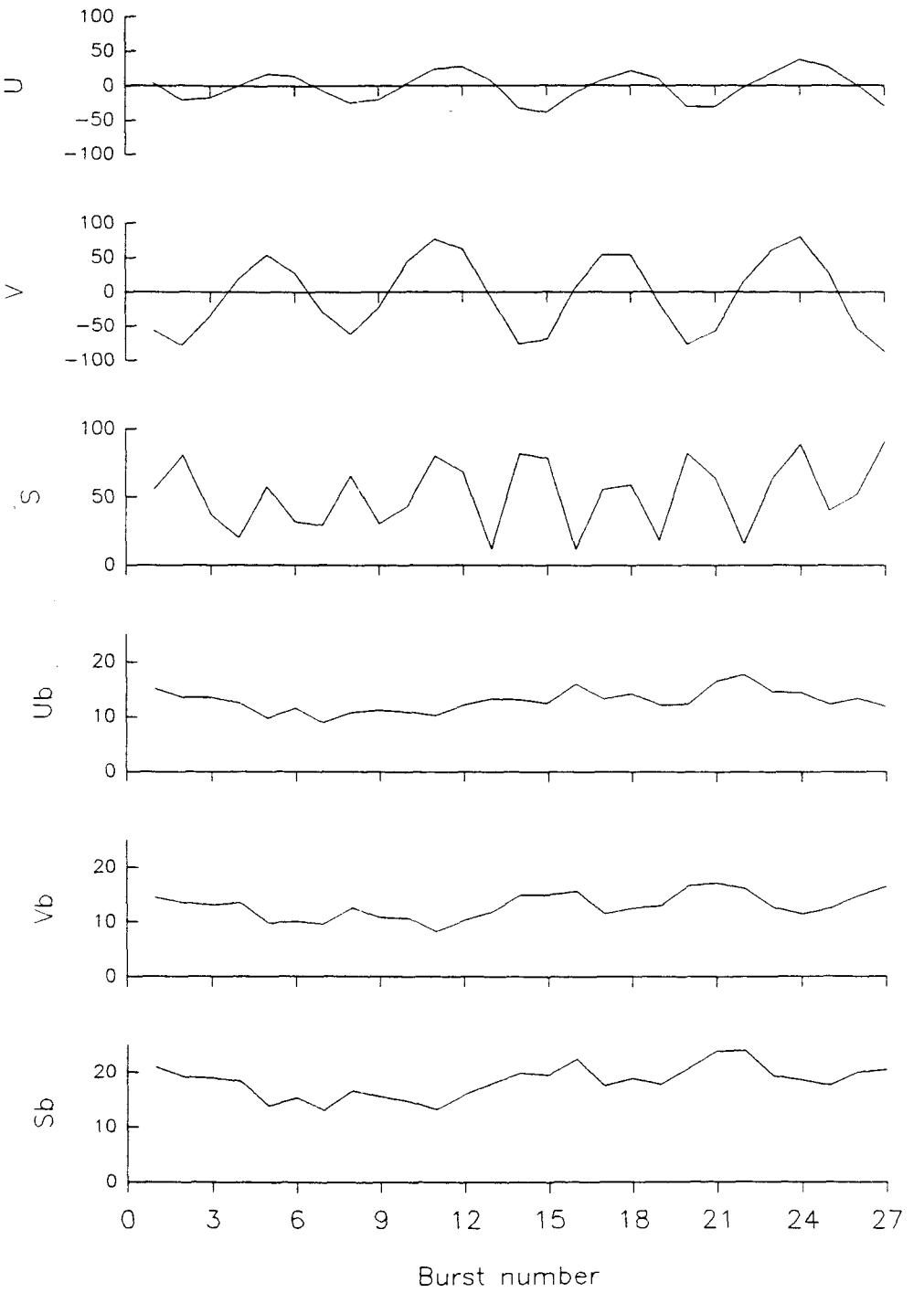

Figure 5.4b As for Figure 5.4a, data recorded at 80 cm above the bed.

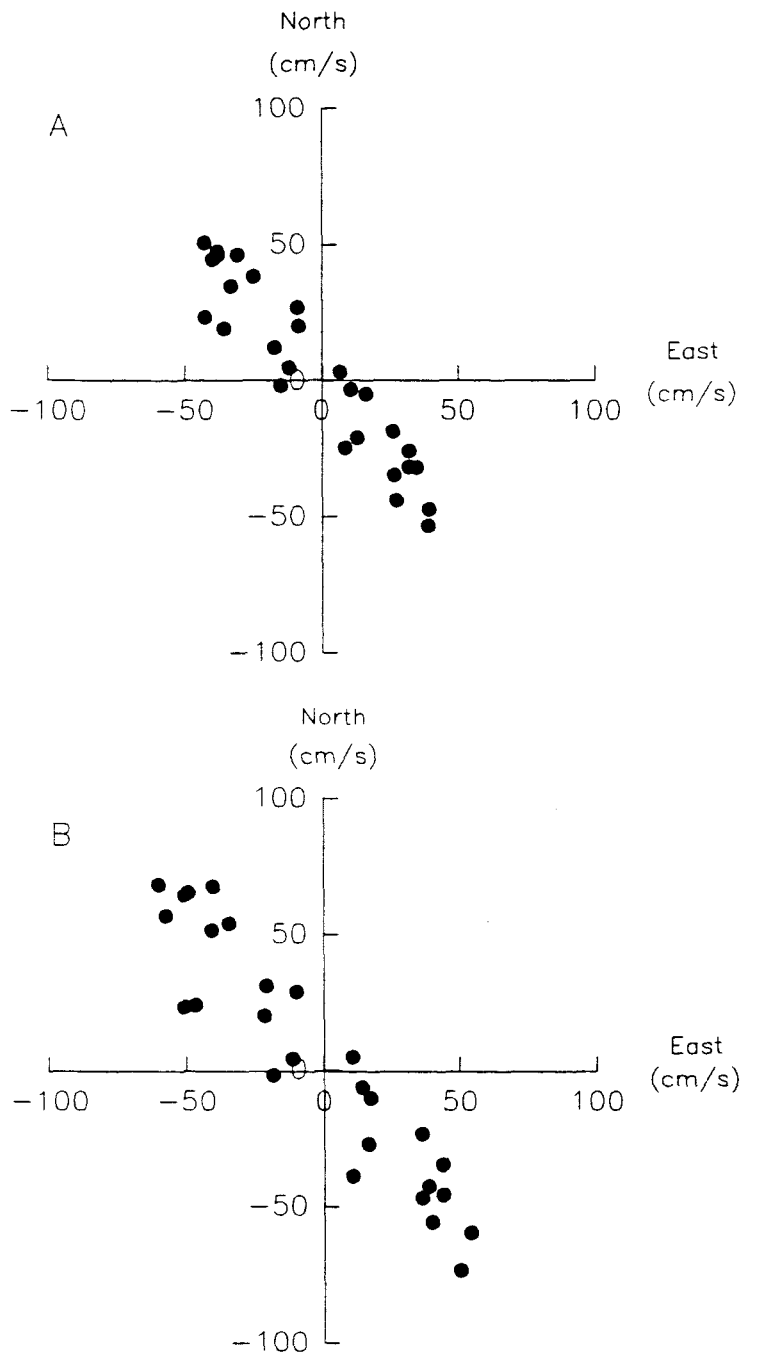

Figure 5.5 Burst-averaged steady current velocities recorded by the STABLE tripod, plotted on north-south, east-west axes. Data were recorded at 41 cm above the bed (Graph A) and 80 cm above the bed (Graph B).

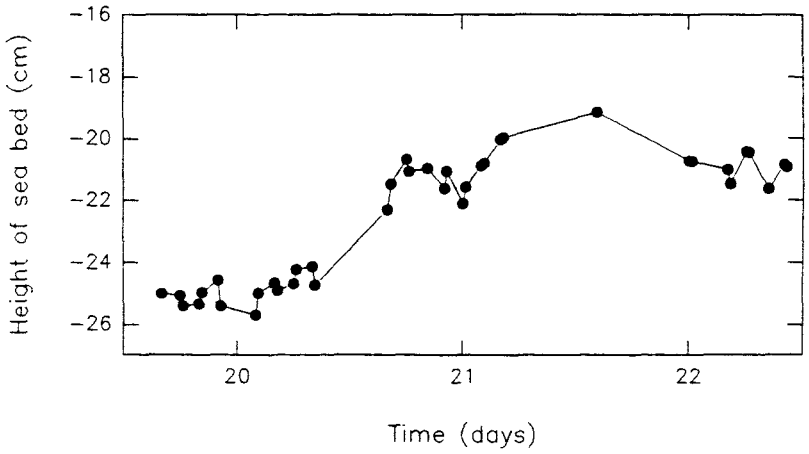

Figure 5.6 Elevation of the sea bed, relative to the shadow bar, during the period of the deployment.

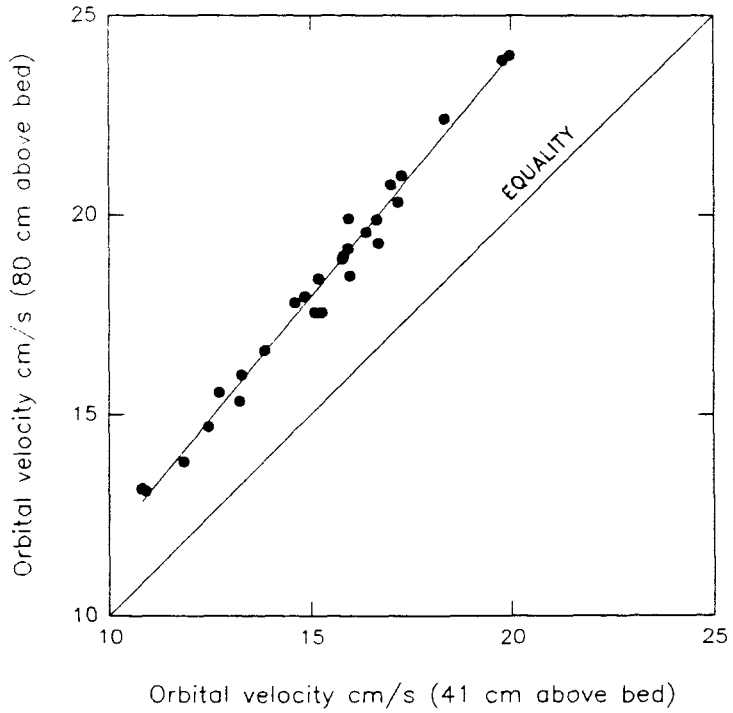

Figure 5.7 Wave orbital velocities recorded at 80 cm above the bed compared with those recorded at 41 cm above the bed, with a regression line passing through data. Also shown is the line representing equality between the two groups of data.

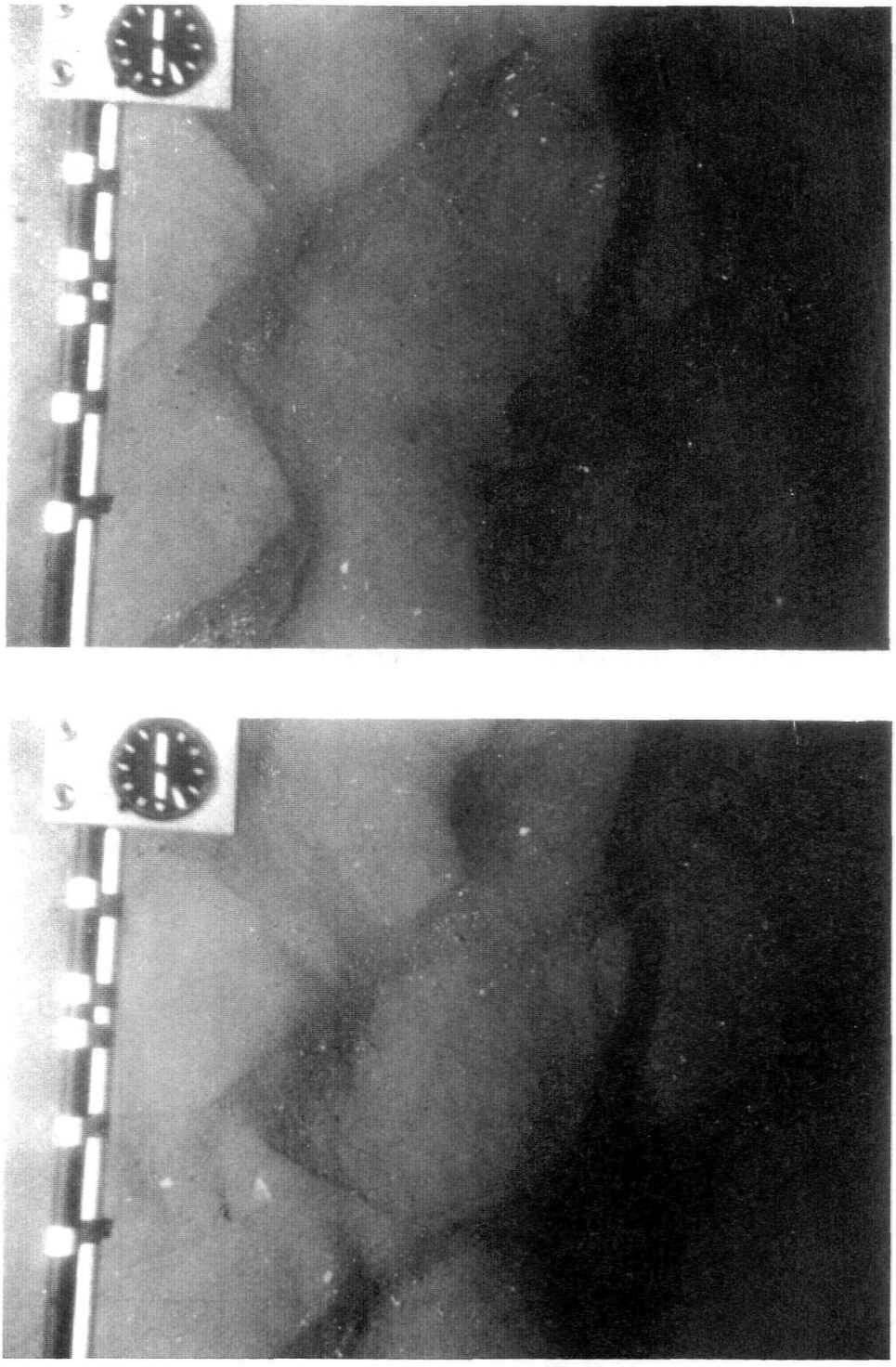

Figure 5.8 Consecutive photographs of the sea bed obtained during the STABLE deployment. The photographs shown were taken at the beginning (top) and end (bottom) of Burst 17. Shown also in each photograph are the compass and shadow bars.

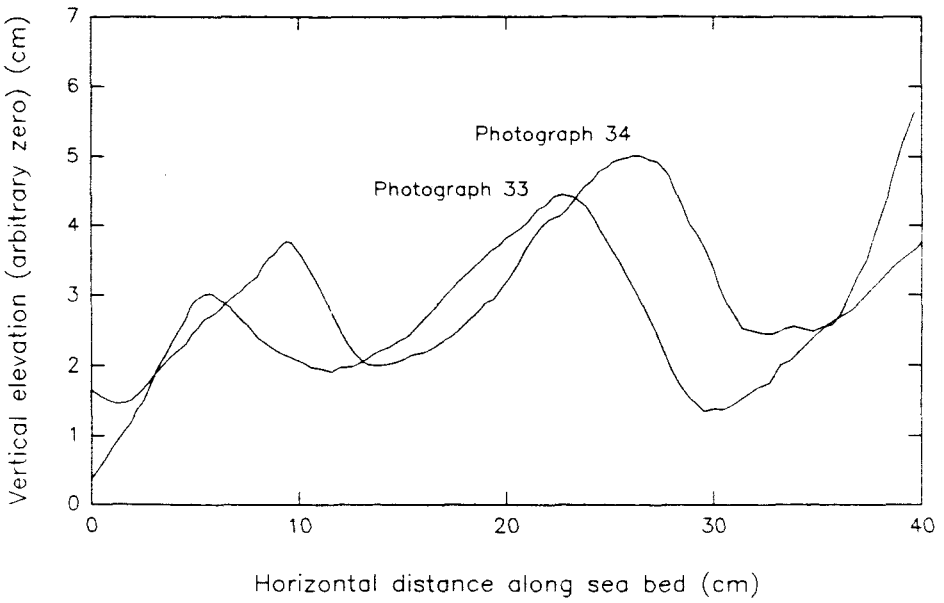

Figure 5.9 Sea bed profiles obtained from the photographs shown in Figure 5.8.

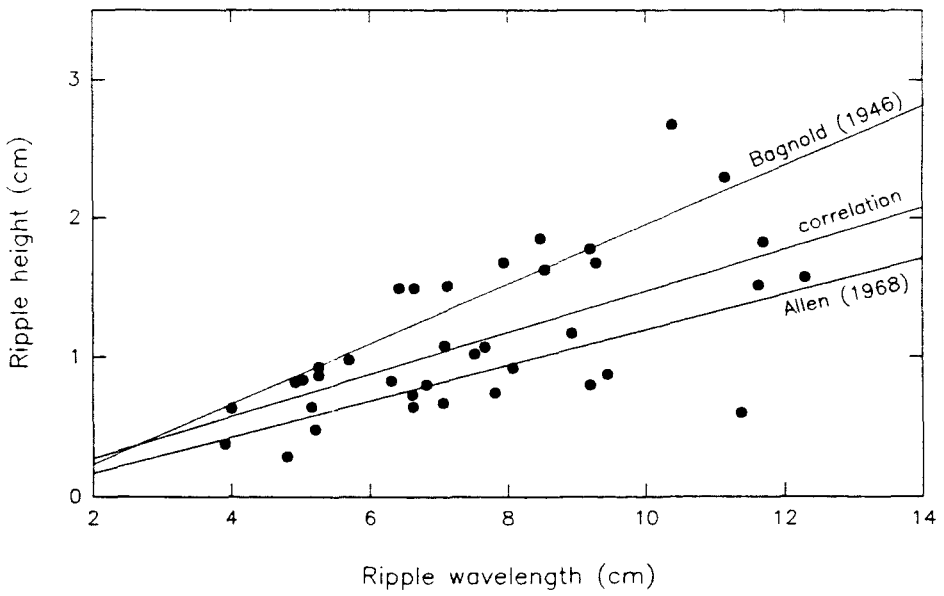

Figure 5.10 Ripple height plotted against ripple wavelength for the bedforms observed as part of the present investigation. Also presented are the steepness formulae of Bagnold (1946) and Allen (1968) (Equation 5.49).

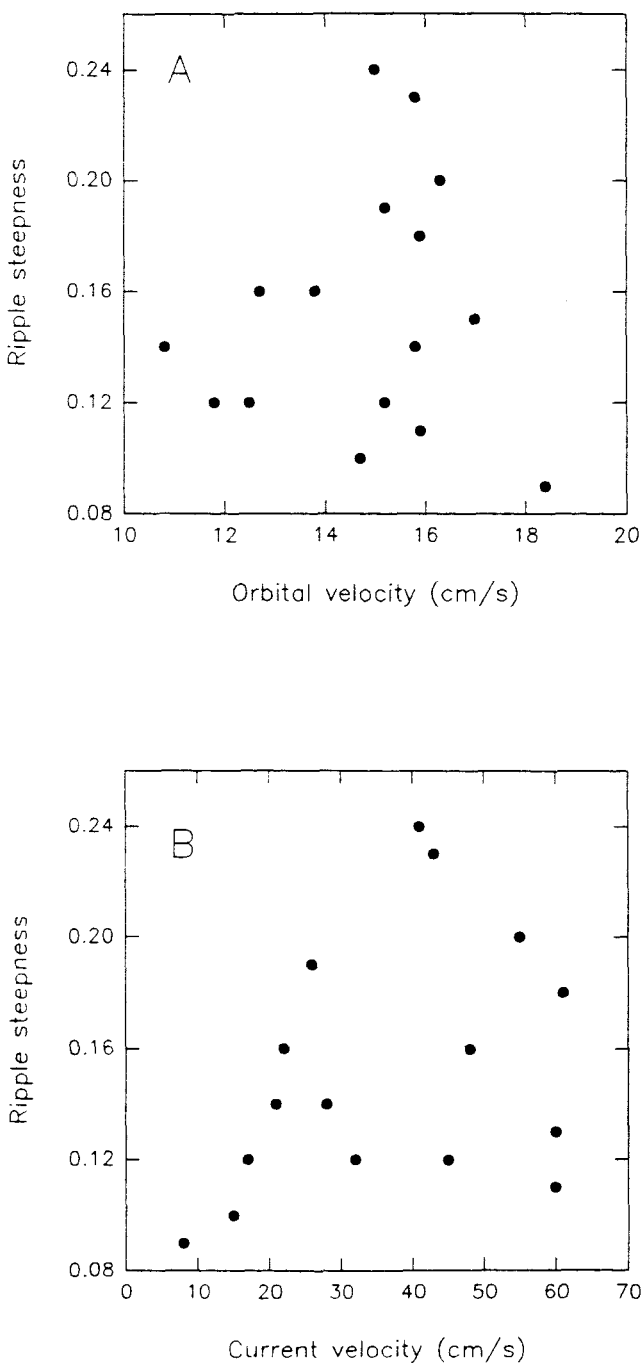

Figure 5.11 Ripple steepness plotted against rms wave-induced orbital velocity (Graph A) and tidal current velocity (Graph B).

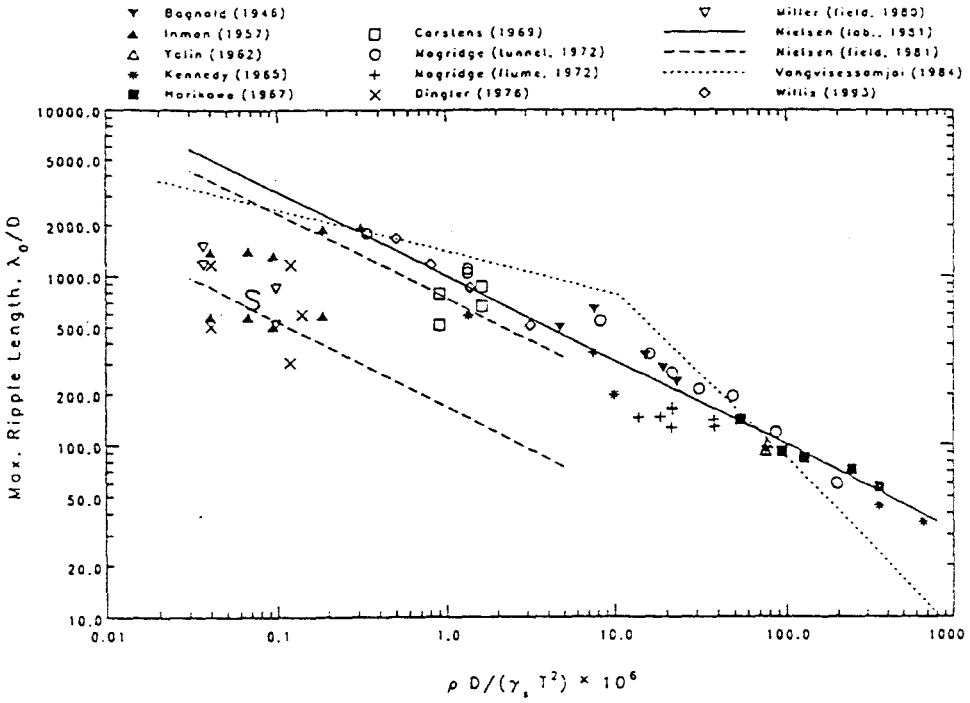

Figure 5.12 Ripple wavelength shown in relation to the (wave) period parameter. The data obtained during the present investigation are shown (after Mogridge *et al.*, 1994). (centre of S=STABLE data).

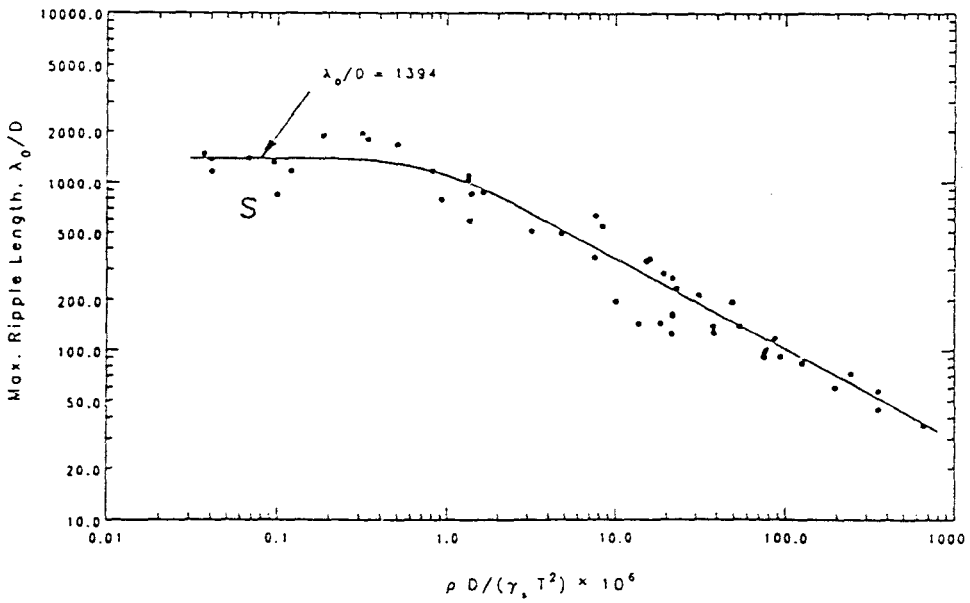

Figure 5.13 Results of the curve fitting exercise performed by Mogridge *et al.* on the maximum bedform length data. Also shown are the data obtained during the present investigation (after Mogridge *et al.*, 1994). (S=STABLE data).

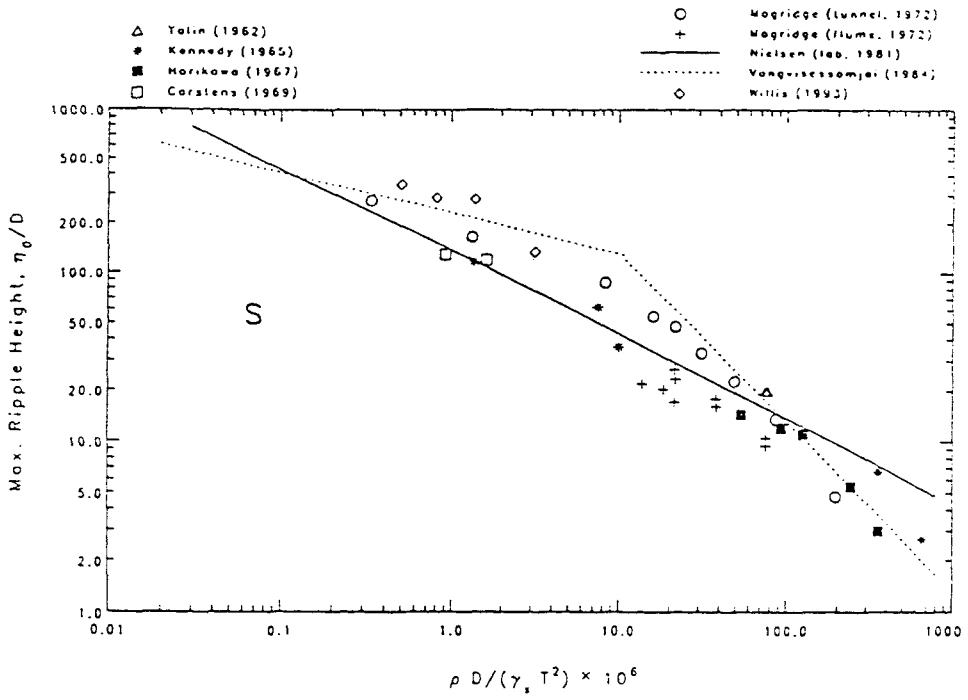

Figure 5.14 Ripple height shown in relation to the (wave) versus period parameter. The data obtained during the present investigation are shown (after Mogridge *et al.*, 1994). (S=STABLE data).

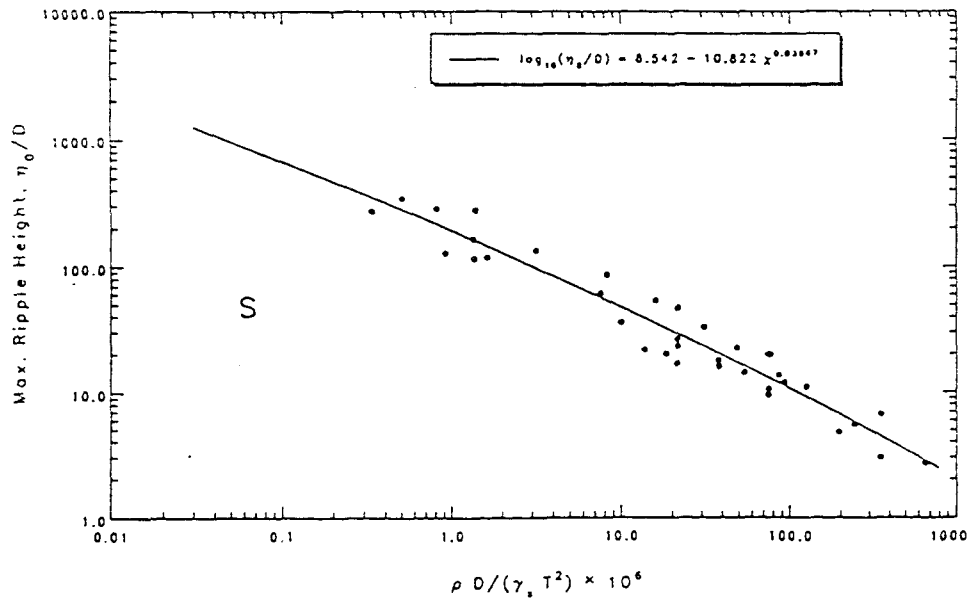

Figure 5.15 Results of the curve fitting exercise performed by Mogridge *et al.* on the maximum bedform height data. Also shown are the data obtained during the present investigation (after Mogridge *et al.*, 1994). (S=STABLE data).

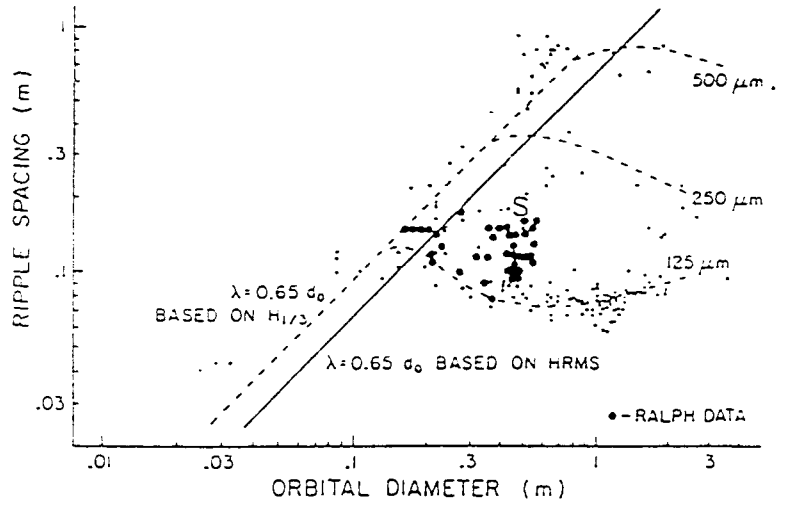

Figure 5.16 Comparison of the data from the present investigation with those obtained by Amos *et al.* (1988) and from the investigation of Miller and Komar (1980a) (after Amos *et al.*, 1988). (S=STABLE data).

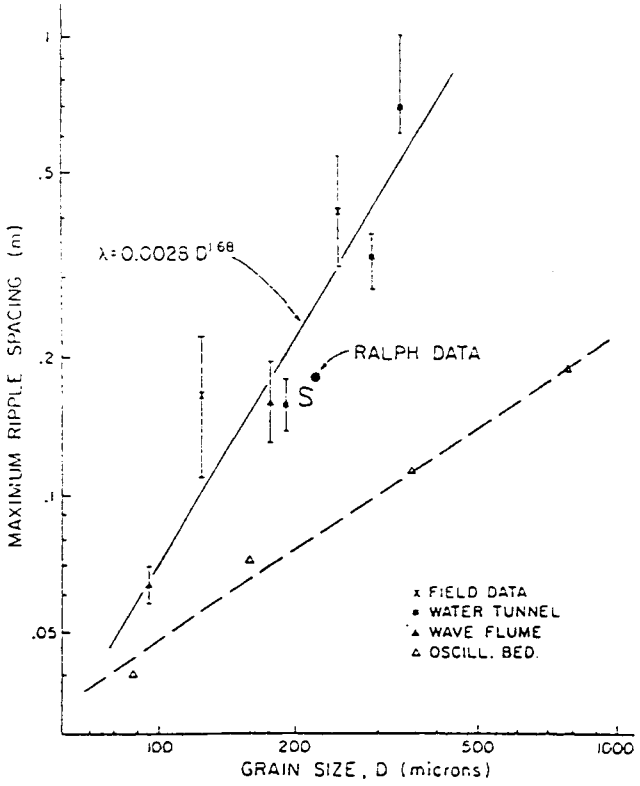

Figure 5.17 Comparison of the data from the present investigation with those obtained by Amos *et al.* (1988) and from the investigation of Miller and Komar (1980a) (after Amos *et al.*, 1988). (S=STABLE data).

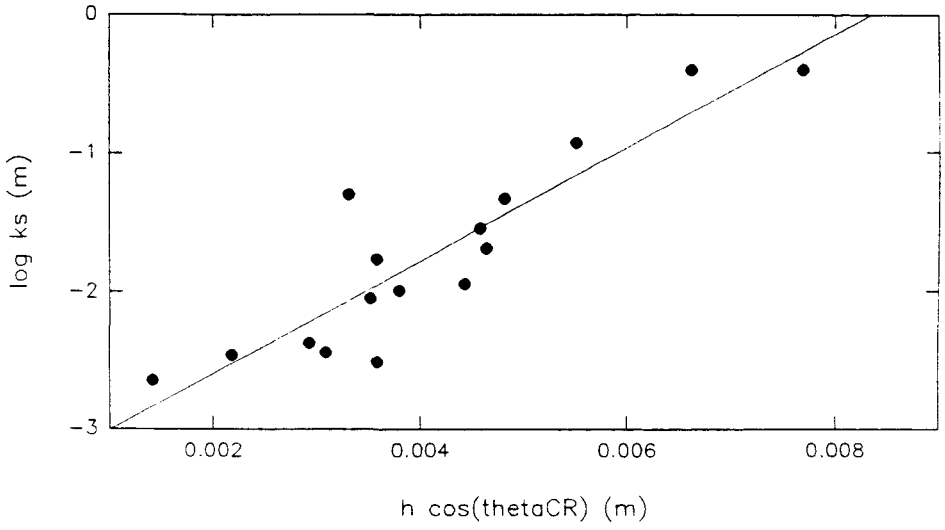

Figure 5.18 Dependence of the bed roughness (k_s) upon the ripple height (h) and the angle made between the current direction and the ripple crests (thetaCR $\equiv \theta_{cr}$).

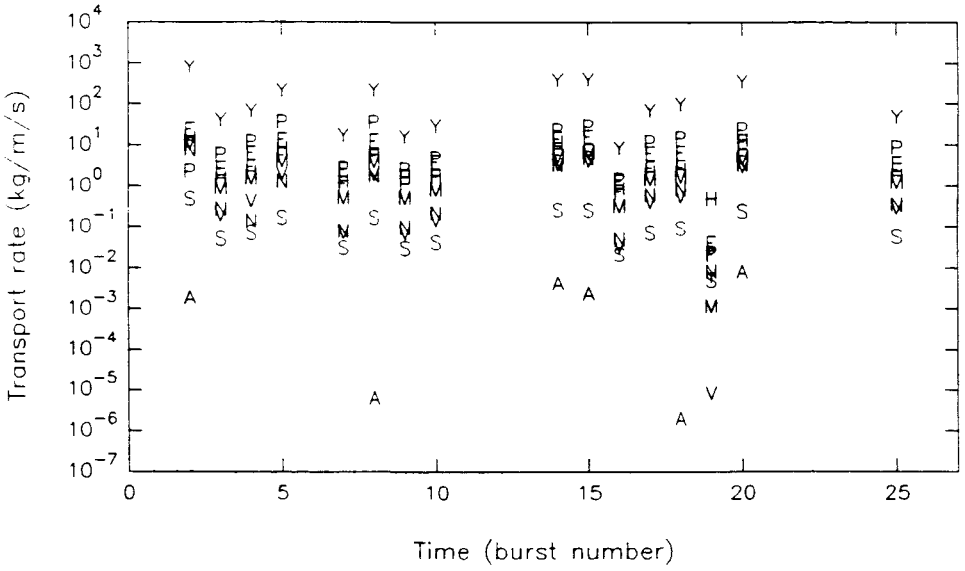

Figure 5.19 Bedload transport rates predicted by the (ten) formulae investigated here as part of the present investigation.
Key: M=Meyer-Peter and Müller (1948); E=Einstein (1950); F=Kalinske-Frijlink (1951); Y=Yalin (1963); N=Engelund and Hansen (1967); P=Paintal (1971); A=Ackers and White (1973); H=Hardisty (1983, 1990); V=van Rijn (1986); and S=Soulsby (1993).

Chapter 6
REGIONAL SEDIMENT TRANSPORT PATTERNS

6.1 INTRODUCTION

Tidal sand banks are the largest bedform, orientated sub-parallel to the flow, of continental shelves associated with strong tidal currents. Offshore examples, which are active in European seas at the present time, can be up to 50 km long, 3 km wide and rising 40 m in height above the surrounding sea bed (Stride, 1982).

Stride (1963) has investigated the regional sediment transport patterns prevailing around the southern UK continental shelf, concluding that the status of the sand banks lying off the Norfolk coastline is somewhat uncertain. Inferred diverging sand streams, from both ends of the East Anglian banks, suggest that they should be diminishing in size; however, this has not been established. Indeed, coastal erosion must be supplying sand to the system. A mechanism to explain such a movement has been established recently by Stride (1988). A complex pattern of transport, related to partial separation of the pathways of the ebb and flood currents between the banks is evident; however, this does indicate the overall pattern of sediment transport. Rather, storm-induced offshore transport of sand-sized material must be included in the regional budget.

An understanding of the sediment transport processes active within the present study area is important for navigation purposes, for pipeline integrity, and for the dredging industry. Such interests are in addition to the long-term scientific interest in understanding the sediment transport regime in the vicinity of linear sand banks. In this Chapter, the patterns of movement of sediment transported as bedload around the Broken Bank are investigated. Bedload transport rates are presented here in terms of mass transport rates (g cm^{-1} s^{-1}), so that direct comparison can be undertaken with similar studies (undertaken elsewhere) and previous investigations in the area.

6.2 METHODOLOGY

The approach adopted in previous investigations (see for example Heathershaw, 1981; Lees, 1983b) has been based upon the application of (physically-based) empirical sediment transport formulae, derived and applied to near-bed self-recording current meter observations from the marine environment (Heathershaw, *op. cit.*; Pattiaratchi and Collins, 1984). Sediment transport rates and directions have been determined for unidirectional tidal currents alone and under the superimposed influence of waves, as a combined flow.

The present investigation differs from many that have been undertaken previously, in that sediment transport pathways are predicted using two methods. The first approach adopts widely-accepted empirical methods. Within the second method, an attempt has been made to determine more accurately the bed shear stresses induced under the combined wave and current conditions. Such shear stresses have been evaluated using a recently-derived combined boundary layer model (see below). Further, an attempt has been made to incorporate accurately into the analysis the influence of bedforms on the rate at which sediment is transported.

The distribution of sea bed sediments over the study area has been determined on a regional basis around and including the Broken Bank; this was established on the basis of extensive grab sampling (53 sites) of the area around the sand bank (Shimwell, 1990). The sediment was found to be composed of well sorted sands, with a mean diameter of 0.2 mm (with a standard deviation of 0.03 mm). This grain size compares well with median grain sizes ranging from 0.2 mm to 0.3 mm found on the adjacent Well Bank (Houbolt, 1968). In all the sediment transport calculations, the density of the grains has been taken as that of quartz ($2.65\ g\ cm^{-3}$).

Regional (sediment) transport pathways have been inferred from the (self-recording) current meter records obtained at 2 m above the bed, at 5 Stations around Broken Bank (Chapter 4).

The derived sediment transport rates are based generally upon the exceedence of a critical threshold condition, between 'no movement' and 'some movement' of the sediment. Many investigators have proposed various definitions for this threshold (Section 3.1.3). In this investigation, the threshold of movement for the sediment has been determined using Yalin's (1972) modification of the Shield's (1936) curve (Section 3.1.3). In this approach, a critical friction velocity (u_{*cr}) is established; this is based upon the sediment grain size (diameter) found at a particular location. Such a value must be exceeded before the sediment can be transported. Many transport formulae incorporate excess stress ($\tau - \tau_{cr}$) or excess velocity ($u - u_{cr}$) terms relating to some height above the bed (typically 1 m). The assumed velocity profile (see below) can be used then to convert the critical friction velocity to a threshold value representative of this particular height above the bed (u_{100cr}); this value is used in the equation for deriving predicted bedload transport rates.

6.2.1 Method 1

This approach is based primarily on the self-recording current meter observations obtained for this current-dominated ($\tau_{cu} > \tau_w$) environment (Chapter 5). The effect of waves, in enhancing the bed shear stresses, are included at the end of the procedure. For unidirectional flow, the general procedure adopted here for the determination of transport rates is outlined below:

(i) Selection of an appropriate and representative (a) grain size, (b) roughness length (z_0), as required by the assumption of a logarithmic velocity profile (see below);

(ii) Use the velocity profile to determine bed shear stresses from the current meter observations, at 2 m above the bed.

(iii) Use of the velocity profile to obtain an effective flow velocity at 1 m above the bed (u_{100}), for this fraction of the total bed shear stresses.

(iv) Compare this value of u_{100}, with the threshold condition.

And, finally, (v) if the threshold is exceeded, use of a transport equation (Equation 5.61) to calculate the bedload transport rate.

Sediment transport on the inner continental shelf is the result mainly of combined wave activity and tidal currents. The effect of waves on the predicted sediment transport rates has been determined here through the adoption of the formulae of Bijker (1967) (Section 3.3.1). In this way, the rates of sediment movement under a combined wave and current regime can be calculated.

Throughout this particular investigation, it has been assumed that there was no directional veering within the current boundary layer (see, for example, Gill, 1968). Therefore, the resultant direction of sediment (bedload) transport was taken to be that of the tidal current flow at 2 m above the sea bed.

(a) Assumption of a velocity profile

Tidal current observations have been obtained at five locations around the Broken Bank (Figure 4.1). The current meters were located near-bed (2 m) and at mid-depth (10 m and/or 12 m) elevations above the sea bed. The sediment transport predictions have been obtained on the basis of the flow variations recorded at 2 m above the bed. In order that these observations can be transformed into the parameters used in the prediction of sediment transport rates, an assumption has to be made regarding the structure of the velocity profile. For this investigation, the von Karman Prandtl logarithmic velocity profile (Equation 3.4) has been used for the determination of the friction velocity from the observed current speeds. The bed shear stress (τ_0) can be determined subsequently from Equation 3.5. Various field measurements (Charnock, 1959; Caldwell and Chriss, 1979; and Soulsby and Dyer, 1981) have confirmed that a value of the von Karman's constant of 0.4 is appropriate for use in the marine environment. The assumption of a logarithmic velocity profile requires specification of a roughness length (z_0) (see below).

Sternberg (1968) has investigated the occurrence of logarithmic velocity distributions within the current boundary layer (up to 1.5 m above the bed) in several channels within Puget Sound, Washington. The bed sediment related to each of the channels was different and it was found that logarithmic velocity

distributions occurred, on average, 85% of the time. However, the sandy channels experienced logarithmic velocity distributions in excess of 90% of the time. In an investigation carried out to the west of Well Bank, current speed profiles have indicated that there is a logarithmic velocity distribution within the lowest 5 m of the water column (Harvey and Vincent, 1977). Combining measurements obtained around Well Bank, Howarth and Huthnance (1984) identified that the current velocity profile was logarithmic throughout the water depth (cf. Figure 3.1).

However, in such a dynamic environment, the velocity profile may not always be logarithmic. Deviation of the velocity profile, away from a logarithmic structure, can be most significant during periods of highest flow acceleration and deceleration (Dyer, 1980). This divergence could have important repercussions in determining the accuracy of the derivation of the bed shear stresses (and transport rates). However, the greatest changes in the velocity structure are likely to occur at the beginning and end of a tidal cycle. At such times, the current speeds are lowest, hence, they are likely to be below the threshold conditions for sediment movement. It is considered reasonable to assume, therefore, that a logarithmic velocity profile exists in the lower 2 m of the water column and over periods when sediment transport will be initiated and maintained.

(b) Selection of a suitable roughness length

The assumption of a logarithmic velocity profile requires now the selection of a value for the roughness length (z_0). This decision influences directly the estimated values of the bed shear stress, from the current meter data. Hence, some considerable care must be taken to ensure that an appropriate value is selected.

Considerable uncertainty exists in the z_0 value to be adopted for any particular situation. HR (1991), for the hydrodynamic data presented in Chapter 5, predicted z_0 values around 5 cm. However, z_0 values obtained from the equations of Lettau (1969) and Wooding *et al.* (1973), using ripple dimensions observed during the same deployment, produced z_0 values which were an order of magnitude lower

than the widely published value (0.5 cm) given typically for a rippled sand bed. A compilation of the many measurements of sea bed roughness lengths which can be used for predictive purposes is presented in Table 3.2. In the marine environment, considerable variation around these values is observed. The range of values is encompassed generally by a factor of about 3 (Dyer, 1986); empirically, this takes into account effects such as biological activity, or bioturbation, in roughening the bed. These latter factors can be significant, however, with Nowell *et al.* (1981) reporting a doubling of the roughness (length) caused by animal tracks across muddy sands.

The relationship between the flow speed at 1 m above the bed (u_{100}), the roughness length and the resulting bed shear stress (τ) has been investigated here. In particular, the influence of z_0 (from zero to 1 cm) on transport rates has been determined. Such a range encompasses values for z_0 quoted widely in the literature for a fine sand bed i.e. 0.05 cm for a planar sand bed, and 0.5 cm for a rippled sand bed. Two representations of this relationship are shown on Figure 6.1. The 2-D plot shows that the dotted lines representing shear stress lie almost parallel to the z_0 (y) axis for the majority of the graph. This result indicates that, for most of the range of z_0 values investigated here, little influence on the τ values can be perceived i.e. τ is controlled primarily by variation in the u_{100} values.

The lower end of the graph displays rapidly varying values of τ, for z_0 values up to 0.1 cm. It is over this particular portion of the graph, therefore, that the roughness length has most influence; this suggests that it is the order of magnitude of z_0 which is of primary interest, rather than its absolute value.

On the basis of previous work (e.g. Heathershaw (1981) Table III, p.85; Lees (1983b) Table 3, p.469), a value of z_0=0.5 cm was taken for z_0 and used in the present investigation.

(c) Wave enhancement of current-only transport rates

The current-only approach, as described above, can be modified easily to include the effects of waves on the predicted (current-only) sediment transport rates. Combined wave-current transport rates can be achieved by incorporating the formulae of Bijker (1967) into the process (see, for example, Heathershaw, 1981; Lees, 1983b). Water depth and surface wave characteristics are the only additional information necessary (Section 3.3.1). The influence of this combined approach, on the enhancement of the (near-bed) shear stress and transport rates, is shown in Figure 6.2.

6.2.2 Method 2

The second approach adopted here to determine sediment transport rates is based upon recent research into the wave-current boundary layer. This approach, used in the determination of bedload sediment transport rates under the combined influence of waves and currents, is described in Chapter 5. Here, the boundary layer model of Sleath (1991) has been used to obtain wave- and current-induced bed shear stresses, on the basis of wave data recorded during the STABLE deployment and the current meter data recorded at 2 m above the bed, respectively. Wave-induced orbital velocities, at a level of 2 m above the bed, have been determined assuming first-order linear wave theory. A roughness parameter appropriate to the location, derived on the basis of a k_s value determined from the STABLE deployment (Chapter 5) has been used. Thus, one source of significant uncertainty (namely, the appropriate description of bed roughness) has been removed from the predictive process. The absolute shear stress values have been reduced, in order to accommodate the influence of bedforms (as form drag) in the analysis. The resulting shear stresses, assumed to be acting directly on the bed sediment alone (as skin friction), are used then within the transport relationships presented in Section 5.4.4 (Equation 5.61).

The ability of existing sediment transport formulae to predict accurately rates of

sediment movement was described in Chapter 5. Here, this approach has been extended to include directional considerations within the context of sediment transport patterns. The relationship between the parameters involved in this method, in terms of a definition sketch, is shown as Figure 5.3.

Net bedload transport rates have been determined for typical spring and neap tidal cycles, together with that representing the overall current meter record length i.e. up to approximately 11 days.

Bed form influence on sediment transport

Photographic data obtained during the STABLE deployment have revealed the presence of ripples on the sea bed, over this particular area of investigation. The total shear stress applied to the sea bed can be divided into skin friction (τ') and the form drag (see above) in relation to the bedforms (τ'') (Einstein and Barbarossa, 1952). Since it is the skin friction which acts on the sediment and causes movement, the applied force will move sediment only when the total drag over the bedform produces a skin friction greater than the threshold value. The effect of form drag is to reduce, therefore, the bed shear stress available for transporting individual sediment grains. Transport rates determined without considering form drag would be expected, consequently, to overestimate the rate of sediment movement around Broken Bank (or, indeed, other areas where the sea bed exhibits longitudinal or transverse bedform features). Accurate predictions of sediment transport rates and directions must consider, therefore, the effect of bedforms on transport predictions.

The investigation undertaken previously (Chapter 5) describes the incorporation of a rippled sand bed into the analyses. Namely, that the friction velocity related to flow speed at 80 cm above the bed is caused by both the grain roughness and the presence of bedforms. The velocity profile is modified, therefore, to provide a u_* value based upon sediment grain characteristics alone. The ratio of the two u_* values provides an indication of the component of the friction velocity dedicated to

overcoming form drag (some 42% of the total friction velocity (Section 5.4.4)); this, therefore, is not responsible for movement of any sediment.

6.3 RESULTS AND DISCUSSION

6.3.1 Exceedence of critical velocities

Variations in velocity are compared now with the critical velocity required to initiate sediment movement. The threshold value for the initiation of movement, for a mean grain (sand) size of 0.2 mm, has been taken as 17 cm s^{-1} at 1 m above the bed. The results of this part of the investigation are summarised in Table 6.1. Three groups of results are presented for each station; the upper values listed (a) describe the percentage of time over which threshold was exceeded; this might be expected to vary with recording period (overall deployment record; spring or neap tidal cycles), with the highest exceedence over springs and the lowest over neaps. This pattern is observed generally around the Broken Bank. The values derived for the complete deployment are likely to be biased, as the length of deployment was less than 14 days; consequently, tidal current velocities over a complete spring-neap cycle were not recorded. On average, at all the stations, the threshold velocity at
1 m above the bed was exceeded for 68.2% of the time during neap tides, 76.7% of the time during spring tides and 74.8% of the time over the complete period of deployment. On the basis of these observations, the sandy sea bed in the vicinity of the Norfolk Banks may be regarded as highly mobile; this feature of the investigation is discussed more fully in Section 6.4.

Once threshold is exceeded, the flows related to spring tidal conditions are significantly greater than those on neaps; around the bank, the spring condition results in current speeds which average 26.5 cm s^{-1} greater than the threshold. Under neap tidal conditions, this value falls to 10.7 cm s^{-1}.

6.3.2 Sediment transport predictions (Method 1)

Sediment transport pathways are predicted initially using Method 1 based on tidal current variations only.

(a) Scalar transport rates

The predicted transport rates for each station are presented in Table 6.1. These values are scalar mean transport rates and are based, therefore, upon *speed* variations in the tidal current data. They are indicative of the volume of sediment that is mobile during the period of the deployment and have been calculated using the bedload transport formula described in Chapter 5 (Equation 5.61)

As anticipated, the bedload transport rates correlate well with the pattern of excess velocities. During the spring tidal cycle, the predicted rates are an order of magnitude greater than during neap tidal conditions. The only exception is the predicted transport rate at Station H, where the rates are of the same order of magnitude; however, the spring rate is over 4 times that predicted under neap conditions.

During neap tidal conditions, the rates along the eastern flank of the Broken Bank (Stations B and C) are greater than those to the west of the bank (Station E). During spring tidal conditions, the predicted rates on either side of the sand bank are similar; this indicates that similar volumes of sediment are mobile on each side of the Broken Bank. The highest transport rates over the area, for all record lengths, are found adjacent to the Well Bank (Station H).

(b) Sediment transport patterns around Broken Bank

Vector transport rates predicted in the vicinity of the Broken Bank, using the formula described in Chapter 5 (Equation 5.61), are presented in Table 6.2. Bedload transport vectors have been derived on the basis of records obtained for

the complete length of the deployment of the current meters, together with those representing typical spring and neap tidal cycles.

The transport vectors, in contrast to the scalar rates, indicate net movement of the sediment (sand) around the bank; here, the direction of each instantaneous current recording (and associated sediment movement) is considered, as well as the instantaneous rate. The results demonstrate clearly well-defined areas of flood and ebb bedload transport dominance. The predominant direction of transport along the eastern side of Broken Bank is towards the southeast. Over the same period, the transport direction on the western side of the Bank is more variable. At Station E, the direction of neap transport is low and directed towards the south. This rate is small compared with the rate of transport directed towards the northwest over a spring tidal cycle and over the whole of the record. The direction of transport is variable also at Station G; movement here may be directed through an arc of approximately 110° (cf. Stride, 1988). The flow at Station H, in common with the flow along the eastern flank of Broken Bank, is directed largely parallel to the axis of the Well Bank. The highest rates of sediment transport within the area are found along the eastern flank of the Well Bank. As a result, bedload transport across the width of the interbank channel, exhibits substantial directional variation. Such variability is particularly pronounced during the neap tidal cycle. Huntley *et al.* (1993) have suggested that such variability may be occurring as a result of the formation of a new sand bank in the central swale area.

The highest rates of bedload transport (for each section of the record investigated (overall, neap, spring)) around the Broken Bank are observed along the eastern flank. Sediment transport rates during the spring tidal cycle reach 3.0×10^{-2} g cm^{-1} s^{-1} at Station B. The predicted transport rates are lower along the western side of the bank. The location of Station H is sufficiently close to the Well Bank to be within the southeasterly dominated transport along its eastern flank; this is similar to the transport regime found adjacent to the eastern side of Broken Bank.

In comparison with the scalar rates, the vector sediment movement at stations

located on the eastern flanks of banks is of the same order of magnitude. This similarity suggests that the flow regime at these locations is biased strongly in a particular direction (towards the southeast). Flow away from this direction, when it occurs, appears to be mostly below the threshold condition for sediment movement. At Stations E and G sand movement is found to be variable, with relatively high rates of transportation (high scalar means); however, vector rates are substantially lower (by up to an order of magnitude) than the scalar rates. This indicates that once threshold has been exceeded by the flow to the west of the Broken Bank, a regime is established in which northwesterly and southeasterly transport rates are similar; this results in low net transport rates.

Whilst the highest transport rates occur along the eastern side of the Broken Bank, often by as much as an order of magnitude, the angle between the predominant transport direction and the bank's axis is small. Hence, only a relatively small component of the bedload transport along this side of the bank is directed towards the crestline of the bank. At Station E, a greater angle between the transport vector and the axis of the bank is associated with the spring tidal cycle and predictions based upon the entire record. During the neap tidal cycle, transport is directed largely southward; this results in transport directed away from the bank. In the mid-swale region (Station G), the transport is directed towards the bank. In summary, therefore, results presented here suggest that the supply of sand to the Broken Bank occurs intermittently on the western side and continuously on the eastern side.

(c) Transport rates under combined (wave and current) flows

The results presented above have been derived on the basis of tidal current variations alone.

The results obtained from the STABLE deployment, in which current- and wave-induced velocities could be separated from one another (see Chapter 5), showed that the area under investigation is dominated by tidal current action. The initial

approach to predicting sediment transport rates, described above, was adopted on the basis of its simplicity and widespread use. However, measurements collected during the STABLE deployment (HR, 1991) indicate that waves were present throughout the observational period. Hence, the method of analysis has been revised in order to incorporate the effects of waves on sediment transport rates using the formulae of Bijker (1967) (Section 3.3.1)

A preliminary investigation into the enhancement, by waves, of unidirectional transport rates is undertaken now. A mean water depth for the present study area and an average wave height (derived using first-order linear wave theory and orbital velocities recorded at 80 cm above the bed from the STABLE deployment), have been used to determine the enhancement (by wave action) of the current-only bed shear stresses. An average water depth (27 m), wave-induced orbital velocity (20 cm s^{-1}) and tidal current speed (35 cm s^{-1}) at 2 m above the bed, have all been assumed. The z_0 value has been kept equal to 0.5 cm (Section 6.2.1). The resulting rate of sediment transport for this particular tidal current, in the absence of wave influence, is 1.6 x 10^{-2} g cm^{-1} s^{-1}. When wave action is integrated within the predictive process, the bed shear stress is approximately 5 times that under currents alone. This level of increase more than doubles the effective flow velocity at 2 m above the bed, generating a predicted transport rate of 2.4 x 10^{-1} g cm^{-1} s^{-1}. The wave-current transport rate is an order of magnitude (some 15 times) greater than the transport rate predicted under currents alone.

The approach adopted here for predicting sediment transport rates under combined wave and current action, enhances considerably the current-only transport rates. Under the low wave conditions (1 m wave height, 10 s period in 27 m water depth) experienced during the present investigation, wave orbital velocities were lower than the tidal currents. Given these values, this level of enhancement seems unrealistic and consideration must be given to the applicability of this approach.

6.3.3 Discussion of Method 1

The results presented in this section have been based upon a method accepted as an engineering approach; namely, the use of the assumed logarithmic velocity profile with a specified roughness length and a selected transport formula. The effects of waves have been incorporated through the use of the Bijker (1967) formulae. This particular approach involves considerable assumptions, as demonstrated below.

Firstly, the assumption of a logarithmic velocity profile requires the specification of a roughness parameter. For rippled sandy beds, the value of z_0 has been accepted elsewhere as being 0.5 cm. A single z_0 value is unlikely, however, to represent adequately the roughness of the potential range of rippled sand beds present on the inner continental shelf. Such an observation is particularly relevant to combined flows, where significant wave-induced orbital velocities may occur and are likely to influence bedform geometry. Interestingly, only limited investigations have been undertaken into the relationship between ripple geometry and roughness lengths. The roughness for a rippled sand bed (0.5 cm) is based upon measurements reported by various investigators (see Table III, Heathershaw, 1981), whilst the influence of z_0 on bed shear stresses values has been presented earlier (Figure 3.1). Further, the gradient of the logarithmic velocity profile is comparatively insensitive to changes in z_0: for example, a 20% increase in z_0 causes only a 4% increase in u_*. Dyer (1980) suggested that, as the bedforms change in their shape and position on the bed, z_0 may vary by as much as 1 to 2 orders of magnitude over a tidal cycle. However, this magnitude of variation appears large when due to changes of bedform *shape* and *position* only. It is possible that some non-logarithmic profiles have been considered as logarithmic within this analysis (S. Gao, pers. comm.). A more strict definition of logarithmic flow structure has been presented by Collins *et al.* (1995b).

Additional errors may be introduced if z_0 values derived from laboratory flume experiments are used in the marine environment. Undisturbed (planar) sea bed

samples and those samples reconstructed after grain measurement analysis can produce z_0 values an order of magnitude different (Whitcombe, 1995); z_0 values specified from laboratory experiments may not accurately represent, therefore, the sea bed roughness in the marine environment. Further, accurate determination of the proportion of the friction velocity dedicated solely to transporting sediment grains over a rippled bed may not be possible by the selection of a single roughness length value (Section 3.4).

Whilst considerable variation in derived u_* values (and subsequent transport rates) can be obtained as a result of the selection of a z_0 value, this variation is limited in comparison with that produced by different transport formulae. Bedload transport rates predicted by (nine of) the formulae investigated in Chapter 5 varied by 3 orders of magnitude.

Various previous investigations have supported the use of the bedload transport formula suggested by Gadd *et al.* (1978), which is based upon previously-established physical principles. For example, Heathershaw and Carr (1977) and Heathershaw and Hammond (1979) have described an investigation using radioactive tracer techniques to determine bedload transport rates in Swansea Bay (South Wales). Elsewhere, Heathershaw (1981) has compared the performance of several predictive transport equations, with the measured rates. On the basis of these investigations, Heathershaw and Hammond (*op. cit.*) and Heathershaw (*op. cit.*) supported the use of the Gadd *et al.* (*op. cit.*) modification to Bagnold's (1963) formula for tidally-dominated environments on the inner continental shelf. Recently, Grochowski *et al.* (1993) have advocated also the use of this particular transport equation. For the North Sea itself, in comparing several sediment transport formulae against the observation of ripple migration rates, Huntley *et al.* (1991) found that the Gadd *et al.* (*op. cit.*) and the Einstein-Brown (1950) formulae were the most successful in reproducing the observed sediment transport rates.

Gadd *et al.* (1978) formulated the 'excess velocity' equation:

$$q = \beta\ (u_{100} - u_{100cr})^3 \qquad (6.1)$$

where q is the bedload transport rate (g cm^{-1} s^{-1}), ß is a calibration coefficient, and u_{100cr} is the threshold term. These investigators suggest that ß has a value of 7.22 x 10^{-5} g cm^{-4} s^2 for 0.18 mm median grain size sand and 1.73 x 10^{-5} g cm^{-4} s^2 for 0.45 mm sand; they suggest also that a mean value of ß for both grain sizes (4.48 x 10^{-5} g cm^{-4} s^2), is suitable for sands ranging in size from 0.11 mm to 0.56 mm.

Both the equations of Gadd *et al.* (1978) and Hardisty (1983, 1990) (Section 3.4.8) are derivatives of the original work undertaken by Bagnold (1963, 1966). Hardisty's (*op. cit*) approach is closer, however, to the original concepts of Bagnold; it retains the idea of an excess *stress* required to initiate and support sediment movement, rather than an excess velocity suggested by Gadd *et al.* (*op. cit*). The performance of the Hardisty equation was investigated earlier (Chapter 5), where it was found to over-predict the bedload transport rates observed at the present study location.

The bedload transport rates predicted by these two equations, under unidirectional currents ranging between 0 and 100 cm s^{-1} at 1 m above the bed and for a grain size of 0.2 mm and a roughness length of 0.5 cm, are shown in Figure 6.3. The threshold condition used in the computations was determined by adopting the Shields parameter (Section 3.1.3). Once threshold has been exceeded, the rapid development of sediment movement is predicted by the Hardisty equation (1983, 1990). However, this situation prevails only for a small range of flow rates (up to $u_{100} \approx 20$ cm s^{-1}). For the majority of the flow rates encountered around Broken Bank (Table 4.3), the Gadd *et al.* (*op. cit.*) equation predicts substantially higher bedload transport rates than those predicted by the Hardisty equation.

From the results presented in Chapter 5, it may be seen that the Hardisty bedload sediment transport equation overpredicts substantially the bedload transport rates over this particular area. The relationship between the rates predicted by the Gadd

et al. and Hardisty equations (Figure 6.3) suggests that the bedload transport equation suggested by Gadd *et al.* (1978) would have overestimated also the rates observed here. Heathershaw and Hammond (1979) and Heathershaw (1981), when advocating the use of the Gadd *et al.* equation, were investigating sediment transport patterns in an area of high wave and tidal current energy (the Bristol Channel). Hence, this latter location and the present study area represent very different hydrodynamic regimes.

Bedload transport vector predictions under the action of tidal currents alone have been discussed in detail (see above). Under the combined action of tidal currents and waves, the threshold of sediment movement will now be exceeded in directions other than those of the (unidirectional) residuals identified earlier. However, sediment transport rates, observed as part of the investigation described in Chapter 5, are proportional to the cube of the friction velocity (see Equation 5.61). Thus, transport patterns which were the result of strong currents alone, will be increased substantially. Transport patterns under combined flow bear a strong resemblance, therefore, to those identified under currents alone: net movements of sand under wave- and current-induced shear stresses are directed towards the southeast on the eastern side of Broken Bank, and towards the northwest along its western side. The predicted directions agree well with observed patterns of sand wave orientation observed around the Broken Bank (Caston, 1972).

The combined rates presented here are not considered reasonable; the approach adopted involves a linear addition of the wave and current shear stresses. However, a number of investigators (e.g. Grant and Madsen, 1979; Christoffersen and Jonsson, 1985; Sleath, 1991) suggest that wave and current stresses cannot be considered separately and then superimposed. Non-linear interaction occurs between the steady current and oscillatory flow which alters both from their pure form; the current in the region above the wave boundary layer experiences a shear stress which depends not only on the roughness but also on the wave boundary layer characteristics.

A typical sequence of sea bed topographic changes during the period of a sampling burst using STABLE is presented in Figure 5.8. The ripple crest located in the centre of the photograph has moved approximately 5 cm during the 17 min period. If the transport rates predicted under tidal currents alone are accepted as an accurate representation of the sediment movement, inferred rates of ripple migration would be (at least) 50 cm during the period of the burst. The photographs obtained by STABLE recorded information across approximately 45 cm of sea bed in the direction of ripple migration. On the basis of this rate of ripple migration, it is necessary to accept that the same ripples are not being identified in consecutive sea bed photographs. However, there is strong evidence to suggest that the high migration rate, inferred by Method 1, is not occurring. Consecutive sea bed profiles are presented in Figure 5.9. The two sea bed profiles are very similar; this suggests that the same portion of the ripple profile is being identified in the succeeding photograph. When wave activity is incorporated into Method 1, predicted transport rates are a further order of magnitude higher; these (combined wave-current) rates infer a ripple migration rate higher than that discounted under the action of currents alone.

Results using Method 2, which encompasses the non-linearity of wave-current interaction, are presented below.

6.3.4 Sediment transport predictions (Method 2)

Bedload transport rates derived using this particular approach are presented in Table 6.3.

(a) Rates of predicted sediment movement

Over the complete period of the deployment, the predicted residual rates are highest along the eastern flank of the Broken Bank. Scalar mean transport rates (Q_{scal}) are similar on both sides of the bank, suggesting similar instantaneous transport rates throughout the duration of the records. Variation in transport rate

vectors (Q_b) around the sand bank suggest that the hydrodynamic regime to the west of the bank is relatively balanced between the flood and ebb phases of tidal cycles. An equivalent similarity between northwesterly and southeasterly sediment movement is observed at the interbank location (Station G); here, there is a small residual sediment movement, in relation to a large scalar mean rate.

During a spring tidal cycle, the scalar transport rates are similar throughout the study area, with the residual movements being slightly greater along the eastern side of the sand bank. For example, the transport predicted for Station G is approximately one third of the rates predicted for a location along the western flank (Station E).

The predicted patterns during a neap tidal cycle are, as might be expected, more variable. The rates predicted for the western side of the bank (Station E) are the lowest of those stations lying adjacent to the bank, although the scalar mean rates are similar at all the measurement locations. The predicted movement of material at Station G is, on this occasion, comparable with the movements predicted for elsewhere throughout the area.

(b) Progressive vector transport rates

Sediment transport rate vectors, over successive tidal days (24 hrs 50 mins) and throughout the entire period of deployment, were calculated on the basis of the addition of the northerly and easterly components of the sediment transport rates (predicted for each current velocity recording during these intervals). The results are displayed in Figure 6.4.

The results obtained for all the stations show lower rates of sediment transport during the early part of the record; these coincide with a period of lower tidal ranges (cf. Figure 4.4). For stations located to the east of the banks (Stations B, C and H) there is a consistent prediction of the southeasterly movement of sand. At Station E, there is more variation in predictions relating to the earlier and later

parts of the record: low rates, towards different directions, are predicted during the early part of the record. Sediment transport is directed consistently towards the north during the latter part of the record. Sediment transport predictions for the central swale location (Station G) exhibit also considerable variability during the early (neap tide) part of the record; easterly movement becomes apparent during the latter part of the deployment.

(c) Patterns of sediment movement

Patterns of sediment transport, in the vicinity of the Broken Bank, are presented in Table 6.4 and Figure 6.5.

Overall record

Strong southeasterly transport is evident along the eastern side of the Broken Bank, with more variable transport directions predicted for the west of the sand bank (Stations E and G), producing weak northwesterly sediment movement at Station E. Even weaker (towards the bank) transport is predicted at Station G. At Station H, a southeasterly transport pattern is apparent to the east of the Well Bank.

Spring tidal cycle

Under spring tidal conditions, the anticipated pattern of flood and ebb dominance (southeasterly on the eastern side of bank, northwesterly on the western side of bank (see, for example, Caston, 1972)) on either side of the bank is observed clearly. The strong southeasterly movement on the eastern side of the bank, identified over the entire record (see above), is predicted also over the spring tidal cycles. To the west of the bank, the northwesterly-moving sandstream is more pronounced; its rate of movement is almost the same as the rates predicted at Stations B and C. Once again, the pattern of sediment transport predicted for the central swale location is somewhat variable, with sand transport being directed

largely towards the Broken Bank. At Station H, the southeasterly movement of sediment is evident, once again; these rates are the highest predicted for the region.

Neap tidal cycle

Relatively strong and consistent southeasterly movement of sediment is predicted for the eastern flank of the Broken Bank. A very low sediment transport rate, directed away from the sand bank, is predicted for Station E. Sediment movement at Station G is directed towards approximately 25° to the west of north. At Station H, the southeasterly movement of sediment predicted also during the neap tidal cycle.

(d) Sand bank maintenance

Predicted sediment transport rates have been described and discussed within the context of temporal and spatial variability. Such vectors are directed at an angle to the crestline of the bank; as such, they have a component of transport directed perpendicularly towards, or away from, the bank. In this way, the bank may acquire (or lose) material and will be maintained (or eroded).

The component of sediment transport directed towards the crestline of the bank has been determined for Stations B, C, E and G; these are listed in Table 6.4.

Sediment transport pathways on the eastern flank of the bank are largely parallel to the axis of the sand bank; therefore sediment transport directed towards the crestline of the Broken Bank constitutes a small component of the total transport along this flank of the bank. To the west of the bank, bank-directed transport represents a greater proportion of the sediment movement; indicating generally the greater angles between the sediment transport directions and the axis of the bank.

On-bank movement from the east of Broken Bank is relatively constant at Station

C occurring over all tidal conditions. In contrast to the regime found on the eastern flank, considerable variability is experienced on the west of the Broken Bank. During the overall deployment period, on-bank transport from the western flank is the same magnitude as that from the eastern side of the bank, during the spring tidal cycle, it is an order of magnitude larger; during the neap tidal cycle, sediment transport, though considerably weaker (two orders of magnitude lower) than the spring on-bank component, is directed away from the bank.

The steep side of such a bank may be a reflection of the dominant northwesterly sediment movement on the western flank of the bank (Caston, 1972; Kenyon *et al.*, 1981). On average, therefore, the upstream (western) side of the bank should be eroded with the downstream (eastern) side accreting (Smith, 1969). This may produce a lateral migration to the northeast, though limited movement only has been detected by Collins *et al.* (1995a). However, the supply of sand towards the crestline of the Broken Bank occurs intermittently on the western flank. At Station E, only transport directed towards the crestline during the spring tidal cycle is greater than that from the eastern flank.

6.3.5 Discussion of Method 2

The 'sensitivity' of Method 2 to wave enhancement of the predicted bedload transport rates has been investigated. The influence of waves has been investigated for 10 ratios, between zero and 1, of wave-induced orbital velocity to steady current velocity. Likewise, variation in the predicted transport rates in relation to the wave-current interaction angle (ϕ_{wc}) has been investigated.

The transport rates under combined flows presented here have been calculated using an orbital velocity of approximately 18 cm s^{-1} (the average value recorded during the STABLE deployment). The wave period selected was 10 s; this is approximately the average of that recorded during the deployment. An average value of 35 cm s^{-1} was used for the tidal current speed recorded at 2 m above the bed (see Table 4.3). Hence, the u_{rms}/u_z ratio used for the present investigation is

approximately 0.5; this lies mid-way along the range of (x-axis) values investigated.

First-order linear wave theory has been assumed. Here, the effects of waves are considered only as a 'stirring' mechanism, producing no net movement of sediment in themselves. On the basis of this theory, wave-current interaction angles of between 0 and 90° have been investigated; these allow for all wave-current interaction angles. An average water depth for the (5) stations around the bank (of 27 m) has been used in the analysis.

The results of this part of the investigation are presented in Figure 6.6; here the ratio of transport rates predicted under the combined influence of waves and currents (Q(wc)) to those predicted under currents alone (Q(c)) are presented. An increase in the predicted transport rates is apparent when the influence of waves are included in the predictive process; this suggests that waves can have a significant influence on sand transport in the area. The predicted transport rates are greatest for the codirectional case ($\phi_{wc}=0°$), with the lowest rates occurring when the direction of wave propagation is perpendicular to that of the tidal current direction ($\phi_{wc}=90°$).

The influence of the interaction angle (ϕ_{wc}) on the transport rate is seen to be much less than that of the wave-induced orbital velocity (u_{rms}). The maximum influence of the angle is encountered between $0.1 < u_{rms}/u_z < \sim 0.4$. At $u_{rms}/u_z=0.5$ (representative of the present investigation), there is little difference between the enhancement influence of waves at varying angles to the current.

For the present investigation ($u_{rms}/u_z \approx 0.5$), the superimposed effects of waves upon a tidal current results in predicted transport rates which are approximately 20 times greater than those relating to the (unidirectional) current alone. However, only small changes in the rate of sediment transport are predicted in relation to variation in the wave-current interaction angle (Figure 6.6). Locally, the tidal currents are highly rectilinear, with their main axes lying essentially parallel to the

axis of the bank (315°-135°). The direction of wave propagation is, on average, towards 165°N (see Chapter 5). Therefore the predominant wave-current interaction angle will be essentially constant (approximately 30°) for significant periods of time.

Independent sediment transport rates have been determined from a fluorescent sand tracer study carried out around Broken Bank (Shimwell, 1990). Observed rates and those derived using Method 2 rates differ by 3 orders of magnitude. However, the rates observed by Shimwell (1990) were subject to navigation errors due to the use of the Decca (Main Chain) position fixing system (i.e. $\pm$150 m), and to bias in the sampling positions to one side of the tracer injection sites. The transport rates observed by Shimwell (1990) are very similar to those observed by Heathershaw (1981) for a nearshore, high energy (6000 km wave fetch and 10 m spring tidal range) environment (Swansea Bay, Bristol Channel), and Lees (1981) who measured transport rates adjacent to the coast of East Anglia. In would seem, therefore, that the rates observed from the fluorescent sand tracer deployment around Broken Bank may not be truly representative of the naturally-occurring transport rates.

6.4 DISCUSSION

Tidal current velocities have revealed that the threshold for sediment transport may be exceeded for as much as 77% of the time during the period of a spring tidal cycle. The rate and direction of the resulting sediment transport have been predicted (utilising two approaches) for the study area. The performance of the approaches has been assessed.

Broken Bank is located between sandstreams moving in opposite directions, the present investigation has provided further evidence for the pattern of residual (water and sand) circulation around a linear sand bank (Caston, 1970; Caston and Stride, 1972; Kenyon *et al.*, 1981; Huthnance, 1982a, 1982b); sand movements predicted here have been towards the southeast on the eastern side and towards the

northwest on the western side of the bank. Whilst the hydrodynamic regimes on either sides of the Broken Bank are equally capable of transporting sediment, net sediment movement towards the southeast (on the eastern flank) is substantially greater than the corresponding northwesterly rates (on the western flank). This suggests greater asymmetry in the tidal current pattern along the eastern side of the bank which leads to a general southerly movement over the area. This observation is consistent with southerly movement inferred from the presence of a bedload parting to the north of the present study area (Stride, 1963; Kenyon and Stride, 1970; see also Chang and Evans, 1992).

Previous investigations undertaken over the Norfolk Banks region (e.g. Caston, 1972) have suggested that the asymmetrical cross-sectional shape of the sand banks, with the steeper side facing towards the northeast, is a result of the dominance of a northwesterly-moving sand stream. However, the rate of the movement of sediment predicted here towards the northwest is consistently lower than that directed towards the southeast, along the eastern flank of the Broken Bank. Further, the identified northwestward movement does not produce consistently higher transport directed towards the crestline of the Broken Bank. That the steeper side of the Broken Bank, facing towards the northeast, is a reflection of the dominance of the (northwesterly) sandstream on the western flank of the bank (Caston, 1972) has not been presented here; indeed, the results obtained suggest another, more variable, pattern of sand movement and sand bank maintenance on the western flank of the bank.

Sediment transport in the centre of the swale between the Well and Broken Banks (Station G) indicates a movement towards the northeast (offshore). These pathways may be the result of the formation of a new sand bank at this particular location (Huntley *et al.*, 1993; Collins *et al.*, 1995a). For the same area, Stride (1988) has suggested that movement of sediment offshore will occur under storm conditions with the banks acting as 'stepping stones', transporting sand seaward from the East Anglian coastline. However, transport patterns which are consistent with this concept have been shown here to occur under hydrodynamic conditions associated

with tidal currents and low wave activity. Such results are consistent with previous investigations into regional residual water movement (Maier-Reimer, 1977).

Sediment transport rates have been predicted using two fundamentally different approaches; discussion of the different approaches adopted to predict sediment transport pathways is presented here. Both the methods adopted predict similar transport directions (typically within 5°) for each of the recording stations and various record length intervals. These patterns of sediment movement are essentially similar to the observed pattern of water movements over the study area (Chapter 4).

The rates of transport predicted under the combined action of waves and currents, using Method 2, are typically an order of magnitude lower than corresponding rates predicted using Method 1. The approaches use very different estimates of the bed roughness. Method 1 adopts a widely quoted roughness length value (z_0) of 0.5 cm. Method 2 uses a bed roughness parameter (k_s=0.4 cm) which has been calibrated against observed ripple geometry on the sea bed (Section 5.4.3) which makes an allowance for form drag. The roughness parameter adopted in each method influences strongly the value of the predicted shear stress acting on the sediment grains. The relationship between these parameters (z_0 and k_s) is given by:

$$k_s = 30 z_0 \qquad (6.2)$$

for rough turbulent flow. A z_0 value of 0.5 cm corresponds to a k_s value of 15 cm; this suggests that the methods adopted here utilise roughness scales which are approximately 35 times different.

The (two) predictive methods adopted here have been compared with photographic data presented earlier (Chapter 5) and with the results of previous investigations. On the basis of these comparisons, it is considered that Method 2 predicts more realistic rates of sediment transport. As part of this approach, care has been taken to specify an accurate roughness condition, and to use a locally-calibrated transport formula; it is suggested, therefore, that the predictive process (Method 2) has

produced accurate estimates of sediment transport patterns present in the vicinity of the Broken Bank.

6.5 CONCLUDING REMARKS

The present study area is one of active sediment transport; the threshold of movement may be exceeded by up to 77% of the time during a spring tidal cycle.

To the west of Broken Bank, a northwesterly moving sandstream is evident; to the east of the bank, a southeasterly moving sandstream is evident.

On the western flank of the bank, residual rates are low; this suggests that the southeasterly movement on the flood is comparable with that directed towards the northwest on the ebb. On the eastern flank of the bank (where the highest transport rates are observed) the (southeasterly) sandstream on the flood is significantly larger than the ebb (northwesterly) movement, producing a high (southeasterly) residual transport rate. The imbalance between the residual sediment movements on each side of the bank suggests a net southerly movement over the area.

Sediment movement in the swale between the Broken and Well Banks, under 'normal' hydrodynamic conditions, is directed towards the northeast (offshore).

Two approaches have been adopted initially to predict sediment transport pathways. Both approaches predict similar sediment transport *directions* for all stations within the present study area. However, significant differences between the transport *rates* predicted by the two methods are obtained. Method 1, based largely on engineering practices, has been shown to inaccurately reproduce locally observed sediment transport rates. Method 2, based on an improved wave-current boundary layer model which incorporates a roughness parameter (important in determining bed shear stress) calibrated *in-situ*, is suggested to predict more accurately the naturally occurring sediment transport patterns.

STATION		NEAP	SPRING	ALL
B-2	(a)	56.8	77.5	70.9
	(b)	10.5	24.5	21.0
	(c)	7.2×10^{-3}	5.0×10^{-2}	3.5×10^{-2}
C-2	(a)	52.3	75.1	71.8
	(b)	11.6	25.9	22.7
	(c)	8.7×10^{-3}	5.3×10^{-2}	4.1×10^{-2}
E-2	(a)	60.1	72.1	76.0
	(b)	8.1	28.6	22.9
	(c)	4.7×10^{-3}	5.9×10^{-2}	4.2×10^{-2}
G-2	(a)	90.7	77.3	76.9
	(b)	9.2	24.5	19.7
	(c)	8.7×10^{-3}	4.8×10^{-2}	3.3×10^{-2}
H-2	(a)	81.3	81.3	78.3
	(b)	14.1	28.8	24.9
	(c)	1.8×10^{-2}	7.7×10^{-2}	5.7×10^{-2}

Table 6.1 (a) Percentage of time over which the threshold of sediment movement is exceeded (%); together with (b) the average velocity of those currents which exceed the threshold for sediment motion (cm s^{-1}); and (c) the scalar transport rate (g cm^{-1} s^{-1}) predicted by the formula presented in Section 5.4.4 (Equation 5.61).

Station		Neap	Spring	Overall
B-2	(a)	$2.6x10^{-3}$	$3.0x10^{-2}$	$2.2x10^{-2}$
	(b)	138.4	139.3	141.1
	(c)	36.1	60.0	62.9
C-2	(a)	$6.5x10^{-3}$	$2.4x10^{-2}$	$2.4x10^{-2}$
	(b)	135.8	131.7	135.3
	(c)	74.7	45.3	58.5
E-2	(a)	$4.5x10^{-4}$	$1.8x10^{-2}$	$3.9x10^{-3}$
	(b)	177.9	333.0	336.9
	(c)	9.6	30.5	9.3
G-2	(a)	$2.8x10^{-3}$	$5.9x10^{-3}$	$2.4x10^{-3}$
	(b)	324.3	11.9	71.7
	(c)	32.2	12.3	7.27
H-2	(a)	$6.6x10^{-3}$	$4.3x10^{-2}$	$3.6x10^{-2}$
	(b)	123.7	135.8	137.0
	(c)	36.7	55.8	63.2

Table 6.2 (a) Sediment transport rates (g cm^{-1} s^{-1}) predicted using Method 1 for (unidirectional) tidal currents only, vectorially-averaged (over the respective record length); (b) direction of sediment transport (°N); and (c) sediment transport vector expressed as a percentage of the scalar transport rate predicted for each station (Table 6.1).

Station	Q_E (g cm^{-1} s^{-1})	Q_N (g cm^{-1} s^{-1})	Q_b (g cm^{-1} s^{-1})	Q_{bdir} (°N)	Q_{scal} (g cm^{-1} s^{-1})	Ex (%)
Overall record						
B	3.3 x10^{-4}	-4.8 x10^{-4}	5.8 x10^{-4}	145.5	9.2 x10^{-4}	100
C	4.0 x10^{-4}	-4.9 x10^{-4}	6.42 x10^{-4}	140.7	1.1 x10^{-3}	100
E	-3.4 x10^{-5}	1.0 x10^{-4}	1.1 x10^{-4}	341.5	1.1 x10^{-3}	100
G	5.7 x10^{-5}	1.2 x10^{-5}	5.8 x10^{-5}	78.2	8.4 x10^{-4}	100
H	5.8 x10^{-4}	-7.5 x10^{-4}	9.5 x10^{-4}	142.1	1.5 x10^{-3}	100
Spring tidal cycle						
B	4.7 x10^{-4}	-6.3 x10^{-4}	7.9 x10^{-4}	143.4	1.3 x10^{-3}	100
C	4.4 x10^{-4}	-4.7 x10^{-4}	6.4 x10^{-4}	137.0	1.4 x10^{-3}	100
E	-1.9 x10^{-4}	4.3 x10^{-4}	4.7 x10^{-4}	335.7	1.5 x10^{-3}	100
G	4.2 x10^{-5}	1.5 x10^{-4}	1.5 x10^{-4}	15.9	1.2 x10^{-3}	100
H	7.5 x10^{-4}	-8.9 x10^{-4}	1.2 x10^{-3}	139.9	2.0 x10^{-3}	100
Neap tidal cycle						
B	3.1 x10^{-5}	-4.4 x10^{-5}	5.3 x10^{-5}	145.2	2.0 x10^{-4}	100
C	8.8 x10^{-5}	-1.2 x10^{-4}	1.5 x10^{-4}	144.0	2.4 x10^{-4}	100
E	-4.1 x10^{-6}	-9.0 x10^{-7}	4.2 x10^{-6}	257.5	1.6 x10^{-4}	100
G	-2.9 x10^{-5}	6.1 x10^{-5}	6.8 x10^{-5}	334.4	2.5 x10^{-4}	100
H	1.2 x10^{-4}	-1.0 x10^{-4}	1.6 x10^{-4}	130.0	4.6 x10^{-4}	100

Table 6.3 Bedload sediment transport rates determined under combined waves and tidal currents predicted using Method 2.
Key: Q_E, Q_N - easterly and northerly, respectively, components of the transport rate; Q_b - sediment transport rate; Q_{bdir} - direction of Q_b; Q_{scal} - scalar transport rate over the same period; and Ex - percentage of time over which the threshold of sediment motion is exceeded.

Station	Q_b (g cm^{-1} s^{-1})	Q_{bdir} (°N)	α (°)	Q_{OB} (g cm^{-1} s^{-1})	$\%Q_b$
Overall record					
B	5.8×10^{-4}	145.5	10.5	1.1×10^{-4}	18.2
C	6.4×10^{-4}	140.7	5.7	6.3×10^{-5}	9.9
E	1.1×10^{-4}	341.5	26.5	4.8×10^{-5}	44.6
G	5.8×10^{-5}	78.2	56.8	4.8×10^{-5}	83.7
Spring tidal cycle					
B	7.9×10^{-4}	143.4	8.4	1.1×10^{-4}	14.6
C	6.4×10^{-4}	137.0	2.0	2.2×10^{-5}	3.4
E	4.7×10^{-4}	335.7	20.7	1.7×10^{-4}	35.4
G	1.5×10^{-4}	15.9	60.9	1.4×10^{-4}	87.4
Neap tidal cycle					
B	5.3×10^{-5}	145.2	10.2	9.4×10^{-6}	17.7
C	1.5×10^{-4}	144.0	9.0	2.3×10^{-5}	15.7
E	4.2×10^{-6}	257.5	57.5	-3.5×10^{-6}	-84.3
G	6.8×10^{-5}	334.4	19.4	2.2×10^{-5}	33.3

Table 6.4 Components of sediment transport (predicted using Method 2) directed perpendicular to the crestline of the Broken Bank.
Key: Q_b - sediment transport rate; Q_{bdir} - direction of Q_b; α - angle made between the direction of sediment movement and the direction perpendicular to the crestline of the bank; Q_{OB} - transport directed perpendicularly towards (or away from) the bank (+ve on-bank, -ve off-bank); $\%Q_b$ - Q_{OB} expressed as a percentage of Q_b.

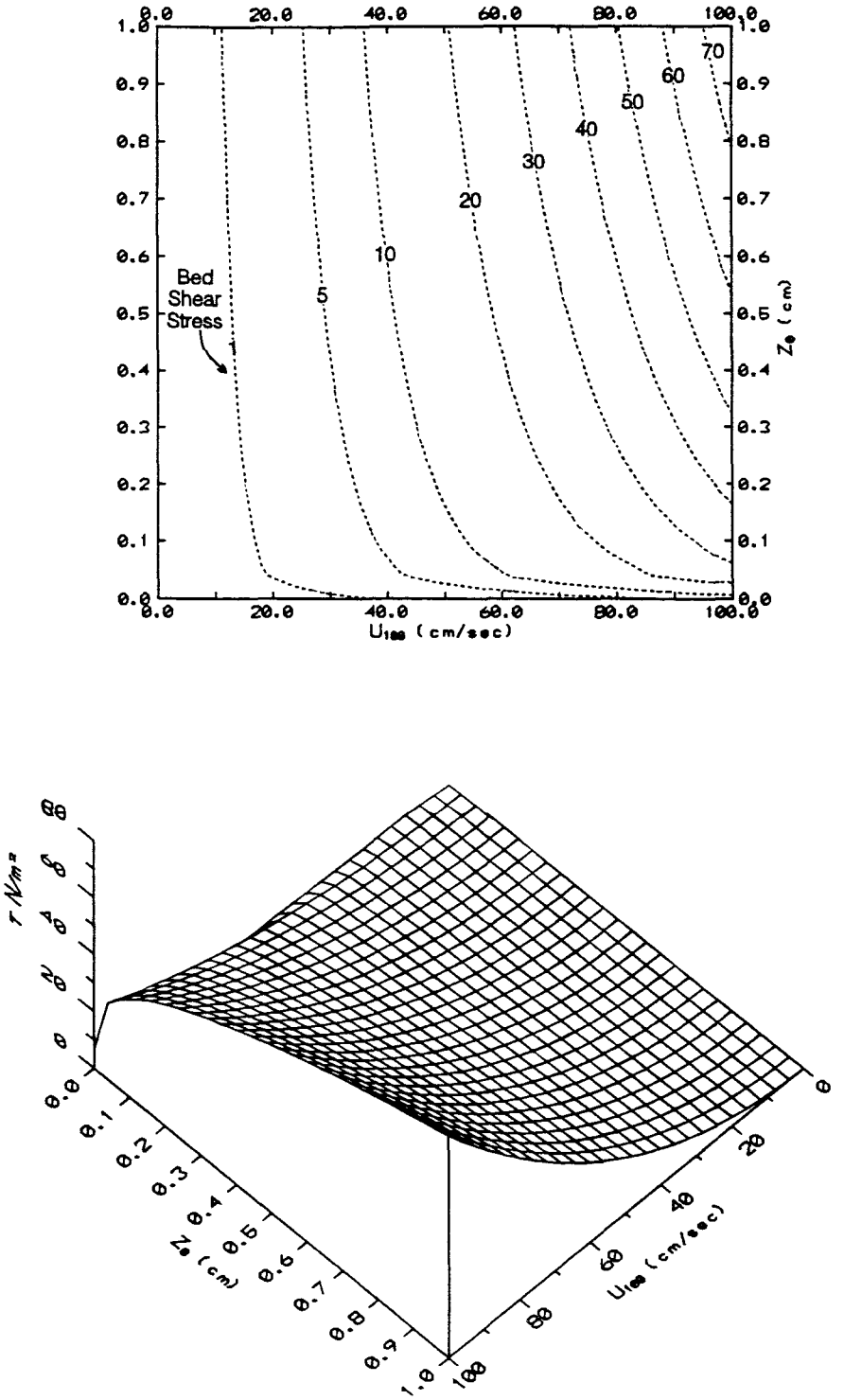

Figure 6.1 Contour and 3-d representation of the relationship between bed shear stress (τ), flow velocity 1 m above the bed (u_{100}), and the roughness length (z_0).

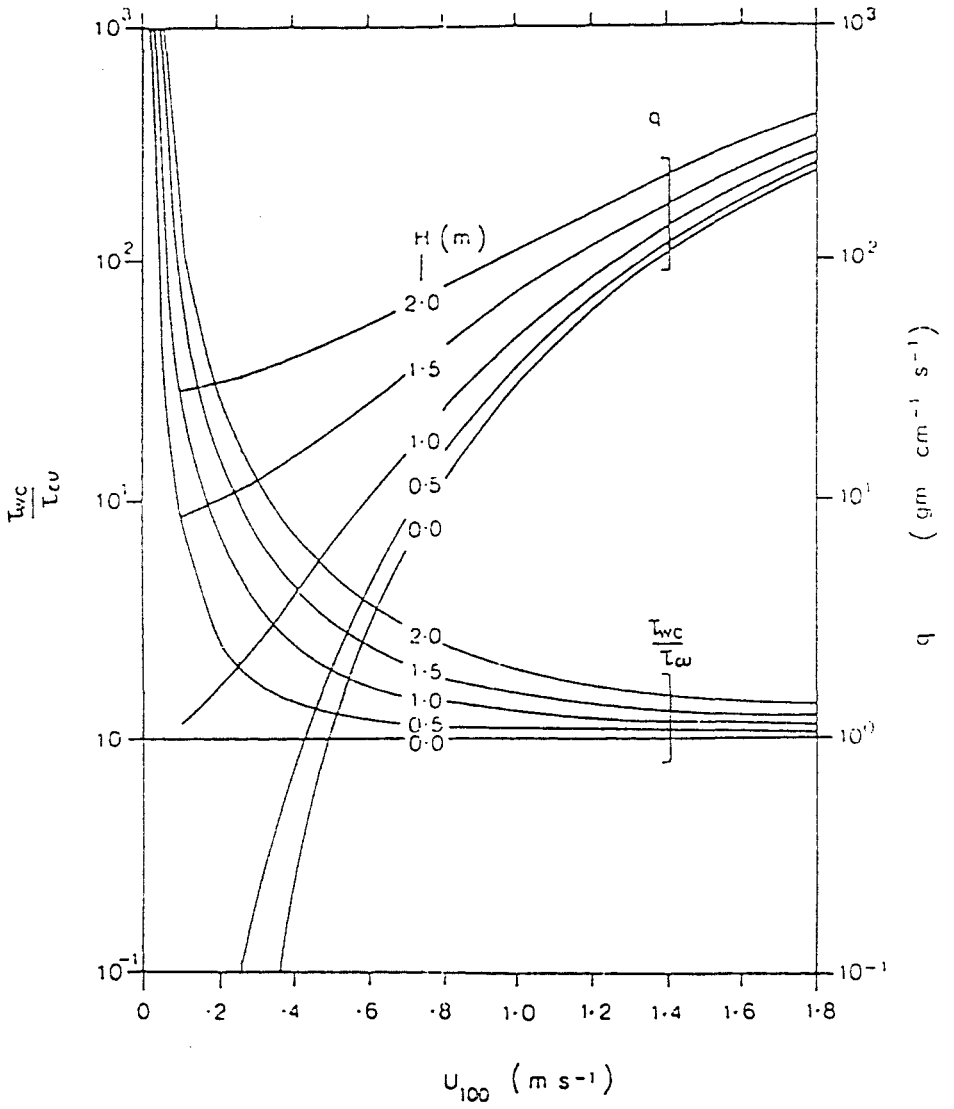

Figure 6.2 The ratio of the bed shear stress due to waves and currents (τ_{wc}) to the bed shear stress due to currents alone (τ), calculated using Bijker's (1967) formulae, in terms of the near-bed current (u_{100}). Shown also is the effect of increasing wave height (H) on sediment transport rates (after Heathershaw, 1981).

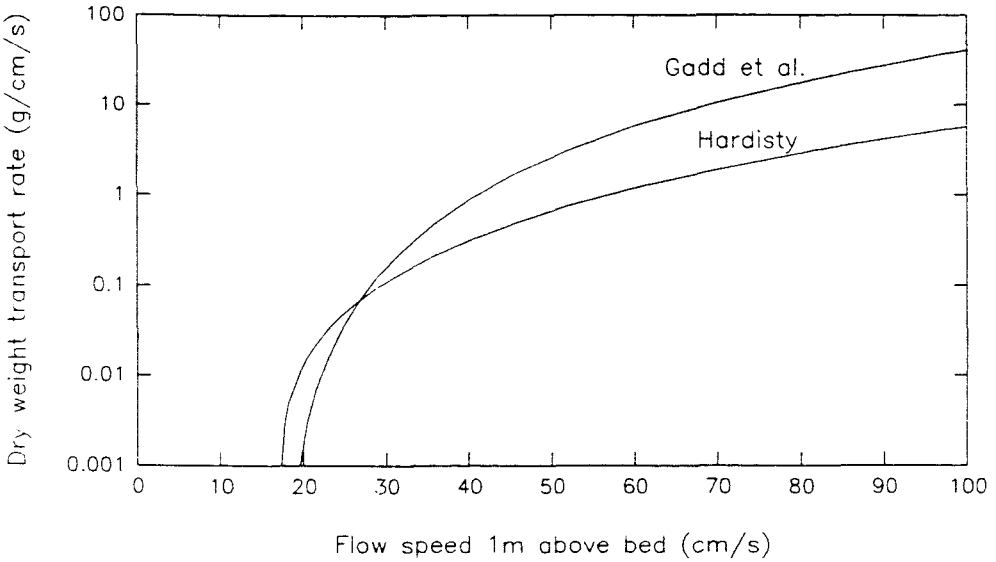

Figure 6.3 Bedload sediment transport rates predicted by the Gadd *et al.* (1978) and Hardisty (1983), 1990) equations, in relation to flow at 1 m above the bed.

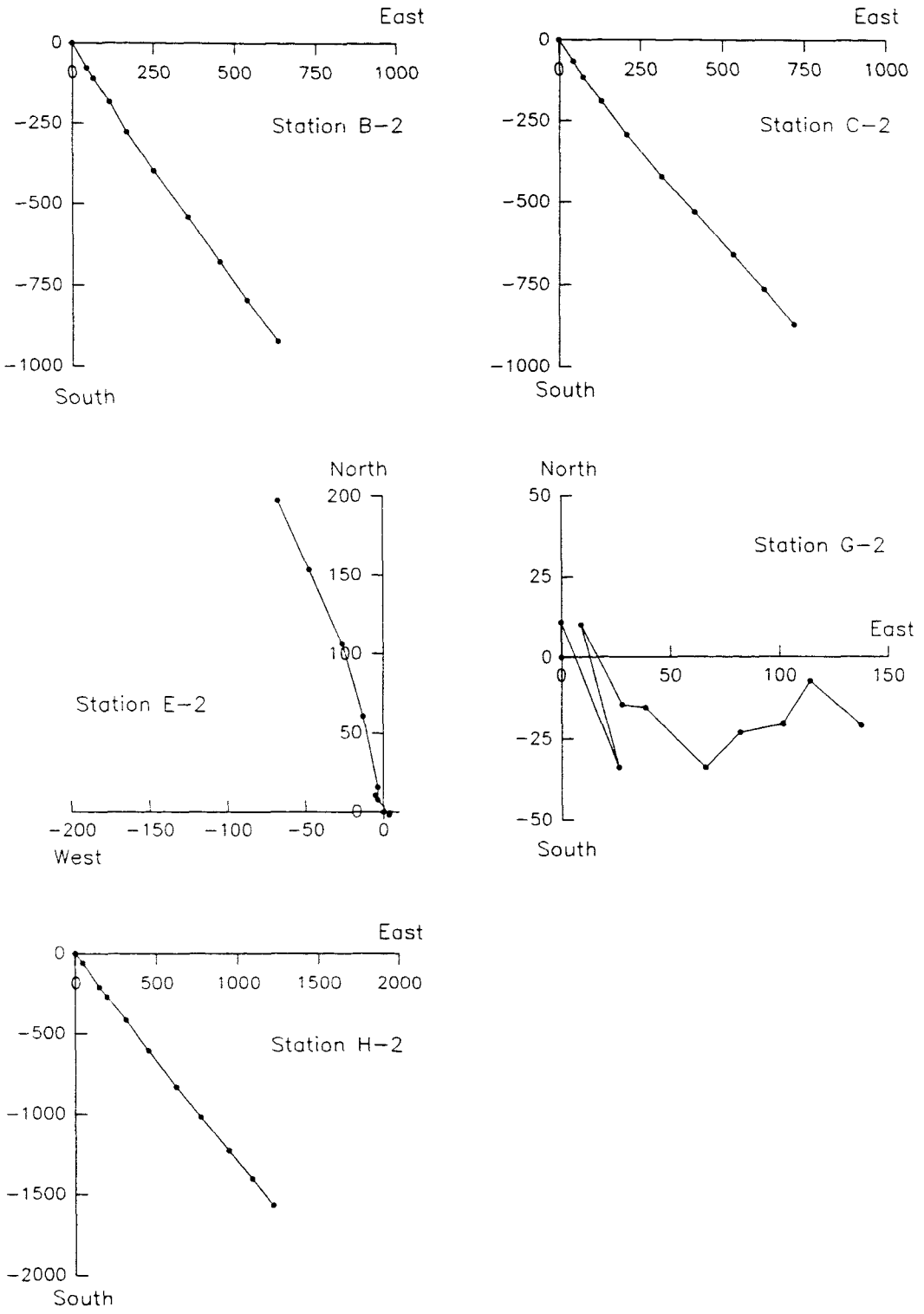

Figure 6.4 Progressive vector diagrams of the predicted bedload transport rates. Points are plotted for successive tidal days during the deployment. All axes are presented in g cm^{-1} tidal day^{-1}.

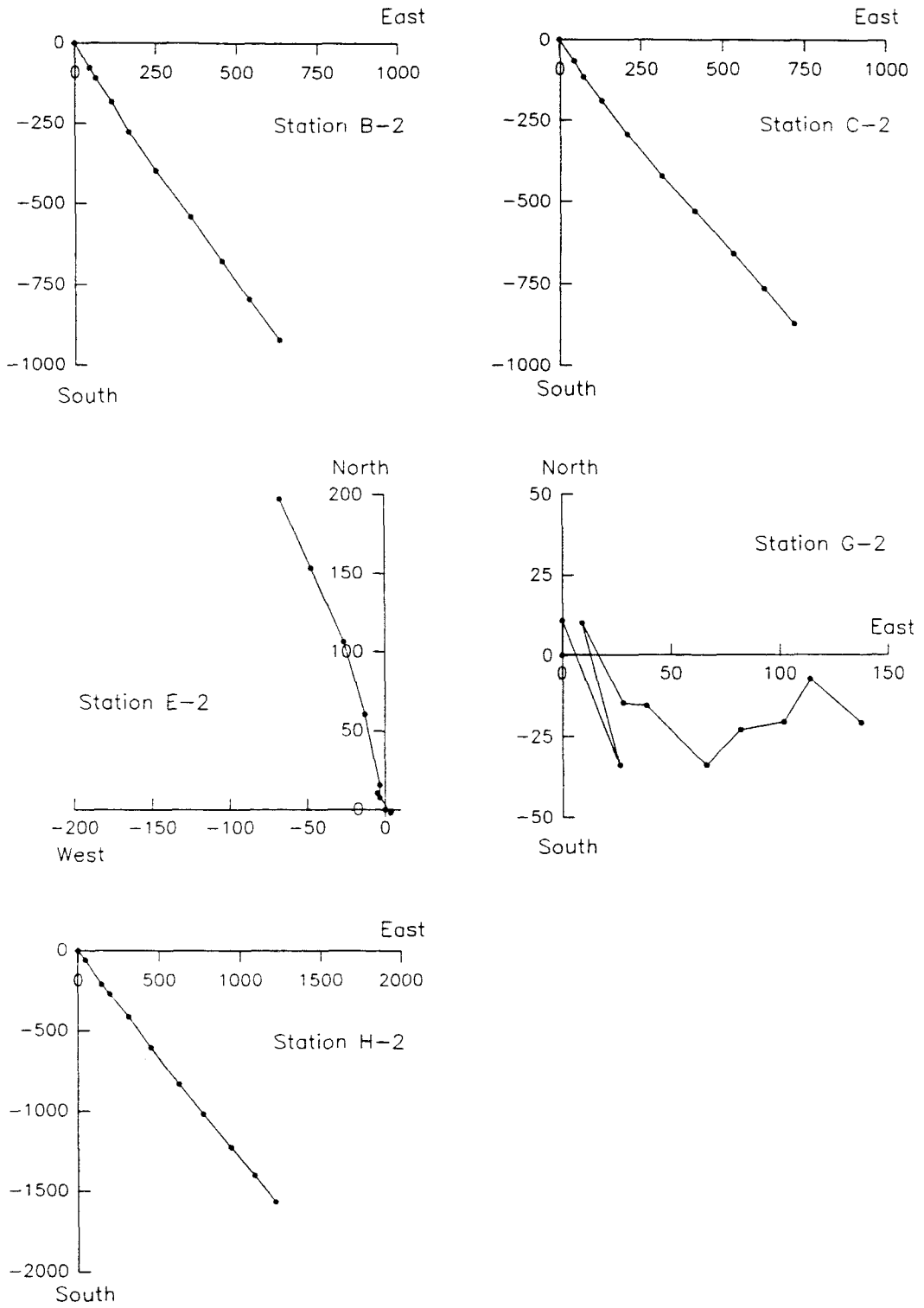

Figure 6.4 Progressive vector diagrams of the predicted bedload transport rates. Points are plotted for successive tidal days during the deployment. All axes are presented in g cm^{-1} tidal day^{-1}.

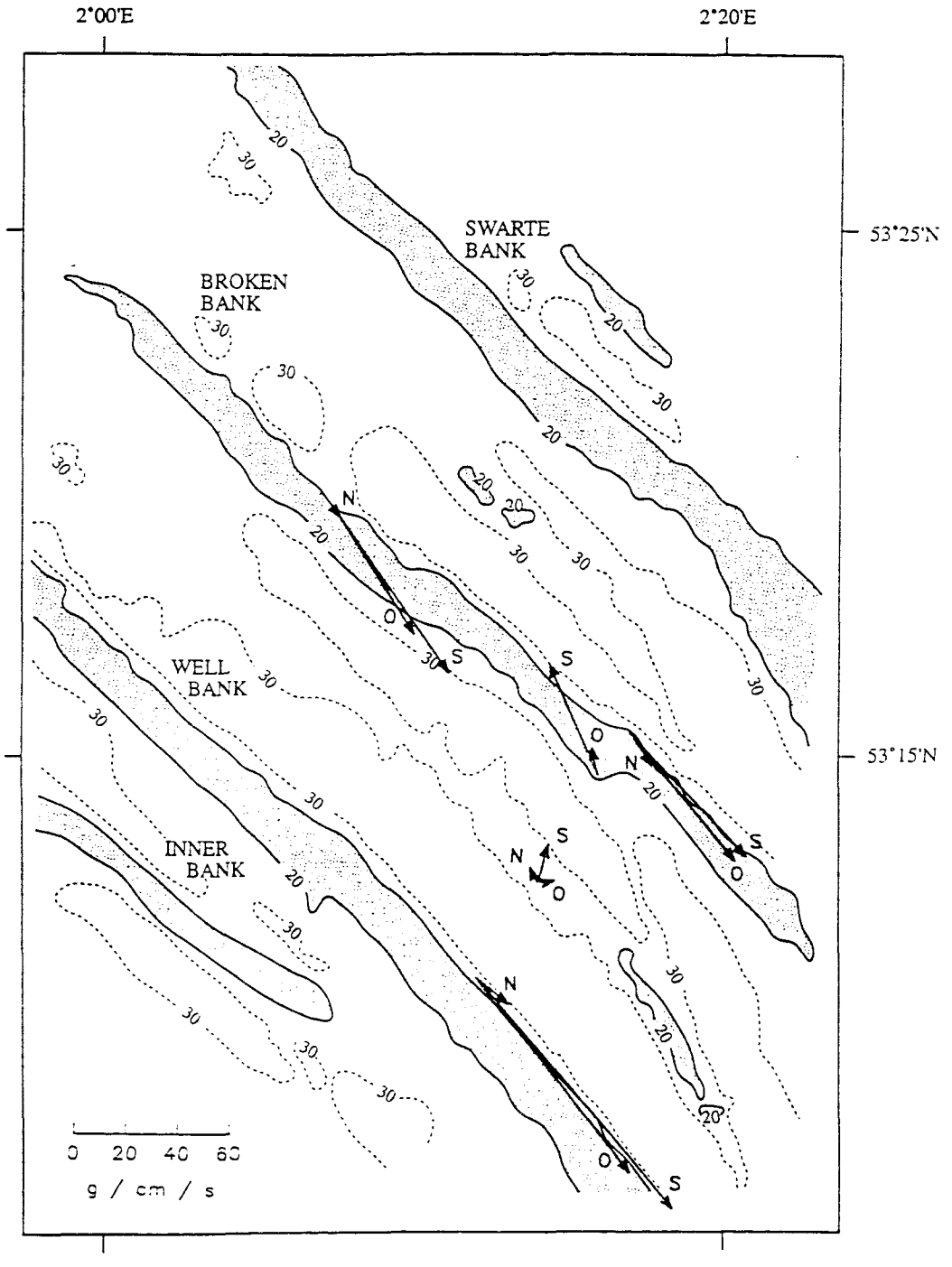

Figure 6.5 Sediment transport vectors for combined wave and current action, predicted using Method 2. Key: N= neap tidal cycle; O= overall record; and S= spring tidal cycle. Note: Transport at Station E over a neap tidal cycle was too low to be represented here.

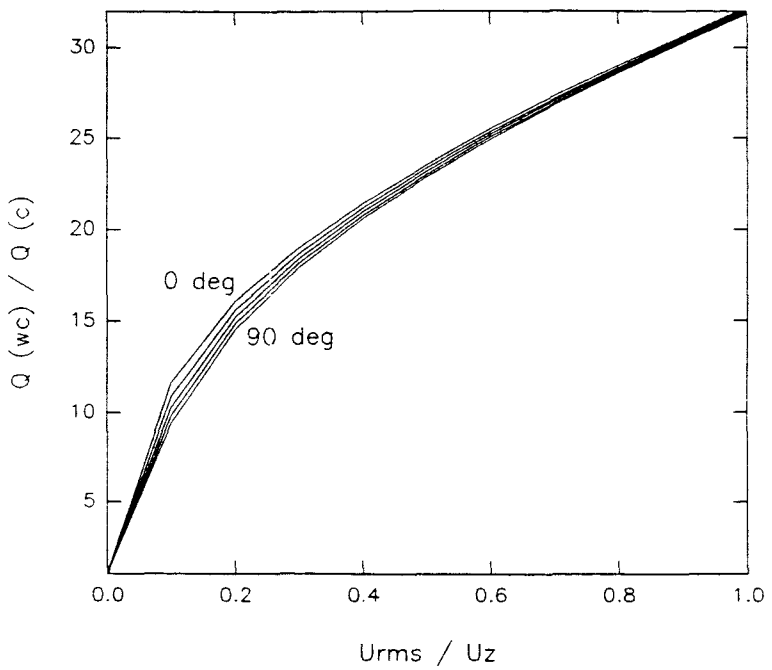

Figure 6.6 The enhanced (wave-current) sediment transport (Q(wc)) rates compared against current-only transport rates (Q(c)) are investigated for a range of wave/current conditions, combined with wave-current interaction angles of 0°, 30°, 45°, 60° and 90°.

Chapter 7
DISCUSSION

7.1 TIME-SCALES

An area of considerable interest to coastal engineers and oceanographers alike is the definition of time-scales within coastal hydrodynamics and processes of sediment dynamics. The present study is concerned with a number of processes that occur over a range of (temporal and spatial) scales. Within this context, together with other investigations in the same research area, references have been made to short- and long-term changes. These terms, however, are rarely defined. Horikawa (1981), in a review of coastal sedimentary processes, identified that many of these processes are understood only in a qualitative sense. A particular problem is that the various processes operate at quite different scales, both in time and space. Horikawa (*op. cit.*) proposed a classification, based on three time/space categories: (a) macroscale (year/kilometre); (b) mesoscale (day-hour/metre); and (c) microscale (second/millimetre). There is considerable interest in macroscale changes. Observations of this nature are difficult to obtain and measurements of a particular process are obtained frequently at meso- and micro-scales. These measurements are extrapolated to the macroscale, and the results must be viewed with some uncertainty. The problem is that all the processes operating within the marine environment do so at various rates, whilst measurements of these are made often at widely-differing time intervals. The problems caused by the definition of a suitable scale can best be described by the following example.

Long-term changes to a major area of sea bed, such as that covered by the Norfolk Banks will occur over many 100's of years; in this case, 'short-term' will be a period of several years. Hydrographic surveys are a time-consuming and expensive undertaking; revisions to charts, therefore, are made only occasionally (revisions to the chart relating to the Norfolk Banks are undertaken approximately every four years), except in areas where rapid changes are known to occur and

such information is important to maintain safe inshore navigation. For comparison, a period of only a few years will be considered 'long-term' when monitoring sediment transport in response to tidal currents. 'Short-term' changes in these rates can define a time interval which may incorporate only a single storm period of one or two days, or even a single tidal cycle. The different measuring intervals of the various processes, with their associated rates of change, provides the terminology with a degree of flexibility. Consequently, defining a particular (time or length) scale is difficult.

7.2 PATTERNS OF REGIONAL WATER MOVEMENT

Self-recording current meter data have been obtained successfully from several locations around Broken Bank. From these data, horizontal and vertical water movements have been identified.

Information has been derived from a wide variety of sources/techniques; these include: current meters, sea surface elevation, form factor calculations and energy frequency distributions. The tidal wave propagates through the present study area as a progressive wave and is strongly semidiurnal in nature. For the water movements recorded at most locations and elevations in the present study area, the M_2 harmonic is dominant (except at Station G-12). Throughout the area the amplitude of the M_4 harmonic is considerably smaller than that of the M_2 harmonic; it is more distinctive, however, at locations adjacent to the banks than in the central swale location. This may be indicative of local (topographic) generation of M_4 tidal currents.

The change of water speed with height above the sea bed is spatially variable; theoretically, near-bed currents should reach their maximum values before the mid-depth flow (Mofjeld, 1976; Pugh, 1987). However, considerable variation exists through the present investigation area; to the west of the Broken Bank mid-depth flow lags near-bed flow, on the eastern side mid-depth *leads* near-bed flow (though the difference is small). Changes in the phase of the tidal currents with

height above the sea bed have been identified by Huntley *et al.* (1993) as a possible source of error in the comparison between measured and depth-averaged currents for this area. Detailed investigation of this phenomenon, as part of the present investigation, was not possible due to the limited number of current meters deployed at each location, and the relatively coarse sampling interval of the current meters.

The directional structure of the tidal currents with height above the sea bed at Station B (the only station with current meters at three elevations above the bed) indicates that the observed pattern of veering through the water column is not consistent with the pattern of water movements expected for a (secondary) helical flow (Houbolt, 1968). This suggests that maintenance of the Broken Bank does not appear to be occurring as a result of sediment transport due to such secondary helical flow cells. Similar observations have been made by Harvey and Vincent (1977) and McCave (1979).

The pattern of horizontal water movements around the Broken Bank is one of strongly rectilinear tidal currents producing narrow tidal ellipses. The axis of the Broken Bank is, on average, orientated at approximately 20° in an anticlockwise sense to the direction of dominant flow; considerable agreement is obtained, therefore, with the modelling approach of Huthnance (1982b) in which the range of values was found to be 18° to 48°, with maximum growth occurring for an angle of 27°.

Residual flow patterns around the Broken Bank have been identified; on the eastern flank, residual flow is directed consistently towards the southeast and is, therefore, largely parallel to the axis of the Broken Bank. On the western flank, the flow is more variable but directed generally towards the northwest. In the swale between the Well and Broken Banks, the observed near-bed residual current is in an offshore (northeasterly) direction. Such water movement contrasts with the result of Caston and Stride (1970), where long-term residual currents in the swale between the Well and Leman Banks were towards the northwest. Such differences

may be influenced by the growth of a new sand bank in this region (Huntley *et al.*, 1993) or may be the result of prevailing meterological conditions during each particular period of measurement. Indeed, an oscillation with a period substantially longer than the tidal period, can be observed within the self-recording current meter data obtained at Station G. Nevertheless, there is a northerly residual flow component evident in data from both investigations.

Therefore, the crest of the Broken Bank forms a partition between variable flow on the western flank, and flow on the eastern flank which is characterised by its strong dominance in the southeasterly direction. As such, the Broken Bank may be considered as a bedload parting zone (Harris *et al.*, 1995).

7.3 PREDICTIVE SEDIMENT TRANSPORT TECHNIQUES

Part of the present study has investigated the influence of a number of aspects (first order wave theory, bed roughness and sediment transport formulae) of the predictive methods, with a view to developing an accurate model with which to predict regional patterns of sediment transport.

Most coastal processes are subject to some degree of wave influence. It is important, therefore, to determine accurately the wave-induced bed shear stress. As part of the investigation into such processes, first order (linear) wave theory is normally used. On the basis of results presented here, however, it seems that this theory may not be valid in the present study area. Further investigation is required into the form of the wave-induced near-bed velocity profile.

Sea bed characteristics have been interpreted successfully from sea bed photographs. The dimensions of ripples observed as part of the present investigation do not exhibit any obvious agreement with concurrently recorded hydrodynamic data. Ripple height and wavelength data show considerable agreement with similar data presented by Amos *et al.* (1988). Further, ripple wavelength data from the present investigation exhibits considerable agreement

with wave-generated bedform data and relationships derived by Mogridge *et al.* (1994). No (field) height data were provided by these investigators, thus making any comparison with results from the present study impossible. However, the ripples observed here show little agreement with the steepness formula suggested by Bagnold (1946) for wave-generated ripples. On the basis of these comparisons, it would appear that ripple dimensions in wave-current flows must be related to both the wave and current components of the flow.

Difficulty arises in relating ripple dimensions to hydrodynamic flow data that has been obtained from discrete 'bursts', as a lag exists between maximum tidal current velocity and maximum sediment transport which influences ripple shape.

Coastal processes which result from the combined influence of waves and tidal currents are now frequently modelled numerically. A knowledge of the near-bed current structure in tidal seas is essential for sediment transport studies. A key component of any wave-current interaction model is the accurate specification of the sea bed roughness (k_s). There seems, however, little agreement on the method by which bed roughness may be determined accurately; existing roughness formulae have been shown to exhibit considerable scatter when using the same input data. A new roughness formula has been suggested here which improves considerably on the performance of existing formulae for the data from the present study area. In contrast to the majority of previous investigations, the formula derived as part of the present investigation for determining k_s takes into account the angle made between the ripple crests and the tidal current. The range of results obtained suggests that the k_s value may be very site-specific and that further observations may be necessary before consensus is reached.

Before accurate prediction of sediment transport rates can be made with any confidence in the coastal marine environment, the techniques adopted must be checked for accuracy and suitability. An essential component of this process is the comparison of results from the predictive method against (independent) observed transport rates. The observational process should be non-intrusive and so have

with wave-generated bedform data and relationships derived by Mogridge *et al.* (1994). No (field) height data were provided by these investigators, thus making any comparison with results from the present study impossible. However, the ripples observed here show little agreement with the steepness formula suggested by Bagnold (1946) for wave-generated ripples. On the basis of these comparisons, it would appear that ripple dimensions in wave-current flows must be related to both the wave and current components of the flow.

Difficulty arises in relating ripple dimensions to hydrodynamic flow data that has been obtained from discrete 'bursts', as a lag exists between maximum tidal current velocity and maximum sediment transport which influences ripple shape.

Coastal processes which result from the combined influence of waves and tidal currents are now frequently modelled numerically. A knowledge of the near-bed current structure in tidal seas is essential for sediment transport studies. A key component of any wave-current interaction model is the accurate specification of the sea bed roughness (k_s). There seems, however, little agreement on the method by which bed roughness may be determined accurately; existing roughness formulae have been shown to exhibit considerable scatter when using the same input data. A new roughness formula has been suggested here which improves considerably on the performance of existing formulae for the data from the present study area. In contrast to the majority of previous investigations, the formula derived as part of the present investigation for determining k_s takes into account the angle made between the ripple crests and the tidal current. The range of results obtained suggests that the k_s value may be very site-specific and that further observations may be necessary before consensus is reached.

Before accurate prediction of sediment transport rates can be made with any confidence in the coastal marine environment, the techniques adopted must be checked for accuracy and suitability. An essential component of this process is the comparison of results from the predictive method against (independent) observed transport rates. The observational process should be non-intrusive and so have

minimal effects on the rates of transport observed. In the present investigation independent rates have been inferred from bedform migration rates.

Coastal sediment transport pathways are derived usually on the basis of steady-current and wave-induced shear stresses exerted on the sea bed. These stresses are used then in a sediment transport formula. However, a considerable number of formulae are available to the coastal engineer/oceanographer, and it is in this last stage that much variation is encountered with the various formulae producing widely differing sediment transport rates for the same input data (Chapter 5), and may fail to reproduce accurately the observed rates. On the basis of detailed comparison between predicted transport rates and observed rates of ripple migration, a new calibration of an existing transport formula has been suggested in order to obtain improved agreement between observed and predicted transport rates. Though considerable improvement in the predictive technique is obtained here using the new transport formula, further investigation is required to assess the more widespread applicability of this formula.

A number of shortcomings of the techniques used to interpret the photographic data have become apparent. For any given hydrodynamic conditions, the time interval between successive photographs will influence the amount of ripple migration observed. In area such as the North Sea, a large range of current speeds and, hence, ripple migration rates can be experienced. The time interval between successive photographs needs to be chosen, therefore, to allow maximum ripple migration within the field of view. This choice will be complicated if, as in the present investigation, a fixed time interval is employed over a period of several tidal cycles. Further inaccuracies may be encountered as sediment transport is assumed to be occurring as a result of the migration of the ripple forms. No account is made of the possibility of ripple bypassing or the variable depth of the mobile layer. However, the effects of ripple bypassing are likely to be minimal during the lower flow periods represented by the photographs used here.

7.4 REGIONAL SEDIMENT TRANSPORT PATTERNS

During geological time the North Sea basin has been uplifted and submerged a number of times. Owing to the periodic interchange of land and sea, older sediment deposits have been covered by more recent ones, laid bare, reworked or destroyed. Deposits from various geological periods have been recognised in different parts of the North Sea, suggesting that the existing pattern of sediment distribution has not been created to a significant extent by the currents of the present North Sea. Instead, it can be mostly assumed that, the present distribution of sediments was formed by the Pleistocene glacial periods which has not been concealed or destroyed by the alterations which have followed (Edelman, 1939).

Within this context, the sediments of the southern North Sea continue to be modified by hydrodynamic processes. Medium-grained sandy sediments are dominant over much of the offshore area. However, significant geographical variation of the heavy mineral content of the sands is evident (Baak, 1936). Much of the sand is mobile under present-day hydrodynamic conditions, and therefore its distribution is related to modern sand transport processes. Large areas of coarse sand are present off the German and Danish coasts, and at several points along the English coast. In the central section of the North Sea only a few small areas of coarse sand are found. Sand and fine mud occupy the largest part of the sea basin and are the main types of sediment present. Mud and sandy mud cover a large area along the Norwegian coast, in the vicinity of the Norwegian Trough, but elsewhere are present to only a small extent. Fine-grained sand occurs in the mouths of estuaries. Very fine-grained sands are found mostly on intertidal flats.

The largest area of gravelly sediments occurs between the north Norfolk coast and Flamborough Head. These sediments are mostly less than a few tens of centimetres thick, and are overlain in places by deposits of sand, including the Norfolk Banks. Patches of gravelly sediment are found on the Dogger Bank and on the sea floor off eastern East Anglia and in the Dover Strait (Cameron *et al.*, 1992).

7.4 REGIONAL SEDIMENT TRANSPORT PATTERNS

During geological time the North Sea basin has been uplifted and submerged a number of times. Owing to the periodic interchange of land and sea, older sediment deposits have been covered by more recent ones, laid bare, reworked or destroyed. Deposits from various geological periods have been recognised in different parts of the North Sea, suggesting that the existing pattern of sediment distribution has not been created to a significant extent by the currents of the present North Sea. Instead, it can be mostly assumed that, the present distribution of sediments was formed by the Pleistocene glacial periods which has not been concealed or destroyed by the alterations which have followed (Edelman, 1939).

Within this context, the sediments of the southern North Sea continue to be modified by hydrodynamic processes. Medium-grained sandy sediments are dominant over much of the offshore area. However, significant geographical variation of the heavy mineral content of the sands is evident (Baak, 1936). Much of the sand is mobile under present-day hydrodynamic conditions, and therefore its distribution is related to modern sand transport processes. Large areas of coarse sand are present off the German and Danish coasts, and at several points along the English coast. In the central section of the North Sea only a few small areas of coarse sand are found. Sand and fine mud occupy the largest part of the sea basin and are the main types of sediment present. Mud and sandy mud cover a large area along the Norwegian coast, in the vicinity of the Norwegian Trough, but elsewhere are present to only a small extent. Fine-grained sand occurs in the mouths of estuaries. Very fine-grained sands are found mostly on intertidal flats.

The largest area of gravelly sediments occurs between the north Norfolk coast and Flamborough Head. These sediments are mostly less than a few tens of centimetres thick, and are overlain in places by deposits of sand, including the Norfolk Banks. Patches of gravelly sediment are found on the Dogger Bank and on the sea floor off eastern East Anglia and in the Dover Strait (Cameron *et al.*, 1992).

Muddy sediments in the southern North Sea are confined mostly to intertidal areas within estuaries and tidal inlets.

Investigation of the temporal variation of the occurrence of sediment transport reveals that the area of the Norfolk Banks is highly dynamic. The present study area is one of active sediment transport; the threshold of movement may be exceeded by as much as 77% of the time during a spring tidal cycle.

Rates of (scalar) sediment transport indicate that the tidal currents on either side of the Broken Bank are equally competent in transporting sediment. When the current direction is considered, sediment transport pathways are identified: southeasterly transport is prevalent on the eastern side of the bank whilst on the western flank of the bank, the movement is directed predominantly towards the northwest. Further, these transport rates show that, along the eastern flank of Broken Bank, southeasterly sediment transport is substantially greater than that directed towards the northwest. Along the western flank of the bank, transport of sand to the northwest and southeast is similar which produces only a small (northwesterly) residual transport rate.

The sediment transport pattern identified here produces a net southward movement of sand over the area which appears to be consistent with the regional sediment transport patterns. To the north of the study area, a bedload parting zone has been identified, which indicates net southeasterly movement over the sand bank areas (Stride, 1963; Kenyon and Stride, 1970; see also Chang and Evans, 1992). The bedload transport rates derived here, using empirical formulae and self-recording current meter data, indicate higher rates of transport in a southeasterly direction on the eastern side of the Broken Bank, than on the western side. This is consistent with the results of the present investigation, but not with those of earlier studies. Caston and Stride (1970) and Caston (1972) have suggested that the steep side of banks such as the Broken Bank, which faces to the northeast, is a reflection of the cross-bank directed component of the dominant northwesterly sediment movement. However, long-term wave measurements may reveal the ability of extreme events

to enhance considerably the sandstream directed towards the northwest.

The residual water and sand movement, identified as part of the present investigation, is indicative of water and sand circulation cells associated with the North Sea sand bank systems. Net sand transport directions have been inferred from the asymmetry of sand waves adjacent to the banks (Collins *et al.*, 1995a). The patterns are consistent with a clockwise pattern of (residual) water movement around the banks (as observed here). Such an observation is in agreement with the earlier findings of Caston and Stride (1970) who proposed a clockwise circulation of sand around the Leman and Well Banks.

Sediment movement is directed at an angle to the axis of the Broken Bank and, hence, has a component of movement directed to (or away from) the bank. This movement can be postulated to either maintain or erode the bank. This bank-directed movement occurs consistently along the eastern flank of the Broken Bank. To the west, it is more variable. During periods when the bank is being supplied with sediment from the western flank, the magnitude of sediment movement directed towards the crestline is greater than that from the eastern flank.

Sand may be supplied to the banks by secondary currents. However, water movement patterns observed as part of the present investigation contradict the patterns expected for the 'helical flow' concept (Houbolt, 1968). However, the understanding of secondary circulation effects requires detailed information on the vertical current structure; these data have not been obtained as part of the present investigation.

Caston (1972), in relation to Houbolt's (1968) original observations, explained the crestline as a line of convergence of sand waves veering towards the bank crest. The sand waves changed their orientation as they approached the bank crestline, from being normal to the crestline in the swales adjacent to the bank, to almost parallel to the axis on either side of the crest. This interpretation was based upon data collected in the vicinity of the Leman and Ower Banks; it corresponds to the

sand wave orientation data presented by Collins *et al.* (1995a). A mechanism was thus suggested whereby material is constantly transported to the crest, thus perpetuating the form of the sand bank. Cross-sectional asymmetry of the bank was assumed to reflect the dominance of one of the (crestward) sandstreams. In the case of the Norfolk Banks, this indicates a northeasterly (offshore) movement of material.

Within the swale between the Broken and Well Banks, there is a high incidence of sand waves indicating a component of sand transport in a northeasterly direction (Collins *et al.*, *op. cit.*). Self-recording current meter data recorded at Station G as part of the present investigation, indicate near-bed residual water movement and sediment transport directed towards the northeast. Although no direct evidence of such sand wave migration appears to have been reported elsewhere, investigators have suggested sand transport directed towards the northeast, based upon: (a) internal bedding directions, sand bank movement and asymmetry of the banks themselves (Houbolt, 1968); and (b) prediction of long-term and overall sand transport directions towards the northeast, based upon the numerical modelling of tidally- and storm surge-induced currents (Stride, 1988).

The data from the present study are indicative of some transport of sand in an offshore (northeasterly) direction in the swales between the banks, which would confirm the hypothesis of Stride (*op. cit.*). This investigator has shown how the combination of storm surge currents with strong tidal currents are veered and amplified as they cross the crests of the Norfolk Banks. These currents are thought to provide a means of transporting sand seawards from the coast. Hence, the banks acts as 'stepping stones', transporting sand from the East Anglian coastline to seaward. Such transport has been shown to occur in this study, not only during storms, but also under 'normal' (tidal and low wave) hydrodynamic conditions. Such an observation is consistent with previous investigations into residual water movement (Maier-Reimer, 1977). It is likely that a combination of the strong instantaneous currents within the swales, together with the residual currents directed offshore, causes sediment movement across the swales from the coast

towards deeper waters. Cameron *et al.* (1992) have suggested that erosion of the coast may supply large volumes of sediment which would provide material for the construction and maintenance of sand banks.

The presence of a lag effect between maximum tidal current velocity and maximum sediment transport implies that the net sediment transport direction depends upon the sense of rotation of the tidal current vectors i.e. clockwise or anticlockwise (Stride, 1974). To the south of the bedload parting zone identified by Stride (1963) and Kenyon and Stride (1970), the sense of rotation indicates an offshore transport. Loss of sediment to the offshore has been reported by McCave (1978) and McCave and Balson (1990). This offshore sand movement i.e. to the northeast, is supported also by the observation that the banks have their steepest slopes on their northeast flanks and their internal stratification indicates migration in the same direction (Houbolt, 1968).

The proposed offshore transport pathway may cause the sand banks to grow vertically or laterally in response to deposition, and/or accretion to take place in the offshore waters. Difficulty arises when trying to observe bathymetric changes which support these postulations. Throughout the present study area, mesoscale measurements have been obtained from previous studies, and as part of the present investigation. From these measurements, macroscale changes have been inferred. A comparison of the morphology of the sand banks over time, using sequential bathymetric charts has been undertaken by Collins *et al.* (1995a). These investigators could detect only limited changes.

The sedimentary structure of the southeastern part of the Broken Bank does not provide any evidence of major lateral migration of the main body of the sand bank. Only at the northwestern end is there any (bathymetric) indication that this part of the Bank is moving towards the northeast. The terminations of the sand bank may be dynamically very active in terms of sediment mobility (evidence for this is provided by the fact that the current meters deployed at both ends were lost, in contrast to the recovery of all of the other deployments). However, such

mobility is assessed on a time-scale which is small when compared to that of sand bank migration and development (i.e. 10^2 years) (Huthnance, 1982a; Howarth and Huthnance, 1984). It is suggested, therefore, that the material transported offshore is dissipated partly into deeper waters beyond the sand banks as well as contributing partly to the development and maintenance of the sand bank system itself (perhaps causing slow lateral migration).

The presence of an area of symmetrical sand waves at the ends of a sand bank have been taken to indicate zero net transport by other investigators (Caston, 1972; McCave and Langhorne, 1982). Megaripples trending at very high angles with respect to the bank axis have also been observed here. The presence of these bedforms was believed to be indicative of sediment circulation around the bank. Caston (1981) suggested that sand enters the bank system through a low apron at the broad head of the bank, then leaves by the narrower tail. Hence, there was no evidence for a circulation of sand around the bank. However, for the present investigation, considerable difficulty arises when trying to identify the broad head of the Broken Bank. Due to equipment losses, geophysical data presented by Collins *et al.* (1995a) and tidal current observations presented here do not, unfortunately, cover the extremities of the bank. These theories cannot, therefore, be disputed or confirmed.

The previous discussion relates to the maintenance of linear sand banks. With regard to the formation of such banks, Huthnance (1982a, 1982b) has proposed the requirement for strong currents and the presence of some initial irregularities on the sea bed. However, such conditions may not be necessary i.e. other mechanisms may cause sand bank growth. For example, flat-lying estuarine/coastal deposits or Tertiary bedrock surfaces have been found generally to underlie a number of the North Sea sand banks (Eisma, 1988; Liu *et al.*, 1992; Trentesaux *et al.*, 1993; Berné *et al.*, 1994). Sub-bottom profiler images of the Broken Bank presented by Collins *et al.* (*op. cit.*) show the presence of a flat and featureless base to the sand bank. Although in Huthnance's models no significant sea bed irregularities are needed, together with the fact that conditions at the initial stage

of the sand bank growth cannot be inferred from the underlying deposits, the possibility cannot be excluded that the early stages of bank development is completely controlled hydrodynamically i.e. without any perturbations or humps on the sea bed.

7.5 RECOMMENDATIONS FOR FUTURE RESEARCH

During the period of this research, a number of areas of potential further research have become apparent. These are listed below.

(i) Attempt to determine the pattern of phase differences and veering between near-bed and mid-depth flows which may be indicative of secondary circulation and, hence, sand bank maintenance.

(ii) Within the present study area, it appears that linear wave theory is not an accurate representation of the wave-induced orbital velocities. Further investigation of the properties of near-bed wave dynamics is required.

(iii) Examination of the response of the sea bed (ripple dimensions) to hydrodynamic (wave and current) data.

(iv) Investigation of the depth of the mobile sediment layer, for a rippled sea bed under combined wave and tidal current conditions, and the associated 'velocity profile' within this sedimentary layer.

(v) Evaluation of the bed roughness (Equation 5.55) and bedload transport (Equation 5.61) formulae with data from other geographical areas in order to investigate their wider applicability.

(vi) Investigation of water and sediment movement around the ends of a linear sand bank.

Chapter 8
SUMMARY

The present investigation has been concerned with the water and sediment movements in the vicinity of a linear sand bank. Tidal current information has been obtained through the extensive deployment of self-recording current meters near the bed and at a mid depth elevation above the bed in the vicinity of the Broken Bank, southern North Sea. Sea bed photographs and concurrently recorded high frequency hydrodynamic (wave and tidal current) data have been obtained from the STABLE multi-sensor tripod. Data were obtained also from a pressure sensor deployed adjacent to the Broken Bank.

A summary of the main conclusions of the present investigation is presented here.

8.1 REGIONAL HYDRODYNAMICS

Self-recording current meter data have revealed patterns of water movement in the vicinity of the Broken Bank, southern North Sea. Comparison of water depths and tidal currents has established that the tide propagates through the area as a progressive wave. Harmonic analysis of the self-recording current meter data has shown that the M_2 harmonic is dominant throughout the area. Whilst the amplitude of M_4 component is up to only 10% of that of the M_2 harmonic, it is more distinctive at locations adjacent to the banks within the present study area. This may be indicative of local (topographic) generation of M_4 tidal currents.

Tidal currents in the vicinity of the Broken Bank are strongly rectilinear, creating narrow tidal ellipses. The axis of the bank is, on average, orientated at approximately 20° in an anticlockwise sense to the direction of the dominant flow. This orientation creates a component of flow directed perpendicularly towards the axis of the bank. As such, the supply of sand may be directed towards or away from the bank. Along the eastern flank, sand transport is directed continuously

towards the crestline. Sediment supply from the western flank is, however, more intermittent.

Along the eastern flank of the Broken Bank, the hydrodynamic regime is such that the southeasterly flow is considerably greater than that directed towards the northwest. Hence, residual water flow here is directed towards the southeast and is, therefore, largely parallel to the axis of the Broken Bank. Along the western flank, tidal currents directed towards the northwest and the southeast are comparable. Hence, residual flow rates here are low, but directed generally towards the northwest. In the swale between the Broken and Well Banks, the observed near-bed residual current is directed towards the northeast (offshore).

8.2 WAVE-CURRENT INTERACTION AND SEDIMENT TRANSPORT

Analysis of the hydrodynamic data recorded by the STABLE tripod has revealed that within the present study area, first order wave theory does not reproduce accurately the wave-induced orbital velocities observed near the sea bed.

Concurrently recorded hydrodynamic data reveal that sea bed profiles, interpreted from near-bed photographs, are not controlled explicitly by either waves or currents. Observed ripple dimensions have been found to exhibit some agreement with formulae derived for both wave- and current-dominated conditions.

Estimates of bed shear stress (HR, 1991) have been compared with those inferred from the recorded hydrodynamic data. By matching these estimates, it has been possible to determine values of the bed roughness 'experienced' by the flow. This roughness has been related to the height of the ripples observed on the sea bed, and the angle made between the ripple crests and the direction of tidal current flow. This relationship has been shown to improve considerably on the performance of existing roughness formulae.

Rates of sediment transport have been inferred from rates of ripple migration.

These observed rates and the concurrently recorded hydrodynamic data have been used to investigate the ability of existing predictive sediment transport formulae to reproduce the observed (independent) transport rates. A predictive formula has been presented here which improves significantly on the performance of existing predictive formulae.

8.3 REGIONAL SEDIMENT TRANSPORT PATTERNS

Comparison of the observed tidal current velocities with the velocity required to initiate sediment transport here reveals that the present study area is highly active; critical erosion velocities may be exceeded by up to 77% of the time during a spring tidal cycle. The hydrodynamic conditions on either side of the Broken Bank are equally capable of transporting sediment.

Sediment transport patterns within the present study area have been determined by adopting two approaches. The first is based on (easily applicable) engineering practices; the second is based upon a recent wave-current boundary layer model which incorporates (locally calibrated) roughness values and accounts for the reduction in bed shear stress available to transport sediment (skin friction). When compared with the (independent) rates of sediment transport inferred from the observed rates of ripple migration, transport rates predicted by the first method were considered unreasonably high.

Regional sediment transport patterns have been identified in the vicinity of the Broken Bank; sediment movement is directed predominantly towards the southeast along the eastern flank and towards the northwest on the western flank. This pattern of residual sediment transport is indicative of sediment circulation cells associated with North Sea sand bank systems.

Along the eastern flank of the Broken Bank, water flow to the northwest would appear to be low and largely sub-threshold; thus transport directed towards the southeast is substantially greater than that directed towards the northwest. In

contrast, on the western side, northwesterly and southeasterly sediment movements are comparable; as such the southeasterly sediment movement along the eastern flank is much greater than the northwesterly movement on the western flank. A net southward movement is inferred, therefore, for this area.

The supply of sand to the crestline occurs continuously from the eastern flank and intermittently from the western flank.

Sediment movement in the swale between the Broken and Well Banks is directed towards the northeast. This suggests that sediment is being transported offshore under 'normal' (tidal and low wave) hydrodynamic conditions.

REFERENCES

Ackers P and White WR (1973). Sediment transport: New approach and analysis. Journal of the Hydraulics Division, ASCE, 99(11), 2041-2060.

Allen JRL (1968). Current Ripples. North Holland Publication Company, 211-220.

Allen JRL (1970). Physical Processes and Sedimentation. Unwin, 248pp.

Allen JRL (1982). Sedimentary Structures. Vols I and II. Elsevier, 593pp and 633pp.

Amos CL and King EL (1984). Bedforms of the Canadian eastern seaboard: A comparison with global occurrences. Marine Geology, 57, 167-208.

Amos CL, Bowen AJ, Huntley DA and Lewis CFM (1988). Ripple generation under the combined influences of waves and currents on the Canadian continental shelf. Continental Shelf Research, 8(10), 1129-1153.

Ashley GM (1990). Classification of large-scale subaqueous bedforms: A new look at an old problem. Journal of Sedimentary Petrology, 60, 160-172.

Austin RM (1991). Modelling Holocene tides on the NW European continental shelf. Terra Nova, 3, 276-288.

Baak JA (1936). Regional petrology of the southern North Sea. Wageningen.

Bacon S (1989). Waves recorded at 'Dowsing' light vessel 1979-1985. IOSDL, Report No. 262. 60pp.

Bagnold RA (1941). The Physics of Blown Sand and Desert Dunes. Methuen. Reprint 1973. Chapman and Hall.

Bagnold RA (1946). Motion of waves in shallow water. Interaction between waves and sand bottoms. Proceedings of the Royal Society, London, Ser. A., 187, 1-18.

Bagnold RA (1963). Beach and nearshore processes. Part 1, Mechanics of marine sedimentation. In Hill MN (Ed), The Sea: Vol 3, Wiley-Interscience, New York, 507-528.

Bagnold RA (1966). An approach to the sediment transport problem from general physics. US Geol. Surv. Prof. Pap. 422-I, 137pp.

Bakkar WT and Van Doorn T (1978). Near bottom velocities in waves with a current. Proc. 16th Conf. Coastal Eng., 1394-1413.

Bathurst JC, Thorne CR and Hey RD (1977). Direct measurements of secondary currents in river bends. Nature, 269, 504-506.

Belderson, RH (1986). Offshore tidal and non-tidal sand ridges and sheets: Differences in morphology and hydrodynamic setting. In: Knight RJ and McLean JR (Eds), Shelf Sands and Sandstones, Canadian Society of Petroleum Geologists, Memoir II, 293-301.

Belderson RH, Johnson MA and Kenyon NH (1982). Bedforms. In: Offshore Tidal Sands, Processes and Deposits. Stride AH (Ed). London. Chapman and Hall, 27-57.

Berné S, Trentesaux A, Stolk A, Missaen T and De Batist M (1994). Architecture and long term evolution of a tidal sandbank: The Middlekerke Bank (southern North Sea). Marine Geology, 121, 57-72.

Bijker EW (1967). The increase in bed shear due to wave motion. Proceedings of the 10th Conference on Coastal Engineering, ASCE, 1, 746-765.

Boczar-Karakiewicz B and Bona JL (1986). Wave-dominated shelves: a model of sand-ridge formation by progressive infragravity waves. In: Shelf Sands

REFERENCES

Ackers P and White WR (1973). Sediment transport: New approach and analysis. Journal of the Hydraulics Division, ASCE, 99(11), 2041-2060.

Allen JRL (1968). Current Ripples. North Holland Publication Company, 211-220.

Allen JRL (1970). Physical Processes and Sedimentation. Unwin, 248pp.

Allen JRL (1982). Sedimentary Structures. Vols I and II. Elsevier, 593pp and 633pp.

Amos CL and King EL (1984). Bedforms of the Canadian eastern seaboard: A comparison with global occurrences. Marine Geology, 57, 167-208.

Amos CL, Bowen AJ, Huntley DA and Lewis CFM (1988). Ripple generation under the combined influences of waves and currents on the Canadian continental shelf. Continental Shelf Research, 8(10), 1129-1153.

Ashley GM (1990). Classification of large-scale subaqueous bedforms: A new look at an old problem. Journal of Sedimentary Petrology, 60, 160-172.

Austin RM (1991). Modelling Holocene tides on the NW European continental shelf. Terra Nova, 3, 276-288.

Baak JA (1936). Regional petrology of the southern North Sea. Wageningen.

Bacon S (1989). Waves recorded at 'Dowsing' light vessel 1979-1985. IOSDL, Report No. 262. 60pp.

Bagnold RA (1941). The Physics of Blown Sand and Desert Dunes. Methuen. Reprint 1973. Chapman and Hall.

Bagnold RA (1946). Motion of waves in shallow water. Interaction between waves and sand bottoms. Proceedings of the Royal Society, London, Ser. A., 187, 1-18.

Bagnold RA (1963). Beach and nearshore processes. Part 1, Mechanics of marine sedimentation. In Hill MN (Ed), The Sea: Vol 3, Wiley-Interscience, New York, 507-528.

Bagnold RA (1966). An approach to the sediment transport problem from general physics. US Geol. Surv. Prof. Pap. 422-I, 137pp.

Bakkar WT and Van Doorn T (1978). Near bottom velocities in waves with a current. Proc. 16th Conf. Coastal Eng., 1394-1413.

Bathurst JC, Thorne CR and Hey RD (1977). Direct measurements of secondary currents in river bends. Nature, 269, 504-506.

Belderson, RH (1986). Offshore tidal and non-tidal sand ridges and sheets: Differences in morphology and hydrodynamic setting. In: Knight RJ and McLean JR (Eds), Shelf Sands and Sandstones, Canadian Society of Petroleum Geologists, Memoir II, 293-301.

Belderson RH, Johnson MA and Kenyon NH (1982). Bedforms. In: Offshore Tidal Sands, Processes and Deposits. Stride AH (Ed). London. Chapman and Hall, 27-57.

Berné S, Trentesaux A, Stolk A, Missaen T and De Batist M (1994). Architecture and long term evolution of a tidal sandbank: The Middlekerke Bank (southern North Sea). Marine Geology, 121, 57-72.

Bijker EW (1967). The increase in bed shear due to wave motion. Proceedings of the 10th Conference on Coastal Engineering, ASCE, 1, 746-765.

Boczar-Karakiewicz B and Bona JL (1986). Wave-dominated shelves: a model of sand-ridge formation by progressive infragravity waves. In: Shelf Sands

REFERENCES

Ackers P and White WR (1973). Sediment transport: New approach and analysis. Journal of the Hydraulics Division, ASCE, 99(11), 2041-2060.

Allen JRL (1968). Current Ripples. North Holland Publication Company, 211-220.

Allen JRL (1970). Physical Processes and Sedimentation. Unwin, 248pp.

Allen JRL (1982). Sedimentary Structures. Vols I and II. Elsevier, 593pp and 633pp.

Amos CL and King EL (1984). Bedforms of the Canadian eastern seaboard: A comparison with global occurrences. Marine Geology, 57, 167-208.

Amos CL, Bowen AJ, Huntley DA and Lewis CFM (1988). Ripple generation under the combined influences of waves and currents on the Canadian continental shelf. Continental Shelf Research, 8(10), 1129-1153.

Ashley GM (1990). Classification of large-scale subaqueous bedforms: A new look at an old problem. Journal of Sedimentary Petrology, 60, 160-172.

Austin RM (1991). Modelling Holocene tides on the NW European continental shelf. Terra Nova, 3, 276-288.

Baak JA (1936). Regional petrology of the southern North Sea. Wageningen.

Bacon S (1989). Waves recorded at 'Dowsing' light vessel 1979-1985. IOSDL, Report No. 262. 60pp.

Bagnold RA (1941). The Physics of Blown Sand and Desert Dunes. Methuen. Reprint 1973. Chapman and Hall.

Bagnold RA (1946). Motion of waves in shallow water. Interaction between waves and sand bottoms. Proceedings of the Royal Society, London, Ser. A., 187, 1-18.

Bagnold RA (1963). Beach and nearshore processes. Part 1, Mechanics of marine sedimentation. In Hill MN (Ed), The Sea: Vol 3, Wiley-Interscience, New York, 507-528.

Bagnold RA (1966). An approach to the sediment transport problem from general physics. US Geol. Surv. Prof. Pap. 422-I, 137pp.

Bakkar WT and Van Doorn T (1978). Near bottom velocities in waves with a current. Proc. 16th Conf. Coastal Eng., 1394-1413.

Bathurst JC, Thorne CR and Hey RD (1977). Direct measurements of secondary currents in river bends. Nature, 269, 504-506.

Belderson, RH (1986). Offshore tidal and non-tidal sand ridges and sheets: Differences in morphology and hydrodynamic setting. In: Knight RJ and McLean JR (Eds), Shelf Sands and Sandstones, Canadian Society of Petroleum Geologists, Memoir II, 293-301.

Belderson RH, Johnson MA and Kenyon NH (1982). Bedforms. In: Offshore Tidal Sands, Processes and Deposits. Stride AH (Ed). London. Chapman and Hall, 27-57.

Berné S, Trentesaux A, Stolk A, Missaen T and De Batist M (1994). Architecture and long term evolution of a tidal sandbank: The Middlekerke Bank (southern North Sea). Marine Geology, 121, 57-72.

Bijker EW (1967). The increase in bed shear due to wave motion. Proceedings of the 10th Conference on Coastal Engineering, ASCE, 1, 746-765.

Boczar-Karakiewicz B and Bona JL (1986). Wave-dominated shelves: a model of sand-ridge formation by progressive infragravity waves. In: Shelf Sands

REFERENCES

Ackers P and White WR (1973). Sediment transport: New approach and analysis. Journal of the Hydraulics Division, ASCE, 99(11), 2041-2060.

Allen JRL (1968). Current Ripples. North Holland Publication Company, 211-220.

Allen JRL (1970). Physical Processes and Sedimentation. Unwin, 248pp.

Allen JRL (1982). Sedimentary Structures. Vols I and II. Elsevier, 593pp and 633pp.

Amos CL and King EL (1984). Bedforms of the Canadian eastern seaboard: A comparison with global occurrences. Marine Geology, 57, 167-208.

Amos CL, Bowen AJ, Huntley DA and Lewis CFM (1988). Ripple generation under the combined influences of waves and currents on the Canadian continental shelf. Continental Shelf Research, 8(10), 1129-1153.

Ashley GM (1990). Classification of large-scale subaqueous bedforms: A new look at an old problem. Journal of Sedimentary Petrology, 60, 160-172.

Austin RM (1991). Modelling Holocene tides on the NW European continental shelf. Terra Nova, 3, 276-288.

Baak JA (1936). Regional petrology of the southern North Sea. Wageningen.

Bacon S (1989). Waves recorded at 'Dowsing' light vessel 1979-1985. IOSDL, Report No. 262. 60pp.

Bagnold RA (1941). The Physics of Blown Sand and Desert Dunes. Methuen. Reprint 1973. Chapman and Hall.

Bagnold RA (1946). Motion of waves in shallow water. Interaction between waves and sand bottoms. Proceedings of the Royal Society, London, Ser. A., 187, 1-18.

Bagnold RA (1963). Beach and nearshore processes. Part 1, Mechanics of marine sedimentation. In Hill MN (Ed), The Sea: Vol 3, Wiley-Interscience, New York, 507-528.

Bagnold RA (1966). An approach to the sediment transport problem from general physics. US Geol. Surv. Prof. Pap. 422-I, 137pp.

Bakkar WT and Van Doorn T (1978). Near bottom velocities in waves with a current. Proc. 16th Conf. Coastal Eng., 1394-1413.

Bathurst JC, Thorne CR and Hey RD (1977). Direct measurements of secondary currents in river bends. Nature, 269, 504-506.

Belderson, RH (1986). Offshore tidal and non-tidal sand ridges and sheets: Differences in morphology and hydrodynamic setting. In: Knight RJ and McLean JR (Eds), Shelf Sands and Sandstones, Canadian Society of Petroleum Geologists, Memoir II, 293-301.

Belderson RH, Johnson MA and Kenyon NH (1982). Bedforms. In: Offshore Tidal Sands, Processes and Deposits. Stride AH (Ed). London. Chapman and Hall, 27-57.

Berné S, Trentesaux A, Stolk A, Missaen T and De Batist M (1994). Architecture and long term evolution of a tidal sandbank: The Middlekerke Bank (southern North Sea). Marine Geology, 121, 57-72.

Bijker EW (1967). The increase in bed shear due to wave motion. Proceedings of the 10th Conference on Coastal Engineering, ASCE, 1, 746-765.

Boczar-Karakiewicz B and Bona JL (1986). Wave-dominated shelves: a model of sand-ridge formation by progressive infragravity waves. In: Shelf Sands

REFERENCES

Ackers P and White WR (1973). Sediment transport: New approach and analysis. Journal of the Hydraulics Division, ASCE, 99(11), 2041-2060.

Allen JRL (1968). Current Ripples. North Holland Publication Company, 211-220.

Allen JRL (1970). Physical Processes and Sedimentation. Unwin, 248pp.

Allen JRL (1982). Sedimentary Structures. Vols I and II. Elsevier, 593pp and 633pp.

Amos CL and King EL (1984). Bedforms of the Canadian eastern seaboard: A comparison with global occurrences. Marine Geology, 57, 167-208.

Amos CL, Bowen AJ, Huntley DA and Lewis CFM (1988). Ripple generation under the combined influences of waves and currents on the Canadian continental shelf. Continental Shelf Research, 8(10), 1129-1153.

Ashley GM (1990). Classification of large-scale subaqueous bedforms: A new look at an old problem. Journal of Sedimentary Petrology, 60, 160-172.

Austin RM (1991). Modelling Holocene tides on the NW European continental shelf. Terra Nova, 3, 276-288.

Baak JA (1936). Regional petrology of the southern North Sea. Wageningen.

Bacon S (1989). Waves recorded at 'Dowsing' light vessel 1979-1985. IOSDL, Report No. 262. 60pp.

Bagnold RA (1941). The Physics of Blown Sand and Desert Dunes. Methuen. Reprint 1973. Chapman and Hall.

Bagnold RA (1946). Motion of waves in shallow water. Interaction between waves and sand bottoms. Proceedings of the Royal Society, London, Ser. A., 187, 1-18.

Bagnold RA (1963). Beach and nearshore processes. Part 1, Mechanics of marine sedimentation. In Hill MN (Ed), The Sea: Vol 3, Wiley-Interscience, New York, 507-528.

Bagnold RA (1966). An approach to the sediment transport problem from general physics. US Geol. Surv. Prof. Pap. 422-I, 137pp.

Bakkar WT and Van Doorn T (1978). Near bottom velocities in waves with a current. Proc. 16th Conf. Coastal Eng., 1394-1413.

Bathurst JC, Thorne CR and Hey RD (1977). Direct measurements of secondary currents in river bends. Nature, 269, 504-506.

Belderson, RH (1986). Offshore tidal and non-tidal sand ridges and sheets: Differences in morphology and hydrodynamic setting. In: Knight RJ and McLean JR (Eds), Shelf Sands and Sandstones, Canadian Society of Petroleum Geologists, Memoir II, 293-301.

Belderson RH, Johnson MA and Kenyon NH (1982). Bedforms. In: Offshore Tidal Sands, Processes and Deposits. Stride AH (Ed). London. Chapman and Hall, 27-57.

Berné S, Trentesaux A, Stolk A, Missaen T and De Batist M (1994). Architecture and long term evolution of a tidal sandbank: The Middlekerke Bank (southern North Sea). Marine Geology, 121, 57-72.

Bijker EW (1967). The increase in bed shear due to wave motion. Proceedings of the 10th Conference on Coastal Engineering, ASCE, 1, 746-765.

Boczar-Karakiewicz B and Bona JL (1986). Wave-dominated shelves: a model of sand-ridge formation by progressive infragravity waves. In: Shelf Sands

and Sandstones, Knight RJ and McLean JR (Eds), Can. Soc. Petr. Geol., Memoir II, 163-179.

Boczar-Karakiewicz B, Amos CL and Drapeau G (1990). The origin and stability of sand ridges on Stable Island Bank, Scotian Shelf. Continental Shelf Research, 10(7), 683-704.

Boczar-Karakiewicz B, Bona JL and Pelchat B (1991). Sand ridges and internal waves on continental shelves. In: Coastal Sediments '91, Kraus NC, Gingerich KS and Kreibel DL (Eds), Vol I, 527-541, ASCE.

Bray M (1990). Patterns of sediment transport. Report to Dorset County Council and West Dorset District Council, January 1990, 797pp.

Cacchione DA and Drake DE (1982). Measurements of storm-generated bottom stresses on the continental shelf. Journal of Geophysical Research, 87, 1952-1960.

Caldwell DR and Chriss TM (1979). The viscous sublayer at the sea floor. Science, 205, 1131-1132.

Cameron TDJ, Crosby A, Balson PS, Jeffery DH, Lott GK, Bulat J and Harrison DJ (1992). The geology of the southern North Sea. British Geological Survey, HMSO, London, 152pp.

Casey HJ (1935). Uber Geschiebebewegung. Milt. d. Preuss. Versuchsanstalt f. Wasserbau u. Schiffbau, Berlin, 19pp.

Caston GF (1981). Potential gain and loss of sand by some sand banks in the southern bight of the North Sea. Marine Geology, 41, 239-250.

Caston VND (1972). Linear sand banks in the southern North Sea. Sedimentology, 18, 63-78.

Caston VND and Stride AH (1970). Tidal sand movement between some linear sand banks in the North Sea off northeast Norfolk. Marine Geology, 9, M38-M42.

Chakhotin PS, Medvedev VS and Longinov VV (1972). Sand ridges and waves on the shelf of tidal seas. Oceanology, 12, 386-394.

Chang SC and Evans G (1992). Sources of sediment and sediment transport on the east coast of England: significant or coincidental? Marine Geology, 9, M38-M42.

Charnock H (1959). Tidal friction from currents near the sea bed. Geophysical Journal of the Royal Astronomical Society, 2, 215-221.

Chriss TM and Caldwell DR (1982). Evidence for the influence of form drag on bottom boundary layer flow. Journal of Geophysical Research, 87(C6), 4148-4154.

Christoffersen JB and Jonsson IG (1985). Bed friction and dissipation in a combined current and wave motion. Ocean Engineering, 12(5), 387-423.

Clayson CH and Ewing JA (1988). Directional wave data recorded in the southern North Sea. IOSDL, Report No. 258. 70pp.

Clayton KM (1989). Sediment input from the Norfolk Cliffs, eastern England- a century of coast protection and its effect. Journal of Coastal research, 5, 433-442.

Clifton HE and Dingler JR (1984). Wave-formed structures and paleoenvironmental reconstruction. Developments in Sedimentology, 39. Greenwood B and Davies Jr. RA (Eds). Elsevier Science Publishers, 165-

198.
Cloet RL (1954). Hydrographic analysis of the Goodwin Sands and the Brake Bank. Geographical Journal, 120, 203-215.
Coffey FC and Nielsen P (1984). Aspects of wave current boundary layer flows. Proc. 19th Conf. Coastal Eng., 2, 2231-2245.
Collins MB, Amos CL and Evans G (1981). Observations of some sediment transport processes over intertidal flats, the Wash, UK. Special Publication, International Association Sedimentologists, 5, 81-98.
Collins MB (1991). RRS Challenger Cruise 40, 15-29 November 1988. Sediment and water movement in the vicinity of a North Sea sandbank. Southampton: Southampton University, Department of Oceanography. 38pp.
Collins MB, Shimwell SJ, Gao S, Powell H, Hewitson C and Taylor JA (1995a). Water and sediment movement in the vicinity of linear sandbanks: the Norfolk Banks, southern North Sea. Marine Geology, 123, 125-142.
Collins MB, Ke X and Gao S (1995b). Tidally-induced flow structure over sandy intertidal flats. Paper submitted to Journal of Geophysical Research.
Davies CM (1980). Evidence for the formation and age of a commercial sand deposit in the Bristol Channel. Estuarine and Coastal Marine Science, 11, 83-101.
Davies AG, Soulsby RL and King HL (1988). A numerical model of the combined wave and current bottom boundary layer. Journal of Geophysical Research, 93(C1), 491-508.
Davis RA and Balson PS (1992). Stratigraphy of a North Sea tidal sand ridge. Journal of Sedimentary Petrology, 62(1), 116-122.
De Vriend HJ (1990). Morphological processes in shallow tidal seas. In: RT Cheng (Ed), Residual Currents and Long-term Transport. Coastal and Estuarine Studies, Vol. 38. Springer-Verlag, New York, 276-301.
Dingler JR and Inman DL (1976). Wave formed ripples in seashore sands. Proc. 15th Conf. Coastal Eng., 2109-2126.
D'Olier B (1981). Sedimentary events during sea level rise in the south-west corner of the North Sea. Special Publication of the International Association of Sedimentologists, 5, 221-227.
Doodson AT (1928). The analysis of tidal observations. Philosophical Transactions of the Royal Society of London, A227, 223-279.
Drake DE, Cacchione DA and Grant WD (1992). Shear stress and bed roughness estimates for combined wave and current flows over a rippled bed. Journal of Geophysical Research, 97(C2), 2319-2326.
Draper L (1968). Waves at Smith's Knoll, North Sea. National Institute of Oceanography Internal Report, Number A33, 16pp.
Duane DB, Field ME, Meisburger EP, Swift DJP and Williams SJ (1972). Linear shoals on the Atlantic inner continental shelf, Florida to Long Island. In: Swift DJP, Duane DB and Pilkey OH (Eds), Shelf Sediment Transport: Processes and Pattern. Dowden, Huthchinson and Ross, 447-498.
Dyer KR (1970). Current velocity profiles in a tidal channel. Geophysical Journal of the Royal Astronomical Society, 22, 153-161.
Dyer KR (1980). Velocity profiles over a rippled bed and the threshold of movement of sand. Estuarine and Coastal Science, 10, 181-199.

Dyer KR (1986). Coastal and Estuarine Sediment Dynamics. Chichester, John Wiley, 342 pp.

Dyer KR and Soulsby RL (1988). Sand transport on the continental shelf. Annual Review of Fluid Mechanics, 20, 295-324.

Eagleson PS, Dean RG and Peralta LA (1959). The mechanics of the motion of discrete spherical bottom sediment particles due to shoaling waves. Journal of the Hydraulics Division, ASCE, 85(HY10), 53-79.

Einstein HA (1950). The bedload function for sediment transportation in open channel flows. Soil Conservation Service US Department of Agriculture Technical Bulletin, No. 1026, 78pp.

Einstein HA and Barbarossa NL (1952). River channel roughness. Transactions, ASCE, 117, 1121-1146.

Eisma D (1981). Supply and deposition of suspended matter in the North Sea. Special Publications of the International Association of Sediment., 5, 415-428.

Eisma D (1988). An introduction to the geology of continental shelves. In: H Postma and JJ Zijlstra (Eds), Continental Shelves. (Ecosystems of the World, 27), Elsevier, Amsterdam, 39-91.

Eisma D and Kalf J (1979). Distribution and particle size of suspended matter in the Southern Bight of the North Sea and the eastern Channel. Netherlands Journal of Sea Research, 13, 298-324.

Edelman CH (1939). Petrological relations of the sediments in the southern North Sea. In: Recent Marine Sediments, Trask PD (Ed), Thomas Murby, 343-347.

Elzerman JJ and Frijlink HC (1951). Present state of the investigation on bedload movement in Holland. 9th Ass. Int. Geodesy Geophys., Brussels, 100-116.

Engelund F and Hansen E (1967). A monograph on sediment transport in alluvial streams. Technical University of Denmark. 62pp.

Fairbanks RG (1989). A 17000-year galcio-eustatic sea level record: influence of glacial melting rates on the younger Dryas event and deep-ocean circulation. Nature, London, 342, 637-642.

Ferentinos G and Collins MB (1980). Effects of shoreline irregularities on the rectilinear tidal current and their significance in sedimentation processes. Journal of Sedimentary Petrology, 50(4), 1081-1094.

Figueiredo AG, Swift DJP, Stubblefield WL and Clarke TL (1981). Sand ridges on the inner Atlantic shelf of North America: morphometric comparisons with Huthnance stability model. Geo-Marine Letters, 1, 187-191.

Flather RA (1987). Estimates of extreme conditions of tide and surge using a numerical model of the north-west European continental shelf. Estuarine, Coastal and Shelf Science, 24, 69-93.

Fredsoe J (1982). Shape and dimensions of stationary dunes in rivers. Journal of the Hydraulics Division, ASCE, 108(8), 932-947.

Gadd PE, Lavelle JW and Swift DJP (1978). Estimates of sand transport on the New York Shelf using near bottom current meter observations. Journal of Sedimentary Petrology 48, 239-252.

Gill MA (1968). Rationalisation of Lacey's regime flow equations. ASCE, 94, HY4, 983-995.

Graff HW (1971). Hydraulics of sediment transport. McGraw-Hill. 513pp.
Grant WD and Glenn SM (1983). Continental shelf bottom boundary layer mode, Vol. 1, Theoretical model development, Woods Hole Oceanographic Institute, 163pp.
Grant WD and Madsen OS (1979). Combined wave and current interaction with a rough bottom. Journal of Geophysical Research, 84(C4), 1797-1808.
Grant WD and Madsen OS (1982). Moveable bed roughness in unsteady oscillatory flow. Journal of Geophysical Research, 87(C1), 469-481.
Grant WD and Madsen OS (1986). The continental-shelf bottom boundary layer. Annual Review of Fluid Mechanics, 18, 265-305.
Grochowski NTL, Collins MB, Boxall SR and Salomon JC (1993). Sediment transport predictions for the English Channel, using numerical models. Journal of the Geological Society, 150, 683-695.
Guy HP, Simons DB and Richardson EV (1966). Summary of alluvial channel data from flume experiments 1955-1961. US Geol. Surv. Prof. Pap. 462-I, 92pp.
Hammond TM and Collins MB (1979). Flume studies of the response of various current meter rotor/propellers to combinations of unidirectional and oscillatory flow. Deutsch Hydrographische Zeitschrift, 32, 39-58.
Hammond TM, Pattiaratchi CB, Osborne MJ and Collins M (1986). Field and flume comparisons of the modified and standard (savonius-rotor) Anderaa self-recording current meters. Deutsche Hydrographische Zeitschrift, H2, 41-63.
Hannay A, Williams JJ, West JR and Coates LE (1994). A field study of wave-current interactions over a rippled sand bed. Euromech, Plymouth, 1994, 15pp.
Hardisty J (1983). An Assessment and Calibration of Formulations for Bagnold's Bedload Equation. Journal of Sedimentary Petrology 53, 1007-1010.
Hardisty J (1990). Basic sediment transport. In: Beaches, Form and Process, 113-136.
Harris PT, Pattiaratchi CB, Cole AR and Keene JB (1992). Evolution of subtidal sandbanks in Moreton Bay, eastern Australia. Marine Geology, 103(1/3), 225-247.
Harris PT, Pattiaratchi CB, Collins MB and Dalrymple RW (1995). What is a bedload parting? Spec. Publs int. Ass. Sediment., 24, 3-18.
Harvey JG and Vincent CE (1977). Observations of shear in near-bed currents in the southern North Sea. Estuarine and Coastal Marine Science, 5, 715-731.
Heaps NS (1978). Linearised vertically integrated equations for residual circulations in coastal seas. Deutsche Hydrographische Zeitschrift, 31, 147-169.
Heathershaw, A.D. (1981). Comparisons of Measured and Predicted Sediment Transport Rates in Tidal Currents. Developments in Sedimentology 32-Sediment Dynamics of Continental Shelves. ed C.A. Nittrouer, 75-104.
Heathershaw AD (1988). Sediment transport in the sea, on beaches and in rivers: Part I- Fundamental Principles. J.N.S., 14(3), 154-170.
Heathershaw AD (1988). Sediment transport in the sea, on beaches and in rivers: Part II- Sediment movement. J.N.S., 14(3), 221-234.

Graff HW (1971). Hydraulics of sediment transport. McGraw-Hill. 513pp.

Grant WD and Glenn SM (1983). Continental shelf bottom boundary layer mode, Vol. 1, Theoretical model development, Woods Hole Oceanographic Institute, 163pp.

Grant WD and Madsen OS (1979). Combined wave and current interaction with a rough bottom. Journal of Geophysical Research, 84(C4), 1797-1808.

Grant WD and Madsen OS (1982). Moveable bed roughness in unsteady oscillatory flow. Journal of Geophysical Research, 87(C1), 469-481.

Grant WD and Madsen OS (1986). The continental-shelf bottom boundary layer. Annual Review of Fluid Mechanics, 18, 265-305.

Grochowski NTL, Collins MB, Boxall SR and Salomon JC (1993). Sediment transport predictions for the English Channel, using numerical models. Journal of the Geological Society, 150, 683-695.

Guy HP, Simons DB and Richardson EV (1966). Summary of alluvial channel data from flume experiments 1955-1961. US Geol. Surv. Prof. Pap. 462-I, 92pp.

Hammond TM and Collins MB (1979). Flume studies of the response of various current meter rotor/propellers to combinations of unidirectional and oscillatory flow. Deutsch Hydrographische Zeitschrift, 32, 39-58.

Hammond TM, Pattiaratchi CB, Osborne MJ and Collins M (1986). Field and flume comparisons of the modified and standard (savonius-rotor) Anderaa self-recording current meters. Deutsche Hydrographische Zeitschrift, H2, 41-63.

Hannay A, Williams JJ, West JR and Coates LE (1994). A field study of wave-current interactions over a rippled sand bed. Euromech, Plymouth, 1994, 15pp.

Hardisty J (1983). An Assessment and Calibration of Formulations for Bagnold's Bedload Equation. Journal of Sedimentary Petrology 53, 1007-1010.

Hardisty J (1990). Basic sediment transport. In: Beaches, Form and Process, 113-136.

Harris PT, Pattiaratchi CB, Cole AR and Keene JB (1992). Evolution of subtidal sandbanks in Moreton Bay, eastern Australia. Marine Geology, 103(1/3), 225-247.

Harris PT, Pattiaratchi CB, Collins MB and Dalrymple RW (1995). What is a bedload parting? Spec. Publs int. Ass. Sediment., 24, 3-18.

Harvey JG and Vincent CE (1977). Observations of shear in near-bed currents in the southern North Sea. Estuarine and Coastal Marine Science, 5, 715-731.

Heaps NS (1978). Linearised vertically integrated equations for residual circulations in coastal seas. Deutsche Hydrographische Zeitschrift, 31, 147-169.

Heathershaw, A.D. (1981). Comparisons of Measured and Predicted Sediment Transport Rates in Tidal Currents. Developments in Sedimentology 32-Sediment Dynamics of Continental Shelves. ed C.A. Nittrouer, 75-104.

Heathershaw AD (1988). Sediment transport in the sea, on beaches and in rivers: Part I- Fundamental Principles. J.N.S., 14(3), 154-170.

Heathershaw AD (1988). Sediment transport in the sea, on beaches and in rivers: Part II- Sediment movement. J.N.S., 14(3), 221-234.

Heathershaw AD and Carr AP (1977). Measurements of sediment transport rates using radioactive tracers. Coastal Sediments, ASCE, 399-416.

Heathershaw AD and Hammond FDC (1979). Swansea Bay (SKER) Project Topic Report, 6. Offshore sediment movement and its relation to observed tidal current and wave data. Institute of Oceanographic Sciences Report, 93, 119pp.

Heathershaw AD and Hammond FDC (1980a). Transport and deposition of non-cohesive sediments in Swansea Bay. In Industrial Embayments and their Environmental Problems: A Case Study of Swansea Bay (Ed MB Collins et al.), Pergammon Press, Oxford, 215-248.

Heathershaw AD and Hammond FDC (1980b). Secondary circulations near sand banks and in coastal embayments. Deutsche Hydrographische Zeitschrift, H4, 135-151.

Hill HW and Ramster JW (1972). Variability in current meter records in the Irish Sea. Rapp. P.-v. Reun. Cons. int. Explor. Mer., 162, 232-247.

Hjulstrom F (1935). Studies in the morphological activity of rivers as illustrated by the River Fyris. Geological Institute of the University of Upsala Bulletin, 25, 221-528.

Hjulstrom F (1939). Transportation of detritus by moving water. In: Recent Marine Sediments, Trask PD (Ed), Thomas Murby, 5-31.

Horikawa K (1981). Coastal sediment processes. Annual Review of Fluid Mechanics, 13, 9-32.

Horikawa K and Watanabe A (1967). A study of sand movement due to wave action. Coastal Engineering in Japan, 10, 39-57.

Houbolt JJHC (1968). Recent sediments in the southern bight of the North Sea. Geologie en Mijnbouw, 47(4), 245-273.

Howarth MJ and Huthnance JM (1984). Tidal and residual currents around a Norfolk sandbank. Estuarine, Coastal and Shelf Science, 19, 105-117.

Howarth MJ and Pugh DT (1983). Observations of tides over the continental shelf of northwest Europe. In: Physical Oceanography of Coastal and Shelf Seas. B Johns (Ed). Elsevier Oceanography Series 35, Elsevier, Amsterdam, 135-185.

Hulscher SJMH, De Swart HE and De Vriend HJ (1993). The generation of offshore tidal sand banks and sand waves. Continental Shelf Research, 13(11), 1183-1204.

Humphery JD (1987). STABLE- an instrument for studying current structure and sediment transport in the benthic boundary layer. Proc. Electronics for Ocean Technology Conf. Endinburgh.

Huntley DA, Amos CL, Williams JJ and Humphery JD (1991). Estimating bedload transport on continental shelves by observations of ripple migration - An assessment. In: Euromech 262 - Sand Transport in Rivers, Estuaries and the Sea, RL Soulsby and R Bettes (Eds), Rotterdam, Balkema, 17-24.

Huntley DA, Huthnance JM, Collins, MB, Liu C-L, Nicholls RJ, and Hewitson C (1993). Hydrodynamics and sediment dynamics of North Sea sand waves and sand banks. Philosophical Transactions of the Royal Society, London, A343, 461-474.

Huthnance JM (1973). Tidal current asymmetries over the Norfolk Sandbanks.

Estuarine, Coastal and Shelf Science, 1, 89-99.
Huthnance JM (1982a). On one mechanism forming linear sand banks. Estuarine, Coastal and Shelf Science, 14, 79-99.
Huthnance JM (1982b). On the formation of sand banks of finite extent. Estuarine, Coastal and Shelf Science, 15, 277-299.
Huthnance JM (1991). Physical oceanography of the North Sea. Ocean and Shoreline Management, 16, 199-231.
HR (1991). Norfolk Sand Banks, Analysis of STABLE data. Hydraulics Research, Wallingford, Report EX 2345, 18pp.
Inman DL (1949). Sorting of sediment in light of fluid mechanics. Journal of Sedimentary Petrology, 22, 125-145.
Inman DL (1957). Wave generated ripples in nearshore sands. US Army Beach Erosion Board, Tech. Memo. No. 100
IOS (1983). Harmonic analysis of time series data. Institute of Oceanographic Sciences.
Jonsson IG (1967). Wave boundary layers and friction factors. In: Proc. 13th Conf. Coastal Eng., 1, 127-148.
Jonsson IG and Carlsen NA (1976). Experimental and theoretical investigations in an oscillatory turbulent boundary layer. Journal of Hydraulic Research, 14, 45-60.
Kachel NB and Sternberg RW (1971). Transport of bedload as ripples during an ebb current. Marine Geology, 10, 229-244.
Kalinske AA (1947). Movement of sediment as bed-load in rivers. Transactions of the American Geophysical Union, 28, 615-620.
Kapdasli MS (1990). Threshold condition of sand particles under codirectional combined wave and current flow. Geo-Marine Letters, 10, 45-49.
Kapdasli MS and Dyer KR (1986). Threshold conditions for sand movement on a rippled bed. Geo-Marine Letters, 6, 161-164.
Kemp PH and Simons RR (1982). The interaction between waves and a turbulent current; waves propagating with the current. Journal of Fluid Mechanics, 130, 73-89.
Kemp PH and Simons RR (1983a). The interaction between waves and a turbulent current; waves propagating against the current. Journal of Fluid Mechanics, 116, 227-250.
Kemp PH and Simons RR (1983b). Sediment transport due to waves and tidal currents. In: Proceedings of Seabed Mechanics, B Denness (Ed), Newcastle Upon Tyne, 197-206.
Kenyon NH and Stride AH (1970). The tide-swept continental shelf sediments between the Shetland islands and France. Sedimentology, 14, 159-173.
Kenyon NH, Belderson RH, Stride AH and Johnson MA (1981). Offshore tidal sand-banks as indicators of net sand transport and as potential deposits. In: Holocene Marine Sedimentation in the North Sea Basin. NIO S-D, Shuttenhelm RTE and van Veering TjCE (Eds), Blackwell, 257-268.
Khanna SD (1970). Experimental investigation of the form of bed roughness. ASCE, 96, HY10, 2029-2040.
Komar PD and Miller MC (1973). The threshold of sediment movement under oscillatory waves. Journal of Sedimentary Petrology, 43, 1101.

Komar PD and Miller MC (1975). Sediment threshold under oscillatory waves. Proc. 14th Coastal Eng Conf, Copenhagen: 756-775.

Lamb H (1932). Hydrodynamics, 6th edn. Cambridge. 738pp.

Lambrakos KF (1982). Seabed wave boundary layer measurements and analysis. Journal of Geophysical Research, (C6), 1471-1489.

Langhorne DN (1981). An evaluation of Bagnold's dimensionless coefficient of proportionality using measurements of sandwave movement. Marine Geology, 43, 49-64.

Langhorne DN (1982). A study of the dynamics of a marine sandwaves. Sedimentology, 29(4), 571-594.

Le Méhauté B, Divorky D, and Lin A (1968). Shallow water waves: a comparison of theories and experiments. Proc. 11th Conf. Coastal Eng., 1, 86-107.

Lees BJ (1981). Sediment transport measurements in the Sizewell-Dunwich Banks area, East Anglia, U.K.. In: Holocene Marine Sedimentation in the North Sea Basin. NIO, S-D., Shuttenhelm, R.T.E. and Van Veering, Tj.C.E. Editors. Blackwell Scientific Publications, Oxford, 269-281.

Lees BJ (1983a). Observations of tidal and residual currents in the Sizewell-Dunwich area, East Anglia. Deutsche Hydrographische Zeitschrift, 36, 1-24.

Lees BJ (1983b). The relationship of sediment transport rates and paths to sandbanks in a tidally dominated area off the coast of East Anglia, U.K.. Sedimentology, 30, 461-483.

Lettau H (1969). Note on aerodynamic roughness parameter estimation on the basis of roughness-element description. Journal of Applied Meteorology, 8, 828-832.

Liu AC, Missiaen T and Henriet JP (1992). The morphology of the top-Tertiary erosion surface in the Belgian sector of the North Sea. Marine Geology, 105, 275-284.

Ludwick JC (1972). Migration of tidal sand waves in Chesapeake Bay entrance. In: Swift DJP, Duane DB and Pilkey OH (Eds), Shelf Sediment Transport: Processes and Pattern. Dowden, Huthchinson and Ross, 377-410.

Maier-Reimer E (1977). Residual circulation in the North Sea due to the M_2 tide and mean annual wind stress. Dtsch. Hydrgr. Z., 30, 253-262.

Manohar M (1955). Mechanics of bottom sediment movement due to wave action. US Army Beach Erosion Board, Tech. Memo. No. 75, 121pp.

Mardell GT and Pingree RD (1981). Half-wave rectification of tidal vorticity near headlands as determined from current meter measurements. Oceanologica Acta, 4, 63-68.

McCave IN (1971). Sand waves in the North Sea off the coast of Holland. Marine Geology, 10, 199-225.

McCave IN (1978). Grain-size trends and transport along beaches: example from eastern England. Marine Geology, 28, M43-M51.

McCave IN (1979). Tidal currents at the North Hinder Lightship, southern North Sea: Flow directions and turbulence in relation to maintenance of sand banks. Marine Geology, 31, 101-114.

McCave IN and Balson PS (1990). Recent sedimentation of the East Anglian coast and southern North Sea. 13th Int. Sedimentol. Conf., Field Guide No.1,

17pp.
McCave IN and Langhorne DN (1982). Sand waves and sediment transport around the end of a tidal sand bank. Sedimentology, 29, 95-110.
Meyer-Peter E and Müller R (1948). Formulae for bedload transport. Proc. 2nd Conf. Int. Assoc. Hydraul. Res., Stockholm, 2, 39-64.
Miller MC and Komar PD (1980a). Oscillation sand ripples generated by laboratory apparatus. Journal of Sedimentary Petrology, 50(1), 173-182.
Miller MC and Komar PD (1980b). A field investigation of the relationship between oscillation ripple spacing and the near-bottom water orbital motions. Journal of Sedimentary Petrology, 50(1), 183-191.
Miller MC, McCave IN, and Komar PD (1977). Threshold of sediment motion under unidirectional currents. Sedimentology, 24, 507-527.
Mofjeld HO (1976). Tidal currents. In: Marine sediment transport and environmental management. Eds Stanley DJ and Swift JP. Wiley Interscience.
Mogridge GR, Davies MH and Willis DH (1994). Geometry prediction for wave-generated bedforms. Coastal Engineering, 22, 255-286.
Nielsen P (1981). Dynamics and geometry of wave-generated ripples. Journal of Geophysical Research, 86(C7), 6467-6472.
Nielsen P (1983). Analytical determination of nearshore wave height variation due to refraction shoaling and friction. Coastal Engineering, 7, 233-251.
Nowell ARM, Jumars PA and Eckman JE (1981). Effects of biological activity on the entrainment of marine sediments. Marine Geology, 42, 133-153.
Off T (1963). Rhythmic linear sand bodies caused by tidal currents. Bulletin of the American Association of Petroleum Geologists, 47(2), 324-341.
Paintal AS (1971). A stochastic model of bedload transport. Journal of Hydraulic Research, 9(4), 527-554
Pantin HM, Hamilton D and Evans CDR (1981). Secondary flow caused by differential roughness, Langmuir circulations, and their effect on the developments of sand ribbons. Geo-Marine Letters, 1, 255-260.
Parker G, Lanfredi NW and Swift DJP (1982). Seafloor response to flow in a southern hemisphere sand ridge field: Argentine inner shelf. Sedimentary Geology, 33, 195-216.
Pattiaratchi CB (1981). Estimates of sand transport under waves and currents. Unpublished M.Sc thesis, University of Wales. 194pp.
Pattiaratchi CB (1985). Hydrography and sedimentology of a headland associated linear sandbank: Scarweather Sands, northern Bristol Channel. Unpublished Ph.D thesis, University of Wales. 294pp.
Pattiaratchi CB and Collins MB (1984). Sediment transport under waves and tidal currents: a case study from the northern Bristol Channel, U.K.. Marine Geology, 56, 27-40.
Pattiaratchi CB and Collins MB (1985). Sand transport under the combined influence of waves and tidal currents: an assessment of available formulae. Marine Geology, 67, 83-100.
Pattiaratchi C and Collins M (1987). Mechanisms for linear sandbank formation and maintenance in relation to dynamical oceanographic observations. Progress in Oceanography, 19, 117-176.

17pp.
McCave IN and Langhorne DN (1982). Sand waves and sediment transport around the end of a tidal sand bank. Sedimentology, 29, 95-110.
Meyer-Peter E and Müller R (1948). Formulae for bedload transport. Proc. 2nd Conf. Int. Assoc. Hydraul. Res., Stockholm, 2, 39-64.
Miller MC and Komar PD (1980a). Oscillation sand ripples generated by laboratory apparatus. Journal of Sedimentary Petrology, 50(1), 173-182.
Miller MC and Komar PD (1980b). A field investigation of the relationship between oscillation ripple spacing and the near-bottom water orbital motions. Journal of Sedimentary Petrology, 50(1), 183-191.
Miller MC, McCave IN, and Komar PD (1977). Threshold of sediment motion under unidirectional currents. Sedimentology, 24, 507-527.
Mofjeld HO (1976). Tidal currents. In: Marine sediment transport and environmental management. Eds Stanley DJ and Swift JP. Wiley Interscience.
Mogridge GR, Davies MH and Willis DH (1994). Geometry prediction for wave-generated bedforms. Coastal Engineering, 22, 255-286.
Nielsen P (1981). Dynamics and geometry of wave-generated ripples. Journal of Geophysical Research, 86(C7), 6467-6472.
Nielsen P (1983). Analytical determination of nearshore wave height variation due to refraction shoaling and friction. Coastal Engineering, 7, 233-251.
Nowell ARM, Jumars PA and Eckman JE (1981). Effects of biological activity on the entrainment of marine sediments. Marine Geology, 42, 133-153.
Off T (1963). Rhythmic linear sand bodies caused by tidal currents. Bulletin of the American Association of Petroleum Geologists, 47(2), 324-341.
Paintal AS (1971). A stochastic model of bedload transport. Journal of Hydraulic Research, 9(4), 527-554
Pantin HM, Hamilton D and Evans CDR (1981). Secondary flow caused by differential roughness, Langmuir circulations, and their effect on the developments of sand ribbons. Geo-Marine Letters, 1, 255-260.
Parker G, Lanfredi NW and Swift DJP (1982). Seafloor response to flow in a southern hemisphere sand ridge field: Argentine inner shelf. Sedimentary Geology, 33, 195-216.
Pattiaratchi CB (1981). Estimates of sand transport under waves and currents. Unpublished M.Sc thesis, University of Wales. 194pp.
Pattiaratchi CB (1985). Hydrography and sedimentology of a headland associated linear sandbank: Scarweather Sands, northern Bristol Channel. Unpublished Ph.D thesis, University of Wales. 294pp.
Pattiaratchi CB and Collins MB (1984). Sediment transport under waves and tidal currents: a case study from the northern Bristol Channel, U.K.. Marine Geology, 56, 27-40.
Pattiaratchi CB and Collins MB (1985). Sand transport under the combined influence of waves and tidal currents: an assessment of available formulae. Marine Geology, 67, 83-100.
Pattiaratchi C and Collins M (1987). Mechanisms for linear sandbank formation and maintenance in relation to dynamical oceanographic observations. Progress in Oceanography, 19, 117-176.

Pingree RD (1978). The formation of the Shambles and other banks by tidal stirring of the seas. Journal of the Marine Biological Association of the United Kingdom, 58, 211-226.

Pingree RD and Griffiths DK (1979). Sand transport paths around the British Isles resulting from M_2 and M_4 tidal interactions. Journal of the Marine Biological Association of the United Kingdom, 59, 497-513.

Pingree RD and Maddock L (1978). The M_4 tide in the English Channel derived from a non-linear model of the M_2 tide. Deep-Sea Research, 25, 53-63.

Pingree RD and Maddock L (1979). The tidal physics of headland flows and offshore tidal bank formation. Marine Geology, 32, 269-289.

Prandtl L (1927). Uber die ausgebildte turbulenz. Proc. 2nd Int. Congr. App. Mech., Zurich, 62-96.

Proudman J (1953). Dynamical Oceanography. London, Methuen and Co., 409pp.

Pugh DT (1987). Tides, Surges and Mean Sea-Level. Chichester, John Wiley and Sons, 472pp.

Ramster JW, Hughes DG and Furness GK (1978). A 'steadiness' factor for estimating the variability of residual drift in current meter records. Dt. hydrogr. Z. 31, 230-236.

Rance PJ and Warren NF (1969). The threshold of coarse material in oscillatory flow. Proc. 11th Conf. Coastal Eng., 487-491.

Raudkivi AJ (1990). Loose boundary hydraulics. 3rd ed, Pergammon Press, 533pp.

Reineck HE and Singh IB (1980). Depositional Sedimentary Environments, with reference to Terrigenous clastics, Springer-Verlag, Berlin, 2nd ed., 549pp.

Richards KJ (1982). Turbulent flow over ripples and their effective roughness. In: Mechanics of Sediment Transport, Summer BM and Muller A (Eds), Euromech 156, Istanbul, AA Balkema, Rotterdam, 127-132.

Rigler JK and Collins MB (1983). Initial grain motion under oscillatory flow: A comparison of some threshold criteria. Geo-Marine Letters, 3, 43-48

Robinson AHW (1966). Residual currents in relation to shoreline evolution of the East Anglian coast. Marine Geology, 4, 57-84.

Robinson IS (1981). Tidal vorticity and residual circulation. Deep-Sea Research, 28, 195-212.

Robinson IS (1983). Tidally induced residual flows. In: Physical Oceanography of Coastal and Shelf Seas. B Johns (Ed). Elsevier Oceanography Series 35, Elsevier, Amsterdam, 321-356.

Rubin DM and McCulloch DS (1980). Single and superimposed bedforms: a synthesis of San Francisco Bay and flume observations. Sedimentary Geology, 26, 207-231.

Shennan I (1989). Holocene crustal movements and sea-level changes in Great Britain. Journal of Quarternary Science, 4, 77-89.

Shields IA (1936). Application of similarity principles and turbulence research to bed-load movement. Translated by Ott WP and van Uchelen JC. WM Keck Laboratory of Hydraulics and Water Resources, Report 167, 26pp.

Shimwell SJ (1990). Sand transport paths in the vicinity of a North Sea sandbank. Unpublished B.Sc thesis, University of Southampton. 152pp.

Shinohara K and Tsubaki T (1959). On the characteristics of sand waves formed

upon beds of open channels and rivers. Reports of Research Institute for Applied Mechanics, Kyushu University, Japan, 7, No. 25.

Silvestor R and Mogridge GR (1971). Reach of waves to the bed of the continental shelf. Proc. 12th Conf. Coastal Eng., 651-667.

Sleath JFA (1974). Stability of laminar flow at seabed. Journal of the Waterways, Harbors and Coastal Engineering Division, ASCE, 100(WW2), 105-122.

Sleath JFA (1984). Sea Bed Mechanics. John Wiley & Sons.

Sleath, J.F.A. (1990). Velocities and bed friction in combined flows. In: Proc. 22nd Conf. Coastal Eng., 1, 450-463.

Sleath JFA (1991). Velocities and shear stresses in wave-current flows. Journal of Geophysical Research, 96(C8), 15237-15244.

Smith JD (1969). Geomorphology of a sand ridge. Journal of Geology, 77, 39-55.

Smith JD (1977). Modelling of sediment transport on continental shelves. In: The Sea, Vol. 6, Goldberg ED, McCave IN, O'Brien JJ, Steele JH (Eds), 539-577. New York: Wiley-Interscience.

Smith JD and McLean SR (1977). Spatially averaged flow over a wavy surface. Journal of Geophysical Research, 82(12), 1735-1746.

Soulsby RL (1981). Measurements of the Reynolds Stress components close to a marine sand bank. Marine Geology, 42, 35-47.

Soulsby RL (1983). The bottom boundary layer of shelf seas. In: Physical Oceanography of Coastal and Shelf Seas. Johns B (Ed). Elsevier Oceanography Series 35, Elsevier, Amsterdam, 189-266.

Soulsby RL (1993). Manual of Marine Sands. HR Wallingford Report SR 351, Wallingford, Oxon, UK.

Soulsby RL and Dyer KR (1981). The form of the near-bed velocity profile in a tidally accelerating flow. Journal of Geophysical Research, 86(C9), 8067-8074.

Soulsby RL and Humphery JD (1989). Field observations of wave-current interaction at the sea bed. In: Proc Advanced Workshop on Water Wave Linematics, Torum A (Ed), Molde, Norway. Kluner.

Sternberg RW (1967). Measurements of sediment movement and ripple migration in a shallow marine environment. Marine Geology, 5, 195-205.

Sternberg RW (1968). Friction factors in tidal channels with differing bed roughness. Marine Geology, 6, 243-260.

Stride AH (1963). Current-swept sea floors near the southern half of Great Britain. Quarterly Journal of the Geological Society of London, 119, 175-199.

Stride AH (1974). Indications of long term, tidal control of net sand loss or gain by European coasts. Estuarine and Coastal Marine Science, 2, 27-36.

Stride AH (Ed) (1982). Offshore Tidal Sands. Processes and Deposits. Chapman and Hall, London, 222pp.

Stride AH (1988). Indications of long term episodic suspension transport of sand across the Norfolk Banks, North Sea. Marine Geology, 79, 55-64.

Stride AH (1989). Modern deposits, quasi-deposits and some Holocene? in the Southern Bight, North Sea. In: The Quarternary and Tertiary geology of the Southern Bight, North Sea. Henriet JP and De Moor G (Eds). Brussels, Belgian Geological Society, 149-159.

Stride AH, Belderson RH, Kenyon NH and Johnson MA (1982). Offshore tidal deposits: sand sheet and sand bank facies. In: Offshore Tidal Sands: Processes and Deposits. Stride AH (Ed). London, Chapman and Hall, 95-125 .

Sundborg A (1956). The River Klaralven. A study of fluvial processes. Geografiska Annaler, Ser. A., 115, 127-316.

Swart DH (1976). Predictive equations regarding coastal transport. Proc 15th Conf. Coastal Eng.,1113-1132.

Swift DJP (1975). Tidal sand ridges and shoal-retreat massifs. Marine Geology, 18, 105-134.

Swift DJP and Field ME (1981). Evolution of a classic sand ridge field: Maryland sector, North American inner shelf. Sedimentology, 28, 461-482.

Swift DJP, Duane DB and McKinney TF (1973). Ridge and swale topography of the middle Atlantic Bight, North America: Secular response to the Holocene hydraulic regime. Marine Geology, 15, 227-247.

Swift DJP, Parker G, Lanfredi NW, Perillo, G and Figge K (1978). Shoreface connected sand ridges on American and European shelves- a comparison. Estuarine Coastal Marine Science, 7, 257-273.

Tanner WF (1963). Spiral flow in rivers, shallow seas, dust devils and models. Science, 134, 41-42.

Taylor PA, Gent PR and Keen JM (1976). Some numerical solutions for turbulent boundary layer flow above fixed, rough, wavy surfaces. Geophy. J. R. Astron. Soc., 44, 177.

Tee KT (1976). Tide-induced residual currents, a 2-D non-linear tidal model. Journal of Marine Research, 34, 603-608.

Terwindt JHJ (1971). Sand waves in the southern bight of the North Sea. Marine Geology, 10, 51-67.

Thorne CR and Hey RD (1979). Direct measurements of secondary currents at a river inflection point. Nature, 280, 226-228.

Tomlinson BN (1993). Erosion studies of mixed beds under the combined action of waves and currents. Unpublished Ph.D thesis, University of Southampton. 267pp.

Trentesaux A, Berné S, De Batist M and Chamley H (1993). Internal structure of a tidal sand bank in the southern North Sea. C. R. Acad. Sci. Paris, 316(Ser.II), 99-106.

de Vriend HJ (1990). Morphological processes in shallow tidal seas. In: Residual Currents and Long-term Transport. RT Cheng (Ed). Springer-Verlag, Coastal and Estuarine Studies, 38, 276-301.

van den Berg JH (1987). Bedform migration and bed-load transport in some rivers and tidal environments. Sedimentology, 34, 681-698.

van Doorn TH (1981). Experimental investigation of near bottom velocities in water waves with and without a current. Delft Hydraulics Laboratory, Report No. M1423, Part I.

van Doorn TH (1982). Experimental investigation of the velocity field in the turbulent bottom boundary layer in an oscillating water tunnel. Delft Hydraulics Laboratory, Report No. M1562-b.

van Rijn LC (1982). Equivalent roughness of an alluvial bed. Journal of the

Stride AH, Belderson RH, Kenyon NH and Johnson MA (1982). Offshore tidal deposits: sand sheet and sand bank facies. In: Offshore Tidal Sands: Processes and Deposits. Stride AH (Ed). London, Chapman and Hall, 95-125 .

Sundborg A (1956). The River Klaralven. A study of fluvial processes. Geografiska Annaler, Ser. A., 115, 127-316.

Swart DH (1976). Predictive equations regarding coastal transport. Proc 15th Conf. Coastal Eng.,1113-1132.

Swift DJP (1975). Tidal sand ridges and shoal-retreat massifs. Marine Geology, 18, 105-134.

Swift DJP and Field ME (1981). Evolution of a classic sand ridge field: Maryland sector, North American inner shelf. Sedimentology, 28, 461-482.

Swift DJP, Duane DB and McKinney TF (1973). Ridge and swale topography of the middle Atlantic Bight, North America: Secular response to the Holocene hydraulic regime. Marine Geology, 15, 227-247.

Swift DJP, Parker G, Lanfredi NW, Perillo, G and Figge K (1978). Shoreface connected sand ridges on American and European shelves- a comparison. Estuarine Coastal Marine Science, 7, 257-273.

Tanner WF (1963). Spiral flow in rivers, shallow seas, dust devils and models. Science, 134, 41-42.

Taylor PA, Gent PR and Keen JM (1976). Some numerical solutions for turbulent boundary layer flow above fixed, rough, wavy surfaces. Geophy. J. R. Astron. Soc., 44, 177.

Tee KT (1976). Tide-induced residual currents, a 2-D non-linear tidal model. Journal of Marine Research, 34, 603-608.

Terwindt JHJ (1971). Sand waves in the southern bight of the North Sea. Marine Geology, 10, 51-67.

Thorne CR and Hey RD (1979). Direct measurements of secondary currents at a river inflection point. Nature, 280, 226-228.

Tomlinson BN (1993). Erosion studies of mixed beds under the combined action of waves and currents. Unpublished Ph.D thesis, University of Southampton. 267pp.

Trentesaux A, Berné S, De Batist M and Chamley H (1993). Internal structure of a tidal sand bank in the southern North Sea. C. R. Acad. Sci. Paris, 316(Ser.II), 99-106.

de Vriend HJ (1990). Morphological processes in shallow tidal seas. In: Residual Currents and Long-term Transport. RT Cheng (Ed). Springer-Verlag, Coastal and Estuarine Studies, 38, 276-301.

van den Berg JH (1987). Bedform migration and bed-load transport in some rivers and tidal environments. Sedimentology, 34, 681-698.

van Doorn TH (1981). Experimental investigation of near bottom velocities in water waves with and without a current. Delft Hydraulics Laboratory, Report No. M1423, Part I.

van Doorn TH (1982). Experimental investigation of the velocity field in the turbulent bottom boundary layer in an oscillating water tunnel. Delft Hydraulics Laboratory, Report No. M1562-b.

van Rijn LC (1982). Equivalent roughness of an alluvial bed. Journal of the

Stride AH, Belderson RH, Kenyon NH and Johnson MA (1982). Offshore tidal deposits: sand sheet and sand bank facies. In: Offshore Tidal Sands: Processes and Deposits. Stride AH (Ed). London, Chapman and Hall, 95-125 .

Sundborg A (1956). The River Klaralven. A study of fluvial processes. Geografiska Annaler, Ser. A., 115, 127-316.

Swart DH (1976). Predictive equations regarding coastal transport. Proc 15th Conf. Coastal Eng.,1113-1132.

Swift DJP (1975). Tidal sand ridges and shoal-retreat massifs. Marine Geology, 18, 105-134.

Swift DJP and Field ME (1981). Evolution of a classic sand ridge field: Maryland sector, North American inner shelf. Sedimentology, 28, 461-482.

Swift DJP, Duane DB and McKinney TF (1973). Ridge and swale topography of the middle Atlantic Bight, North America: Secular response to the Holocene hydraulic regime. Marine Geology, 15, 227-247.

Swift DJP, Parker G, Lanfredi NW, Perillo, G and Figge K (1978). Shoreface connected sand ridges on American and European shelves- a comparison. Estuarine Coastal Marine Science, 7, 257-273.

Tanner WF (1963). Spiral flow in rivers, shallow seas, dust devils and models. Science, 134, 41-42.

Taylor PA, Gent PR and Keen JM (1976). Some numerical solutions for turbulent boundary layer flow above fixed, rough, wavy surfaces. Geophy. J. R. Astron. Soc., 44, 177.

Tee KT (1976). Tide-induced residual currents, a 2-D non-linear tidal model. Journal of Marine Research, 34, 603-608.

Terwindt JHJ (1971). Sand waves in the southern bight of the North Sea. Marine Geology, 10, 51-67.

Thorne CR and Hey RD (1979). Direct measurements of secondary currents at a river inflection point. Nature, 280, 226-228.

Tomlinson BN (1993). Erosion studies of mixed beds under the combined action of waves and currents. Unpublished Ph.D thesis, University of Southampton. 267pp.

Trentesaux A, Berné S, De Batist M and Chamley H (1993). Internal structure of a tidal sand bank in the southern North Sea. C. R. Acad. Sci. Paris, 316(Ser.II), 99-106.

de Vriend HJ (1990). Morphological processes in shallow tidal seas. In: Residual Currents and Long-term Transport. RT Cheng (Ed). Springer-Verlag, Coastal and Estuarine Studies, 38, 276-301.

van den Berg JH (1987). Bedform migration and bed-load transport in some rivers and tidal environments. Sedimentology, 34, 681-698.

van Doorn TH (1981). Experimental investigation of near bottom velocities in water waves with and without a current. Delft Hydraulics Laboratory, Report No. M1423, Part I.

van Doorn TH (1982). Experimental investigation of the velocity field in the turbulent bottom boundary layer in an oscillating water tunnel. Delft Hydraulics Laboratory, Report No. M1562-b.

van Rijn LC (1982). Equivalent roughness of an alluvial bed. Journal of the

Stride AH, Belderson RH, Kenyon NH and Johnson MA (1982). Offshore tidal deposits: sand sheet and sand bank facies. In: Offshore Tidal Sands: Processes and Deposits. Stride AH (Ed). London, Chapman and Hall, 95-125 .

Sundborg A (1956). The River Klaralven. A study of fluvial processes. Geografiska Annaler, Ser. A., 115, 127-316.

Swart DH (1976). Predictive equations regarding coastal transport. Proc 15th Conf. Coastal Eng.,1113-1132.

Swift DJP (1975). Tidal sand ridges and shoal-retreat massifs. Marine Geology, 18, 105-134.

Swift DJP and Field ME (1981). Evolution of a classic sand ridge field: Maryland sector, North American inner shelf. Sedimentology, 28, 461-482.

Swift DJP, Duane DB and McKinney TF (1973). Ridge and swale topography of the middle Atlantic Bight, North America: Secular response to the Holocene hydraulic regime. Marine Geology, 15, 227-247.

Swift DJP, Parker G, Lanfredi NW, Perillo, G and Figge K (1978). Shoreface connected sand ridges on American and European shelves- a comparison. Estuarine Coastal Marine Science, 7, 257-273.

Tanner WF (1963). Spiral flow in rivers, shallow seas, dust devils and models. Science, 134, 41-42.

Taylor PA, Gent PR and Keen JM (1976). Some numerical solutions for turbulent boundary layer flow above fixed, rough, wavy surfaces. Geophy. J. R. Astron. Soc., 44, 177.

Tee KT (1976). Tide-induced residual currents, a 2-D non-linear tidal model. Journal of Marine Research, 34, 603-608.

Terwindt JHJ (1971). Sand waves in the southern bight of the North Sea. Marine Geology, 10, 51-67.

Thorne CR and Hey RD (1979). Direct measurements of secondary currents at a river inflection point. Nature, 280, 226-228.

Tomlinson BN (1993). Erosion studies of mixed beds under the combined action of waves and currents. Unpublished Ph.D thesis, University of Southampton. 267pp.

Trentesaux A, Berné S, De Batist M and Chamley H (1993). Internal structure of a tidal sand bank in the southern North Sea. C. R. Acad. Sci. Paris, 316(Ser.II), 99-106.

de Vriend HJ (1990). Morphological processes in shallow tidal seas. In: Residual Currents and Long-term Transport. RT Cheng (Ed). Springer-Verlag, Coastal and Estuarine Studies, 38, 276-301.

van den Berg JH (1987). Bedform migration and bed-load transport in some rivers and tidal environments. Sedimentology, 34, 681-698.

van Doorn TH (1981). Experimental investigation of near bottom velocities in water waves with and without a current. Delft Hydraulics Laboratory, Report No. M1423, Part I.

van Doorn TH (1982). Experimental investigation of the velocity field in the turbulent bottom boundary layer in an oscillating water tunnel. Delft Hydraulics Laboratory, Report No. M1562-b.

van Rijn LC (1982). Equivalent roughness of an alluvial bed. Journal of the

Stride AH, Belderson RH, Kenyon NH and Johnson MA (1982). Offshore tidal deposits: sand sheet and sand bank facies. In: Offshore Tidal Sands: Processes and Deposits. Stride AH (Ed). London, Chapman and Hall, 95-125 .

Sundborg A (1956). The River Klaralven. A study of fluvial processes. Geografiska Annaler, Ser. A., 115, 127-316.

Swart DH (1976). Predictive equations regarding coastal transport. Proc 15th Conf. Coastal Eng.,1113-1132.

Swift DJP (1975). Tidal sand ridges and shoal-retreat massifs. Marine Geology, 18, 105-134.

Swift DJP and Field ME (1981). Evolution of a classic sand ridge field: Maryland sector, North American inner shelf. Sedimentology, 28, 461-482.

Swift DJP, Duane DB and McKinney TF (1973). Ridge and swale topography of the middle Atlantic Bight, North America: Secular response to the Holocene hydraulic regime. Marine Geology, 15, 227-247.

Swift DJP, Parker G, Lanfredi NW, Perillo, G and Figge K (1978). Shoreface connected sand ridges on American and European shelves- a comparison. Estuarine Coastal Marine Science, 7, 257-273.

Tanner WF (1963). Spiral flow in rivers, shallow seas, dust devils and models. Science, 134, 41-42.

Taylor PA, Gent PR and Keen JM (1976). Some numerical solutions for turbulent boundary layer flow above fixed, rough, wavy surfaces. Geophy. J. R. Astron. Soc., 44, 177.

Tee KT (1976). Tide-induced residual currents, a 2-D non-linear tidal model. Journal of Marine Research, 34, 603-608.

Terwindt JHJ (1971). Sand waves in the southern bight of the North Sea. Marine Geology, 10, 51-67.

Thorne CR and Hey RD (1979). Direct measurements of secondary currents at a river inflection point. Nature, 280, 226-228.

Tomlinson BN (1993). Erosion studies of mixed beds under the combined action of waves and currents. Unpublished Ph.D thesis, University of Southampton. 267pp.

Trentesaux A, Berné S, De Batist M and Chamley H (1993). Internal structure of a tidal sand bank in the southern North Sea. C. R. Acad. Sci. Paris, 316(Ser.II), 99-106.

de Vriend HJ (1990). Morphological processes in shallow tidal seas. In: Residual Currents and Long-term Transport. RT Cheng (Ed). Springer-Verlag, Coastal and Estuarine Studies, 38, 276-301.

van den Berg JH (1987). Bedform migration and bed-load transport in some rivers and tidal environments. Sedimentology, 34, 681-698.

van Doorn TH (1981). Experimental investigation of near bottom velocities in water waves with and without a current. Delft Hydraulics Laboratory, Report No. M1423, Part I.

van Doorn TH (1982). Experimental investigation of the velocity field in the turbulent bottom boundary layer in an oscillating water tunnel. Delft Hydraulics Laboratory, Report No. M1562-b.

van Rijn LC (1982). Equivalent roughness of an alluvial bed. Journal of the

Hydraulics Division, ASCE, 108, 1215-1218.
van Rijn LC (1986). Applications of sediment pick-up functions. Journal of Hydraulic Engineering, ASCE, 112(9), 867-874.
van Veen J (1936). Onderzoeckingen in de Hoofden. Algemeene Landsdrukkerij, s'Gravenhage, 252pp.
Vanoni VA (1977). Sedimentation Engineering. ASCE, 745pp.
Whitcombe LJ (1995). Sediment transport processes, with particular reference to Hayling Island. Unpublished Ph.D thesis, University of Southampton. 300pp.
White WR, Milli H and Crabbe AD (1975). Sediment transport theories: a review. Proceedings of the Institution of Civil Engineers, 59, 2: 265-292.
Wiberg PL and Harris CK (1994). Ripple geometry in wave-dominated environments. Journal of Geophysical Research, 99(C1), 775-789.
Wiberg PL and Nelson JM (1992). Unidirectional flow over asymmetric and symmetric ripples. Journal of Geophysical Research, 97(C8), 12745-12761.
Wiberg P and Smith JD (1983). A comparison of field data and theoretical models for wave-current interactions at the sea bed on the continental shelf. Continental Shelf Research, 2, 147-162.
Wilkinson RH (1984). A method for evaluating statistical errors associated with logarithmic velocity profiles. Geo-Marine Letters, 3, 49-52.
Wilkinson RH (1986). Variation of roughness length of a mobile sand bed in a tidal flow. Geo-Marine Letters, 5, 231-239.
Wilkinson RH, Moore EJ and Salkield AP (1985). Photogrammetry in sediment transport studies. In: Underwater Photography and Television for Scientists, George JD, Lythgoe GI and Lythgoe JN (Eds), Underwater Assoc. Spec. Vol., 2. Clarendon, 13pp.
Williams GP (1967). Flume experiments on the transport of a coarse sand. U.S. Geological Survey Professional Paper 562-B.
Williams JJ, Thorne PD and Heathershaw AD (1989). Comparisons between acoustic measurements and predictions of the bedload transport of marine gravels. Sedimentology, 36, 973-979.
Wooding RA, Bradley EF and Marshall JK (1973). Drag due to regular arrays of roughness elements of varying geometry. Boundary-Layer Meteorology, 5, 285-308.
Wright LD and Thom BG (1977). Coastal depositional landforms - a morphodynamic approach. Prog. P. Geo., 1(3), 412-459.
Xu JP and Wright LD (1995). Tests of bed roughness models using field data from the Middle Atlantic Bight. Continental Shelf Research, 15, 1409-1434.
Yalin MS (1963). An expression for bedload transportation. Journal of the Hydraulic Division, ASCE, 89(HY3), 221-250.
Yalin MS (1972). Mechanics of sediment Transport. Pergammon Press, Oxford, 290pp.
Yalin MS (1977). On the determination of ripple length. ASCE, HY4, 439-442.
Yang C-S (1986). On Bagnold's sediment transport equation in tidal marine environments and the practical definition of bedload. Sedimentology, 33(4), 465-486.

You Z-J (1996). Moveable bed roughness and current profiles in the presence of irregular waves with an arbitrary angle to currents. Ocean Engineering, 23(3), 225-242.

Zanke U (1987). Sedimenttransportformeln fur bed-load im vergleich.

Zimmerman JTF (1981). Dynamics, diffusion and geomorphological significance of tidal residual eddies. Nature, 290, 549-555.

APPENDIX 1

Collins MB, Shimwell SJ, Gao S, Powell H, Hewitson C and Taylor JA (1995). Water and sediment movement in the vicinity of linear sandbanks: the Norfolk Banks, southern North Sea. Marine Geology, 123, 125-142.

The present author was involved in the computation of the bedload transport rates and in the joint preparation of the manuscript.

APPENDIX 1

Collins MB, Shimwell SJ, Gao S, Powell H, Hewitson C and Taylor JA (1995). Water and sediment movement in the vicinity of linear sandbanks: the Norfolk Banks, southern North Sea. Marine Geology, 123, 125-142.

The present author was involved in the computation of the bedload transport rates and in the joint preparation of the manuscript.

ELSEVIER

Marine Geology 123 (1995) 125–142

MARINE GEOLOGY
INTERNATIONAL JOURNAL OF MARINE GEOLOGY GEOCHEMISTRY AND GEOPHYSICS

Water and sediment movement in the vicinity of linear sandbanks: the Norfolk Banks, southern North Sea

M.B. Collins, S.J. Shimwell, S. Gao *, H. Powell, C. Hewitson, J.A. Taylor

Department of Oceanography, The University, Southampton SO17 1BJ, UK

Received 15 August 1994; revision accepted 25 January 1995

Abstract

Geophysical surveys, current meter measurements and fluorescent sand tracer experiments were undertaken in the vicinity of the Broken Bank. The data are used to establish localised and regional patterns of water and sediment movement.

The results obtained confirm mechanisms proposed previously for sandbank growth, with particular reference to the North Sea; these include the clockwise circulation of water and sand, with convergence at the crestline. Secondary helical water circulations do not appear to be a dominant process influencing sandbank *maintenance*. However, such circulation may still be important in the initial *formation* of linear sandbanks and or at some stages in the bank development.

On a regional basis, residual currents, bedform asymmetries and tracer dispersion indicate an offshore sediment transport component. This observation supports the hypothesis of other investigators, formed on the basis of geomorphological observations and numerical model predictions, concerning the movement of sand under extreme conditions. Moreover, these transport pathways may persist under low wave and tidally-dominated conditions, as opposed to being restricted to storm activity.

1. Introduction

Linear sandbanks, or tidal sand ridges, are the largest bedforms found on tidally-dominated continental shelves; they have maximum dimensions of 55 km in length, 6 km in width, and up to 40 m in height above the surrounding seabed. Such bedforms are found often as groups of banks, at locations with sufficient sand availability and strong tidal currents (Off, 1963). Such sandbanks have been shown to be orientated obliquely to the tidal current maxima (and the resultant net sand transport direction) by as much as 20°, with the offset being typically anticlockwise in the Northern Hemisphere (Kenyon et al., 1981). Most linear sandbanks are asymmetric in cross-section, with their steep face or lee slope reaching a maximum angle of 6° to the horizontal.

Sandbanks can be divided between those which are maintained actively by the modern (Late Holocene) tidal current regime and those formed at periods of lower sea level. The latter are now inactive (moribund) banks, occurring in deeper waters where the prevailing tidal current regime is too weak to cause active sediment movement. Both types of sandbanks have been found to be present in the southern North Sea, with the moribund banks located in deeper offshore waters (Belderson, 1986).

Several theories have been proposed to explain the formation and maintenance of sandbanks (for

* Corresponding author.

SSDI 0025-3227(95)00010-0

a review, see Pattiaratchi and Collins, 1987). Helical spiral water circulations, with flow divergence (at depth) in the swales between the banks and convergence over the crestline, have been postulated. Such a mechanism would transport sand from the swales and onto a bank, resulting in the continued growth and maintenance of the system (Houbolt, 1968). Likewise, lateral migration of sandbanks has been suggested, combined with the existence of flood- and ebb-dominated flows on either side of the bank; this results in an inequality in the sand transport rates (Caston, 1972). Such an imbalance causes the crestline of the bank to curve, becoming progressively more sigmoidal. Eventually, such a bank would divide into two smaller parallel banks, separated by a channel or swale.

A stratigraphic model for the evolution of these large-scale bedforms associated with sea level rises has been described (Swift, 1975). These low and broad sand bodies are considered to mark, as massifs, the retreat path of the coastline during periods of marine transgression. A sand body is considered to accumulate in areas where the littoral drift of sand along the coastline converges; this is attached to the shoreline. In response to sea level rise, a sequence of offshore sand bodies would result, as the tidal ridges became detached from their nearshore origins. Once isolated from the nearshore sand supply, a linear tidal ridge would interact with the regional tidal flow field. The bedform would reach then an equilibrium state, with sand transport continuing within the ridge/swale system.

Using numerical models, Huthnance (1982a,b) has shown that strong currents (1 m s^{-1}, on average) and the presence of initial irregularities or humps on the seabed are sufficient to form and maintain linear sandbanks. The growth of the bank is assumed to adopt the fastest possible rate (dependent upon sand availability), resulting in certain spacing and orientation of the bank axis. Eventually, equilibrium morphology of a bank will be reached, which may be characterised by a flattened top caused by wave action and an asymmetric cross-section in response to asymmetric current activity. Hence, other mechanisms, including secondary circulation, internal tides, the lag of sediment transport behind the instantaneous current, and spatial changes in bed roughness, may not be necessary (Huthnance, 1982a). Under some conditions, however, they may cause sandbank growth.

The validation of the various (conceptual and mathematical) models proposed for sandbank formation and maintenance requires in situ oceanographic and sedimentological measurements. Current meter observations have been used, in previous studies, for comparison with model predictions (e.g. McCave, 1979; Huthnance, 1982a).

The present investigation is concerned with water and sediment movement in the vicinity of a sequence of tidal sandbanks (the Norfolk Banks) in the Southern Bight of the North Sea. Observations used in the analyses were obtained using geophysical survey techniques (side-scan sonar and shallow sub-bottom profiling), self-recording current meter deployments and longer-term fluorescent sand tracer investigations. Hence, an integrated data set is available to study the prevailing localised hydrodynamic and sediment dynamic conditions. Furthermore, interaction of the sandbanks with regional sediment transport pathways in the southern North Sea is examined.

2. Area under investigation

The Norfolk Banks consist of a group of offshore sandbanks, located some 100 km to seaward of the East Anglian coastline and lying in water depths of 18 to 40 m (Fig. 1). Some of the banks rise from the sea-floor to within 5 m of the sea surface; however, those lying in deeper waters have their crestlines submerged at greater depths.

The study has concentrated upon the Well Bank, Broken Bank and Swarte Bank system (Fig. 2). Broken Bank, around which most of the data were collected, has dimensions which are typical of the tidally-controlled sandbanks within the area i.e. 33 km in length, approximately 1 km in width, and rising to a height of 30 m above the surrounding sea-floor. The loosely-consolidated seabed material on and around the Broken Bank consists predominantly of well-sorted, fine-grained sand.

All three banks are asymmetric in their cross-section, with a steep northeasterly facing slope and a more gently sloping southwesterly face. The

a review, see Pattiaratchi and Collins, 1987). Helical spiral water circulations, with flow divergence (at depth) in the swales between the banks and convergence over the crestline, have been postulated. Such a mechanism would transport sand from the swales and onto a bank, resulting in the continued growth and maintenance of the system (Houbolt, 1968). Likewise, lateral migration of sandbanks has been suggested, combined with the existence of flood- and ebb-dominated flows on either side of the bank; this results in an inequality in the sand transport rates (Caston, 1972). Such an imbalance causes the crestline of the bank to curve, becoming progressively more sigmoidal. Eventually, such a bank would divide into two smaller parallel banks, separated by a channel or swale.

A stratigraphic model for the evolution of these large-scale bedforms associated with sea level rises has been described (Swift, 1975). These low and broad sand bodies are considered to mark, as massifs, the retreat path of the coastline during periods of marine transgression. A sand body is considered to accumulate in areas where the littoral drift of sand along the coastline converges; this is attached to the shoreline. In response to sea level rise, a sequence of offshore sand bodies would result, as the tidal ridges became detached from their nearshore origins. Once isolated from the nearshore sand supply, a linear tidal ridge would interact with the regional tidal flow field. The bedform would reach then an equilibrium state, with sand transport continuing within the ridge/swale system.

Using numerical models, Huthnance (1982a,b) has shown that strong currents (1 m s^{-1}, on average) and the presence of initial irregularities or humps on the seabed are sufficient to form and maintain linear sandbanks. The growth of the bank is assumed to adopt the fastest possible rate (dependent upon sand availability), resulting in certain spacing and orientation of the bank axis. Eventually, equilibrium morphology of a bank will be reached, which may be characterised by a flattened top caused by wave action and an asymmetric cross-section in response to asymmetric current activity. Hence, other mechanisms, including secondary circulation, internal tides, the lag of sediment transport behind the instantaneous current, and spatial changes in bed roughness, may not be necessary (Huthnance, 1982a). Under some conditions, however, they may cause sandbank growth.

The validation of the various (conceptual and mathematical) models proposed for sandbank formation and maintenance requires in situ oceanographic and sedimentological measurements. Current meter observations have been used, in previous studies, for comparison with model predictions (e.g. McCave, 1979; Huthnance, 1982a).

The present investigation is concerned with water and sediment movement in the vicinity of a sequence of tidal sandbanks (the Norfolk Banks) in the Southern Bight of the North Sea. Observations used in the analyses were obtained using geophysical survey techniques (side-scan sonar and shallow sub-bottom profiling), self-recording current meter deployments and longer-term fluorescent sand tracer investigations. Hence, an integrated data set is available to study the prevailing localised hydrodynamic and sediment dynamic conditions. Furthermore, interaction of the sandbanks with regional sediment transport pathways in the southern North Sea is examined.

2. Area under investigation

The Norfolk Banks consist of a group of offshore sandbanks, located some 100 km to seaward of the East Anglian coastline and lying in water depths of 18 to 40 m (Fig. 1). Some of the banks rise from the sea-floor to within 5 m of the sea surface; however, those lying in deeper waters have their crestlines submerged at greater depths.

The study has concentrated upon the Well Bank, Broken Bank and Swarte Bank system (Fig. 2). Broken Bank, around which most of the data were collected, has dimensions which are typical of the tidally-controlled sandbanks within the area i.e. 33 km in length, approximately 1 km in width, and rising to a height of 30 m above the surrounding sea-floor. The loosely-consolidated seabed material on and around the Broken Bank consists predominantly of well-sorted, fine-grained sand.

All three banks are asymmetric in their cross-section, with a steep northeasterly facing slope and a more gently sloping southwesterly face. The

a review, see Pattiaratchi and Collins, 1987). Helical spiral water circulations, with flow divergence (at depth) in the swales between the banks and convergence over the crestline, have been postulated. Such a mechanism would transport sand from the swales and onto a bank, resulting in the continued growth and maintenance of the system (Houbolt, 1968). Likewise, lateral migration of sandbanks has been suggested, combined with the existence of flood- and ebb-dominated flows on either side of the bank; this results in an inequality in the sand transport rates (Caston, 1972). Such an imbalance causes the crestline of the bank to curve, becoming progressively more sigmoidal. Eventually, such a bank would divide into two smaller parallel banks, separated by a channel or swale.

A stratigraphic model for the evolution of these large-scale bedforms associated with sea level rises has been described (Swift, 1975). These low and broad sand bodies are considered to mark, as massifs, the retreat path of the coastline during periods of marine transgression. A sand body is considered to accumulate in areas where the littoral drift of sand along the coastline converges; this is attached to the shoreline. In response to sea level rise, a sequence of offshore sand bodies would result, as the tidal ridges became detached from their nearshore origins. Once isolated from the nearshore sand supply, a linear tidal ridge would interact with the regional tidal flow field. The bedform would reach then an equilibrium state, with sand transport continuing within the ridge/swale system.

Using numerical models, Huthnance (1982a,b) has shown that strong currents (1 m s^{-1}, on average) and the presence of initial irregularities or humps on the seabed are sufficient to form and maintain linear sandbanks. The growth of the bank is assumed to adopt the fastest possible rate (dependent upon sand availability), resulting in certain spacing and orientation of the bank axis. Eventually, equilibrium morphology of a bank will be reached, which may be characterised by a flattened top caused by wave action and an asymmetric cross-section in response to asymmetric current activity. Hence, other mechanisms, including secondary circulation, internal tides, the lag of sediment transport behind the instantaneous current, and spatial changes in bed roughness, may not be necessary (Huthnance, 1982a). Under some conditions, however, they may cause sandbank growth.

The validation of the various (conceptual and mathematical) models proposed for sandbank formation and maintenance requires in situ oceanographic and sedimentological measurements. Current meter observations have been used, in previous studies, for comparison with model predictions (e.g. McCave, 1979; Huthnance, 1982a).

The present investigation is concerned with water and sediment movement in the vicinity of a sequence of tidal sandbanks (the Norfolk Banks) in the Southern Bight of the North Sea. Observations used in the analyses were obtained using geophysical survey techniques (side-scan sonar and shallow sub-bottom profiling), self-recording current meter deployments and longer-term fluorescent sand tracer investigations. Hence, an integrated data set is available to study the prevailing localised hydrodynamic and sediment dynamic conditions. Furthermore, interaction of the sandbanks with regional sediment transport pathways in the southern North Sea is examined.

2. Area under investigation

The Norfolk Banks consist of a group of offshore sandbanks, located some 100 km to seaward of the East Anglian coastline and lying in water depths of 18 to 40 m (Fig. 1). Some of the banks rise from the sea-floor to within 5 m of the sea surface; however, those lying in deeper waters have their crestlines submerged at greater depths.

The study has concentrated upon the Well Bank, Broken Bank and Swarte Bank system (Fig. 2). Broken Bank, around which most of the data were collected, has dimensions which are typical of the tidally-controlled sandbanks within the area i.e. 33 km in length, approximately 1 km in width, and rising to a height of 30 m above the surrounding sea-floor. The loosely-consolidated seabed material on and around the Broken Bank consists predominantly of well-sorted, fine-grained sand.

All three banks are asymmetric in their cross-section, with a steep northeasterly facing slope and a more gently sloping southwesterly face. The

a review, see Pattiaratchi and Collins, 1987). Helical spiral water circulations, with flow divergence (at depth) in the swales between the banks and convergence over the crestline, have been postulated. Such a mechanism would transport sand from the swales and onto a bank, resulting in the continued growth and maintenance of the system (Houbolt, 1968). Likewise, lateral migration of sandbanks has been suggested, combined with the existence of flood- and ebb-dominated flows on either side of the bank; this results in an inequality in the sand transport rates (Caston, 1972). Such an imbalance causes the crestline of the bank to curve, becoming progressively more sigmoidal. Eventually, such a bank would divide into two smaller parallel banks, separated by a channel or swale.

A stratigraphic model for the evolution of these large-scale bedforms associated with sea level rises has been described (Swift, 1975). These low and broad sand bodies are considered to mark, as massifs, the retreat path of the coastline during periods of marine transgression. A sand body is considered to accumulate in areas where the littoral drift of sand along the coastline converges; this is attached to the shoreline. In response to sea level rise, a sequence of offshore sand bodies would result, as the tidal ridges became detached from their nearshore origins. Once isolated from the nearshore sand supply, a linear tidal ridge would interact with the regional tidal flow field. The bedform would reach then an equilibrium state, with sand transport continuing within the ridge/swale system.

Using numerical models, Huthnance (1982a,b) has shown that strong currents (1 m s^{-1}, on average) and the presence of initial irregularities or humps on the seabed are sufficient to form and maintain linear sandbanks. The growth of the bank is assumed to adopt the fastest possible rate (dependent upon sand availability), resulting in certain spacing and orientation of the bank axis. Eventually, equilibrium morphology of a bank will be reached, which may be characterised by a flattened top caused by wave action and an asymmetric cross-section in response to asymmetric current activity. Hence, other mechanisms, including secondary circulation, internal tides, the lag of sediment transport behind the instantaneous current, and spatial changes in bed roughness, may not be necessary (Huthnance, 1982a). Under some conditions, however, they may cause sandbank growth.

The validation of the various (conceptual and mathematical) models proposed for sandbank formation and maintenance requires in situ oceanographic and sedimentological measurements. Current meter observations have been used, in previous studies, for comparison with model predictions (e.g. McCave, 1979; Huthnance, 1982a).

The present investigation is concerned with water and sediment movement in the vicinity of a sequence of tidal sandbanks (the Norfolk Banks) in the Southern Bight of the North Sea. Observations used in the analyses were obtained using geophysical survey techniques (side-scan sonar and shallow sub-bottom profiling), self-recording current meter deployments and longer-term fluorescent sand tracer investigations. Hence, an integrated data set is available to study the prevailing localised hydrodynamic and sediment dynamic conditions. Furthermore, interaction of the sandbanks with regional sediment transport pathways in the southern North Sea is examined.

2. Area under investigation

The Norfolk Banks consist of a group of offshore sandbanks, located some 100 km to seaward of the East Anglian coastline and lying in water depths of 18 to 40 m (Fig. 1). Some of the banks rise from the sea-floor to within 5 m of the sea surface; however, those lying in deeper waters have their crestlines submerged at greater depths.

The study has concentrated upon the Well Bank, Broken Bank and Swarte Bank system (Fig. 2). Broken Bank, around which most of the data were collected, has dimensions which are typical of the tidally-controlled sandbanks within the area i.e. 33 km in length, approximately 1 km in width, and rising to a height of 30 m above the surrounding sea-floor. The loosely-consolidated seabed material on and around the Broken Bank consists predominantly of well-sorted, fine-grained sand.

All three banks are asymmetric in their cross-section, with a steep northeasterly facing slope and a more gently sloping southwesterly face. The

a review, see Pattiaratchi and Collins, 1987). Helical spiral water circulations, with flow divergence (at depth) in the swales between the banks and convergence over the crestline, have been postulated. Such a mechanism would transport sand from the swales and onto a bank, resulting in the continued growth and maintenance of the system (Houbolt, 1968). Likewise, lateral migration of sandbanks has been suggested, combined with the existence of flood- and ebb-dominated flows on either side of the bank; this results in an inequality in the sand transport rates (Caston, 1972). Such an imbalance causes the crestline of the bank to curve, becoming progressively more sigmoidal. Eventually, such a bank would divide into two smaller parallel banks, separated by a channel or swale.

A stratigraphic model for the evolution of these large-scale bedforms associated with sea level rises has been described (Swift, 1975). These low and broad sand bodies are considered to mark, as massifs, the retreat path of the coastline during periods of marine transgression. A sand body is considered to accumulate in areas where the littoral drift of sand along the coastline converges; this is attached to the shoreline. In response to sea level rise, a sequence of offshore sand bodies would result, as the tidal ridges became detached from their nearshore origins. Once isolated from the nearshore sand supply, a linear tidal ridge would interact with the regional tidal flow field. The bedform would reach then an equilibrium state, with sand transport continuing within the ridge/swale system.

Using numerical models, Huthnance (1982a,b) has shown that strong currents (1 m s^{-1}, on average) and the presence of initial irregularities or humps on the seabed are sufficient to form and maintain linear sandbanks. The growth of the bank is assumed to adopt the fastest possible rate (dependent upon sand availability), resulting in certain spacing and orientation of the bank axis. Eventually, equilibrium morphology of a bank will be reached, which may be characterised by a flattened top caused by wave action and an asymmetric cross-section in response to asymmetric current activity. Hence, other mechanisms, including secondary circulation, internal tides, the lag of sediment transport behind the instantaneous current, and spatial changes in bed roughness, may not be necessary (Huthnance, 1982a). Under some conditions, however, they may cause sandbank growth.

The validation of the various (conceptual and mathematical) models proposed for sandbank formation and maintenance requires in situ oceanographic and sedimentological measurements. Current meter observations have been used, in previous studies, for comparison with model predictions (e.g. McCave, 1979; Huthnance, 1982a).

The present investigation is concerned with water and sediment movement in the vicinity of a sequence of tidal sandbanks (the Norfolk Banks) in the Southern Bight of the North Sea. Observations used in the analyses were obtained using geophysical survey techniques (side-scan sonar and shallow sub-bottom profiling), self-recording current meter deployments and longer-term fluorescent sand tracer investigations. Hence, an integrated data set is available to study the prevailing localised hydrodynamic and sediment dynamic conditions. Furthermore, interaction of the sandbanks with regional sediment transport pathways in the southern North Sea is examined.

2. Area under investigation

The Norfolk Banks consist of a group of offshore sandbanks, located some 100 km to seaward of the East Anglian coastline and lying in water depths of 18 to 40 m (Fig. 1). Some of the banks rise from the sea-floor to within 5 m of the sea surface; however, those lying in deeper waters have their crestlines submerged at greater depths.

The study has concentrated upon the Well Bank, Broken Bank and Swarte Bank system (Fig. 2). Broken Bank, around which most of the data were collected, has dimensions which are typical of the tidally-controlled sandbanks within the area i.e. 33 km in length, approximately 1 km in width, and rising to a height of 30 m above the surrounding sea-floor. The loosely-consolidated seabed material on and around the Broken Bank consists predominantly of well-sorted, fine-grained sand.

All three banks are asymmetric in their cross-section, with a steep northeasterly facing slope and a more gently sloping southwesterly face. The

a review, see Pattiaratchi and Collins, 1987). Helical spiral water circulations, with flow divergence (at depth) in the swales between the banks and convergence over the crestline, have been postulated. Such a mechanism would transport sand from the swales and onto a bank, resulting in the continued growth and maintenance of the system (Houbolt, 1968). Likewise, lateral migration of sandbanks has been suggested, combined with the existence of flood- and ebb-dominated flows on either side of the bank; this results in an inequality in the sand transport rates (Caston, 1972). Such an imbalance causes the crestline of the bank to curve, becoming progressively more sigmoidal. Eventually, such a bank would divide into two smaller parallel banks, separated by a channel or swale.

A stratigraphic model for the evolution of these large-scale bedforms associated with sea level rises has been described (Swift, 1975). These low and broad sand bodies are considered to mark, as massifs, the retreat path of the coastline during periods of marine transgression. A sand body is considered to accumulate in areas where the littoral drift of sand along the coastline converges; this is attached to the shoreline. In response to sea level rise, a sequence of offshore sand bodies would result, as the tidal ridges became detached from their nearshore origins. Once isolated from the nearshore sand supply, a linear tidal ridge would interact with the regional tidal flow field. The bedform would reach then an equilibrium state, with sand transport continuing within the ridge/swale system.

Using numerical models, Huthnance (1982a,b) has shown that strong currents (1 m s^{-1}, on average) and the presence of initial irregularities or humps on the seabed are sufficient to form and maintain linear sandbanks. The growth of the bank is assumed to adopt the fastest possible rate (dependent upon sand availability), resulting in certain spacing and orientation of the bank axis. Eventually, equilibrium morphology of a bank will be reached, which may be characterised by a flattened top caused by wave action and an asymmetric cross-section in response to asymmetric current activity. Hence, other mechanisms, including secondary circulation, internal tides, the lag of sediment transport behind the instantaneous current, and spatial changes in bed roughness, may not be necessary (Huthnance, 1982a). Under some conditions, however, they may cause sandbank growth.

The validation of the various (conceptual and mathematical) models proposed for sandbank formation and maintenance requires in situ oceanographic and sedimentological measurements. Current meter observations have been used, in previous studies, for comparison with model predictions (e.g. McCave, 1979; Huthnance, 1982a).

The present investigation is concerned with water and sediment movement in the vicinity of a sequence of tidal sandbanks (the Norfolk Banks) in the Southern Bight of the North Sea. Observations used in the analyses were obtained using geophysical survey techniques (side-scan sonar and shallow sub-bottom profiling), self-recording current meter deployments and longer-term fluorescent sand tracer investigations. Hence, an integrated data set is available to study the prevailing localised hydrodynamic and sediment dynamic conditions. Furthermore, interaction of the sandbanks with regional sediment transport pathways in the southern North Sea is examined.

2. Area under investigation

The Norfolk Banks consist of a group of offshore sandbanks, located some 100 km to seaward of the East Anglian coastline and lying in water depths of 18 to 40 m (Fig. 1). Some of the banks rise from the sea-floor to within 5 m of the sea surface; however, those lying in deeper waters have their crestlines submerged at greater depths.

The study has concentrated upon the Well Bank, Broken Bank and Swarte Bank system (Fig. 2). Broken Bank, around which most of the data were collected, has dimensions which are typical of the tidally-controlled sandbanks within the area i.e. 33 km in length, approximately 1 km in width, and rising to a height of 30 m above the surrounding sea-floor. The loosely-consolidated seabed material on and around the Broken Bank consists predominantly of well-sorted, fine-grained sand.

All three banks are asymmetric in their cross-section, with a steep northeasterly facing slope and a more gently sloping southwesterly face. The

a review, see Pattiaratchi and Collins, 1987). Helical spiral water circulations, with flow divergence (at depth) in the swales between the banks and convergence over the crestline, have been postulated. Such a mechanism would transport sand from the swales and onto a bank, resulting in the continued growth and maintenance of the system (Houbolt, 1968). Likewise, lateral migration of sandbanks has been suggested, combined with the existence of flood- and ebb-dominated flows on either side of the bank; this results in an inequality in the sand transport rates (Caston, 1972). Such an imbalance causes the crestline of the bank to curve, becoming progressively more sigmoidal. Eventually, such a bank would divide into two smaller parallel banks, separated by a channel or swale.

A stratigraphic model for the evolution of these large-scale bedforms associated with sea level rises has been described (Swift, 1975). These low and broad sand bodies are considered to mark, as massifs, the retreat path of the coastline during periods of marine transgression. A sand body is considered to accumulate in areas where the littoral drift of sand along the coastline converges; this is attached to the shoreline. In response to sea level rise, a sequence of offshore sand bodies would result, as the tidal ridges became detached from their nearshore origins. Once isolated from the nearshore sand supply, a linear tidal ridge would interact with the regional tidal flow field. The bedform would reach then an equilibrium state, with sand transport continuing within the ridge/swale system.

Using numerical models, Huthnance (1982a,b) has shown that strong currents (1 m s^{-1}, on average) and the presence of initial irregularities or humps on the seabed are sufficient to form and maintain linear sandbanks. The growth of the bank is assumed to adopt the fastest possible rate (dependent upon sand availability), resulting in certain spacing and orientation of the bank axis. Eventually, equilibrium morphology of a bank will be reached, which may be characterised by a flattened top caused by wave action and an asymmetric cross-section in response to asymmetric current activity. Hence, other mechanisms, including secondary circulation, internal tides, the lag of sediment transport behind the instantaneous current, and spatial changes in bed roughness, may not be necessary (Huthnance, 1982a). Under some conditions, however, they may cause sandbank growth.

The validation of the various (conceptual and mathematical) models proposed for sandbank formation and maintenance requires in situ oceanographic and sedimentological measurements. Current meter observations have been used, in previous studies, for comparison with model predictions (e.g. McCave, 1979; Huthnance, 1982a).

The present investigation is concerned with water and sediment movement in the vicinity of a sequence of tidal sandbanks (the Norfolk Banks) in the Southern Bight of the North Sea. Observations used in the analyses were obtained using geophysical survey techniques (side-scan sonar and shallow sub-bottom profiling), self-recording current meter deployments and longer-term fluorescent sand tracer investigations. Hence, an integrated data set is available to study the prevailing localised hydrodynamic and sediment dynamic conditions. Furthermore, interaction of the sandbanks with regional sediment transport pathways in the southern North Sea is examined.

2. Area under investigation

The Norfolk Banks consist of a group of offshore sandbanks, located some 100 km to seaward of the East Anglian coastline and lying in water depths of 18 to 40 m (Fig. 1). Some of the banks rise from the sea-floor to within 5 m of the sea surface; however, those lying in deeper waters have their crestlines submerged at greater depths.

The study has concentrated upon the Well Bank, Broken Bank and Swarte Bank system (Fig. 2). Broken Bank, around which most of the data were collected, has dimensions which are typical of the tidally-controlled sandbanks within the area i.e. 33 km in length, approximately 1 km in width, and rising to a height of 30 m above the surrounding sea-floor. The loosely-consolidated seabed material on and around the Broken Bank consists predominantly of well-sorted, fine-grained sand.

All three banks are asymmetric in their cross-section, with a steep northeasterly facing slope and a more gently sloping southwesterly face. The

a review, see Pattiaratchi and Collins, 1987). Helical spiral water circulations, with flow divergence (at depth) in the swales between the banks and convergence over the crestline, have been postulated. Such a mechanism would transport sand from the swales and onto a bank, resulting in the continued growth and maintenance of the system (Houbolt, 1968). Likewise, lateral migration of sandbanks has been suggested, combined with the existence of flood- and ebb-dominated flows on either side of the bank; this results in an inequality in the sand transport rates (Caston, 1972). Such an imbalance causes the crestline of the bank to curve, becoming progressively more sigmoidal. Eventually, such a bank would divide into two smaller parallel banks, separated by a channel or swale.

A stratigraphic model for the evolution of these large-scale bedforms associated with sea level rises has been described (Swift, 1975). These low and broad sand bodies are considered to mark, as massifs, the retreat path of the coastline during periods of marine transgression. A sand body is considered to accumulate in areas where the littoral drift of sand along the coastline converges; this is attached to the shoreline. In response to sea level rise, a sequence of offshore sand bodies would result, as the tidal ridges became detached from their nearshore origins. Once isolated from the nearshore sand supply, a linear tidal ridge would interact with the regional tidal flow field. The bedform would reach then an equilibrium state, with sand transport continuing within the ridge/swale system.

Using numerical models, Huthnance (1982a,b) has shown that strong currents (1 m s^{-1}, on average) and the presence of initial irregularities or humps on the seabed are sufficient to form and maintain linear sandbanks. The growth of the bank is assumed to adopt the fastest possible rate (dependent upon sand availability), resulting in certain spacing and orientation of the bank axis. Eventually, equilibrium morphology of a bank will be reached, which may be characterised by a flattened top caused by wave action and an asymmetric cross-section in response to asymmetric current activity. Hence, other mechanisms, including secondary circulation, internal tides, the lag of sediment transport behind the instantaneous current, and spatial changes in bed roughness, may not be necessary (Huthnance, 1982a). Under some conditions, however, they may cause sandbank growth.

The validation of the various (conceptual and mathematical) models proposed for sandbank formation and maintenance requires in situ oceanographic and sedimentological measurements. Current meter observations have been used, in previous studies, for comparison with model predictions (e.g. McCave, 1979; Huthnance, 1982a).

The present investigation is concerned with water and sediment movement in the vicinity of a sequence of tidal sandbanks (the Norfolk Banks) in the Southern Bight of the North Sea. Observations used in the analyses were obtained using geophysical survey techniques (side-scan sonar and shallow sub-bottom profiling), self-recording current meter deployments and longer-term fluorescent sand tracer investigations. Hence, an integrated data set is available to study the prevailing localised hydrodynamic and sediment dynamic conditions. Furthermore, interaction of the sandbanks with regional sediment transport pathways in the southern North Sea is examined.

2. Area under investigation

The Norfolk Banks consist of a group of offshore sandbanks, located some 100 km to seaward of the East Anglian coastline and lying in water depths of 18 to 40 m (Fig. 1). Some of the banks rise from the sea-floor to within 5 m of the sea surface; however, those lying in deeper waters have their crestlines submerged at greater depths.

The study has concentrated upon the Well Bank, Broken Bank and Swarte Bank system (Fig. 2). Broken Bank, around which most of the data were collected, has dimensions which are typical of the tidally-controlled sandbanks within the area i.e. 33 km in length, approximately 1 km in width, and rising to a height of 30 m above the surrounding sea-floor. The loosely-consolidated seabed material on and around the Broken Bank consists predominantly of well-sorted, fine-grained sand.

All three banks are asymmetric in their cross-section, with a steep northeasterly facing slope and a more gently sloping southwesterly face. The

a review, see Pattiaratchi and Collins, 1987). Helical spiral water circulations, with flow divergence (at depth) in the swales between the banks and convergence over the crestline, have been postulated. Such a mechanism would transport sand from the swales and onto a bank, resulting in the continued growth and maintenance of the system (Houbolt, 1968). Likewise, lateral migration of sandbanks has been suggested, combined with the existence of flood- and ebb-dominated flows on either side of the bank; this results in an inequality in the sand transport rates (Caston, 1972). Such an imbalance causes the crestline of the bank to curve, becoming progressively more sigmoidal. Eventually, such a bank would divide into two smaller parallel banks, separated by a channel or swale.

A stratigraphic model for the evolution of these large-scale bedforms associated with sea level rises has been described (Swift, 1975). These low and broad sand bodies are considered to mark, as massifs, the retreat path of the coastline during periods of marine transgression. A sand body is considered to accumulate in areas where the littoral drift of sand along the coastline converges; this is attached to the shoreline. In response to sea level rise, a sequence of offshore sand bodies would result, as the tidal ridges became detached from their nearshore origins. Once isolated from the nearshore sand supply, a linear tidal ridge would interact with the regional tidal flow field. The bedform would reach then an equilibrium state, with sand transport continuing within the ridge/swale system.

Using numerical models, Huthnance (1982a,b) has shown that strong currents (1 m s^{-1}, on average) and the presence of initial irregularities or humps on the seabed are sufficient to form and maintain linear sandbanks. The growth of the bank is assumed to adopt the fastest possible rate (dependent upon sand availability), resulting in certain spacing and orientation of the bank axis. Eventually, equilibrium morphology of a bank will be reached, which may be characterised by a flattened top caused by wave action and an asymmetric cross-section in response to asymmetric current activity. Hence, other mechanisms, including secondary circulation, internal tides, the lag of sediment transport behind the instantaneous current, and spatial changes in bed roughness, may not be necessary (Huthnance, 1982a). Under some conditions, however, they may cause sandbank growth.

The validation of the various (conceptual and mathematical) models proposed for sandbank formation and maintenance requires in situ oceanographic and sedimentological measurements. Current meter observations have been used, in previous studies, for comparison with model predictions (e.g. McCave, 1979; Huthnance, 1982a).

The present investigation is concerned with water and sediment movement in the vicinity of a sequence of tidal sandbanks (the Norfolk Banks) in the Southern Bight of the North Sea. Observations used in the analyses were obtained using geophysical survey techniques (side-scan sonar and shallow sub-bottom profiling), self-recording current meter deployments and longer-term fluorescent sand tracer investigations. Hence, an integrated data set is available to study the prevailing localised hydrodynamic and sediment dynamic conditions. Furthermore, interaction of the sandbanks with regional sediment transport pathways in the southern North Sea is examined.

2. Area under investigation

The Norfolk Banks consist of a group of offshore sandbanks, located some 100 km to seaward of the East Anglian coastline and lying in water depths of 18 to 40 m (Fig. 1). Some of the banks rise from the sea-floor to within 5 m of the sea surface; however, those lying in deeper waters have their crestlines submerged at greater depths.

The study has concentrated upon the Well Bank, Broken Bank and Swarte Bank system (Fig. 2). Broken Bank, around which most of the data were collected, has dimensions which are typical of the tidally-controlled sandbanks within the area i.e. 33 km in length, approximately 1 km in width, and rising to a height of 30 m above the surrounding sea-floor. The loosely-consolidated seabed material on and around the Broken Bank consists predominantly of well-sorted, fine-grained sand.

All three banks are asymmetric in their cross-section, with a steep northeasterly facing slope and a more gently sloping southwesterly face. The

a review, see Pattiaratchi and Collins, 1987). Helical spiral water circulations, with flow divergence (at depth) in the swales between the banks and convergence over the crestline, have been postulated. Such a mechanism would transport sand from the swales and onto a bank, resulting in the continued growth and maintenance of the system (Houbolt, 1968). Likewise, lateral migration of sandbanks has been suggested, combined with the existence of flood- and ebb-dominated flows on either side of the bank; this results in an inequality in the sand transport rates (Caston, 1972). Such an imbalance causes the crestline of the bank to curve, becoming progressively more sigmoidal. Eventually, such a bank would divide into two smaller parallel banks, separated by a channel or swale.

A stratigraphic model for the evolution of these large-scale bedforms associated with sea level rises has been described (Swift, 1975). These low and broad sand bodies are considered to mark, as massifs, the retreat path of the coastline during periods of marine transgression. A sand body is considered to accumulate in areas where the littoral drift of sand along the coastline converges; this is attached to the shoreline. In response to sea level rise, a sequence of offshore sand bodies would result, as the tidal ridges became detached from their nearshore origins. Once isolated from the nearshore sand supply, a linear tidal ridge would interact with the regional tidal flow field. The bedform would reach then an equilibrium state, with sand transport continuing within the ridge/swale system.

Using numerical models, Huthnance (1982a,b) has shown that strong currents (1 m s^{-1}, on average) and the presence of initial irregularities or humps on the seabed are sufficient to form and maintain linear sandbanks. The growth of the bank is assumed to adopt the fastest possible rate (dependent upon sand availability), resulting in certain spacing and orientation of the bank axis. Eventually, equilibrium morphology of a bank will be reached, which may be characterised by a flattened top caused by wave action and an asymmetric cross-section in response to asymmetric current activity. Hence, other mechanisms, including secondary circulation, internal tides, the lag of sediment transport behind the instantaneous current, and spatial changes in bed roughness, may not be necessary (Huthnance, 1982a). Under some conditions, however, they may cause sandbank growth.

The validation of the various (conceptual and mathematical) models proposed for sandbank formation and maintenance requires in situ oceanographic and sedimentological measurements. Current meter observations have been used, in previous studies, for comparison with model predictions (e.g. McCave, 1979; Huthnance, 1982a).

The present investigation is concerned with water and sediment movement in the vicinity of a sequence of tidal sandbanks (the Norfolk Banks) in the Southern Bight of the North Sea. Observations used in the analyses were obtained using geophysical survey techniques (side-scan sonar and shallow sub-bottom profiling), self-recording current meter deployments and longer-term fluorescent sand tracer investigations. Hence, an integrated data set is available to study the prevailing localised hydrodynamic and sediment dynamic conditions. Furthermore, interaction of the sandbanks with regional sediment transport pathways in the southern North Sea is examined.

2. Area under investigation

The Norfolk Banks consist of a group of offshore sandbanks, located some 100 km to seaward of the East Anglian coastline and lying in water depths of 18 to 40 m (Fig. 1). Some of the banks rise from the sea-floor to within 5 m of the sea surface; however, those lying in deeper waters have their crestlines submerged at greater depths.

The study has concentrated upon the Well Bank, Broken Bank and Swarte Bank system (Fig. 2). Broken Bank, around which most of the data were collected, has dimensions which are typical of the tidally-controlled sandbanks within the area i.e. 33 km in length, approximately 1 km in width, and rising to a height of 30 m above the surrounding sea-floor. The loosely-consolidated seabed material on and around the Broken Bank consists predominantly of well-sorted, fine-grained sand.

All three banks are asymmetric in their cross-section, with a steep northeasterly facing slope and a more gently sloping southwesterly face. The

a review, see Pattiaratchi and Collins, 1987). Helical spiral water circulations, with flow divergence (at depth) in the swales between the banks and convergence over the crestline, have been postulated. Such a mechanism would transport sand from the swales and onto a bank, resulting in the continued growth and maintenance of the system (Houbolt, 1968). Likewise, lateral migration of sandbanks has been suggested, combined with the existence of flood- and ebb-dominated flows on either side of the bank; this results in an inequality in the sand transport rates (Caston, 1972). Such an imbalance causes the crestline of the bank to curve, becoming progressively more sigmoidal. Eventually, such a bank would divide into two smaller parallel banks, separated by a channel or swale.

A stratigraphic model for the evolution of these large-scale bedforms associated with sea level rises has been described (Swift, 1975). These low and broad sand bodies are considered to mark, as massifs, the retreat path of the coastline during periods of marine transgression. A sand body is considered to accumulate in areas where the littoral drift of sand along the coastline converges; this is attached to the shoreline. In response to sea level rise, a sequence of offshore sand bodies would result, as the tidal ridges became detached from their nearshore origins. Once isolated from the nearshore sand supply, a linear tidal ridge would interact with the regional tidal flow field. The bedform would reach then an equilibrium state, with sand transport continuing within the ridge/swale system.

Using numerical models, Huthnance (1982a,b) has shown that strong currents (1 m s^{-1}, on average) and the presence of initial irregularities or humps on the seabed are sufficient to form and maintain linear sandbanks. The growth of the bank is assumed to adopt the fastest possible rate (dependent upon sand availability), resulting in certain spacing and orientation of the bank axis. Eventually, equilibrium morphology of a bank will be reached, which may be characterised by a flattened top caused by wave action and an asymmetric cross-section in response to asymmetric current activity. Hence, other mechanisms, including secondary circulation, internal tides, the lag of sediment transport behind the instantaneous current, and spatial changes in bed roughness, may not be necessary (Huthnance, 1982a). Under some conditions, however, they may cause sandbank growth.

The validation of the various (conceptual and mathematical) models proposed for sandbank formation and maintenance requires in situ oceanographic and sedimentological measurements. Current meter observations have been used, in previous studies, for comparison with model predictions (e.g. McCave, 1979; Huthnance, 1982a).

The present investigation is concerned with water and sediment movement in the vicinity of a sequence of tidal sandbanks (the Norfolk Banks) in the Southern Bight of the North Sea. Observations used in the analyses were obtained using geophysical survey techniques (side-scan sonar and shallow sub-bottom profiling), self-recording current meter deployments and longer-term fluorescent sand tracer investigations. Hence, an integrated data set is available to study the prevailing localised hydrodynamic and sediment dynamic conditions. Furthermore, interaction of the sandbanks with regional sediment transport pathways in the southern North Sea is examined.

2. Area under investigation

The Norfolk Banks consist of a group of offshore sandbanks, located some 100 km to seaward of the East Anglian coastline and lying in water depths of 18 to 40 m (Fig. 1). Some of the banks rise from the sea-floor to within 5 m of the sea surface; however, those lying in deeper waters have their crestlines submerged at greater depths.

The study has concentrated upon the Well Bank, Broken Bank and Swarte Bank system (Fig. 2). Broken Bank, around which most of the data were collected, has dimensions which are typical of the tidally-controlled sandbanks within the area i.e. 33 km in length, approximately 1 km in width, and rising to a height of 30 m above the surrounding sea-floor. The loosely-consolidated seabed material on and around the Broken Bank consists predominantly of well-sorted, fine-grained sand.

All three banks are asymmetric in their cross-section, with a steep northeasterly facing slope and a more gently sloping southwesterly face. The

a review, see Pattiaratchi and Collins, 1987). Helical spiral water circulations, with flow divergence (at depth) in the swales between the banks and convergence over the crestline, have been postulated. Such a mechanism would transport sand from the swales and onto a bank, resulting in the continued growth and maintenance of the system (Houbolt, 1968). Likewise, lateral migration of sandbanks has been suggested, combined with the existence of flood- and ebb-dominated flows on either side of the bank; this results in an inequality in the sand transport rates (Caston, 1972). Such an imbalance causes the crestline of the bank to curve, becoming progressively more sigmoidal. Eventually, such a bank would divide into two smaller parallel banks, separated by a channel or swale.

A stratigraphic model for the evolution of these large-scale bedforms associated with sea level rises has been described (Swift, 1975). These low and broad sand bodies are considered to mark, as massifs, the retreat path of the coastline during periods of marine transgression. A sand body is considered to accumulate in areas where the littoral drift of sand along the coastline converges; this is attached to the shoreline. In response to sea level rise, a sequence of offshore sand bodies would result, as the tidal ridges became detached from their nearshore origins. Once isolated from the nearshore sand supply, a linear tidal ridge would interact with the regional tidal flow field. The bedform would reach then an equilibrium state, with sand transport continuing within the ridge/swale system.

Using numerical models, Huthnance (1982a,b) has shown that strong currents (1 m s^{-1}, on average) and the presence of initial irregularities or humps on the seabed are sufficient to form and maintain linear sandbanks. The growth of the bank is assumed to adopt the fastest possible rate (dependent upon sand availability), resulting in certain spacing and orientation of the bank axis. Eventually, equilibrium morphology of a bank will be reached, which may be characterised by a flattened top caused by wave action and an asymmetric cross-section in response to asymmetric current activity. Hence, other mechanisms, including secondary circulation, internal tides, the lag of sediment transport behind the instantaneous current, and spatial changes in bed roughness, may not be necessary (Huthnance, 1982a). Under some conditions, however, they may cause sandbank growth.

The validation of the various (conceptual and mathematical) models proposed for sandbank formation and maintenance requires in situ oceanographic and sedimentological measurements. Current meter observations have been used, in previous studies, for comparison with model predictions (e.g. McCave, 1979; Huthnance, 1982a).

The present investigation is concerned with water and sediment movement in the vicinity of a sequence of tidal sandbanks (the Norfolk Banks) in the Southern Bight of the North Sea. Observations used in the analyses were obtained using geophysical survey techniques (side-scan sonar and shallow sub-bottom profiling), self-recording current meter deployments and longer-term fluorescent sand tracer investigations. Hence, an integrated data set is available to study the prevailing localised hydrodynamic and sediment dynamic conditions. Furthermore, interaction of the sandbanks with regional sediment transport pathways in the southern North Sea is examined.

2. Area under investigation

The Norfolk Banks consist of a group of offshore sandbanks, located some 100 km to seaward of the East Anglian coastline and lying in water depths of 18 to 40 m (Fig. 1). Some of the banks rise from the sea-floor to within 5 m of the sea surface; however, those lying in deeper waters have their crestlines submerged at greater depths.

The study has concentrated upon the Well Bank, Broken Bank and Swarte Bank system (Fig. 2). Broken Bank, around which most of the data were collected, has dimensions which are typical of the tidally-controlled sandbanks within the area i.e. 33 km in length, approximately 1 km in width, and rising to a height of 30 m above the surrounding sea-floor. The loosely-consolidated seabed material on and around the Broken Bank consists predominantly of well-sorted, fine-grained sand.

All three banks are asymmetric in their cross-section, with a steep northeasterly facing slope and a more gently sloping southwesterly face. The

a review, see Pattiaratchi and Collins, 1987). Helical spiral water circulations, with flow divergence (at depth) in the swales between the banks and convergence over the crestline, have been postulated. Such a mechanism would transport sand from the swales and onto a bank, resulting in the continued growth and maintenance of the system (Houbolt, 1968). Likewise, lateral migration of sandbanks has been suggested, combined with the existence of flood- and ebb-dominated flows on either side of the bank; this results in an inequality in the sand transport rates (Caston, 1972). Such an imbalance causes the crestline of the bank to curve, becoming progressively more sigmoidal. Eventually, such a bank would divide into two smaller parallel banks, separated by a channel or swale.

A stratigraphic model for the evolution of these large-scale bedforms associated with sea level rises has been described (Swift, 1975). These low and broad sand bodies are considered to mark, as massifs, the retreat path of the coastline during periods of marine transgression. A sand body is considered to accumulate in areas where the littoral drift of sand along the coastline converges; this is attached to the shoreline. In response to sea level rise, a sequence of offshore sand bodies would result, as the tidal ridges became detached from their nearshore origins. Once isolated from the nearshore sand supply, a linear tidal ridge would interact with the regional tidal flow field. The bedform would reach then an equilibrium state, with sand transport continuing within the ridge/swale system.

Using numerical models, Huthnance (1982a,b) has shown that strong currents (1 m s^{-1}, on average) and the presence of initial irregularities or humps on the seabed are sufficient to form and maintain linear sandbanks. The growth of the bank is assumed to adopt the fastest possible rate (dependent upon sand availability), resulting in certain spacing and orientation of the bank axis. Eventually, equilibrium morphology of a bank will be reached, which may be characterised by a flattened top caused by wave action and an asymmetric cross-section in response to asymmetric current activity. Hence, other mechanisms, including secondary circulation, internal tides, the lag of sediment transport behind the instantaneous current, and spatial changes in bed roughness, may not be necessary (Huthnance, 1982a). Under some conditions, however, they may cause sandbank growth.

The validation of the various (conceptual and mathematical) models proposed for sandbank formation and maintenance requires in situ oceanographic and sedimentological measurements. Current meter observations have been used, in previous studies, for comparison with model predictions (e.g. McCave, 1979; Huthnance, 1982a).

The present investigation is concerned with water and sediment movement in the vicinity of a sequence of tidal sandbanks (the Norfolk Banks) in the Southern Bight of the North Sea. Observations used in the analyses were obtained using geophysical survey techniques (side-scan sonar and shallow sub-bottom profiling), self-recording current meter deployments and longer-term fluorescent sand tracer investigations. Hence, an integrated data set is available to study the prevailing localised hydrodynamic and sediment dynamic conditions. Furthermore, interaction of the sandbanks with regional sediment transport pathways in the southern North Sea is examined.

2. Area under investigation

The Norfolk Banks consist of a group of offshore sandbanks, located some 100 km to seaward of the East Anglian coastline and lying in water depths of 18 to 40 m (Fig. 1). Some of the banks rise from the sea-floor to within 5 m of the sea surface; however, those lying in deeper waters have their crestlines submerged at greater depths.

The study has concentrated upon the Well Bank, Broken Bank and Swarte Bank system (Fig. 2). Broken Bank, around which most of the data were collected, has dimensions which are typical of the tidally-controlled sandbanks within the area i.e. 33 km in length, approximately 1 km in width, and rising to a height of 30 m above the surrounding sea-floor. The loosely-consolidated seabed material on and around the Broken Bank consists predominantly of well-sorted, fine-grained sand.

All three banks are asymmetric in their cross-section, with a steep northeasterly facing slope and a more gently sloping southwesterly face. The

a review, see Pattiaratchi and Collins, 1987). Helical spiral water circulations, with flow divergence (at depth) in the swales between the banks and convergence over the crestline, have been postulated. Such a mechanism would transport sand from the swales and onto a bank, resulting in the continued growth and maintenance of the system (Houbolt, 1968). Likewise, lateral migration of sandbanks has been suggested, combined with the existence of flood- and ebb-dominated flows on either side of the bank; this results in an inequality in the sand transport rates (Caston, 1972). Such an imbalance causes the crestline of the bank to curve, becoming progressively more sigmoidal. Eventually, such a bank would divide into two smaller parallel banks, separated by a channel or swale.

A stratigraphic model for the evolution of these large-scale bedforms associated with sea level rises has been described (Swift, 1975). These low and broad sand bodies are considered to mark, as massifs, the retreat path of the coastline during periods of marine transgression. A sand body is considered to accumulate in areas where the littoral drift of sand along the coastline converges; this is attached to the shoreline. In response to sea level rise, a sequence of offshore sand bodies would result, as the tidal ridges became detached from their nearshore origins. Once isolated from the nearshore sand supply, a linear tidal ridge would interact with the regional tidal flow field. The bedform would reach then an equilibrium state, with sand transport continuing within the ridge/swale system.

Using numerical models, Huthnance (1982a,b) has shown that strong currents (1 m s^{-1}, on average) and the presence of initial irregularities or humps on the seabed are sufficient to form and maintain linear sandbanks. The growth of the bank is assumed to adopt the fastest possible rate (dependent upon sand availability), resulting in certain spacing and orientation of the bank axis. Eventually, equilibrium morphology of a bank will be reached, which may be characterised by a flattened top caused by wave action and an asymmetric cross-section in response to asymmetric current activity. Hence, other mechanisms, including secondary circulation, internal tides, the lag of sediment transport behind the instantaneous current, and spatial changes in bed roughness, may not be necessary (Huthnance, 1982a). Under some conditions, however, they may cause sandbank growth.

The validation of the various (conceptual and mathematical) models proposed for sandbank formation and maintenance requires in situ oceanographic and sedimentological measurements. Current meter observations have been used, in previous studies, for comparison with model predictions (e.g. McCave, 1979; Huthnance, 1982a).

The present investigation is concerned with water and sediment movement in the vicinity of a sequence of tidal sandbanks (the Norfolk Banks) in the Southern Bight of the North Sea. Observations used in the analyses were obtained using geophysical survey techniques (side-scan sonar and shallow sub-bottom profiling), self-recording current meter deployments and longer-term fluorescent sand tracer investigations. Hence, an integrated data set is available to study the prevailing localised hydrodynamic and sediment dynamic conditions. Furthermore, interaction of the sandbanks with regional sediment transport pathways in the southern North Sea is examined.

2. Area under investigation

The Norfolk Banks consist of a group of offshore sandbanks, located some 100 km to seaward of the East Anglian coastline and lying in water depths of 18 to 40 m (Fig. 1). Some of the banks rise from the sea-floor to within 5 m of the sea surface; however, those lying in deeper waters have their crestlines submerged at greater depths.

The study has concentrated upon the Well Bank, Broken Bank and Swarte Bank system (Fig. 2). Broken Bank, around which most of the data were collected, has dimensions which are typical of the tidally-controlled sandbanks within the area i.e. 33 km in length, approximately 1 km in width, and rising to a height of 30 m above the surrounding sea-floor. The loosely-consolidated seabed material on and around the Broken Bank consists predominantly of well-sorted, fine-grained sand.

All three banks are asymmetric in their cross-section, with a steep northeasterly facing slope and a more gently sloping southwesterly face. The

a review, see Pattiaratchi and Collins, 1987). Helical spiral water circulations, with flow divergence (at depth) in the swales between the banks and convergence over the crestline, have been postulated. Such a mechanism would transport sand from the swales and onto a bank, resulting in the continued growth and maintenance of the system (Houbolt, 1968). Likewise, lateral migration of sandbanks has been suggested, combined with the existence of flood- and ebb-dominated flows on either side of the bank; this results in an inequality in the sand transport rates (Caston, 1972). Such an imbalance causes the crestline of the bank to curve, becoming progressively more sigmoidal. Eventually, such a bank would divide into two smaller parallel banks, separated by a channel or swale.

A stratigraphic model for the evolution of these large-scale bedforms associated with sea level rises has been described (Swift, 1975). These low and broad sand bodies are considered to mark, as massifs, the retreat path of the coastline during periods of marine transgression. A sand body is considered to accumulate in areas where the littoral drift of sand along the coastline converges; this is attached to the shoreline. In response to sea level rise, a sequence of offshore sand bodies would result, as the tidal ridges became detached from their nearshore origins. Once isolated from the nearshore sand supply, a linear tidal ridge would interact with the regional tidal flow field. The bedform would reach then an equilibrium state, with sand transport continuing within the ridge/swale system.

Using numerical models, Huthnance (1982a,b) has shown that strong currents (1 m s^{-1}, on average) and the presence of initial irregularities or humps on the seabed are sufficient to form and maintain linear sandbanks. The growth of the bank is assumed to adopt the fastest possible rate (dependent upon sand availability), resulting in certain spacing and orientation of the bank axis. Eventually, equilibrium morphology of a bank will be reached, which may be characterised by a flattened top caused by wave action and an asymmetric cross-section in response to asymmetric current activity. Hence, other mechanisms, including secondary circulation, internal tides, the lag of sediment transport behind the instantaneous current, and spatial changes in bed roughness, may not be necessary (Huthnance, 1982a). Under some conditions, however, they may cause sandbank growth.

The validation of the various (conceptual and mathematical) models proposed for sandbank formation and maintenance requires in situ oceanographic and sedimentological measurements. Current meter observations have been used, in previous studies, for comparison with model predictions (e.g. McCave, 1979; Huthnance, 1982a).

The present investigation is concerned with water and sediment movement in the vicinity of a sequence of tidal sandbanks (the Norfolk Banks) in the Southern Bight of the North Sea. Observations used in the analyses were obtained using geophysical survey techniques (side-scan sonar and shallow sub-bottom profiling), self-recording current meter deployments and longer-term fluorescent sand tracer investigations. Hence, an integrated data set is available to study the prevailing localised hydrodynamic and sediment dynamic conditions. Furthermore, interaction of the sandbanks with regional sediment transport pathways in the southern North Sea is examined.

2. Area under investigation

The Norfolk Banks consist of a group of offshore sandbanks, located some 100 km to seaward of the East Anglian coastline and lying in water depths of 18 to 40 m (Fig. 1). Some of the banks rise from the sea-floor to within 5 m of the sea surface; however, those lying in deeper waters have their crestlines submerged at greater depths.

The study has concentrated upon the Well Bank, Broken Bank and Swarte Bank system (Fig. 2). Broken Bank, around which most of the data were collected, has dimensions which are typical of the tidally-controlled sandbanks within the area i.e. 33 km in length, approximately 1 km in width, and rising to a height of 30 m above the surrounding sea-floor. The loosely-consolidated seabed material on and around the Broken Bank consists predominantly of well-sorted, fine-grained sand.

All three banks are asymmetric in their cross-section, with a steep northeasterly facing slope and a more gently sloping southwesterly face. The

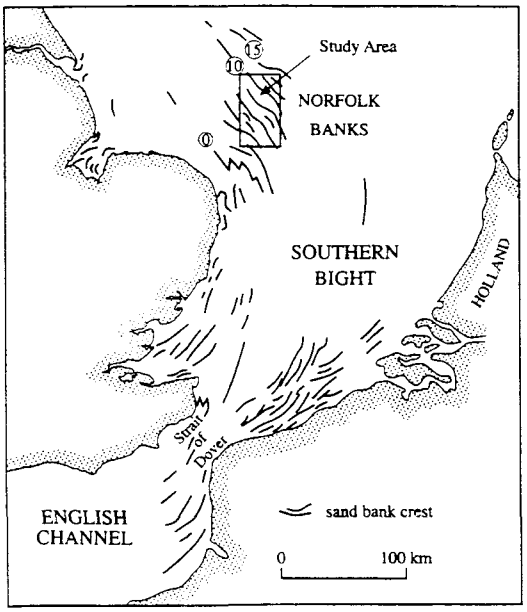

Fig. 1. Location of the Norfolk Banks and the study area (the numbers in circle represent water depth along the bank crestline, in terms of Chart Datum), in relation to the southern North Sea (after Kenyon et al., 1981).

maximum angle of the steeper slope decreases to seawards, from 6° for the Broken Bank to 2° for the Swarte Bank. Shallow-seismic profiles, collected by the British Geological Survey over the region, show the sandbanks to lie essentially on a flat surface (Fig. 3).

Active and moribund sandbanks are contained within the Norfolk Banks, but the area of the present investigation represents only active systems. Here, sandwaves (with heights of up to 4 m and wavelengths of 50 m) are maintained by the modern tidal current regime. The sandwaves are oriented in different directions on either side of the sandbanks, veering towards the crestline (Houbolt, 1968; Caston and Stride, 1970; Caston, 1972).

Tides over the area are controlled by a progressive tidal wave, moving down the coastline of England. Tidal ranges over the Broken Bank, measured during the course of the present investigation, ranged between 1.2 and 2.8 m (i.e. micro–mesotidal). Similarly, analysis of the tidal current data (see below) has shown that maximum velocities occur towards High and Low Water, with a slight velocity-asymmetry towards the southeast. Peak surface currents are oriented approximately NW–SE, with speeds of 1.6 m s^{-1} and 1.0 m s^{-1} on springs and neaps, respectively (Balson and Harrison, 1988).

To the southwest of the Well Bank, near-bed residual tidal currents have been observed elsewhere to be strongest towards the crestline and in opposing directions on either side of the bank (Caston and Stride, 1970; Caston, 1972). Similarly, on the basis of measurements on each side of the Well Bank, the current records obtained were dominated by semi-diurnal tides (M_2 surface amplitude being around 0.75 m s^{-1}) and residual flows of around 0.05 m s^{-1} (Howarth and Huthnance, 1984). The dominant semi-diurnal constituents were rectilinear, with their axis lying approximately parallel to the bank alignment (E40°S). Near-bed residual currents, averaged over a tidal cycle, were always in the sense of a clockwise circulation around the Well Bank.

The importance of episodic currents over the Norfolk Banks, induced by storm surges and causing sand transport in directions other than those caused by the tidal currents alone, has been investigated recently. Using numerical model predictions of the 50 year maximum storm surge currents (Flather, 1987), combined with observed tidal flows (Venn and D'Olier, 1983), sand transport has been shown to be oblique to the tidal currents and towards the northeast (Stride, 1988). Hence, through the banks acting as "stepping stones", it has been postulated that sand is transported from the coastline of East Anglia up to about 100 km to seaward.

The wave climate of the sea area to the north of the sandbank field has been investigated by Draper (1968). Over the course of a year, marked seasonality in wave characteristic is evident. During the winter months, the significant wave height (H_s) at the 50% exceedence level is of the order of 1.3 m; this reduces to 0.7 m during summer. Wave periods, presented in terms of the zero crossing period (T_z), cluster around 5.8 s and range between 3.5 and 9.5 s. Statistical analysis of the data has shown that the wave period tends to be greater during winter than in the other seasons.

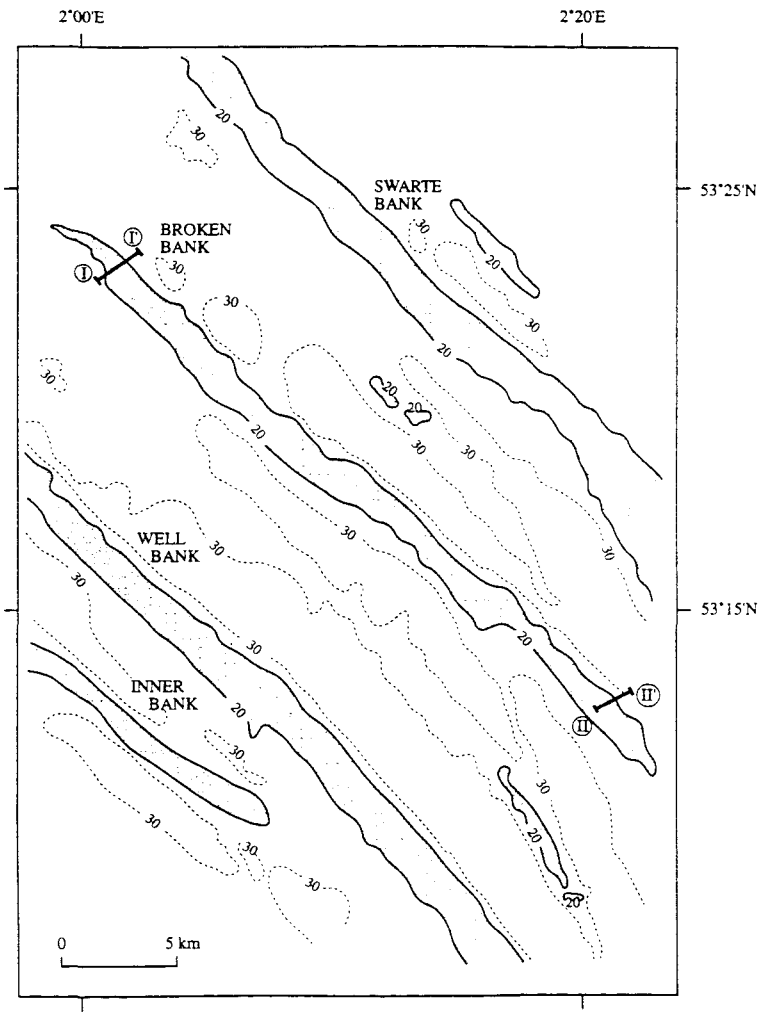

Fig. 2. Bathymetry (in metres) of the Well Bank, Broken Bank and Swarte Bank system. The positions of two sub-bottom (boomer) survey profile lines are also shown.

The highest wave recorded in the data set analysed (Draper, 1968) had a height of 8.0 m and a period of 8.4 s. The observations demonstrated also that the wave field acting on the sandbanks was locally generated, rather than propagating in from the northern North Sea. This interpretation is based upon the absence of T_z values exceeding 10 s, which typify conditions in the Norwegian Sea.

3. Data collection and analysis

3.1. Data collection

The hydrographic data used in this study were collected during RRV *Challenger* Cruise 40 (15–29 November, 1988), as part of the (NERC) North Sea Community Programme.

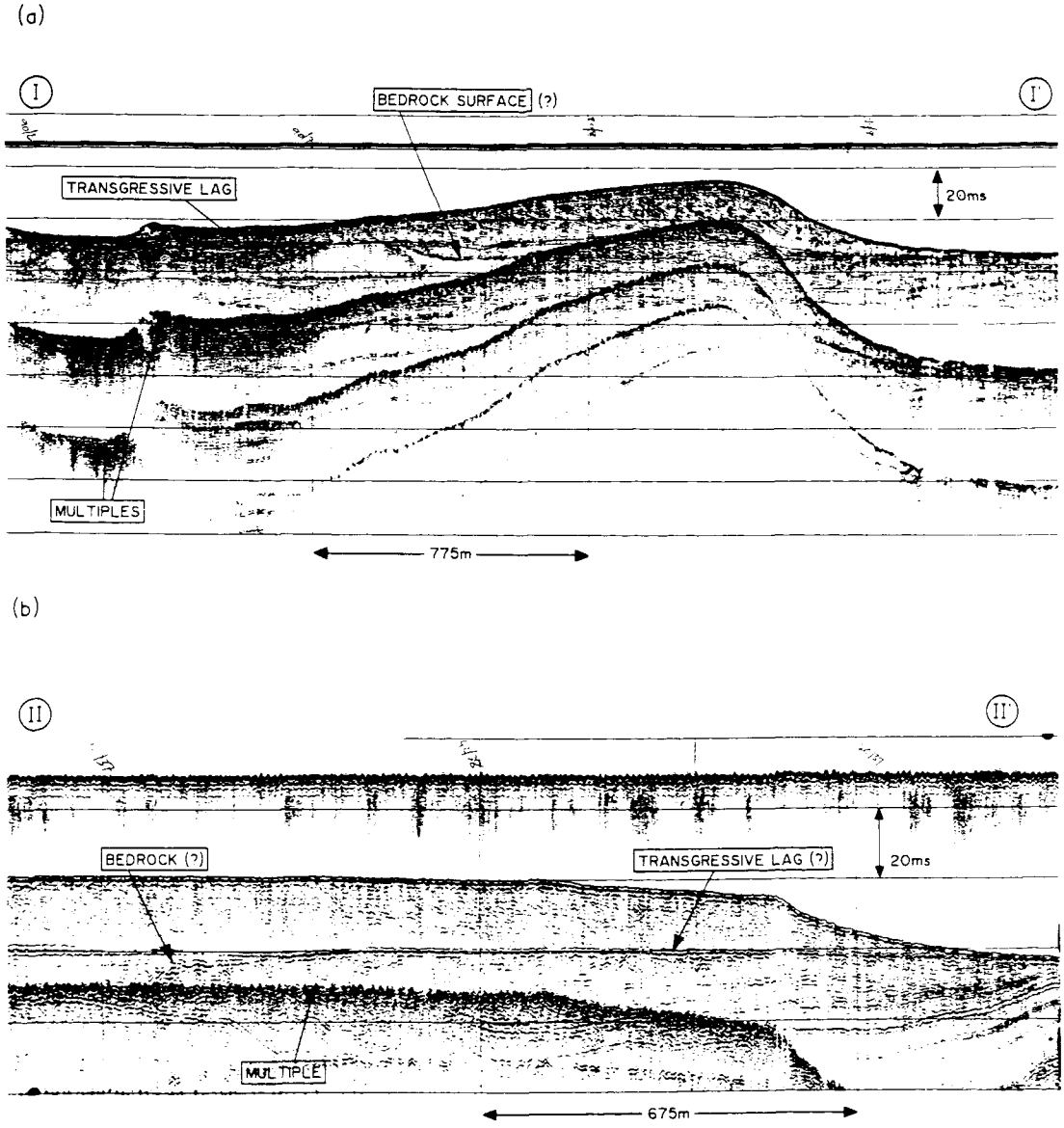

Fig. 3. Boomer record of: (A) Profile I–I'; and (B) Profile II–II' (for locations of the profiles, see Fig. 2) (made available to the authors by the British Geological Survey). In the vertical scale, 20 ms represents approximately 15 m within the water column and 18 m within the sediment.

Water movement around the Broken Bank was established through the 10 day deployment of 8 moorings (Fig. 4), with Anderra self-recording current meters positioned at 2 m above the bed and at mid-depths (Table 1). Current velocities were recorded at 10 min intervals. The stations

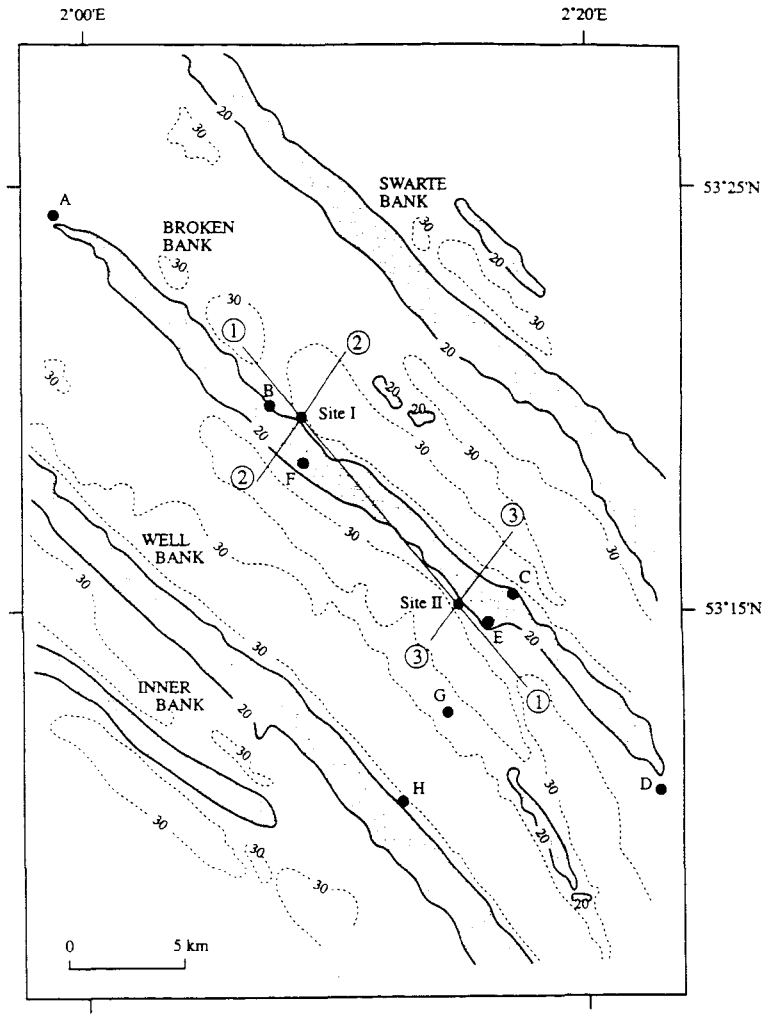

Fig. 4. Self-recording current meter mooring stations around the Broken Bank, together with locations of the fluorescent sand tracer release (Sites *I* and *II*) and (approximate) sediment sampling profiles (*1*, *2* and *3*).

were located mid-way across the stoss and lee sides of the banks, established on the basis of repeated echo-sounder surveys across the features.

Side-scan sonar surveys were undertaken during several days (using an EG&G system) over the Broken Bank area. The records obtained have a swath width of 150 m. During the survey, the vessel speed was maintained at 4 to 5 knots. These records have been analysed here to identify seabed characteristics (i.e. bedforms and the nature of the seabed).

Furthermore, an artificial sand tracer experiment was undertaken at two sites on either side of the Broken Bank (Stations I and II, Fig. 4). At each of the stations, 1000 kg of fluorescently-

Table 1
Self-recording current meter deployments within the Norfolk Banks system

Stn	Latitude	Longitude	Meter type	Meter height above bed (m)	Deployment (h)
A	53°24.6'N	01°58.2'E			Mooring Lost
B	53°19.9'N	02°06.5'E	RCM45	2	231.7
			RCM45	10	
			UCM2	12	
C	53°15.4'N	02°16.2'E	RCM45	2	239.9
			RCM45	12	
			UCM2	14	
D	53°10.7'N	02°22.2'E			No data*
E	53°14.9'N	02°15.3'E	RCM45	2	242.2
			RCM45	10	
			UCM2	12	
F	53°18.6'N	02°08.1'E	RCM45	2	263.6
			RCM45	12	
G	53°12.7'N	02°13.4'E	RCM45	2	263.5
			UCM2	12	
H	53°10.7'N	02°11.2'E	RCM45	2	259.4
			UCM2	12	

* Recovered, but no intelligible data. RCM45 = Aanderra Current Meter; UCM2 = Simrad Ultrasonic Current Meter (see text).

dyed sand of a mean grain size similar to that determined for the study area was deposited. The tracer injection (at the bed, through the inversion of an airline cargo bag (cf. Lees, 1979) was undertaken on 15 November, around High Water and 4 days after the maximum spring tides around this period. Subsequent sampling of the sea-floor was undertaken using a Shipek grab around the sand tracer deposition sites, some 6 to 8 days after the release of the tracer (during RRV *Challenger* Cruise 40, when 118 samples were taken) and 9 months after injection [in August 1989, when 70 samples were collected along three profiles (Fig. 4)].

The position fixing system used for most of the survey work was Decca Main Chain which, for the study area, had an error estimate of the order of a few hundred metres. This accuracy was improved upon, during both the release of the tracer and the first post-injection survey, through radar fixing from adjacent gas production platforms. At such times, position fixing errors of ±150 m were anticipated.

3.2. Current meter data and bedload transport formulae

Emphasis is placed here upon the horizontal displacement of water particles (rather than the analysis of vertical currents measured by the ultrasonic current meters, which will be attempted elsewhere). Hence, current meter data from each of the stations were incorporated into empirically-derived formulae to predict bedload transport.

Bedload transport rates under unidirectional (tidal) currents were derived on the basis of the Gadd et al. (1978) and Hardisty (1983) equations, which have been used widely in similar investigations in the marine environment. According to Gadd et al. (1978):

$$\mathbf{q}_b = \beta(|\mathbf{U}_{100}| - U_{100.cr})^3 \frac{\mathbf{U}_{100}}{|\mathbf{U}_{100}|} \quad (1)$$

where $\mathbf{q}_b$ is bedload transport rate, β is a proportionality coefficient, and variables in bold form denote vector quantities. The Hardisty (1983)

equation adopts a somewhat different form:

$$\mathbf{q}_b = k_1(|\mathbf{U}_{100}|^2 - U_{100.cr}^2)\mathbf{U}_{100} \quad (2)$$

where k_1 is a parameter relating to grain diameter. In order to determine the parameters β and k_1, grain size analysis was undertaken on 53 samples covering the whole of the Broken Bank. On the basis of this approach, the mean grain size for each of the samples was calculated.

In both equations, $U_{100.cr}$ is determined from the critical near-bed shear stress $\tau_{0.cr}$, using the relationship:

$$\tau_{0.cr} = C_d \rho U_{100.cr}^2 \quad (3)$$

where C_d is the mean drag coefficient, taken as 3×10^{-3} (Sternberg, 1972) (this parameter has been observed over the study area to range between 1.9×10^{-3} and 4.3×10^{-3} (Huntley et al., 1993)). $\tau_{0.cr}$ is determined using a modified Shields curve (Yalin, 1972).

To predict the mode of sediment transport (cf. Sternberg et al., 1985) in the vicinity of the Norfolk sandbanks, currents measured at 2 m above the seabed were converted using the logarithmic velocity profile law to those at 1 m, through:

$$\mathbf{U}_{100} = \frac{\ln 100 - \ln Z_0}{\ln 200 - \ln Z_0}\mathbf{U}_{200} \quad (4)$$

In order to undertake a preliminary investigation of the influence of storm waves on sediment transport rates, the Hardisty equation was used, but with $\mathbf{U}_{100}$ being replaced by $\mathbf{U}_{100.wc}$. $\mathbf{U}_{100.wc}$ was determined from the vector τ_{wc}, calculated using the Bijker (1967) method:

$$\tau_{wc} = \tau_c + \tau_1 + \tau_2 \quad (5)$$

where τ_c is the near-bed shear stress due to tidal currents, τ_1 is the component of the wave-induced near-bed shear stress parallel to the direction of the currents, and τ_2 is the perpendicular component. The magnitude of these two quantities can be expressed as:

$$\frac{\tau_1}{\tau_c} = 1 + (0.36\text{-}0.14\cos^2\theta)\left(\zeta\frac{U_0}{U_d}\right)^2 \quad (6)$$

and

$$\frac{\tau_2}{\tau_c} = 0.205\sin^2\theta\left(\zeta\frac{U_0}{U_d}\right)^{0.125} \quad (7)$$

where θ is the angle between the shear stresses due to the tidal currents and wave-induced currents, U_0 is instantaneous wave-induced orbital speed, and U_d is the depth-averaged current speed. In Eqs. 6 and 7:

$$\zeta = 0.45\ln\left(\frac{h}{Z_0} + 1\right) \quad (8)$$

where h is the water depth and Z_0 is the seabed roughness length (taken as 0.5 cm for such environments).

3.3. Bedform and fluorescent sand tracer analyses

Information on sediment transport pathways, obtained on the basis of the asymmetric sandwave profile patterns, was extracted from the side-scan sonar records. Locations where sandwaves were present were identified along the survey tracks. The trending direction of the sandwave crestline, in relation to the direction in which the vessel was moving, was calculated then using a distortion correction algorithm (Voulgaris and Collins, 1991). Finally, any asymmetry present in the bedforms was used as an indication of net bedload transport directions.

For the tracer experiment, each of the grab samples was wet sieved through a 0.063 mm mesh to remove any fine-grained material and salt. The sample was subsequently dried and split, using a riffle box. A sub-sample was spread out thinly over a black piece of card, marked with a grid and placed under an ultra-violet light. The number of fluorescent grains present in each sub-sample was counted, with concentrations in terms of the number of grains per kilogramme.

In order to determine sediment transport rates, the centroid of the tracer distribution was calculated using the data collected from Cruise 40 (i.e. 6 to 8 days after release), using the method presented by Heathershaw and Carr (1977). However, because of insufficient spatial sampling coverage and positioning inaccuracy during the subsequent

survey, the use of the tracer data is somewhat limited. Hence, the results of the tracer study were used only qualitatively in the overall interpretation of transport pathways.

4. Results

4.1. Water movement

The observed current velocities, at mid-depth and near the bed, are listed in Table 2. Generally, current speeds recorded at mid-depth were grater than those at 2 m above the bed; similarly, those near to the crestline of the Broken Bank were slightly higher than those recorded in the intervening swales.

The mid-depth and near-bed residuals are indicative of a clockwise pattern of water movement around the Broken Bank (Table 2; Fig. 5). At the same time, the near-bed residuals are more aligned with the axes of the Well and Broken Banks, for those stations located on the flanks of the banks (i.e. Stations C and E). Interestingly, there is some indication of residual water movement *between* the banks within the swales (Station G) in an offshore direction. Although insufficient data were available to carry out a complete analysis of the vertical velocity structure, the near-bed residuals were deflected (clockwise at Station B, but anticlockwise at Stations E and H) relative to those at mid-depth within the water column. Thus, only the currents observed at Station B supported the helical secondary flow hypothesis.

4.2. Sediment transport: modes and rates

The seabed sediments had, on the basis of grain size analysis, a mean grain size of around 0.2 mm. The magnitude of current speeds and the particle size indicated that the transport mode lies approximately at the boundary between material moving in suspension and as bedload (Sternberg et al., 1985). Transport takes place nominally as bedload, under the influence of tidal currents alone, over the region. Nonetheless, only a small increase in the near-bed currents, caused by superimposed wave-induced oscillatory motion or storm surges, could lead to the material being mobilised into suspension. This observation could have important implications in the comparison of localised (tidally-controlled) transport pathways, with regional

Table 2
Observed tidal current velocities (with U_{max}, U_{mean} and U_R representing maximum, mean and residual current velocities, respectively)

Stn	Tide	Height above bed (m)	U_{max} (m s^{-1}) (°N)		U_{mean} (m s^{-1}) (°N)		U_R (m s^{-1}) (°N)
			Flood	Ebb	Flood	Ebb	
B	Spring	2	0.80 (138)	0.54 (320)	0.44 (143)	0.29 (317)	0.09 (152)
		10	0.94 (127)	0.62 (326)	0.52 (130)	0.34 (321)	0.11 (113)
	Neap	2	0.51 (137)	0.41 (314)	0.22 (150)	0.19 (316)	0.01 (144)
		10	0.48 (88)	0.45 (333)	0.25 (121)	0.22 (324)	0.04 (40)
C	Spring	2	0.83 (141)	0.63 (311)	0.42 (142)	0.32 (328)	0.06 (125)
	Neap	2	0.54 (142)	0.36 (336)	0.26 (141)	0.16 (318)	0.04 (148)
E	Spring	2	0.70 (153)	0.84 (329)	0.35 (146)	0.39 (331)	0.05 (349)
	Neap	2	0.41 (154)	0.37 (320)	0.21 (152)	0.19 (327)	0.04 (290)
		10	0.44 (148)	0.39 (321)	0.23 (155)	0.21 (322)	0.05 (296)
G	Spring	2	0.68 (160)	0.73 (343)	0.36 (148)	0.39 (337)	0.03 (41)
		12	0.86 (152)	0.80 (351)	0.49 (150)	0.47 (344)	0.06 (58)
	Neap	2	0.39 (135)	0.40 (332)	0.24 (140)	0.28 (323)	0.05 (330)
		12	0.48 (153)	0.53 (259)	0.26 (156)	0.27 (319)	0.04 (210)
H	Spring	2	0.97 (133)	0.62 (326)	0.50 (142)	0.36 (323)	0.11 (140)
		12	1.12 (146)	0.64 (327)	0.57 (146)	0.39 (325)	0.14 (148)
	Neap	2	0.58 (151)	0.44 (325)	0.33 (135)	0.28 (325)	0.04 (98)
		12	0.63 (149)	0.49 (312)	0.33 (147)	0.27 (310)	0.07 (185)

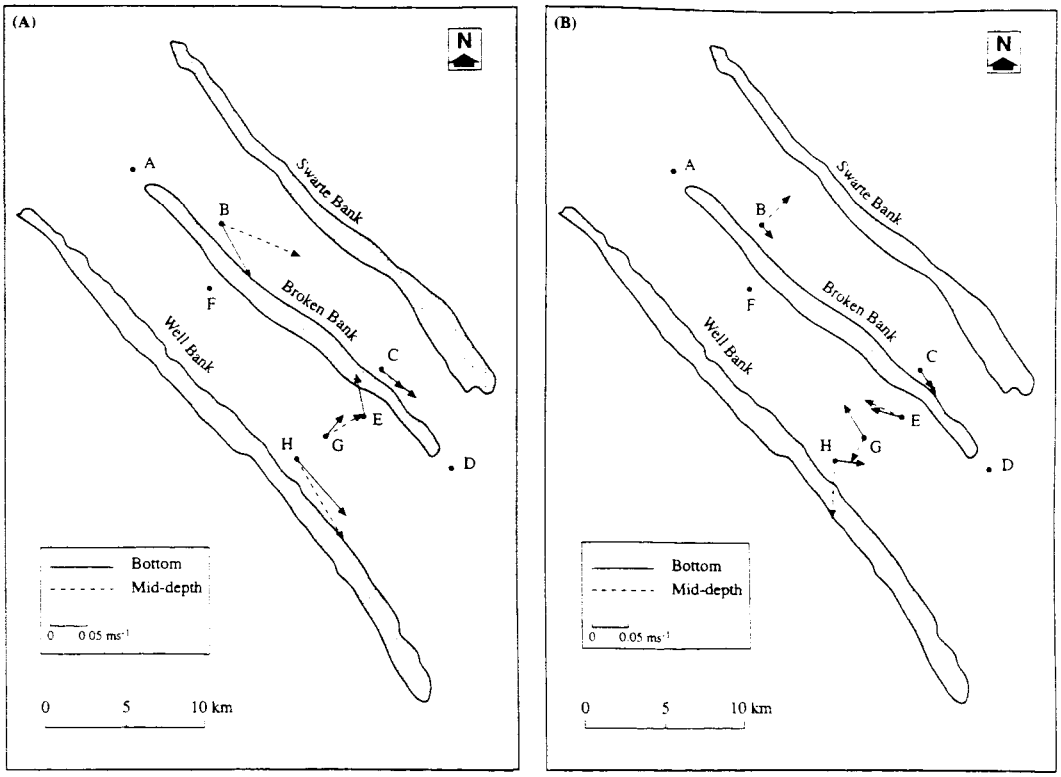

Fig. 5. Residual current speeds around the Norfolk Banks on: (A) springs; and (B) neaps.

patterns of sediment movement, under the influence of storm-induced currents.

Based upon the grain size data, β in Eq. 1 was taken as 4.88 kg m^{-4} s^2, with k_1 in Eq. 2 as 1.2 kg m^{-4} s^2. A roughness length (Z_0) of 0.5 cm was used in Eqs. 4 and 8. Representative transport rates, determined on the basis of the Gadd et al. (1978) and Hardisty (1983) equations, for each of the stations are summarised in Table 3. The results obtained for Stations B and E, located on the northeastern and southwestern flanks of the Broken Bank respectively, are indicative of clockwise bedload transport around the sandbank on both spring and neap tides. Such movement is consistent with that of the residual water movement, described previously. The predicted rates, averaged over a spring-neap tidal cycle, are greater for the eastern sides of the Broken Bank (Stations B and C) and the Well Bank (Station H), than on their western sides and within the swale between the banks (Stations E and G) (Fig. 6).

For the investigation of the superimposed influence of waves on bedload transport, wave conditions typical of the various seasons were used in the calculations for combined flows (i.e. $H_z = 4.5$ m and $T = 8.0$ s for winter; $H_z = 3.5$ m and $T = 7.0$ s for spring; $H_z = 2.5$ m and $T = 7.0$ s for summer; and $H_z = 4.0$ m and $T = 7.5$ s for autumn), as obtained from the available published wave data (Draper, 1968). The resultant net transport rates, in response to wave-current interaction (Fig. 7), show generally that the component directed towards the sandbank crestline increases with an increase in wave height. Thus, wave action tends to intensify the transport of sand towards the crestline of the banks.

Table 3
Characteristic sediment transport rates, calculated using the Gadd et al. (1978) and Hardisty (1981) equations ($q_{sb.max}$, $q_{sb.mean}$ and $q_{sb.R}$ represent maximum, mean and residual transport rates, respectively)

Stn	Tide	Eqn.	$q_{sb.max}$ (kg m^{-1} s^{-1}) (°N)		$q_{sb.mean}$ (kg m^{-1} s^{-1}) (°N)		$q_{sb.R}$ (kg m^{-1} s^{-1}) (°N)
			Flood	Ebb	Flood	Ebb	
B	Spring	GA	1.1 (138)	0.21 (320)	0.24 (143)	0.033 (319)	0.10 (144)
		HA	0.20 (138)	0.031 (320)	0.049 (142)	0.012 (319)	0.019 (145)
	Neap	GA	0.15 (150)	0.054 (314)	0.0099 (141)	0.0025 (315)	0.0036 (143)
		HA	0.045 (150)	0.023 (314)	0.0045 (140)	0.002 (315)	0.0012 (145)
C	Spring	GA	1.3 (142)	0.43 (330)	0.21 (141)	0.057 (331)	0.079 (139)
		HA	0.22 (142)	0.093 (330)	0.043 (142)	0.017 (331)	0.015 (138)
	Neap	GA	0.21 (143)	0.025 (336)	0.021 (141)	0.0006 (327)	0.009 (149)
		HA	0.057 (143)	0.014 (336)	0.0075 (141)	0.0008 (322)	0.0033 (141)
E	Spring	GA	0.66 (153)	1.3 (329)	0.098 (150)	0.19 (333)	0.054 (335)
		HA	0.13 (153)	0.23 (329)	0.026 (149)	0.039 (333)	0.009 (337)
	Neap	GA	0.05 (154)	0.027 (327)	0.0044 (152)	0.0017 (328)	0.0087 (158)
		HA	0.022 (154)	0.015 (327)	0.0029 (153)	0.0017 (328)	0.0013 (180)
G	Spring	GA	0.56 (160)	0.78 (343)	0.098 (147)	0.13 (338)	0.019 (9)
		HA	0.12 (160)	0.15 (343)	0.026 (149)	0.031 (338)	0.007 (8)
	Neap	GA	0.037 (135)	0.048 (332)	0.0059 (147)	0.011 (328)	0.0035 (329)
		HA	0.018 (135)	0.021 (332)	0.0049 (145)	0.0067 (327)	0.0016 (330)
H	Spring	GA	2.4 (133)	0.37 (326)	0.38 (141)	0.077 (324)	0.18 (140)
		HA	0.36 (133)	0.087 (326)	0.072 (141)	0.022 (324)	0.03 (140)
	Neap	GA	0.29 (151)	0.072 (325)	0.044 (137)	0.013 (327)	0.016 (133)
		HA	0.07 (151)	0.027 (325)	0.015 (138)	0.0069 (326)	0.0042 (132)

GA = Gadd et al. (1978); HA = Hardisty (1983).

4.3. Bedform orientation

Side-scan sonar results show there to be mega-ripples present throughout the study area; these are likely to vary in their asymmetry, at different stages of the tidal cycle. The distribution of sandwaves is discontinuous; they are present only over relatively small sections along the survey tracks. The sandwaves are 2 to 4 m in height and around 50 m in wavelength. The asymmetry of such large sandwaves can be related to the net sediment transport direction (e.g. Langhorne, 1982). Net transport pathways, identified on the basis of sandwave asymmetry (Fig. 8) show: (1) the movement of sand around the banks, in a clockwise direction, particularly on either side of the Broken Bank; (2) sand transport onto the banks, from both their gently-sloping southwesterly faces and the more steeply-sloping northeasterly flanks; (3) some indication of sand transfer between the banks, in a northeasterly direction; and (4) in a particular instance, a pattern of sandwave convergence in the northwestern part of the swale *between* the Broken and Well Banks (Location X, on Fig. 8).

The latter feature is of particular interest, in that it may represent an *embryonic* form of sandbank formation (Huntley et al., 1993). Coalescence of sandwaves, to either side of a bathymetric "high" rising only 6 m above the surrounding seabed could represent the processes similar to those identified (i.e. clockwise water and sediment circulations) for a well-developed sandbank within the region. Sand movement to the southeast of this convergence (Location Y, on Fig. 8), as indicated by the sandwave asymmetry, is consistent with the direction of near-bed water movement and the predicted bedload transport pathways (Station G, on Figs. 5 and 6).

On the basis of these observations, there is evidence of tidally-induced transport on either side of the bank, in opposite directions, and onto the bank. There is also some indication of movement between the sandbanks, in a northeasterly direction.

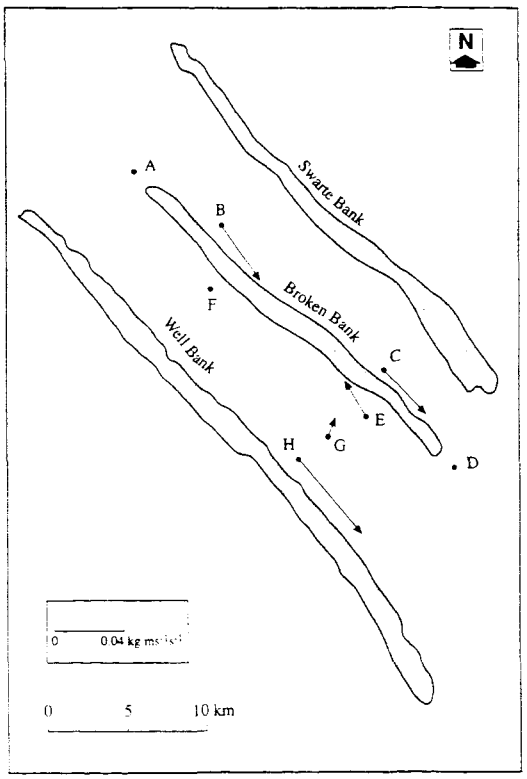

Fig. 6. Net sediment transport rate on springs, on the basis of predictions using the Gadd et al. (1978) equation.

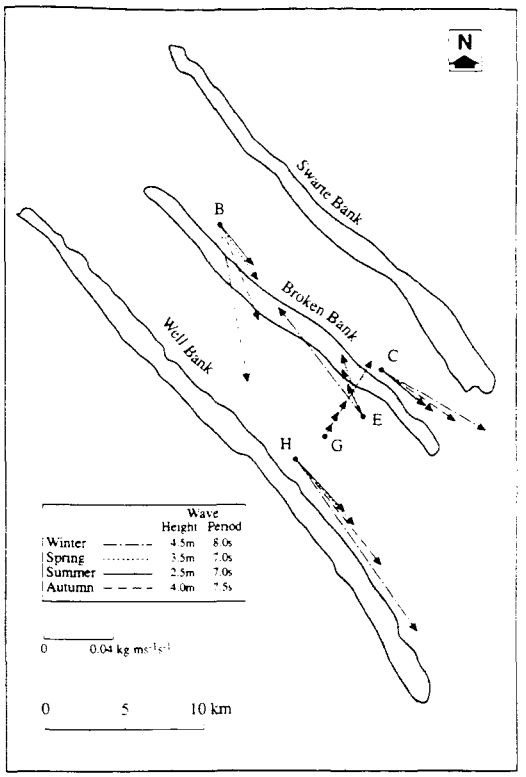

Fig. 7. Vectors of bedload transport rates, under various wave–current combinations, for wave heights and periods representative of different seasons.

4.4. *Fluorescent sand tracer movement*

On the basis of spatially-distributed samples collected during RRS *Challenger* Cruise 40, the movement of the centroid of the fluorescent sand for the period between 15 and 25 November, 1988, has been derived. At Site I, movement of the centroid was shown to be directed towards N50°W. The movement at Site II was towards N70°W. However, the distance identified in both cases was within the error range of the Decca (Main Chain) position fixing (i.e. ±150 m) and, therefore, unreliable. For the data collected during subsequent (*Challenger*) cruises, most of the sampling positions were biased towards one side of the tracer injection sites. Thus, the results obtained cannot be used to derive bedload transport rates. Notwithstanding these limitations, the preliminary analysis presented here is based upon samples collected some 267 days after release (when sampling took place essentially parallel to the crestline and along two cross-sections of the bank).

Seabed samples collected during August, 1989, show fluorescent sand concentrations of around 3000 grains per kilogramme at Site I and 1000 to 2000 at Site II (Fig. 9). Along a direction approximately parallel to the crestline of the sandbank, sand movement appears to be towards the south-east at both sites. Such an interpretation is based upon the inferred location of the centroid. [Note: the observed peak in concentration at sampling location 55 may represent a tidally-induced "bias" introduced at the time of release (see above)].

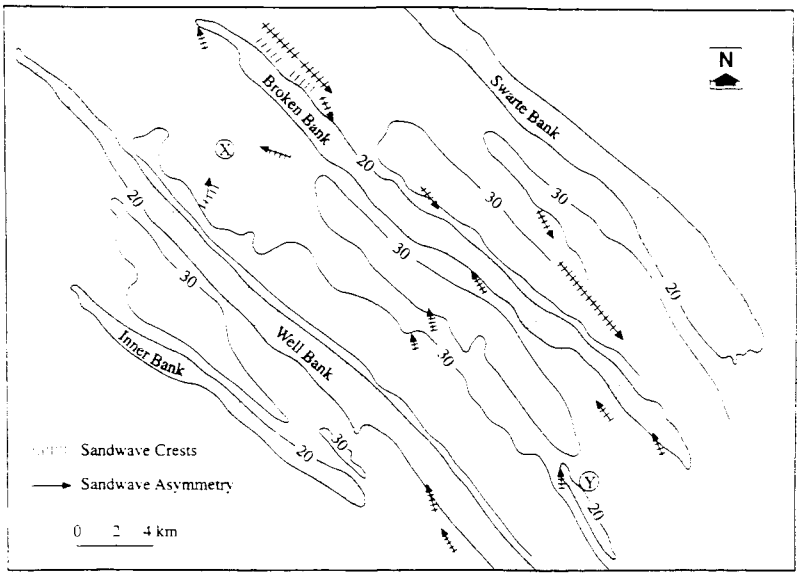

Fig. 8. Sandwave distribution and patterns of (asymmetric) crestline orientation (along the survey track lines *only*) over the Broken Bank (for locations *X* and *Y*, see text).

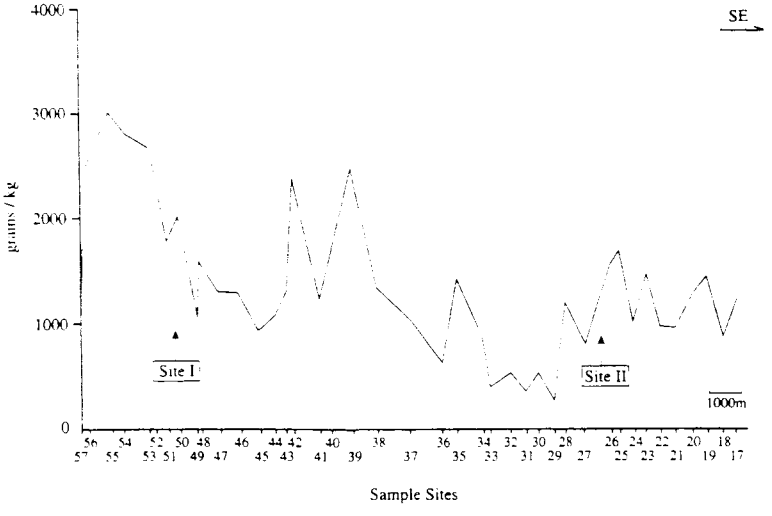

Fig. 9. Concentration of fluorescent sand along the axis of the Broken Bank (Sampling Profile 1, see Fig. 4), 267 days after injection of the tracer.

The peaks in concentration along the two sampling profiles across the crestline (Fig. 10) cannot be explained fully. Cross-bank movement can be interpreted as being towards the northeast at Site II, in the apparent direction of centroid movement. Tracer concentrations at Site I are approximately

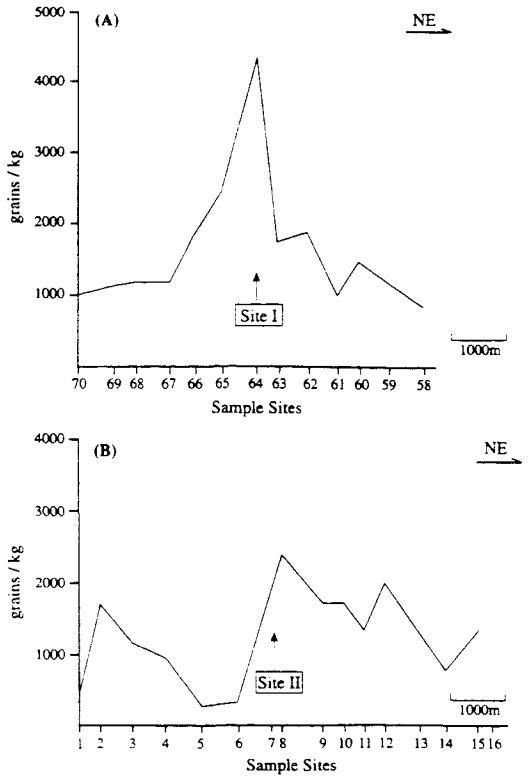

Fig. 10. Distribution of tracer concentration along two profiles across the Broken Bank (Sampling Profiles 2 and 3, see Fig. 4), 267 days after injection of the tracer.

symmetrical about a concentration at the injection point. This latter pattern of movement could represent both clockwise tidally-induced residual circulation and an overall net sediment transport towards offshore.

5. Discussion

5.1. Linear sandbank formation and maintenance

Comparison between mid-depth and near-bed observations of water movement shows some veering in the residual currents. The near-bed residuals near the banks are effectively sub-parallel to the axis of the sandbanks themselves. This pattern is similar for both the Broken and Well Banks and is indicative of clockwise water movement. Elsewhere, on the basis of self-recording current meter measurements along the northwestern part of the Well Bank (Howarth and Huthnance, 1984), residual currents were sub-parallel to the bank but in opposing directions to either side of it. The mean currents on the northeastern side of the bank were stronger than those along the southwestern flank; this is consistent with the results of the present investigation (Table 2).

Such clockwise residual flow, sub-parallel to the axis of the sandbank, could result from the anticlockwise orientation of the sandbank with respect to the tidal flow (Caston and Stride, 1970). The effects of friction and water column stretching would reinforce each other, producing clockwise vorticity and residual circulation (Zimmerman, 1981; Robinson, 1983). The Coriolis and frictional (bottom drag) effects, which are of similar strength over the Norfolk sandbanks, have been shown in a mathematical model (Huthnance, 1973) to produce the observed circulation patterns.

At Station B, veering in the mid-depth currents is away from the bank; this could be an indication of secondary flow patterns in the vicinity of northwestern parts of the sandbanks, consistent with the "helical flow" concept of Houbolt (1968). Nonetheless, at Stations E and H, the observed patterns contradict the "helical flow" concept. To investigate this hypothesis more fully, detailed information on the vertical current structure is required.

Sand transport directions, inferred from the asymmetry sandwaves adjacent to the banks, is consistent with the clockwise pattern of (residual) water movement. Such an observation is, in itself, in agreement with the findings of Caston and Stride (1970) for the Leman and Well Banks. On the basis of their evidence, these investigators postulated the clockwise circulation of sand around the banks. This concept was extended further by Caston (1972), in relation to Houbolt's (1968) original observations, to explain the crestline as a line of convergence of sandwaves veering towards the bank crest. The sandwaves changed their orientation as they approached the bank crestline, from being normal to the crestline in the

swales adjacent to the bank, to almost parallel to the axis on either side of the crest. This interpretation was based upon data collected in the vicinity of the Leman and Ower Banks; it corresponds to the sandwave orientations observed during the present investigation.

Other investigators (Caston, 1972; McCave and Langhorne, 1982) have shown that symmetrical sandwaves occur at the ends of a sandbank, indicating zero net transport, together with megaripples trending at very high angles with respect to the bank axis. Such a pattern was believed to be indicative of sediment circulation around the bank. Caston (1981) suggested, however, that there was no evidence for a circulation of sand around the bank: sand enters the bank system through a low apron at the broad head of the bank, then leaves by the narrower tail. The geophysical data and current observations (due to equipment losses) obtained during this study do not, unfortunately, cover the extreme ends of the bank. Hence, these theories cannot be disputed or confirmed.

On the basis of the above synthesis, the present investigation of water movement and bedload transport pathways has provided further evidence for the pattern of residual circulations around a linear sandbank (Caston, 1970; Caston and Stride, 1972; Kenyon et al., 1981; Huthnance, 1982a, 1982b). Such mechanisms relate to the *maintenance* of sandbanks.

With regard to the initial *formation* of such banks, Huthnance (1982a, 1982b) has proposed the requirement for strong currents and the presence of some initial irregularities, or humps, on the seabed. However, such conditions may not be necessary i.e. other mechanisms may cause sandbank growth. For example, flat estuarine/coastal deposits or Tertiary bedrock surfaces have been found generally to underlie a number of the North Sea sandbanks (Eisma, 1988; Liu et al., 1992; Trentesaux et al., 1993; Berné et al., 1994). For the Broken Bank, the sub-bottom profiler images (Fig. 3) demonstrate, once again, the presence of a flat and featureless base to the sandbank development. Although in Huthnance's models no significant seabed irregularities are needed, combined with the fact that conditions at the initial stage of the sandbank growth cannot be inferred from the underlying deposits, the possibility cannot be excluded that the early stages of bank development is controlled hydrodynamically i.e. without any perturbations or humps on the seabed.

Bedforms revealed on the side-scan sonar records may define a bedload transport convergence at a location within the swale between the bans (Fig. 8); this may represent the initiation of an *embryonic* sandbank. In fact, a number of such smaller-scale sandbanks exist as topographic highs within the swales between the Swarte, Broken and Well Banks (Fig. 2).

Hence, although secondary flows in such an environment have been observed only rarely (McCave, 1979) (in the present investigation, the helical-like flows were observed only at Station B), such a mechanism may be important in terms of sandbank growth at an initial stage. Subsequently, other mechanisms (such as the around-bank residual circulation) may begin to predominate the water and sediment movement, once the initial stage of sandbank development has been completed.

5.2. Regional characteristics

Within the swales of the sandbanks of the region, southeasterly currents are generally stronger than their northwesterly counterparts. This pattern of water movement appears to be consistent with the regional sediment transport patterns: to the northwest of the study area, a bedload parting zone has been identified, which defines southeasterly transport over the sandbank areas (Stride, 1963; see also Chang and Evans, 1992). The bedload transport rates derived here, using empirical formulae and self-recording current meter data, indicate slightly higher rates of transport in a southeasterly direction on the eastern side of the Broken Bank, than on the western side.

In the swale between the Well and Broken Banks, the observed near-bed residual current is in an offshore (northeasterly) direction. Such water movement contrasts with the result of Caston and Stride (1970), where long-term residual currents in the swale between the Well and Leman Banks were towards the northwest. Such differences may represent, however, the prevailing meteorological

conditions during each of the measurement periods. Nevertheless, there is a northerly residual flow component in both data sets.

Along a transect across the banks, incorporating current meter stations H, G, E and C, residual water movement and sediment transport alternates as follows: southeasterly, northeasterly, northwesterly and southeasterly again. Such changes in direction are indicative of water and sand circulation cells associated with the North Sea sandbank systems (Fig. 11).

Within the swales, there is a high incidence of occurrence of sandwaves indicating a component of sand transport in a northeasterly direction: this is confirmed, at Station G, by the near-bed residual water movement (Fig. 5). Although no direct evidence of such sandwave migration appears to have been reported elsewhere, various investigators have suggested sand transport towards the northeast, based upon: (1) internal bedding directions, sandbank movement and asymmetry of the banks themselves (Houbolt, 1968); and (2) prediction of long term and overall sand transport directions towards the northeast, based upon the numerical modelling of tidally- and storm surge-induced currents (Stride, 1988).

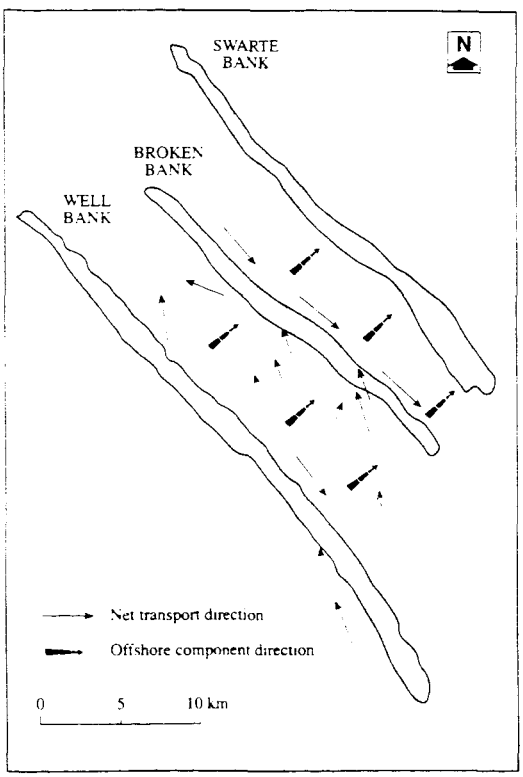

Fig. 11. Regional sediment transport pathways, derived on the basis of current information, bedload transport calculations, geophysical surveys, and (sand) tracer experiments.

The data from the present study are indicative of some transport of sand in an offshore direction between the banks (Fig. 11), which would confirm the hypothesis of Stride (1988). Hence, the banks act as "stepping stones", transporting sand from the East Anglian coastline to seaward. Such transport has been shown here to occur not only during storms, but also under "normal" (tidal and low wave) hydrodynamic conditions; it has been derived also elsewhere on the basis of regional tidal current patterns and grain size trends (I.H. Townend and P. McLaren, pers. commun.). Such an observation is consistent with previous investigations into regional residual water movement (Maier-Reimer, 1977) and that of suspended sediments in the water column (Howarth et al., 1994). It is likely that a combination of the strong instantaneous currents within the swales, together with the residual currents directed offshore, causes sediment movement across the swales from the coast towards the deeper waters.

The proposed offshore transport pathway may cause the sandbanks to grow vertically or laterally in response to deposition, and/or accretion to take place in the offshore waters. A comparison of the morphology of the sandbanks, using historical bathymetric charts (undertaken by some of the present authors, as part of a commercial contract), reveals only limited changes or lateral migration of the features.

The sedimentary structure of the southeastern part of the Broken Bank (Profile II–II', Fig. 3) does not provide any extensive evidence of lateral migration of the sandbank. Only at its northwestern end is there any (sedimentary) indication that this part of the Bank is moving towards the northeast (Profile I–I', Fig. 3). The end parts of the sandbank can be dynamically very active in

terms of sediment mobility (evidence for this may be provided by the fact that the current meters deployed at the both ends were lost, in contrast to the recovery of the other deployments). However, such mobility is assessed on a time scale which is small compared with that for sandbank migration and development (i.e. 10^2 years) (Huthnance, 1982a; Howarth and Huthnance, 1984). It is suggested, therefore, that the material transported offshore is dissipated partly into the deeper waters: it contributes also partly to the development and maintenance of the sandbank system itself (perhaps causing slow lateral migration).

6. Summary

Geophysical surveys, self-recording current meter observations and longer-term fluorescent sand tracer studies have been undertaken to investigate water and sediment movement in the vicinity of some of the Norfolk Banks.

Much of the data presented reinforces the observations and mechanisms for sandbank maintenance presented previously, with particular reference to the North Sea i.e. the clockwise circulation of water and sand around the bank, with sandwaves converging at the crestline. Although helicoidal secondary circulation does not appear to be a predominant process, it may be one of the dominant mechanisms causing the initial growth of such sandbanks.

The regional information, obtained on water movement, sandwave asymmetry and orientation, and the movement of the fluorescent sand tracer, is all indicative of an offshore sand transport component. Such observations support the hypotheses proposed by other investigators, on the basis of geomorphological observations and numerical model predictions for storm conditions. Further, such transport pathways may take place under "normal" hydrodynamic conditions, as opposed to being restricted to storm activity. Material transported offshore is dissipated partly into the deeper water areas, but is also accumulated within the sandbank system.

Acknowledgements

We wish to thank the British Geological Survey, Keyworth (Dr. P.S. Balson) for providing the sub-bottom profiler records across the Broken Bank. Mrs K. Davis kindly assisted in the preparation of the figures. The captain and crew of RRS *Challenger* are acknowledged for their support, together with technicians from RVS Barry and Proudman Oceanographic Laboratory (POC). The study formed part of the (NERC) North Sea Community Programme (Process Studies), undertaken in association with POL (Dr J.M. Huthnance). During the preparation of the manuscript, one of the authors (MBC) was in receipt of an EU MAST Research Grant (CSTAB: Circulation and Sediment Transport Around Banks). Finally, the authors are grateful for the constructive and philosophical comments of Don Swift, Serge Berné and Peter Balson, together with those of an anonymous reviewer.

References

Balson, P.S. and Harrison, D.J., 1988. Marine Aggregate Survey Phase 1: Southern North Sea. Br. Geol. Surv., Mar. Rep., 86 38, 20 pp. (and maps).

Belderson, R.H., 1986. Offshore tidal and non-tidal sand ridges and sheets: differences in morphology and hydrodynamic setting. In: R.J. Knight and J.R. McLean (Editors), Shelf Sands and Sandstone. Can. Soc. Pet. Geol. Mem., 11: 293–301.

Berné, S., Trentesaux, A., Stolk, A., Missiaen, T. and De Batist, M., 1994. Architecture and long term evolution of a tidal sandbank: The Middelkerke Bank (southern North Sea). Mar. Geol., 121: 57–72.

Bijker, E.W., 1967. The increase of bed shear in a current due to wave motion. Proc. 10th Coastal Eng. Conf. ASCE, pp. 746–765.

Caston, G.F., 1981. Potential gain and loss of sand by some sandbanks in the southern North Sea off northeast Norfolk. Mar. Geol., 41: 239–250.

Caston, V.N.D., 1972. Linear sand banks in the southern North Sea. Sedimentology, 18: 63–78.

Caston, V.N.D. and Stride, A.H., 1970. Tidal sand movement between some linear sand banks in the North Sea off northeast Norfolk. Mar. Geol., 9: M38–M42.

Chang, S.C. and Evans, G., 1992. Sources of sediment and sediment transport on the east coast of England: significant or coincidental? Mar. Geol., 107: 283–288.

Draper, L., 1968. Waves at Smith's Knoll, North Sea. Natl. Inst. Oceanogr. Inter. Rep., A33.

Eisma, D., 1988. An introduction to the geology of continental shelves. In: H. Postma and J.J. Zijlstra (Editors), Continental Shelves. (Ecosystems of the World, 27.) Elsevier, Amsterdam, pp. 39–91.

Flather, R.A., 1987. Estimates of extreme conditions of tide and surge using a numerical model of the north-west European continental shelf. Estuarine Coastal Mar. Sci., 24: 69–93.

Gadd, P.E., Lavelle, J.W. and Swift, D.J.P., 1978. Estimates of sand transport on the New York Shelf using near bottom current meter observations. J. Sediment. Petrol., 48: 239–252.

Hardisty, J., 1983. An assessment and calibration of formulations for Bagnold's bedload equation. J. Sediment. Petrol., 53: 1007–1010.

Heathershaw, A.D. and Carr, A.P., 1977. Measurements of sediment transport rates using radioactive tracers. Coastal Sediments. ASCE, pp. 399–416.

Houbolt, J.J.H.C., 1968. Recent sediments in the southern bight of the North Sea. Geol. Mijnbouw, 47(4): 245–273.

Howarth, M.J. and Huthnance, J.M., 1984. Tidal and residual currents around a Norfolk sandbank. Estuarine Coastal Shelf Sci., 19: 105–117.

Howarth, M.J., Dyer, K.R., Joint, I.R., Hydes, D.J., Purdie, D.A., Edmunds,H., Jones, J.E., Lowry, R.K., Moffat, T.J., Pomroy, A.J. and Procter, R., 1994. Seasonal cycles and their spatial variability. Philos. Trans. R. Soc. London, A343: 5–25.

Huntley, D.A., Huthnance, J.M., Collins, M.B., Liu, C.-L., Nicholls, R.J. and Hewitson, C., 1993. Hydrodynamics and sediment dynamics of North Sea sand waves and sand banks. Philos. Trans. R. Soc. London, A343: 461–474.

Huthnance, J.M., 1973. Tidal current asymmetries over the Norfolk sandbanks. Estuarine Coastal Mar. Sci., 1: 89–99.

Huthnance, J.M., 1982a. On one mechanism forming linear sand banks. Estuarine Coastal Shelf Sci., 14: 79–99.

Huthnance, J.M., 1982b. On the formation of sand banks of finite extent. Estuarine Coastal Shelf Sci., 15: 277–299.

Kenyon, N.H., Belderson, R.H., Stride, A.H. and Johnson, M.A., 1981. Offshore tidal sand banks as indicators of net sand transport and as potential deposits. In: S.-D. Nio, R.T.E. Schüttenhelm and Tj.C.E. van Weering (editors), Holocene Marine Sedimentation in the North Sea Basin. Blackwell, Oxford, pp. 257–268.

Langhorne, D.N., 1982. Study of the dynamics of a marine sandwave. Sedimentology, 29: 571–594.

Lees, B.J., 1979. A new technique for injecting fluorescent sand tracers in sediment transport experiments in a shallow marine environment. Mar. Geol., 33: M95–M98.

Liu, A.C., Missiaen, T. and Henriet, J.P., 1992. The morphology of the top-Tertiary erosion surface in the Belgian sector of the North Sea. Mar. Geol., 105: 275–284.

Maier-Reimer, E., 1977. Residual circulation in the North Sea due to the M_2-tide and mean annual wind stress. Dtsch. Hydrogr. Z., 30: 253–262.

McCave, I.N., 1979. Tidal currents at the North Hinder lightship, southern North Sea: flow directions and turbulence in relation to maintenance of sand banks. Mar. Geol., 31: 101–114.

McCave, I.N. and Langhorne, N., 1982. Sand waves and sediment transport around the end of a tidal sandbank. Sedimentology, 29: 95–110.

Off, T., 1963. Rhythmic linear sand bodies caused by tidal currents. Bull. AAPG, 47(2): 324–341.

Pattiaratchi, C. and Collins, M., 1987. Mechanisms for linear sandbank formation and maintenance in relation to dynamical oceanographic observations. Progr. Oceanogr., 19: 117–176.

Robinson, I.S., 1983. Tidally induced residual flows. In: B. Johns (Editor), Physical Oceanography of Coastal and Shelf Seas. Elsevier, Amsterdam, pp. 321–356.

Sternberg, R.W., 1972. Predicting initial motion and bedload transport of sediment particles in the shallow marine environment. In: D.J.P. Swift, D.B. Duane and O.H. Pilkey (Editors), Shelf Sediment Transport: Processes and Pattern. Dowden, Stroudsberg, pp. 61–82.

Sternberg, R.W., Larson, L.H. and Miao, Y.T., 1985. Tidally driven sediment transport on the East China Sea continental shelf. Cont. Shelf Res., 4: 105–120.

Stride, A.H., 1963. Current-swept sea floors near the southern half of Great Britain. Q. J. Geol. Soc. London, 119: 175–199.

Stride, A.H., 1988. Indications of long term episodic suspension transport of sand across the Norfolk banks, North Sea. Mar. Geol., 79: 55–64.

Swift, D.J.P., 1975. Tidal sand ridges and shoal retreat massifs. Mar. Geol., 18: 105–134.

Trentesaux, A., Berné, S., De Batist, M. and Chamley, H., 1993. Internal structure of a tidal sand bank in the southern North Sea. C.R. Acad. Sci. Paris, 316(Ser. II): 99–106.

Venn, J.F. and D'Olier, B., 1983. Preliminary observations for a model of sand bank dynamics. In: J. Sündermann and W. Lenz (Editors), North Sea Dynamics. Springer, Berlin, pp. 472–485.

Voulgaris, G. and Collins, M.B., 1991. Linear features on side-scan sonar images: an algorithm for the correction of angular distortion. Mar. Geol., 96: 187–190.

Yalin, M.S., 1972. Mechanics of Sediment Transport. Pergamon, Oxford, 290 pp.

Zimmerman, J.T.F., 1981. Dynamics, diffusion and geomorphological significance of tidal residual eddies. Nature, 290: 549–555.

SEE RELATED ADMIRALTY PUBLICATIONS: Notices to Mariners (recent, imminent and temporary changes). Sailing Directions (local conditions, directions, regulations, port information). List of Lights, List of Radio Signals (navigational warning and weather transmissions, pilot and port operations services, traffic management, radiobeacons). Tide Tables, Tidal Stream Atlases, The Mariner's Handbook (general information), 5011 (symbols and abbreviations), etc.
ENSURE CHARTS AND PUBLICATIONS ARE KEPT CORRECTED.

Depths are in metres and are reduced to Chart Datum, which is approximately the level of Lowest Astronomical Tide.

Heights are in metres. Underlined figures are drying heights above Chart Datum; all other heights are above Mean High Water Springs.

Navigational marks: IALA Maritime Buoyage System—Region A (Red to port).

Projection: Mercator. Positions are on Ordnance Survey of Great Britain (1936) Datum.

Sources: The origin, scale, date and limits of the hydrographic surveys used in compiling the chart are shown in the Source Data Diagram. The topography is derived chiefly from Ordnance Survey maps.

OIL AND GAS FIELDS

Production platforms and associated structures, including tanker moorings and platforms on pipelines, generally exhibit all or some of the following lights:

Mo(U)W.15s10 or 15M, Mo(U)R.15s2M, aircraft obstruction lights; and sound fog signals: Mo(U)30s.

Unauthorized navigation is prohibited within 500 metres of all such structures. Tankers manœuvring in the vicinity of platforms and moorings should be given a wide berth.

WELLHEADS

Substantial underwater structures, projecting up to 15 metres (50 feet) above the sea bed, are located at wellheads not at present being worked for oil or gas.

CHART 1505: POSITIONS

To agree with the adjoining chart 1505 which is referred to European Datum, positions read from this chart should be moved 0·07 minutes NORTHWARD and 0·03 minutes WESTWARD.

SATELLITE-DERIVED POSITIONS

Positions obtained from satellite navigation systems are normally referred to WGS datum; such positions should be moved 0·02 minutes SOUTHWARD and 0·12 minutes EASTWARD to agree with this chart.

OIL AND GAS PIPELINES

Mariners risk prosecution if they anchor or trawl near a pipeline and so damage it. Gas from a damaged pipeline could cause a fire or loss of a vessel's buoyancy.

WRECKS

Certain inshore wrecks within the 10 metre line are not shown on this chart and less dangerous wrecks in areas covered by larger scale charts may also be omitted.

CAUTION — CHARTED DEPTHS UNRELIABLE

As indicated by the Source Data Diagram, the soundings in the north-western part of this chart are derived from lead-line surveys 1886-1931. The charted depths, particularly on the banks, cannot be relied upon.

DW ROUTE

The Deep Water (DW) route shown on this chart has been specially surveyed for deep-draught ships. Masters must take into account possible changes in depths due to meteorological and other effects.

CAUTION — TRINITY HOUSE NAVAID REVIEW 1987 NEED TO RETAIN PREVIOUS EDITION OF THIS CHART

The details of buoys and other aids to navigation shown on this chart take into account the changes, published in the Trinity House Navaid Review 1987, which are planned to take place during 1988. Until all the changes affecting this chart have been made, mariners should retain the cancelled version, for reference with respect to the old buoyage.

Tidal Levels referred to Datum of Soundings

Place	Lat N	Long E	MHWS	MHWN	MLWN	MLWS
			Heights in metres above datum			
Cromer	52° 56′	1° 18′	5·3	4·2	1·9	0·6
Blakeney Bar	52 59	0 59	5·7	4·5	–	–
Wells Bar	52 59	0 49	6·0	4·8	–	–

For offshore data, see Co-Tidal Chart 5059

Tidal Streams referred to HW at IMMINGHAM

(Hours: Before High Water −6 to −1; High Water 0; After High Water +1 to +6. For each geographical position: Directions of streams (degrees), Rates at spring tides (knots), Rates at neap tides (knots).)

Hours	A 53°14′·5N 0 57·0E			B 53°33′·7N 0 59·3E			C 53°27′·0N 1 05·0E			D 53°05′·4N 1 13·2E			E 52°59′·0N 1 35·0E			F 53°17′·0N 1 38·0E			G 53°37′·5N 1 38·2E			H 53°24′·0N 1 41·0E		
−6	327	1·7	1·0	329	1·7	0·9	324	2·2	0·9	300	1·9	1·0	327	1·7	1·0	327	1·4	0·7	320	1·3	0·7	311	1·2	0·6
−5	313	1·5	0·9	324	1·4	0·7	321	1·7	0·7	296	2·4	1·2	327	2·6	1·5	330	1·6	0·8	319	1·4	0·7	315	1·2	0·6
−4	298	1·3	0·8	310	0·6	0·3	315	0·8	0·4	289	2·4	1·2	327	2·7	1·6	334	1·4	0·7	320	1·1	0·6	317	1·0	0·5
−3	274	0·7	0·4	180	0·5	0·3	172	0·3	0·1	281	1·6	0·8	327	1·9	1·1	331	0·6	0·3	318	0·6	0·3	315	0·6	0·3
−2	196	0·6	0·3	169	1·4	0·7	151	1·4	0·5	248	0·4	0·2	327	0·7	0·5	148	0·1	0·1	135	0·1	0·1	307	0·1	0·1
−1	162	1·2	0·7	162	1·5	0·8	145	1·8	0·7	131	0·7	0·4	147	0·6	0·3	148	0·9	0·5	141	0·8	0·4	137	0·5	0·3
0	149	1·5	0·8	153	1·5	0·8	141	1·7	0·9	120	1·6	0·8	147	1·6	0·9	145	1·3	0·7	143	1·4	0·7	132	1·1	0·6
+1	134	1·5	0·9	147	1·4	0·7	140	1·4	0·7	115	2·1	1·1	147	2·4	1·4	148	1·5	0·8	140	1·4	0·8	131	1·5	0·7
+2	120	1·3	0·8	132	0·9	0·5	135	1·0	0·5	111	2·1	1·1	147	2·4	1·5	149	1·5	0·8	135	1·1	0·6	133	1·4	0·7
+3	105	1·0	0·5	049	0·6	0·3	102	0·3	0·1	109	1·6	0·8	147	1·9	1·2	153	1·1	0·6	135	0·7	0·4	134	0·9	0·5
+4	056	0·5	0·3	357	1·0	0·6	335	0·8	0·3	087	0·6	0·3	147	1·1	0·6	173	0·4	0·2		0·0	0·0	147	0·3	0·2
+5	352	1·0	0·5	337	1·4	0·8	327	1·7	0·7	326	0·6	0·3	327	0·1	0·1	311	0·5	0·3	319	0·7	0·4	294	0·5	0·3
+6	331	1·6	0·9	331	1·6	0·9	325	2·2	0·9	301	1·6	0·8	327	1·3	0·7	324	1·1	0·6	319	1·2	0·6	310	1·0	0·5

Hours	J 53°15′·0N 1 50·5E			K 53°08′·0N 2 02·0E			L 53°04′·5N 2 12·0E			M 52°52′·0N 2 14·0E			N 53°20′·5N 2 17·0E			P 53°28′·0N 2 36·0E			Q 52°56′·5N 2 45·2E			R 53°02′·5N 2 53·0E		
−6	314	1·1	0·6	317	1·1	0·8	312	0·7	0·4	294	0·6	0·3	332	1·1	0·6	310	1·1	0·6	257	0·6	0·3	246	0·6	0·6
−5	319	1·3	0·7	321	1·7	1·1	334	1·6	0·9	317	1·6	0·8	341	1·5	0·8	321	1·3	0·7	331	0·7	0·4	306	0·8	0·5
−4	329	1·5	0·8	321	1·9	1·3	339	2·0	1·1	329	2·3	1·2	346	1·6	0·8	329	1·5	0·8	356	1·1	0·6	342	1·1	0·6
−3	332	1·2	0·6	321	1·7	1·1	338	1·5	0·9	332	2·3	1·2	344	1·1	0·6	341	1·3	0·7	006	1·3	0·7	359	1·3	0·7
−2	344	0·5	0·3	321	0·9	0·6	338	0·8	0·4	337	1·9	0·9	345	0·4	0·2	354	0·8	0·4	004	1·1	0·6	006	1·3	0·7
−1	099	0·5	0·2	090	0·1	0·0	013	0·1	0·1	343	0·9	0·4	116	0·3	0·2	063	0·3	0·2	357	0·6	0·3	020	0·9	0·5
0	120	1·3	0·7	133	1·2	0·8	143	0·7	0·4	124	0·6	0·2	133	1·0	0·6	115	0·7	0·4	010	0·1	0·1	043	0·5	0·3
+1	133	1·6	0·9	140	2·0	1·4	150	1·5	0·8	144	1·7	0·9	145	1·4	0·8	127	1·4	0·7	144	0·5	0·3	132	0·4	0·2
+2	143	1·6	0·8	141	2·1	1·4	153	1·7	1·0	147	2·3	1·2	161	1·7	0·9	142	1·7	0·9	155	1·1	0·6	153	0·6	0·3
+3	158	1·2	0·7	141	1·7	1·1	157	1·5	0·8	149	2·4	1·2	171	1·6	0·8	156	1·6	0·9	162	1·2	0·7	165	1·1	0·6
+4	182	0·7	0·4	145	0·8	0·5	161	0·9	0·5	148	2·0	1·0	191	0·9	0·5	171	1·1	0·6	180	1·1	0·6	172	1·5	0·8
+5	250	0·5	0·3	270	0·1	0·1	174	0·3	0·2	147	1·1	0·5	280	0·5	0·3	242	0·6	0·3	210	0·8	0·4	179	1·3	0·7
+6	302	0·8	0·5	313	0·8	0·5	296	0·4	0·2	234	0·1	0·1	325	1·0	0·5	302	1·0	0·5	245	0·6	0·3	203	0·8	0·5

(1020·0 × 640·0mm)

Published at Taunton 25th March 1977 under the Superintendence of Rear-Admiral D. W. Haslam, O.B.E., Hydrographer of the Navy.
New Editions 24th March 1978, 16th March 1984, 19th February 1988

Positive 1976
AST 1987
A.9-88
A.9-88